Understanding the Role of Ankyrin-G in Synaptic Biology

by

Andrew David Nelson

A dissertation submitted in partial fulfillment
of the requirements for the degree of
Doctor of Philosophy
(Pharmacology)
in the University of Michigan
2019

Doctoral Committee:

Assistant Professor Paul M. Jenkins, Chair
Professor Lori L. Isom
Assistant Professor Kevin S. Jones
Assistant Professor Kenneth Kwan
Research Investigator Heather O'Malley

Andrew David Nelson

andnels@umich.edu

ORCID iD: 0000-0001-8379-3058

Acknowledgements

First, I would like to thank my mentor, Dr. Paul Jenkins for his unconditional support, guidance, and sincere passion for his work. I am extremely lucky he decided to start his own lab just in time for my final rotation. He has been an incredible mentor who has given me every opportunity to be successful and develop as a scientist and student. My experience under his mentorship has been incredibly rewarding and inspiring and fostered my love for science. Secondly, I wish to thank the additional members of my thesis committee: Drs. Lori Isom, Kevin Jones, Kenneth Kwan, and Heather O'Malley. They have provided invaluable insight and guidance on my project and have whole-heartedly encouraged me throughout my training.

Next, I would like to thank all members of the Jenkins laboratory, both past and present, including Julie Philippe, Amanda France, Dr. René Caballero-Florán, Dr. Kathleen Ignatoski, Shruti Arora, Matthew Gologorsky, Randy Strassburg, Zach Bernstein, Katie Hahm, Maxwell Tsai, Marissa Martinelli, and Jaeyoung Choi. They have all made lab a stimulating and supportive environment and provided countless laughs and many good memories.

I would also like to thank the various colleagues and collaborators for their contributions to this thesis. From the University of Michigan, I would like to thank Dr. René Caballero-Florán for a substantial amount of electrophysiological data for studies in Chapter 2, Dr. Lori Isom and her laboratory for helpful discussion, suggestions, and electrophysiological data, Dr. Kevin Jones and Jean Carlos Rodríguez Díaz for establishing techniques to measure gamma oscillations, and

Dr. Melvin Mcinnis for providing patients samples and clinical data from the Heinz C. Pechter Bipolar Research Program. Dr. Vann Bennett from Duke University, Dr. Chao Wang from the School of Life Sciences and Technology of China, Dr. Mingjie Zhang from the University of Hong Kong University of Science and Technology, I would like to thank additional collaborators for their contributions to my graduate work: Dr. Jack Parent from the University of Michigan and Dr. Chris Ross from Johns Hopkins University.

I am also grateful for the funding sources that have supported my graduate studies and thesis work including the Program in Biomedical Sciences (University of Michigan), Heinz C. Pretcher Bipolar Research Fund and Richard Tam Foundation (University of Michigan), Genetics Training Program Fellowship (NIH T32GM007544), Translational Research Education Certificate Program (University of Michigan), and Rackham Predoctoral Fellowship (University of Michigan).

I would like to express gratitude for the administration in the Department of Pharmacology for everything outside of the science including: Lisa Garber, Josh Daniels, Ingrid Shriner-Ward, Dar-Weia Liao, Chereen Mroz, Denise Gakle, Nancy Katon, Dennis Ondreyka, Eileen Ferguson, Audrey Morton-Dziekan, and Elizabeth Oxford.

Finally, I would like to show appreciation to my family, Team Nelson. My parents, Dawn and Steve, as well as my sisters, Taylor, Alyssa, Nicole, and Hannah. I would also like to thank my fiancée, Victoria. Your love and unconditional support have been extremely important to me throughout graduate school. I would not be where I am today without all of you.

Table of Contents

List of Figures

Chapter 1

Chapter 2

Chapter 3

Chapter 4

List of Tables

Abstract

Ankyrin-G is a fundamental scaffolding protein that organizes neuronal excitable membrane domains, including the axon initial segment (AIS) and nodes of Ranvier. A new critical role for ankyrin-G was discovered in the formation of GABAergic inhibitory synapses. GABAergic transmission is essential for the proper synchronization and function of neuronal networks that underlie cognition, mood, and behavior. Recent work has shown ankyrin-G also plays a role in excitatory glutamatergic synapses, important for brain function, by regulating dendritic spine morphology, density, and function. Abnormalities in GABAergic interneuron circuitry and dendritic spines have been linked to neuropsychiatric diseases; however, the underlying cellular and molecular mechanisms remain poorly understood.

Studies designed in this thesis seek to understand the molecular mechanisms of ankyrin-G at inhibitory GABAergic synapses and excitatory dendritic spines. We generated a knock-in mouse model expressing a W1989R mutation in *Ank3*, which completely abolishes the ankyrin-G/$GABA_A$ receptor-associated protein (GABARAP) interaction to understand how ankyrin-G regulates GABAergic circuity *in vivo.* Using confocal microscopy and electrophysiological techniques, we show *Ank3* W1989R mice exhibit a striking reduction in forebrain GABAergic synapse connectivity and function resulting in pyramidal cell hyperexcitability and disrupted network synchronization. Furthermore, we found changes in pyramidal cell dendritic spines and AISs consistent with compensation for hyperexcitability. We identified the *ANK3* W1989R variant in a family with bipolar disorder, suggesting a potential role of this variant in disease. Lastly, this

thesis explores the role of ankyrin-G in regulating dendritic spines to maintain normal neuronal excitability. This work highlights the importance of ankyrin-G in inhibitory and excitatory synapses and provides novel insights into how *ANK3* loss-of-function may contribute to human disease.

CHAPTER 1

General Introduction[1]

Domains of the Neuron and Neuronal Networks

Neurons are highly specialized cells of the nervous system that receive, process, and transmit electrical and chemical signals critical for normal brain function. Neurons are polarized cells made up of structurally and functionally distinct domains, dendrites and axons, which allow for the direct flow of information throughout neuronal networks. The dendrites are often composed of multiple branches and dendritic spines that receive signals from upstream neurons and transmit this information to the axon. The axon propagates electrical signals, known as action potentials, to downstream neurons by the opening of voltage gated-sodium channels at specialized excitable microdomains referred to as the axon initial segment (AIS) and nodes of Ranvier (Fig. 1.1). Action potential initiation at the AIS and efficient propagation across the nodes of Ranvier require the localization of high concentrations of voltage-gated ion channels. In addition, the AIS and nodes also contain high densities of cell adhesion molecules and scaffolding proteins that anchor these critical ion channels to the underlying cytoskeleton networks. Despite similar structural composition between the AIS and the nodes, the mechanisms by which these microdomains form are quite different. The formation of the nodes of Ranvier is strongly influenced by both intrinsic and extrinsic factors, whereas localization of these same protein to the AIS relies mainly on

[1]This review was published in Frontiers in Cellular Neuroscience. Nelson AD, Jenkins PM. Axonal Membranes and their Domains: Assembly and Function of the Axon Initial Segment and Node of Ranvier. 2017 May 9; 11:136. PMCID: PMC5422562.

factors intrinsic to the neuron. The intricate formation and function of excitable axonal microdomains of the vertebrate nervous system plays a critical role in fast neuronal signaling and higher order cognitive processing.

Neurons form complex networks through neuron-to-neuron connections, called synapses, which allow for communication between neurons. A synapse is made up of a presynaptic and postsynaptic terminal. The presynaptic terminal is at the end of the axon and is the site where the action potential, an electrical signal, is converted to a chemical signal, neurotransmitter release. The postsynaptic terminal is located on the downstream receiving neuron and contains specific receptors that the neurotransmitters released from the presynaptic terminal bind to activate. Neuronal networks consist of two main types of neurons: excitatory pyramidal cells and inhibitory interneurons. Pyramidal cells are characterized by the release of the major excitatory neurotransmitter in the brain, glutamate, and interneurons are classified by the principle inhibitory neurotransmitter, GABA. Glutamate acts on three types of ionotropic glutamate receptors (AMPA receptors, NMDA receptors, and kainate receptors), which elicits fast excitatory signaling and depolarizes the postsynaptic neuron. GABA exerts its fast-inhibitory action through $GABA_A$-type ionotropic receptors. GABAergic inhibition balances glutamatergic excitatory transmission to maintain neuron firing and stabilize neuronal networks. The balance between excitatory and inhibitory networks (E/I balance) is important for proper neuronal circuitry function. Abnormal E/I balance has been implicated in a number of diverse pathological conditions including neurodevelopmental and neuropsychiatric disorders (Del Pino, Rico, and Marin 2018; Selten, van Bokhoven, and Nadif Kasri 2018; Sohal and Rubenstein 2019; Tatti et al. 2017). This chapter focuses on recent advances in our understanding of structural and functional mechanisms underlying the formation and function of the AIS and nodes of Ranvier and how disruptions in

these mechanisms influence neurological health and disease. The following chapters are centered on GABAergic inhibitory and glutamatergic excitatory synapses and how their dysfunction may contribute to neuropsychiatric and neurodevelopmental diseases.

Overview of the Function and Intrinsic Assembly of the AIS

The AIS is a specialized membrane domain approximately 10-60 μm long and is generally located at the most proximal region of the axon (Palay et al. 1968). This domain is characterized by high-densities of voltage-gated ion channels and functions as the gatekeeper of action potential initiation as well as axonal polarity (Kole et al. 2008; Bender and Trussell 2012; Kole and Stuart 2012; Jones and Svitkina 2016) (Fig. 1.1). AIS assembly is an intrinsic process within the neuron, in contrast to the formation of nodes of Ranvier, which also require extracellular glial-derived signals. The scaffolding protein ankyrin-G is regarded as the master organizer of the AIS as it coordinates the localization of all known AIS components (Bennett and Baines 2001; Jenkins and Bennett 2001; Leterrier et al. 2017). Other critical proteins involved in AIS assembly and function include Nav channels (Kordeli, Lambert, and Bennett 1995; Zhou et al. 1998), neuronal KCNQ potassium channels (Pan et al. 2006), the cell adhesion molecule neurofascin-186 (NF186) (Jenkins and Bennett 2001; Ango et al. 2004; Davis and Bennett 1994; Dzhashiashvili et al. 2007), casein kinase II (CK2) (Brechet et al. 2008), and βIV spectrin-actin cytoskeletal proteins (Komada and Soriano 2002; Yang et al. 2007) (Fig. 1.1).

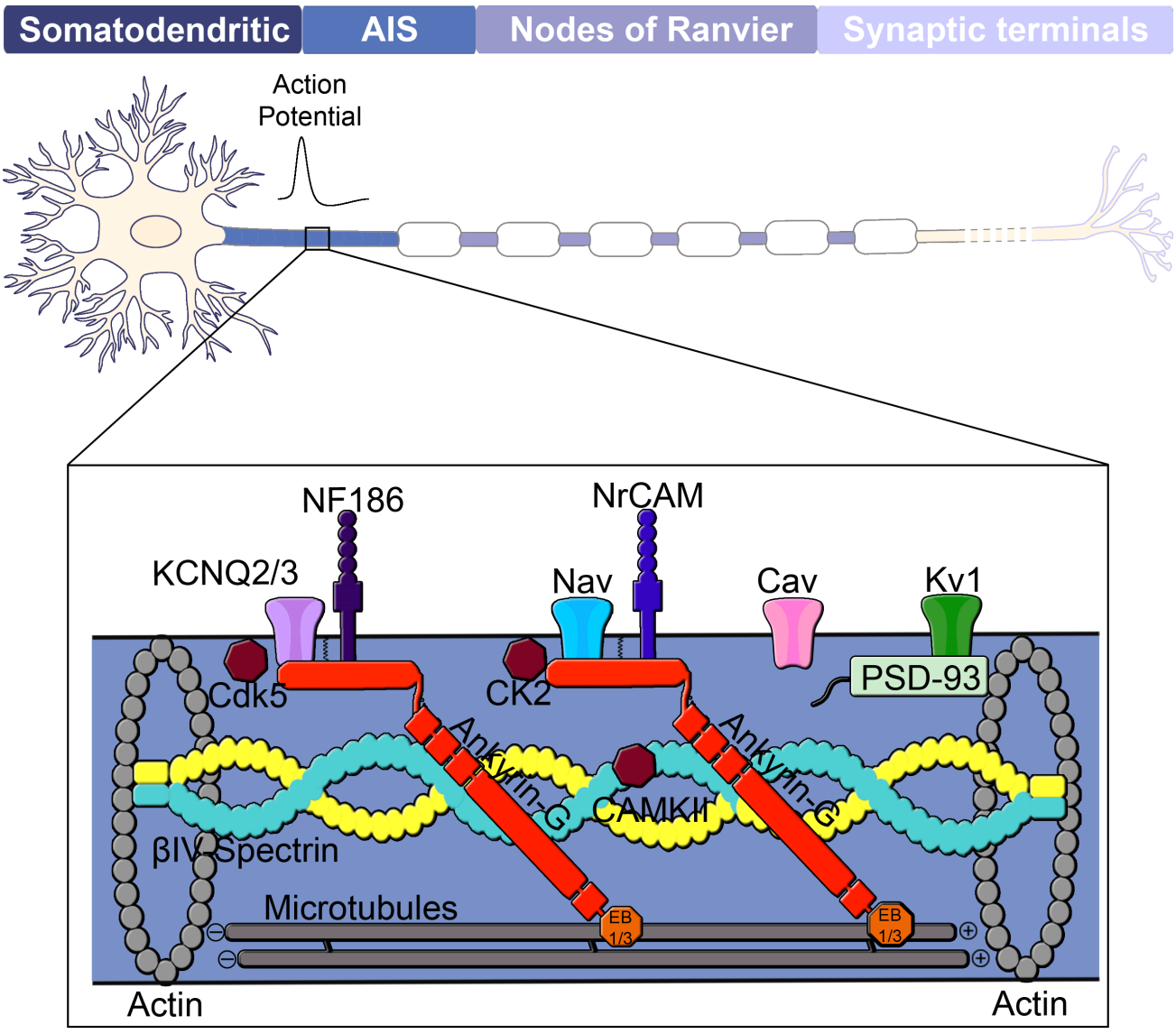

Figure 1.1: Domain organization of a neuron. The neuron consists of a somatodendritic domain, the axon initial segment (AIS), nodes of Ranvier, and presynaptic terminals. The action potential is generated at the AIS, located in the proximal region of the axon, and propagates via saltatory conduction down the nodes of Ranvier of a myelinated axon to the presynaptic terminals. Ankyrin-G (red) is considered the master organizer of the AIS and controls localization of membrane-associated proteins such as Kv and Nav channels as well as the cell adhesion molecules NF186 and NrCAM. Nav channels found at the AIS include Nav 1.1, Nav1.2, and Nav1.6. Ankyrin-G is also linked to the underlying actin cytoskeleton through its interaction with βIV-spectrin and to the microtubule cytoskeleton through interactions with EB1/3 proteins. Other components of the AIS include protein kinases CK2, Cdk5, and CAMKII as well as Cav, Kv1, and PSD-93.

Work from Gary Banker and others with cultured hippocampal neurons has established the nomenclature for stages of neuronal development (Dotti, Sullivan, and Banker 1988). At the start of neuron development, referred to as stage 1, multiple lamellipodia protrude around the entire circumference of the cell. In stage 2, the lamellipodia progress into several short and identical neurites within 12-24 hours of plating. Neuronal polarity begins to develop at 24-48 hours in stage 3 during which one of the immature neurites rapidly elongates and subsequently acquires axonal properties shortly after the formation of the axon, where the remaining immature neurites slowly transition into the dendrites at 3-4 days (Dotti, Sullivan, and Banker 1988). The AIS first forms in cultured hippocampal neurons between stages 3 and 4 (approximately three to four days *in vitro*) indicated by the clustering of ankyrin-G, the first detectable marker of the AIS (Yoshimura and Rasband 2014). *In utero* electroporation of GFP to label neurons *in vivo* revealed the first noticeable accumulation of ankyrin-G occurs in the proximal axon at approximately P1 after most neurons have migrated to their final destination in layer II/III of the cortex (Galiano et al. 2012). In contrast, Gutzmann et al. discovered ankyrin-G appears at the proximal axon at embryonic day 14.5 in the visual cortex (Gutzmann et al. 2014). Further, analysis of AIS formation *in vivo* using spinal motor neurons, demonstrated that ankyrin-G is first expressed along the length of the axon before gradually becoming restricted to the proximal axon at embryonic day 13.5 (Le Bras et al. 2014). It is not clear whether these findings represent a difference in assembly of the AIS in a brain region-specific or cell type-specific manner (i.e. primary motor cortex versus visual cortex versus spinal motor neurons); however, in all cases ankyrin-G is the first resident protein of the AIS to appear.

Giant ankyrins key to axonal structure and function

The vertebrate genome contains three members of the ankyrin gene family: *ANK1*, *ANK2*, and *ANK3* (encoding ankyrin-R, ankyrin-B, and ankyrin-G, respectively). Alternative splicing is a key mechanism underlying the functional diversity and cellular distribution of ankyrins. In addition to the canonical 190 kDa ankyrin-G, alternative splicing of the giant 7.8-kb exon produces a 270 kDa isoform, which only utilizes the first ~2700 nucleotides of the giant exon due to in-frame splicing, and a giant 480 kDa isoform which utilizes the entire giant exon. Similar alternative splicing of *ANK2* gives rise to a 220 kDa isoform and a 440 kDA isoform of ankyrin-B. The giant ankyrin-G differs from the large isoform of ankyrin-B due to the presence of a 40 kDa serine and threonine rich domain located on the N-terminal side that is modified by O-linked *N*-acetylglucosamine residues with unknown function (Vosseller et al. 2006; Zhang and Bennett 1996). Interestingly, giant ankyrins are more prevalent in the genome throughout evolution than originally thought, with many bilaterians expressing giant isoforms with variation between species in the site of insertion (Jegla et al. 2016). Between three species that share homologous insertion sites (*Drosophila*, *Ciona intestinalis*, and *Stronglyocentrotus purpuratus*), there is no significant sequence homology outside of a composition bias of increased usage of serine and glutamic acid and there is a huge variation in exon size (7.8kb in vertebrates versus 13.3kb in *C. intestinalis* and 27.8kb in *Drosophila*). Although the Drosophila giant splice variants also show some ability to restrict ion channel mobility within the axon (Jegla et al. 2016), more work is necessary to determine the functions of these different giant ankyrins.

In vertebrates, the 480 kDa isoform of ankyrin-G is localized to the AIS and nodes of Ranvier in myelinated axons. Recent studies demonstrated that, of all the *ANK3* isoforms, the giant 480 kDa ankyrin-G is specifically required for the proper localization of voltage-gated Nav

channels, KCNQ2/3 channels, NF186, and βIV-spectrin to the AIS (Jenkins et al. 2015). The authors also identified a critical serine residue located within the giant exon, but outside of the canonical binding site of βIV-spectrin, that regulates spectrin localization via a likely phosphorylation-dependent mechanism. Surprisingly, mice lacking the giant 270 kDa and 480k Da splice variants of ankyrin-G survive through weaning, whereas mice lacking all three main isoforms of ankyrin-G die immediately after birth (Jenkins et al. 2015). Survival of mice lacking the giant splice forms of ankyrin-G may be because of a compensatory increase in expression of the smaller 190 kDa isoform. Further, mice lacking giant ankyrin-G demonstrate severe movement defects and significant reductions in higher order cognitive processing such as working memory and sensory stimulation as compared to control littermates (Jenkins et al. 2015). These findings highlight the critical importance of the giant exon of ankyrin-G for normal neuronal function at both the cellular level and for synchronization of complex brain circuits.

In contrast to the giant splice variant of ankyrin-G, the 440 kDa variant of ankyrin-B is found in unmyelinated axons where it interacts with αII-spectrin and βII-spectrin to establish an intra-axonal barrier that limits ankyrin-G expansion within the axon (Fig. 1.2) (Galiano et al. 2012). During postnatal axonal development the majority of the 440 kDa ankyrin-B is replaced by the 220 kDa isoform, lacking the giant insert, which has been shown to be important for the long-range trafficking of cargo down the axon (Lorenzo et al. 2014). Future work will be necessary to fully elucidate the roles of the different splice variants of ankyrin-B and their relationships to ankyrin-G in the proper structure and function of the AIS.

Ankyrins and their spectrin counterparts play a central role in the formation of discrete plasma membrane domains by coordinating the specific subcellular localization of membrane-associated

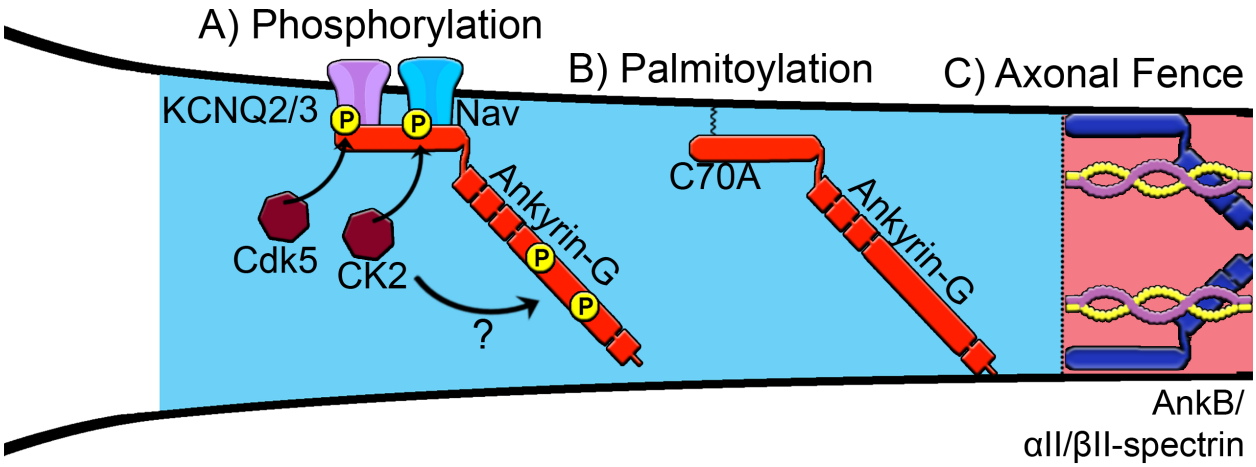

Figure 1.2: Proposed mechanisms of assembly of the AIS. A) Phosphorylation of Nav channels by protein kinase CK2 and KCNQ2/3 channels increases affinity for ankyrin-G. Phosphorylation sites within the giant exon of ankyrin-G (red), potentially regulated by CK2, are important for βIV-spectrin binding. B) Palmitoylation of a critical cysteine 70 residue in the membrane-binding domain of ankyrin-G is necessary to target ankyrin-G to the AIS and recruit known binding partners. C) Ankyrin-B interacts with αII-spectrin and βII-spectrin to establish an intracellular barrier or "axonal fence" and maintain ankyrin-G within the proximal axon.

proteins. Ankyrins interact with their membrane-associated proteins through a membrane-binding domain that consists of 24 ANK repeats folded into an extended solenoid structure on the N-terminus (Bennett and Lorenzo 2013). In canonical ankyrins, the membrane-binding domain is followed by two ZU5 domains, a UPA domain (Wang et al. 2012), a death domain (Wang et al. 2009), and an unstructured C-terminal regulatory domain. The membrane-binding domain of ankyrin-G directly binds to a highly conserved intracellular motif located in the II-III linker domain of Nav channels and to the C-terminus of Kv channels and recruits them to the AIS both *in vivo* and *in vitro* (Gasser et al. 2012; Pan et al. 2006). The cell adhesion molecules NF186 and NrCAM directly interact with the membrane-spanning domain of ankyrin-G through a conserved intracellular five amino acid motif (FIGQY) (Zhong et al. 2014; Zhang et al. 1998). The clustering of ion channels, including Nav and Kv channels, at the AIS is critical for normal neuronal function. The specific subtypes of Nav channels at the AIS include Nav1.1, Nav1.2, and Nav1.6. Early in AIS development, Nav1.2 is the predominant channel found at the AIS; however, as the neuron matures Nav1.6 becomes the primary channel (Boiko et al. 2003; Osorio et al. 2005). The reason for this shift in Nav channel expression and its physiological impact remains poorly understood. Multiple subtypes of Kv channels have also been identified at the AIS, these include Kv1.1, Kv1.2, Kv1.4, Kv2.1, Kv2.2, Kv7.2 (KCNQ2) and Kv7.3 (KCNQ3), which are important for modulating neuronal excitability (Cooper 2011).

Deletion of ankyrin-G prevents clustering of other AIS members including KCNQ2/3 channels, NF186, NrCAM, βIV-spectrin, and Nav channels in the proximal axon (Jenkins et al. 2015; Jenkins and Bennett 2001; Pan et al. 2006; Zhou et al. 1998). Genetic deletion of ankyrin-G in mice or silencing ankyrin-G using shRNA in dissociated neurons results in the loss of Nav channel clustering at the membrane (Fache et al. 2004; Hedstrom, Ogawa, and Rasband 2008;

Zhou et al. 1998). The assembly of the AIS through interaction of both the ion channels and cell adhesion molecules to ankyrin-G is regulated by phosphorylation. Interestingly, the phosphorylation of Nav channels is facilitated by protein kinase CK2, which greatly increases Nav affinity for ankyrin-G (Fig. 1.2) (Brechet et al. 2008), whereas phosphorylation of the FIGQY motif on NF186 and NrCAM inhibits interaction with ankyrin-G (Tuvia, Garver, and Bennett 1997). The NF186-ankyrin-G-Nav channel protein complex is linked to the underlying actin cytoskeleton through ankyrin-G's interactions with βIV-spectrin (Berghs et al. 2000).

Spectrins are a group of cytoskeletal proteins that contribute to the mechanical support of axons through direct interaction with ankyrins. βIV-spectrin is a member of the spectrin family, a group of flexible rod-shaped cytoskeletal proteins that exist as tetramers with two α and two β subunits (Galiano et al. 2012; Ogawa et al. 2006; Uemoto et al. 2007). In mammals, although β-spectrins are encoded by five different genes, only βIV-spectrin is found to be enriched at the AIS and nodes of Ranvier, and its recruitment to these sites depends on the direct interaction with ankyrin-G (Yang et al. 2007). Since all β-spectrins contain the canonical ankyrin-spectrin interaction site (Davis et al. 2009), what is unique about βIV-spectrin that allows its clustering at the AIS and nodes of Ranvier? Studies have shown that the first Zu5 domain of ankyrin is the canonical β-spectrin binding site since this is where βII-spectrin binds to ankyrin-B in neonatal cardiomyocytes and where βI-spectrin binds to ankyrin-R in erythrocytes (Ipsaro et al. 2010; Ipsaro and Mondragon 2010; Mohler, Yoon, and Bennett 2004). However, the presence of the DAR999AAA mutation in the 480 kDa ankyrin-G, which is known to abolish ankyrin-spectrin binding at Zu5, had no effect on its ability to cluster βIV-spectrin to the proximal axon. In addition, knockout and rescue with the 270 kDa ankyrin-G failed to properly localize βIV-spectrin to the AIS despite the fact that all isoforms of ankyrin-G share the Zu5 domain and that 270 kDa ankyrin-

G is capable of interacting with βIV-spectrin in immunoprecipitation experiments (Hedstrom, Ogawa, and Rasband 2008; Jenkins et al. 2015; Komada and Soriano 2002). Interestingly, mutation of a critical S2417A site found within the giant exon of the 480 kDa ankyrin-G greatly reduces βIV-spectrin localization to the AIS. These findings demonstrate that recruitment of βIV-spectrin to the AIS by ankyrin-G occurs independently of the canonical ankyrin-spectrin binding site in the first Zu5 domain and perhaps offers a novel mechanism as to why βIV-spectrin is localized to the AIS. In addition, the 270 residues between the last spectrin repeat and the PH domain of βIV-spectrin, which are not found in other β-spectrins, may play an important role in the noncanonical recruitment of βIV-spectrin to the AIS. Although this stretch is predominantly unstructured, there are ~70 amino acids that are strongly predicted to form alpha helical coils and this may represent an important interaction surface. More work is necessary to determine the precise mechanisms by which ankyrin-G recruits βIV-spectrin to the AIS.

Despite the fact that βIV-spectrin can interact with αII-spectrin (Uemoto et al. 2007); αII-spectrin has not yet been identified at the AIS. In contrast, βII-spectrin and αII-spectrin assemble with one another in the distal axon (Uemoto et al. 2007). βII-spectrin has been implicated in the initial assembly of the AIS as genetic ablation of βII-spectrin in immature neurons alters βIV-spectrin's ability to appropriately accumulate at the AIS (Zhong et al. 2014). βII-spectrin becomes enriched in a periodic arrangement in the AIS very early in development, before the other AIS proteins are detectable, and then migrates to more distal regions within the axon. The migration of βII-spectrin down the axon coincides with the appearance of ankyrin-G and βIV-spectrin at the AIS (Zhong et al. 2014). If βII-spectrin is providing initial structural support, what is the function of the clustered βIV-spectrin? One potential role could be to function as the coordinator of a

signaling platform for calcium-mediated signaling through calmodulin-dependent kinase II (Hund et al. 2010).

Potential mechanisms of ankyrin-G recruitment to the AIS

Increasing evidence supports the role of ankyrin-G as the master organizer of the AIS; however, a major unresolved question is how ankyrin-G itself is recruited to the proximal axon to initiate this process (Fig. 1.2). It has been shown that multiple domains of ankyrin-G cooperate with one another to drive its localization to the AIS (Zhang et al. 1998). He *et al.* demonstrated that the addition of a fatty acid palmitate, termed S-palmitoylation, to a critical cysteine residue in the membrane-binding domain of the 190 kDa ankyrin-G is necessary for ankyrin-G membrane association and proper polarized localization in epithelial cells (He, Jenkins, and Bennett 2012). In addition, palmitoylation of the 270 kDa ankyrin-G at the cysteine 70 site is necessary to target ankyrin-G to the AIS and the presence of a C70A mutation in ankyrin-G fails to cluster at the AIS and cannot recruit neurofascin or Nav channels (He, Jenkins, and Bennett 2012). Of the 23 members of the aspartate-histidine-histidine-cysteine (DHHC)-containing protein palmitoylacyltransferases, zDHHC5 and zDHHC8 were identified as the only family members that localize to the lateral membrane and are responsible for the palmitoylation and targeting of ankyrin-G (He, Abdi, and Bennett 2014). Although the cysteine 70 residue is conserved within all major splice variants of ankyrin-G, it remains unknown which palmitoylacyltransferases localize the giant 480 kDa isoform to the AIS and whether palmitoylation of ankyrin-G occurs specifically at the AIS or within the cell body (Fig. 1.2). Future studies are needed to characterize the palmitoylacyltransferases capable of palmitoylating neuronal ankyrin-G and to evaluate the spatial and temporal regulation of this process during AIS development.

Another important mechanism for the control of AIS formation is phosphorylation of ankyrin-G and its binding partners. Phosphorylation of KCNQ2/3 channels by cyclin-dependent kinase 5 (Cdk5) and phosphorylation of Nav channels by casein kinase (CK2) increase binding affinity to ankyrin-G. Bréchet *et al.* showed that CK2 phosphorylation of various serine residues (S1112, S1124, and S1126) and a glutamate residue (E1111) on Nav1.2 regulates Nav channel association with ankyrin-G (Brechet et al. 2008). These data show that increasing the affinity of ion channels for ankyrin-G is an important regulatory step in the formation of the AIS. Overall, posttranslational modifications are an important step in AIS formation. It will be interesting to see if there are other posttranslational modifications on ankyrin-G and its partners and how these modifications are altered under different signaling conditions.

Lastly, the distal axon cytoskeleton, which is composed of ankyrin-B, αII-spectrin, and βII-spectrin complexes, has been proposed to create a boundary that restricts ankyrin-G to the proximal axon (Fig. 1.2). Manipulating the position of this boundary closer to the soma by overexpression of ankyrin or spectrin resulted in a shorter AIS, whereas shifting the boundary away from the soma caused the AIS to become elongated (Galiano et al. 2012). Silencing of ankyrin-B with short hairpin RNA (shRNA) inhibits AIS assembly and causes ankyrin-G to distribute throughout the distal axon in cultured neurons (Galiano et al. 2012). In contrast, Lorenzo *et al.* observed no gross detectable abnormalities in the AIS in 8 DIV hippocampal neurons derived from ankyrin-B-null mice lacking the 440 kDa and 220 kDa isoforms (Lorenzo et al. 2014). Instead, deletion of ankyrin-B results in shortened axonal tracts and impaired axonal transport due to the loss of ankyrin-B association with dynactin and dynein mediated cargo transport (Lorenzo et al. 2014). Elucidating the role of the ankyrin-B/αII-spectrin/βII-spectrin network in the formation of the AIS *in vivo* will be important for the understanding of human diseases involving

dysfunction of ankyrins and spectrins. In addition, it remains unclear how 480 kDa ankyrin-G, found both at the AIS and at the distal nodes of Ranvier, is able to avoid the restriction at the proximal axon by the ankyrin-B/spectrin cytoskeletal boundary. It is attractive to speculate that nascent ankyrin-G protein is locally translated at the node of Ranvier or perhaps locally palmitoylated; however, the exact mechanisms controlling AIS ankyrin-G versus that found at the node of Ranvier remains poorly understood.

AIS maintenance and analysis of cytoskeletal composition through high-resolution microscopy

A primary function of the AIS is to maintain polarity of the proximal axon. One potential mechanism is the role of the AIS as a diffusion barrier to inhibit the mobility of membrane-associated proteins from dispersing from one neuronal domain to another. To support this theory, Kobayashi *et al*. first suggested the presence of a diffusion barrier at the axonal hillock or AIS after they observed fluorescently labeled phospholipids are static within the axonal membrane in hippocampal cultures, whereas no labeling was observed within the somatodendritic domain (Kobayashi et al. 1992). Winckler *et al.* then showed that the transmembrane protein L1CAM and the GPI-anchored protein Thy-1 display markedly reduced mobility at the AIS and they may be constrained by a cytoplasmic tether to actin filaments since the disruption of actin caused the proteins to freely distribute between the axonal and somatodendritic compartments (Winckler, Forscher, and Mellman 1999). Nakada *et al*. further supported these findings by showing that ankyrin-G accumulation in the AIS at 7-10 DIV of developing hippocampal neurons correlates with a dramatic decrease in the rate of phospholipid and Nav channel diffusion (Nakada et al. 2003).

A more recent study by Song *et al*. proposed a second role of the AIS in which ankyrin-G and actin filaments create a selective filter or intracellular sieve within the cytoplasm that blocks the passage of somatodendritic proteins and large macromolecule from entering the axon (Song et al. 2009). For example, axonal motor proteins of the kinesin superfamily (KIFs) were allowed entry into the axon, whereas dendritic cargos and the microtubule-associated protein 2 (MAP2) were found exclusively in the somatodendritic domain of the neuron and become excluded from the AIS throughout the course of assembly (Song et al. 2009). Silencing ankyrin-G expression in hippocampal neurons or genetic deletion of ankyrin-G *in vivo* results in disassembly of the AIS and causes the proximal portion of the axon to acquire dendritic characteristics including dendritic spines and the presence of MAP2 (Hedstrom, Ogawa, and Rasband 2008; Sobotzik et al. 2009). In addition, Jenkins *et al*. showed invasion of MAP2 into the axonal process in mice lacking only the giant isoforms 270/480 kDa of ankyrin-G, which indicates that the AIS does play a role in determining the site of axonal specification. Interestingly, however, the axonal process eventually excludes MAP2 and acquires the axonal marker, neurofilament, despite a complete lack of the AIS (Jenkins et al. 2015). These data demonstrate that the AIS is critical for maintaining axonal identity in the proximal axon, but also that a transition from dendritic to axonal character can occur in an ankyrin-G-and AIS-independent manner. The exact mechanisms underlying this transition are unknown.

An important prediction of both the diffusion barrier and selective filter models is that dendritic and axonal cargos would randomly mix in the absence of the AIS. Studies evaluating the dendritic-specific cargos, transferrin receptor and TGN38, in neurons completely lacking ankyrin-G showed that these dendritic proteins maintain localization within the dendrites, but were excluded from the distal axon despite the absence of all known AIS components. In addition, the

complete loss of the AIS in ankyrin-G-null neurons revealed anterograde and retrograde transport rates of LAMP-1, a relatively large (50-500nm) lysosome, were indistinguishable between the AIS and distal axon in hippocampal neurons (Jenkins et al. 2015). These findings correspond with other work showing there is no difference in the trafficking of the neuronglia cell adhesion molecule (NgCAM) in the AIS as compared to the distal axon (Petersen, Kaech, and Banker 2014). Furthermore, despite the loss of the AIS in total ankyrin-G-null or 480 kDa ankyrin-G-null neurons, MAP2 remains excluded from the distal axon (Jenkins et al. 2015), which suggests neurons may contain a secondary intrinsic property necessary to maintain distal axonal identity. The exclusion of dendritic cargo from the distal axon in cells lacking ankyrin-G is reminiscent of the separation of dendritic and axonal compartments seen before the AIS has been established (Petersen, Kaech, and Banker 2014; Nakada et al. 2003; Silverman et al. 2001). Future studies need to evaluate additional AIS-independent mechanisms and how they may be critical to establish and maintain distinct axonal and dendritic polarized compartments.

While this work supports the existence of a diffusion barrier or selective filter that restricts phospholipids, membrane and cytoplasmic proteins, and transport vesicles, the molecular composition of the cytoskeletal structure involved in the maintenance of neuronal polarity remains poorly understood. Recent work utilizing light and scanning microscopy showed that dense clusters of actin filaments within the AIS prevented the transport of vesicles that contain dendritic cargo from entering into the axon (Watanabe et al. 2012). Further, live-imaging experiments demonstrated that vesicles containing dendritic cargo enter the axon and dendrites with equal frequency; however, once inside the AIS the vesicles with dendritic proteins reverse directions and proceed toward the somatodendritic domain via an actin and myosin Va-dependent mechanism, whereas vesicles with axonal proteins proceed efficiently down the axon (Al-Bassam et al. 2012).

These findings indicate actin filaments may be a key component for the transport of selective axonal cargo; however, there was still a lack in our understanding regarding actin organization within the AIS. Jones *et al*. recently sought to evaluate the sophisticated architecture of the AIS cytoskeleton in mature hippocampal neurons using platinum replica electron microscopy (PREM). The results showed an array of microtubule bundles covered in a dense submembranous coat comprised of known AIS proteins including ankyrin-G, βIV-spectrin, neurofascin, Nav channels, and actin filaments (Jones, Korobova, and Svitkina 2014). Interestingly, although they failed to identify a dense actin network within the AIS, they discovered subpopulations of actin that alternate between short, stable and longer, flexible filaments.

Recent advances in super resolution microscopy have revealed further insights to the arrangement of the submembranous axonal cytoskeleton and the mechanisms by which the AIS may maintain axonal polarity. A recent study quantitatively sought to determine the nanoscale organization of the AIS using Stochastic Optical Reconstruction Microscopy (STORM). They revealed the actin filaments form "actin rings" that distribute consecutively throughout the entire length of the AIS and are spaced roughly 190nm apart. In addition, they also determined that ankyrin-B was also found to be periodically localized between the adjacent actin rings in the distal axon (Xu, Zhong, and Zhuang 2013). This unique orientation occurs because βIV-spectrin connects between the adjacent actin rings in a lateral, head-to-head orientation. Further, implementation of 3D-STORM, utilizing antibodies directed against epitopes to either end of ankyrin-G, revealed βIV-spectrin binds periodically on the N-terminus of ankyrin-G, whereas the unstructured C-terminal tail extends ~30nm internally into the AIS cytoplasm where it may interact with additional cytoplasmic binding partners (Leterrier et al. 2015).

Axonal polarization and vesicle trafficking

Besides ankyrin-G, βIV-spectrin, and actin, what additional cytoskeletal proteins are important to maintain neuronal polarity? There is strong evidence that microtubule-based motor proteins influence the selective filtering of cargo transport into axons and dendrites, but the mechanisms underlying this process is not well understood (Hoogenraad and Bradke 2009; Witte, Neukirchen, and Bradke 2008). Interestingly, Jacobson *et al*. showed that the axonal transport protein, kinesin-1, accumulates at a single immature neurite before polarization, which suggests that molecular differences between neurites exist long before the emergence of the axon (Jacobson, Schnapp, and Banker 2006). The selective transport of signaling proteins to the axon would allow for axon-specific growth from an individual neurite and the timing of this process throughout neuron development would be critical to initiate and maintain axonal polarity. One model suggests the pre-axonal exclusion zone (PAEZ), which is located within the axon hillock, distinguishes the AIS from the soma and may be important for the sorting of somatodendritic and axonal cargo (Farias et al. 2015) . Here, the carrier vesicles bind to different microtubule motors that mediate transport either towards the dendrites or down the axon. Organelles that normally bind kinesin-1 or other axonal kinesins can migrate across the PAEZ and down the axon; however, vesicles that bind to dynein or other kinesins are directed to the dendrites.

Another model suggests that, since the microtubules within the AIS are primarily oriented with the plus-ends facing away from the cell body and in the dendrites the microtubules are of mixed orientation, the designated kinesins prefer one orientation over the other driving selective axonal or dendritic trafficking (Kapitein and Hoogenraad 2011; Jacobson, Schnapp, and Banker 2006; Hirokawa and Takemura 2005). In further support of this model, recent work showed that microtubule plus-end binding proteins EB1 and EB3 accumulate in the AIS through direct

association with ankyrin-G. Following shRNA-mediated knockdown of ankyrin-G the AIS disassembles and results in a dramatic upregulation in the expression of EB1 and EB2. Thus, it is possible that the C-terminal tail of ankyrin-G extends within the axoplasm to control the proper formation of microtubule bundles and regulate AIS stability. This prediction is consistent with the loss of bundled microtubules seen in the proximal axon of mice lacking ankyrin-G (Sobotzik et al. 2009). Fréal *et al.* showed the cooperative interaction between 480 kDa isoform of ankyrin-G and end-binding proteins of the microtubule cytoskeleton drives AIS assembly and axon polarity and suggests another potential mechanism that drives ankyrin-G localization to the AIS (Freal et al. 2016).

Kinesins motors are mainly involved in the anterograde transport of dendritic cargo by migrating towards microtubule plus-ends, whereas dynein motors move in retrograde fashion towards microtubule minus-ends within axonal tracts. In support of this view, experiments using fluorescently-labeled mutant kinesin motors were conducted to monitor which subtypes of kinesin motors translocate to either dendritic or axonal domains (Nakata et al. 2011). Kuijpers *et al.* discovered that the Nuclear distribution element-like 1 (NDEL1) facilitates dynein activation on somatodendritic cargos that enter the proximal axon and reverses their movement to a retrograde manner (Kuijpers et al. 2016). NDEL1 is highly concentrated in the AIS via a direct link with ankyrin-G through its C-terminus tail and with LIS1 through its N-terminus tail. LIS1 has been shown to be an important regulator of NDEL1-based dynein activity at the AIS (Vallee and Tsai 2006). The knockdown of ankyrin-G, NDEL1, or LIS1 results in the entry of dendritic cargo into the proximal axon, thus these findings suggest a "quick-switch" mechanism for selective vesicle filtering at the AIS. In addition to kinesin and dynein transport, myosin motors have also been

implicated to be important for the sorting of cargo between axonal or dendritic polarized domains by interacting directly with different microtubule components (Lewis et al. 2009).

Electrical activity and plasticity at the AIS

In vertebrate neurons, the AIS is the site of action potential initiation (Kole et al. 2008; Palay et al. 1968). It has recently been proposed that changes in AIS length, location, and/or ion channel expression may occur following varying degrees of neuronal activity (Fig. 1.3) (Yamada and Kuba 2016). This striking plasticity of the AIS arises in an attempt to maintain homeostasis within individual neurons and balance synchronization between complex neuronal circuits. Changes in AIS length were first observed in neurons removed from the avian cochlear nucleus (Kuba, Oichi, and Ohmori 2010). Decreased stimulation of these neurons resulted in elongation of the AIS and an increase in the number of surface Nav channels, which, in turn, enhanced membrane excitability and promoted action potential firing (Kuba, Oichi, and Ohmori 2010). In addition, low-frequency stimulation caused the AIS to shift within about 10μm of the soma, whereas high-frequency stimulation shifted the AIS about 45μm away from the soma (Kuba, Ishii, and Ohmori 2006). A similar observation was seen after chronic stimulation of dissociated hippocampal neurons, which also caused a distal shift in the AIS and a corresponding decrease in membrane excitability (Evans et al. 2013; Grubb and Burrone 2010). These findings suggest changes in electrical activity affect both the dynamics and location of the AIS, but what are the molecular mechanisms that contribute to this plasticity?

Recent studies demonstrated that prolonged depolarization activates L-type and T-type Ca^{2+} channels in pyramidal hippocampal neurons and that the subsequent increase in intracellular

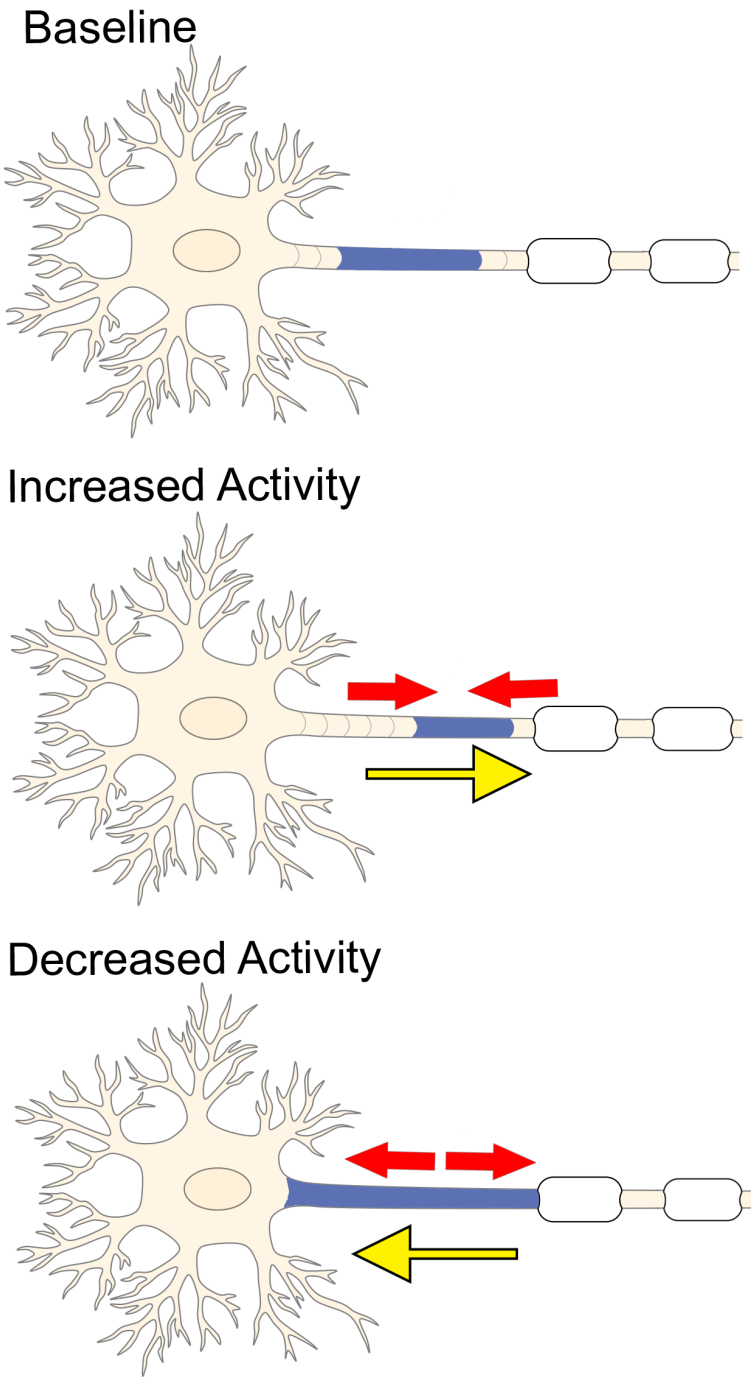

Figure 1.3: Electrical activity and plasticity at the AIS. Increased neuronal activity causes the AIS to shrink (red arrows) and shift more distally away from the soma (yellow arrow). In contrast, inhibiting stimulation of the neuron promotes the AIS to elongate (red arrows) and causes the AIS to shift closer to the soma (yellow arrow).

Ca^{2+} levels activate Ca^{2+}- and calmodulin-dependent protein phosphatases, which may ultimately be responsible for the distal migration and contraction of the AIS (Evans et al. 2015; Evans et al. 2013; Grubb and Burrone 2010; Muir and Kittler 2014). Increased intracellular Ca^{2+} has also been shown to activate cyclin-dependent kinase 5 (cdk5) in olfactory bulb dopaminergic interneurons. In addition, heightened cdk5 activity extended AIS length by as much as 100% in mushroom body neurons of *Drosophila*, while depleting cdk5 causes the AIS to significantly shrink or disappear altogether (Trunova, Baek, and Giniger 2011). To date, the majority of studies that evaluated activity-dependent AIS plasticity and the underlying cellular mechanisms were conducted in fixed cells and these changes were analyzed amongst a population of neurons. The development of innovative tools capable of labeling the AIS for live-imaging experiments will be beneficial to examine AIS plasticity in individual neurons both *in vitro* and *in vivo.* Recently, Dumitrescu *et al*. used a construct consisting of the intracellular domain of a voltage-gated sodium channel Nav1.2 fused to a yellow-fluorescent protein (YFP-NavII-III) to examine the AIS in live neurons (Dumitrescu, Evans, and Grubb 2016). This construct localized specifically to the AIS of dentate granule cells (DGCs) in dissociated hippocampal cultures as well as accurately demonstrated both baseline and activity-induced plasticity changes of the AIS without altering intrinsic neuronal excitability (Dumitrescu, Evans, and Grubb 2016). This construct may be useful in future studies to investigate AIS plasticity in individual neurons. Live-imaging the AIS in individual neurons will reduce cell-to-cell and experimental heterogeneity and provide greater insight to the physiological impact underlying changes in AIS size and position.

Relatively little is known about what happens to the ankyrin-spectrin protein networks during periods of AIS plasticity and the physiological impact these changes have on action potential initiation. Post-translational modifications, such as phosphorylation of Nav channels by

CK2 or palmitoylation of ankyrin-G and NF186, may be involved in this process (Fig. 1.2) (Brechet et al. 2008; He, Jenkins, and Bennett 2012; Ren and Bennett 1998). In addition, the changes in the expression levels of ankyrin could underlie AIS plasticity. In dissociated hippocampal cultures, the overexpression of ankyrin-G was shown to elongate the length of the AIS, whereas overexpression of the distal axon cytoskeletal protein ankyrin-B shortened the AIS (Galiano et al. 2012). While phosphorylation is necessary to assemble and maintain proper AIS structure and function, the Ca^{2+}-dependent cysteine protease calpain works in opposition to promote the degradation and disassembly of the AIS. Calpain activates the proteolysis of the axonal cytoskeletal proteins including ankyrin-G and βIV-spectrin in the proximal axon and ankyrin-B, αII-spectrin, and βII-spectrin in the distal axon (Harada et al. 1997; Czogalla and Sikorski 2005; Bevers and Neumar 2008). In addition, (Schafer et al. 2009) showed that pharmacological inhibition of calpain was sufficient to attenuate degradation and maintain the molecular organization of the AIS both *in vitro* and *in vivo*. It is also possible that the shortened and distal translocation of the AIS is caused by an overload of Ca^{2+} levels and the subsequent potentiation of calpain-mediated proteolysis.

What are the physiological impacts these changes in AIS structure and position may have on action potential generation? Jenkins *et al*. recently showed that mice lacking the giant isoforms (270/480 kDa) of ankyrin-G, and thus all other known components of the AIS, were still able to fire current-induced action potentials with modest effects on action potential frequency and dynamics (Jenkins et al. 2015). One possibility for this phenomenon is that the small 190 kDa ankyrin-G, which displayed a four- to five-fold increase in expression in the giant-exon null mice, is capable of compensating for the 480 kDa ankyrin-G and rescuing Nav channel localization to the plasma membrane. Another possibility is that the action potentials might be generated by Nav

channels clustered locally in the somatodendritic domain (Lai and Jan 2006). If the AIS is dispensable for action potential generation with only minor deficits, what is the evolutionary advantage of having an AIS? One potential answer to this question comes from the abnormalities seen in the gamma oscillations from the EEG recordings of the giant ankyrin-G knockout mice. Gamma oscillations arise through the activity of cortical GABAergic interneurons, which synapse directly on to the AIS and soma of pyramidal neurons and are essential for the proper synchronization of the cortical network (Bartos, Vida, and Jonas 2007; Markram et al. 2004; Somogyi 1977). The AIS thus provides a defined physical location to allow interneurons precise temporal and spatial modulation of action potentials.

Nodes of Ranvier

Following initiation at the AIS, action potentials must travel rapidly across long distances down the axon in order to reach the synapse. In myelinated axons, action potential regeneration occurs at the nodes of Ranvier, which are gaps between myelin sheaths characterized by very high densities of Nav channels (Fig. 1.1). The molecular composition of the nodes of Ranvier and the AIS are very similar in that they both consist of similar ion channels, cell adhesion molecules, and scaffolding proteins (Fig. 1.4) (Rasband 2010). In contrast to the AIS, which is regulated solely by axonal intrinsic signaling, the proper assembly and function of nodes depend on both intrinsic and glial-derived extrinsic mechanisms.

Molecular organization of the Nodes of Ranvier

The complex organization of the Nodes of Ranvier is accomplished in part by myelinating Schwann cells in the peripheral nervous system (PNS) and oligodendrocytes in the central nervous system (CNS). The clustering of Nav channels to the node is critically important for the rapid,

saltatory propagation of action potentials. Myelination divides the axonal membrane into distinct domains including nodes of Ranvier, paranodes, juxtaparanodes, and internodes. The nodes of Ranvier are the sites of action potential repolarization and depolarization due to the clustering of high concentrations of ion channels, including Nav and Kv channels. The complement of Nav and Kv channels at the node are diverse and can include Nav1.1, Nav1.2, Nav1.6, Nav1.7, Nav 1.8, and Nav1.9 which interact with β-subunits Navβ1, Navβ2, and Navβ4 (Boiko et al. 2003; Chen et al. 2002; Fjell et al. 2000; Henry et al. 2005; Duflocq et al. 2008; Black and Waxman 2012). β2-subunits covalently bond with Nav channels via an extracellular disulfide bond and regulate their surface expression (Chen et al. 2012). Kv channels at the node include Kv3.1b, KCNQ2, and KCNQ3 (Cooper 2011). In addition to ion channels, ankyrin-G and βIV-spectrin scaffolding proteins are also highly concentrated at the nodes and, similar to the AIS, anchor the ion channels and cell adhesion molecules NF186 and NrCAM to the underlying cytoskeleton network. Recent studies using STimulated Emission Depleted (STED) microscopy demonstrated a periodic organization of ankyrin-G and βIV-spectrin with the underlying microtubule cytoskeleton at the nodes of Ranvier, similar to that seen in the AIS (D'Este et al. 2015). The paranode flanks the node of Ranvier and is the site where myelinating glial cells form septate-like junctions with the axonal membrane. Ankyrin-G has been shown to be highly enriched within oligodendrocytes on the glial side of the paranodal junction, whereas ankyrin-B is highly expressed at the Schwann cell paranodal membrane (Chang et al. 2014). Glial ankyrins bind to the cell adhesion molecule NF155 at the paranodal junction and contribute to the assembly and maintenance of nodes of Ranvier in both the CNS and PNS. Thus, mutations within *ANK2* or *ANK3* may lead to abnormalities in the AIS and axonal nodes of Ranvier as well as the paranodes within glia. The juxtaparanodes flank the paranodes and are enriched with dense populations of Kv channels known to module action

potential conduction and help maintain internodal resting potential. Finally, the internodes make up the majority of the axon and are found underneath the myelin sheaths.

Assembly of the PNS Nodes of Ranvier

Although the molecular composition between PNS and CNS nodes of Ranvier are similar, the mechanisms involved in their assembly are different mainly due to the glial cells types involved in myelination (Fig. 1.4). In PNS node assembly, Nav channels are initially clustered at the edges of developing myelin sheaths, referred to as the heminodes, by the extracellular matrix molecules gliomedin and neuronal cell adhesion molecule (NrCAM) from Schwann cell microvilli interacting with axonal NF186. (Eshed et al. 2005). (Eshed et al. 2005; Feinberg et al. 2010; Lambert, Davis, and Bennett 1997; Schafer et al. 2006). Secondly, Nav channels are restricted to the nodal gap by the paranodal junction, which consists of glial-derived NF155, found at paranodal region, in conjunction with Caspr and contactin within the axonal membrane. The interaction between NF155 and the Caspr-contactin complex mediates Schwann cell interaction with the axon and formation of the paranodal junction. These paranodal junctions are thought to act as a restriction barrier during node of Ranvier assembly as the nodes are fully capable of forming in NrCAM and gliomedin knockout-mice, despite the fact that NF186 fails to localize to the heminodes of these mice (Feinberg et al. 2010). In addition, the paranodal junction between myelinating Schwann cells of the PNS (and oligodendrocytes in the CNS) may function as a diffusion barrier to prevent the lateral movement of ion channels along the axonal plasma membrane (Pedraza, Huang, and Colman 2001; Rasband et al. 1999). In contrast, the significance of a diffusion barrier remains controversial since disturbing the paranodal junction only slightly perturbed Nav clustering (Bhat et al. 2001; Thaxton et al. 2011). Interestingly, Amor *et al*. recently showed that the paranodal

junctions are sufficient to cluster Nav channels to the node of Ranvier in peripheral sensory neurons and retinal ganglion cells of knockout mice deficient of nodal NF186 (Amor et al. 2017). Further, the authors demonstrate that βII-spectrin plays a role as a diffusion barrier within the paranodal junction to mediate Nav clustering at the node. These findings suggest that the intact paranode can function as a secondary mechanism for Nav nodal clustering independent of axonal NF186 localization by glial-derived proteins.

In addition to gliomedin, other extracellular matrix (ECM) proteins involved in heminode formation include syndecans, laminins, NG2, and versican, all of which also directly interact with NF186 (Occhi et al. 2005). Additional proteins unique to the PNS nodal microvilli are exrin, radixin, moesin, EBP50, dystphin, and utophin (Occhi et al. 2005). The paranodal junction then constrict leading to stabilization of the node by NF186 association with ankyrin-G, which subsequently interacts with and recruits Nav channels, Kv channels, and βIV-spectrin. Nav and Kv channels bind with high affinity to the membrane-binding domain of ankyrin-G at the node via a CK2 phosphorylation-dependent mechanism as seen in the AIS (Wang et al. 2014; Xu and Cooper 2015). Recent studies by Ho *et al.* discovered that in the absence of ankyrin-G Nav channels are still clustered to the node of Ranvier by compensation of ankyrin-R and its binding partner βI-spectrin in peripheral sensory neurons and retinal ganglion cells (Ho et al. 2014). However, the ability of ankyrin-R to compensate for ankyrin-G at the node of Ranvier remains controversial (Saifetiarova et al. 2017).

Assembly of CNS Nodes of Ranvier

Similar to the PNS, glial-derived extrinsic mechanisms contribute to CNS formation; however, in contrast to the microvilli of Schwann cells that make contact to the node in the PNS,

the oligodendrocytes do not directly interact with the nodes in the CNS. Three important components have been proposed to be important for node of Ranvier assembly in the CNS (Fig. 1.4). First, an ECM complex produced by glial cells promotes NF186 to cluster at the node. The ECM in the CNS contains the chondroitin sulfate proteoglycans brevican, versican, neurocan, and phosphacan in addition to tenascin-R, BRal1, and NrCAM. The glial-derived ECM directly interacts with the axonal cell adhesion molecules NF186, NrCAM, contactin-1, and the β-subunit of sodium channel and are likely involved in the long-term maintenance of CNS nodes (Susuki et al. 2013; Weber et al. 1999; Oohashi et al. 2002; Bekku et al. 2009; Dours-Zimmermann et al. 2009; Xiao et al. 1999). Secondly, the paranodal axo-glial complex forms, which consists of three main cell adhesion molecules: neurofascin 155 kDa isoform (NF155) derived from glial cells, and Caspr (contactin-associated protein) and contactin which are generated in the neuron. Lastly, the axonal scaffolding protein ankyrin-G is necessary to cluster and stabilize Nav channels to the node (Gasser et al. 2012). Deletion of the giant splice variants of ankyrin-G resulted in an 80% loss in the number of nodes of Ranvier *in vivo* and the remaining nodes of the corpus callosum were malformed and elongated (Jenkins et al. 2015). Interestingly, while the remaining nodes lacked 480 kDa ankyrin-G and NF186, βIV-spectrin and Nav channels were still present and NF155 persisted at the paranode. Nav channels were clustered at the node, likely due to the dramatic upregulation seen in the 190kDa isoform of ankyrin-G (Jenkins et al. 2015).

Ankyrin-G is referred to as the master organizer of the AIS; however, because the nodes require extrinsic regulation for their proper formation and function, the role of ankyrin-G as the master organizer of the node of Ranvier is less clear. The fact that ankyrin-G contains binding sites for all known nodal components supports the theory that ankyrin-G is necessary and sufficient for node formation (Gasser et al. 2012; Hill et al. 2008). In addition, mutation of the ankyrin-G-

binding domain in NF186 inhibits its ability to cluster at the node (Susuki et al. 2013). Zonta *et al*. demonstrated that genetic deletion of both isoforms of NF186 and NF155 completely disrupted nodal and paranodal complexes; however, the authors show that rescue with either NF186 or NF155 independently can promote the assembly of the nodal complex and recruit Nav channels (Zonta et al. 2008). Since Nav channels, their β subunits, and ankyrin-G can interact with NF186 directly, it may not be a surprise that the addition of NF186 is capable of rescuing the node and may even subsequently promote more delivery of NF186. Rescuing with NF155 is more intriguing as NF155 is not found at the node with ankyrin-G or Nav channels, but is still sufficient to rescue assembly of the node (Zonta et al. 2008). Zhang *et al.* recently discovered a third isoform of neurofascin, NF140, which is highly expressed early in embryonic development and is capable of clustering Nav channels to the developing node of Ranvier independently of NF186 and NF155 (Zhang et al. 2015). Future research should expand on these findings to better understand how deletion of ankyrin-G or neurofascin disrupts Nav clustering throughout CNS, and how this loss of Nav channels at the node impacts brain function.

While the pioneering work on the AIS and nodes of Ranvier done in cultured cells *in vitro* has given us great insights into the formation and function of these critical subcellular domains, recent work has highlighted the need to examine these mechanisms *in vivo* (Amor et al. 2017; Chang et al. 2014; Komada and Soriano 2002; Saifetiarova et al. 2017; Sherman et al. 2005; Susuki et al. 2013; Zonta et al. 2008). Specific knockout animal models have elucidated how the AIS and nodes of Ranvier are formed in the intact organisms and have supported many of the findings from in vitro studies. Importantly, animal models also give us the ability to examine whether the mechanisms are conserved between cell types. For example, much of the work on the mechanisms

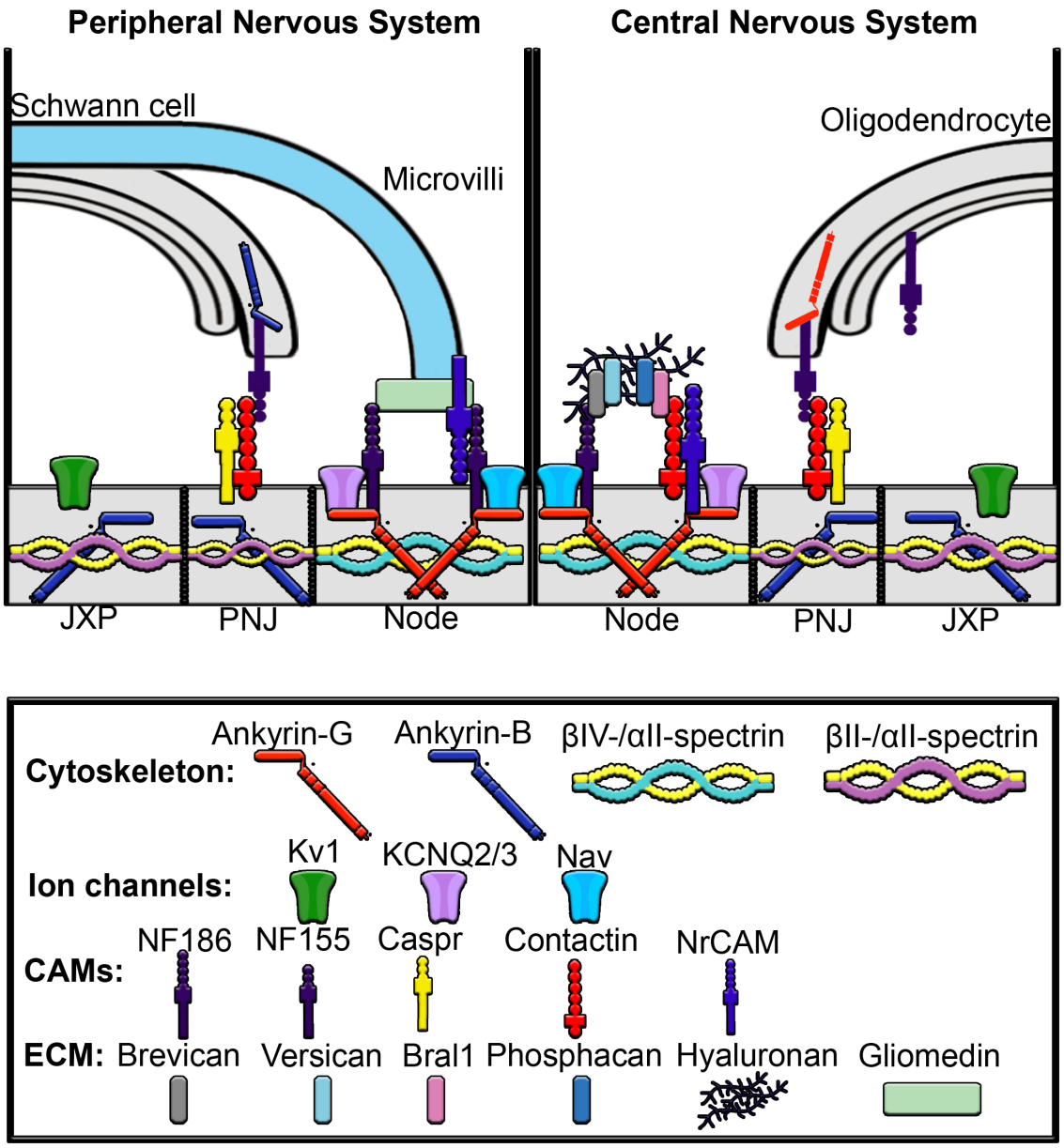

Figure 1.4: Mechanisms underlying assembly of peripheral nervous system (PNS) and central nervous system (CNS) nodes of Ranvier. Axons are myelinated by Schwann cells in the PNS and oligodendrocytes in the CNS. The nodes are gaps in myelinated sheaths and are sites of action potential regeneration. In both the PNS and CNS the node contains high densities of Nav and KCNQ2/3 channels, ankyrin-G, bIV-spectrin, aII-spectrin, NF186 and NrCAM. In the PNS, gliomedin from the microvilli of myelinating Schwann cells directly interacts with NF186 and NrCAM at the node. In contrast, the node of the CNS contains an extracellular matrix (ECM) complex made up of chondroitin sulfate proteoglycans brevican, versican and phosphacan, which interact with contactin, Bral1, hyaluronan and NF186. The paranodal junction (PNJ) flanks the nodes of Ranvier and is the site of Schwann cell contact in the PNS and oligodendrocyte contact in the CNS. In the PNS, Ankyrin-B interacts with NF155 in Schwann cells, which then binds to contactin to connect the myelinating Schwann cell with the axon, whereas in the oligodendrocytes of the CNS, ankyrin-G associates with NF155. Within the paranodal axolemma, ankyrin-B binds bII and aII-spectrin cytoskeleton complexes that play important roles in maintaining paranode barriers. The juxtaparanodes (JXP) are characterized by high-density clustering of Kv1 channels as well as ankyrin-B and bII-spectrin and aII-spectrin tetramers.

of CNS node of Ranvier formation has been done in spinal cord or optic nerve. Are these mechanisms conserved in myelinated axons in the brain?

Axonal Domain Proteins in Disease and Injury

An increasing number of studies have shown that genetic mutations in components of both the AIS and nodes of Ranvier are involved in the pathophysiology of multiple diseases and injuries. As previously mentioned, ankyrin-G is absolutely essential to maintain the structural composition of the AIS and nodes of Ranvier and for normal axonal polarity. Thus, mutations or loss-of-function of *ANK3* might be expected to have a profound effect on neurological function. Consistent with this idea, genome-wide association studies have identified *ANK3* as one of the most significant risk loci for bipolar disorder, and to a lesser degree schizophrenia (Ferreira et al. 2008). Post-mortem brains of schizophrenic patients revealed a 15-20% decrease in ankyrin-G expression at the AIS of pyramidal neurons in the superficial cortical layer as compared to neurotypical controls, while no significant changes in AIS length were observed (Cruz et al. 2009). A recent study by Lopez *et al*. showed that the presence of a bipolar disorder-associated variant in *ANK3* results in reduced expression of the *ANK3* exon 1b isoform in the AIS of parvalbumin-positive (PV) GABAergic interneurons. Interestingly, mice lacking the exon 1b isoform lose Nav channel clustering at the AIS of PV interneurons and demonstrate behavioral characteristics of bipolar disorder, epilepsy, and sudden death (Lopez et al. 2017). In addition**,** *de novo* missense mutations in *ANK3* have been identified in autistic patients as well as severe cognitive deficits, borderline intelligence, severe attention deficit hyperactivity disorder (ADHD), and sleeping problems (Talkowski et al. 2012; Awadalla et al. 2010; Hamdan, Gauthier, Araki, Lin, Yoshizawa, Higashi, Park, Spiegelman, Dobrzeniecka, Piton, Tomitori, Daoud, Massicotte, Henrion, Diallo, Shekarabi,

et al. 2011). The presence of a homozygous premature stop codon predicted to abolish the 480 kDa isoform of ankyrin-G resulted in dramatic cognitive dysfunction and intellectual disability with IQ values below 50 (Iqbal et al. 2015). It will be important to elucidate the precise effects of *ANK3* mutations on neuronal function.

Mutations in voltage-gated sodium channel α subunits and their associated β subunits found at the AIS and nodes of Ranvier have a wide range of profound neurological effects, including epilepsy, neurodegeneration, and sudden death. For example, mutations in *SCN1A* (Nav1.1) are associated with Dravet syndrome, a severe myoclonic epilepsy of infancy, as well as West syndrome, genetic epilepsy with febrile seizures plus (GEFS+), and others (Steinlein 2014). *SCN2A* (Nav1.2) and *SCN8A* (Nav1.6) mutations are found in patients with early infantile epileptic encephalopathy (Steinlein 2014; Wagnon and Meisler 2015). Mutations in the sodium channel β subunits are associated with multiple neurological disorders, including GEFS+, Dravet syndrome, and neurodegenerative disease (O'Malley and Isom 2015). In addition to mutations in sodium channel genes, loss-of-function mutations in both KCNQ2 and KCNQ3 potassium channel genes are linked to benign familial neonatal convulsions (Singh et al. 2003).

Disruptions in spectrin cytoskeletal function and assembly have also been associated with neurological disease. The human spectrin family consists of two alpha- and five beta- spectrin subunits, which form heterodimers that assemble into tetramers through head-to-head and lateral associations (Bennett and Lorenzo 2013). Human dominant in-frame duplications and deletion mutations in *SPTAN1* have been found in patients with early-onset epileptic encephalopathies, hypomyelination, intellectual disability, and blindness starting in children under age 3. (Saitsu et al. 2010; Nicita et al. 2015). Mutations in βIII-spectrin, which is highly expressed in cerebellar Purkinje neurons, have been associated with spinocerebellar ataxia type 5 (Ikeda et al. 2006).

Increasing evidence also suggests degeneration of the axon is an important component underlying multiple sclerosis (MS) pathology; however, the mechanisms that contribute to axonal loss remain elusive (Dutta and Trapp 2007). Patients suffering from MS demonstrated changes in expression and localization of Nav channels and neurofascin, as well as the paranodal protein Caspr (Wolswijk and Balesar 2003; Craner et al. 2004; Howell et al. 2006; Coman et al. 2006). One potential mechanism that contributes to MS may be abnormal axo-glial interaction at the paranode, which would be expected to disrupt axonal transport and alter normal organization of myelinated axons (Sousa and Bhat 2007). Mathey *et al.* identified autoantibodies from MS patients that specifically target the extracellular domains both axonal NF186 and glial NF155, disrupt conduction, and ultimately lead to axonal injury that mimics the pathology of MS (Mathey et al. 2007). In addition to the nodes of Ranvier, the effect of demyelination on the AIS may be another potential mechanism that contributes to MS. Hamada and Kole showed that demyelinating axons using cuprizone caused the AIS to shift more proximal to the soma and reduced action potential initiation (Hamada and Kole 2015). However, they observed no changes in ankyrin-G, βIV-spectrin, and Nav1.6 expression at the AIS following demyelination (Hamada and Kole 2015). Consistent with these findings, Clark *et al*. also found AIS components remained intact following cuprizone-induced demyelination (Clark et al. 2016). In contrast, the authors discovered the proper clustering of ankyrin-G, βIV-spectrin, and Nav1.6 was lost at the AIS of mice after chronic exposure of experimental autoimmune encephalomyelitis (EAE), an inflammatory model of MS (Clark et al. 2016). Ultimately, the AIS is a primary target during inflammation and, in addition to demyelination of the distal axon, may contribute to inflammatory demyelinating diseases such as MS.

In a rat model of mild traumatic brain injury, Baalman *et al.* showed that exposure to a single blast wave results in long-term changes in memory within these rats and, at the cellular level, significant decreases in AIS length (Baalman et al. 2013). These changes in the AIS perhaps highlight a potential mechanism underlying mild traumatic brain injury and future studies will be important to elucidate the specific molecular components that contribute to the structural and functional changes in the AIS.

Overall, changes in excitable domains of the axon or their constituent proteins have profound impact on neurological function. Although many of the proteins of the AIS and nodes of Ranvier have important functions in other cellular domains, the overlapping phenotypes seen with loss of function of different AIS and nodal components suggest that dysfunction of these axonal membrane domains is a major factor in the development of disease. As we increasingly understand the genetic basis of neurological disorders, we will likely uncover more genes involved in the formation and function of axonal domains that can give us more insight into the etiology of human disease.

Conclusion

The structural assembly and maintenance of the axon relies on the precise organization between ankyrins, spectrins, membrane-associated proteins, and actin and microtubule cytoskeletal proteins. The mechanisms underlying the interaction between these components at the AIS and nodes of Ranvier are now becoming more apparent. A better understanding of the organization and maintenance of axonal excitable domains as well as how abnormalities in their signaling may lead to altered axonal function will provide insight to novel therapeutic targets for the treatment of human diseases of the nervous system.

Hypothesis and Aims

The overall goal of the work described in this thesis is to explore new roles of ankyrin-G in GABAergic inhibitory synapses and glutamatergic excitatory synapses, outside of its canonical role at the AIS and nodes of Ranvier. The goals are to determine the mechanisms by which ankyrin-G stabilizes GABAergic synapses onto excitatory pyramidal neurons, determine the effects of loss-of-function ankyrin-G at GABAergic synapses on neuronal circuitry *in vivo*, and to understand mechanisms of ankyrin-G in dendritic spine plasticity and neuronal excitability. Given that the *ANK3* gene, which encodes the protein ankyrin-G, is associated with multiple neuropsychiatric diseases and is one of the strongest genes linked to bipolar disorder, this work will provide data on how mutations in *ANK3* may alter neuronal circuitry and contribute to disease pathophysiology.

Chapter 2: Investigate the effect of loss-of-function ankyrin-G at GABAergic inhibitory synapses on neuronal circuitry in vivo.

GABAergic interneurons synapse onto unique postsynaptic domains on pyramidal neurons; however, the molecular mechanisms that regulate the subcellular organization of GABAergic synapses is not completely understood. Chapter 2 investigates the ankyrin-G/GABARAP mechanism of GABAergic synapse formation onto cortical and hippocampal pyramidal neurons. The studies in this chapter utilize an *Ank3* W1989R knock-in mutant mouse model, immunostaining and confocal microscopy, and whole-cell patch clamp to evaluate the effects of abolishing the ankyrin-G/GABARAP interaction on GABAergic synapse connectivity and function. Further, we use a multi-electrode array to evaluate kainite-induce gamma oscillations, a measure of synchronization of neuronal networks. We then assess the effect of GABAergic synapse loss on pyramidal cell hyperexcitability as well as plasticity changes in

dendritic spines and AISs. Finally, we collaborated with the Heinz C. Prechter Bipolar Research Program at the University of Michigan and found the first family with bipolar disorder with affected individuals heterozygous for *ANK3* W1989R, linking the *ANK3* W1989R variant to human disease. In analyzing the *Ank3* W1989R loss-of-function ankyrin-G model, a greater understanding of the role of ankyrin-G on forebrain neuronal network connectivity and function was uncovered.

Chapter 3: Investigate the role of ankyrin-G in homeostatic scaling of dendritic spines to maintain proper neuron excitability.

Dendritic spines are highly dynamic and spine plasticity is important to regulate synaptic efficacy and maintain neuron excitability within a physiological range. Chapter 3 focuses on the recently discovered role of ankyrin-G in spine morphology, function, and density. We hypothesized that activity-dependent modulation of ankyrin-G regulates dendritic spine density and AMPA receptor-mediated transmission, as a novel intrinsic mechanism to maintain homeostasis of neuronal excitability. We investigated the effect of hyperexcitability in the *Ank3* W1989R mouse model on ankyrin-G expression and dendritic spine density. We evaluated the genetic and post-translational modifications that may contribute to the observed changes in ankyrin-G expression in the *Ank3* W1989R mouse model of hyperexcitability. Furthermore, we tested if pharmacological manipulation of neuron activity with tetrodotoxin (TTX) or bicuculline or chronic depolarization with KCl affected ankyrin-G expression, spine density, and AMPA receptor levels to assess the role of ankyrin-G in homeostatic scaling in wild-type neurons.

Chapter 4: Discussion and Future Directions

CHAPTER 2

Ankyrin-G Regulates Forebrain Connectivity and Network Synchronization via Interaction with GABARAP[2]

Summary

GABAergic circuits are critical for the synchronization and higher order function of brain networks. Defects in this circuitry are linked to neuropsychiatric diseases, including bipolar disorder, schizophrenia, and autism. Work in cultured neurons has shown that ankyrin-G plays a key role in the regulation of GABAergic synapses on the axon initial segment and somatodendritic domain of pyramidal neurons where it interacts directly with the $GABA_A$ receptor associated protein (GABARAP) to stabilize cell surface $GABA_A$ receptors. Here, we generated a knock-in mouse model expressing a mutation that abolishes the ankyrin-G/GABARAP interaction (*Ank3* W1989R) to understand how ankyrin-G and GABARAP regulate GABAergic circuitry *in vivo.* We found that *Ank3* W1989R mice exhibit a striking reduction in forebrain GABAergic synapses resulting in pyramidal cell hyperexcitability and disruptions in network synchronization. In addition, we identified changes in pyramidal cell dendritic spines and axon initial segments consistent with compensation for hyperexcitability. Finally, we identified the *ANK3* W1989R variant in a family with bipolar disorder, suggesting a potential role of this variant in disease. Our

[2]This research was published in Molecular Psychiatry. Nelson AD, Caballero-Florán RN, Rodríguez Díaz JC, Li J, Chen K, Walder KK, Bennett V, Lopez-Santiago LF, McInnis MG, Isom LL, Wang C, Zhang M, Jones KS, Jenkins PM**.** Ankyrin-G Regulates Forebrain Connectivity and Network Synchronization via Interaction with GABARAP. *Molecular Psychiatry* Published online 2018 Nov 20.

results highlight the importance of ankyrin-G in regulating forebrain circuitry and provide novel insights into how *ANK3* loss-of-function variants may contribute to human disease.

Introduction

GABAergic interneurons are essential for the proper synchronization and function of neuronal networks that underlie normal cognition, mood, and behavior. GABAergic interneurons target to unique postsynaptic domains on excitatory neurons; however, the molecular mechanisms underlying the subcellular organization of forebrain GABAergic synapses remain poorly understood. Abnormalities in GABAergic interneuron circuitry and decreased gamma oscillations have been implicated in many neurodevelopmental and neuropsychiatric disorders (Benes 2010; Benes and Berretta 2001; Konradi et al. 2011; Lazarus, Krishnan, and Huang 2015; Ozerdema et al. 2013; Schubert, Focking, and Cotter 2015; Sohal 2012; Torrey et al. 2005). Thus, the understanding of the cellular and molecular mechanisms that contribute to the development and function of GABAergic synapses as well as identification of genetic variants that contribute to neuropsychiatric disorders is critical to the discovery of new therapeutic agents for the treatment of diseases involving altered inhibitory circuits.

ANK3 encodes ankyrin-G, a fundamental scaffolding protein that organizes critical plasma membrane domains (Bennett and Lorenzo 2013; Nelson and Jenkins 2017). Alternative splicing of *ANK3* in the brain gives rise to three main isoforms of ankyrin-G: the canonical 190 kDa isoform, a 270 kDa isoform, and a giant, 480 kDa isoform. The 190 kDa isoform is expressed in most tissues and cell types throughout the body including brain, heart, skeletal muscle, kidney, and retina. The 270 kDa and 480 kDa isoforms of ankyrin-G are predominantly expressed in the nervous system, and arise from alternative splicing of a single 7.8 kb giant exon (Bennett and

Lorenzo 2013; Kordeli, Lambert, and Bennett 1995). The 480 kDa ankyrin-G isoform has been identified as the master organizer of axon initial segments (AIS) and nodes of Ranvier, sites of action potential (AP) initiation and propagation (Nelson and Jenkins 2017). This splice variant is necessary for the proper clustering of voltage-gated sodium channels, KCNQ2/3 potassium channels, the cell adhesion molecule neurofascin-186, and the cytoskeletal protein βIV-spectrin to excitable domains (reviewed in (Nelson and Jenkins 2017)).

Importantly, the 480 kDa ankyrin-G isoform has also been shown to stabilize GABAergic synapses on the soma and AIS of excitatory pyramidal neurons by interacting with the $GABA_A$ receptor-associated protein (GABARAP) to inhibit $GABA_A$ receptor endocytosis (Tseng et al. 2015). GABARAP and GABARAP-like 1, members of the ubiquitin-like LC3 family of microtubule-associated proteins, mediate $GABA_A$ receptor trafficking between the cell surface and intracellular compartments (Chen and Olsen 2007). GABARAP and other members of the LC3 family interact with LC3-interacting region (LIR) motifs (Alemu et al. 2012). The giant exon that encodes the 480 kDa ankyrin-G isoform contains an LIR motif, which includes residue W1989 (Jenkins et al. 2015; Tseng et al. 2015). Mutation of W1989 to arginine (W1989R) completely abolished the binding between ankyrin-G and GABARAP (Tseng et al. 2015). Deletion of wild-type (WT) ankyrin-G and replacement with W1989R 480 kDa ankyrin-G failed to rescue $GABA_A$ receptors to the soma and AIS or restore miniature inhibitory postsynaptic currents (mIPSCs) in cultured mouse hippocampal neurons (Tseng et al. 2015). Taken together, these findings suggested that 480 kDa ankyrin-G plays a critical role in stabilizing GABAergic synapses *in vitro*; however, whether ankyrin-G loss-of-function at GABAergic synapses disrupts forebrain circuitry *in vivo* has not been investigated.

Here, we have generated a novel knock-in mouse model expressing *Ank3* W1989R. This allowed us to study, for the first time, the relationship between the 480 kDa ankyrin-G isoform and GABAergic synapse formation and function *in vivo* in a model that survives to adulthood and is capable of forming the AIS and nodes of Ranvier. We show that the *Ank3* W1989R mutation causes decreases in GABAergic synapses in layer II/III of somatosensory cortex and CA1 of hippocampus, while sparing inhibitory synapses on cerebellar Purkinje neurons and thalamic neurons. The decreases in inhibitory synapses cause hyperexcitability of cortical and hippocampal pyramidal neurons and decreases in gamma oscillations. Interestingly, we also detect changes consistent with compensation for the loss of inhibitory tone, including shortening of the AIS and decreases in dendritic spine density and excitatory postsynaptic currents. Finally, we report the identification of a family with bipolar disorder (BD) that carries the *Ank3* W1989R human variant (rs372922084, c.5965T>C (p.Trp1989Arg)), which may contribute to the pathophysiology of psychiatric disease.

Results

***Ank3* W1989, located within the giant exon of ankyrin-G, is necessary for binding to a hydrophobic pocket in GABARAP**

The 480 kDa *Ank3* splice variant interacts with GABARAP to inhibit $GABA_A$ receptor endocytosis and stabilize GABAergic synapses (Tseng et al. 2015). Here, we explored the molecular basis governing this interaction by resolving the crystal structure of the ankyrin-G/GABARAP complex. Crystallography data show that the LIR motif within the giant exon of ankyrin-G contains aromatic residues, W1989 and F1992, which insert into two hydrophobic pockets of GABARAP (Fig. 2.1a). Moreover, a unique C-terminal helix extension contributes to

ankyrin-G/GABARAP binding by forming a critical salt bridge between residues E1996 of ankyrin-G and R67 of GABARAP and additional hydrophobic interactions with a hydrophobic surface of GABARAP (Fig. 2.2a). This newly defined binding mode with the presence of the C-terminal helix is unique compared to previously known GABARAP/LIR motifs or other LC3 family members/LIR interactions (Fig. 2.1b) (Li et al. 2018), suggesting a specific neuronal function of the ankyrin-G/GABARAP interaction outside the autophagic processes for GABARAP (Rogov et al. 2017). To address the role of the W1989 residue in more detail, we performed Isothermal Titration Calorimetry (ITC) to quantitatively measure the dissociation constant (K_d) between a series of ankyrin-G truncations and GABARAP. Using this approach, we mapped the minimal region of ankyrin-G that is capable of binding to GABARAP to a fragment of 26 amino acids (residues 1985-2010), which included residue W1989 contained within the canonical LIR motif (Fig. 2.2b). This ankyrin-G fragment associated with GABARAP with a K_d of 2.9 nM, which is more than 1000-fold stronger than previously reported interactions between GABARAP and other LIR motifs (Fig. 2.2c and Fig. 2.1b) (Rogov et al. 2017). Mutation of the W1989 residue to R abolished the interaction between ankyrin-G and GABARAP, and decreased the binding affinity to approximately 11 μM, which is 4000-fold weaker than WT ankyrin-G (Fig. 2.2c) (Tseng et al. 2015). Overall, these results demonstrate that ankyrin-G residue W1989 is necessary for high affinity binding to GABARAP, while F1992 and the C-terminal helix extension play important roles in maintaining this interaction.

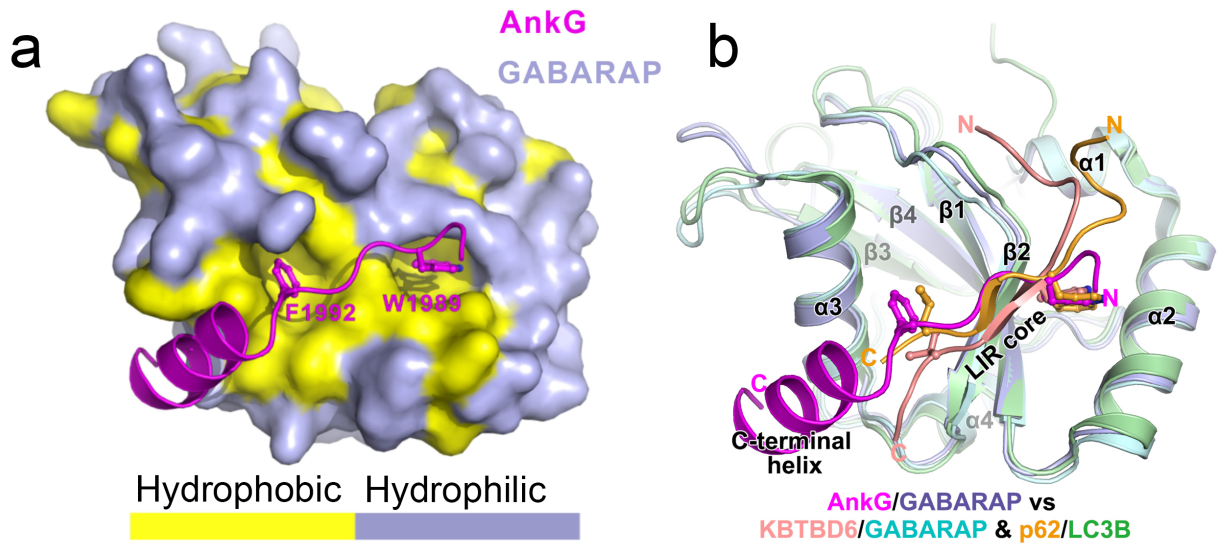

Figure 2.1: Crystal structure of ankyrin-G/GABARAP reveals the critical W1989 residue of ankyrin-G interacts with hydrophobic pocket of GABARAP. (a) Combined surface (GABARAP) and ribbon-stick model (ankyrin-G) showing a hydrophobic pocket of GABARAP is accommodated by the critical W1989 reside within the giant exon of ankyrin-G. The surface for hydrophobic residues of GABARAP are shown in yellow while the hydrophilic surfaces are light purple. The crystal structure of ankyrin-G/GABARAP complex is at a 2.2Å resolution. **(b)** Ribbon-stick model of superposition of ankyrin-G/GABARAP, KBTBD6/GABARAP and p62/LC3B complex structures showing the comparison of ankyrin-G/GABARAP complex with common binding mode of LIR/Atg8s.

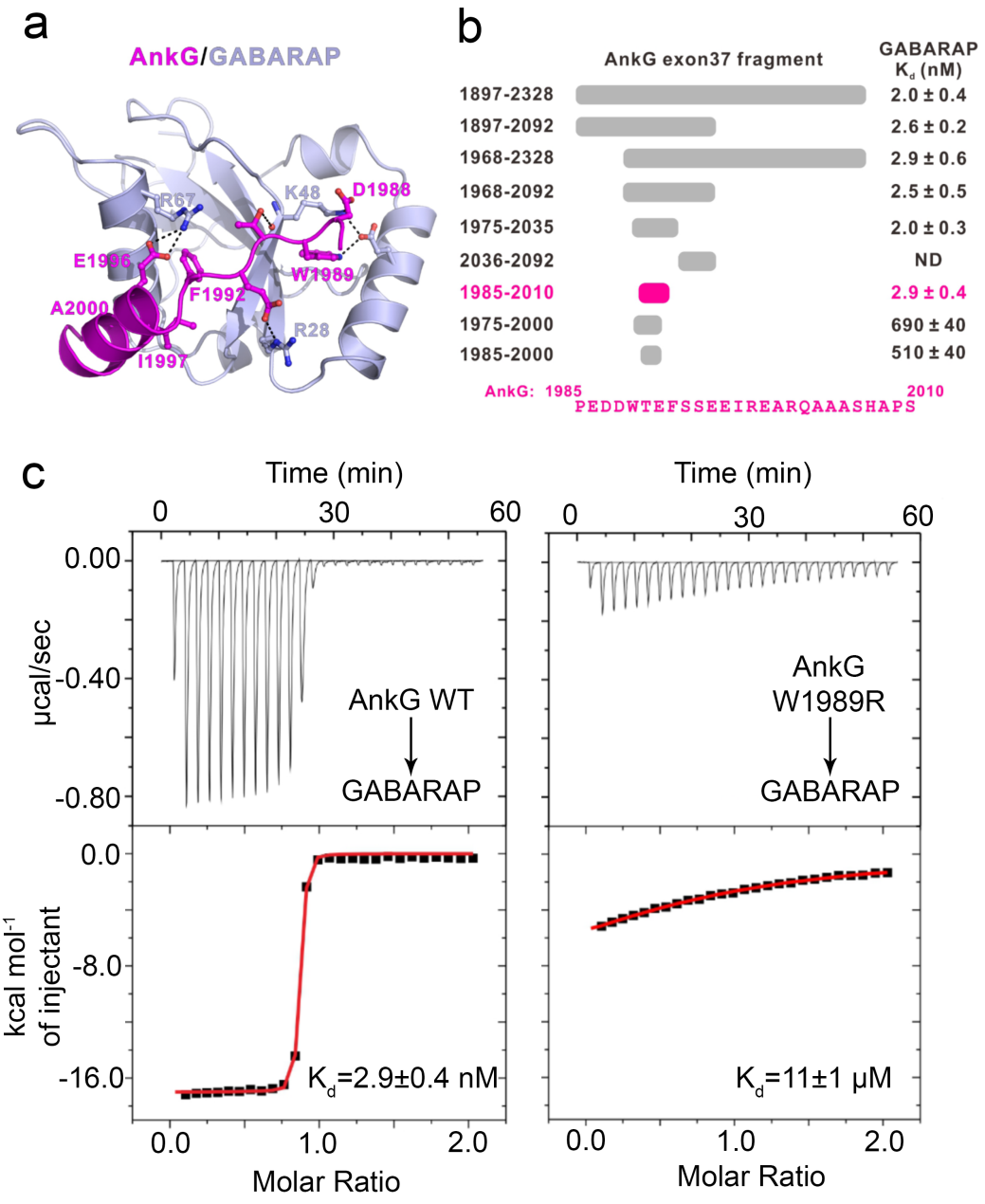

Figure 2.2: W1989 residue in ankyrin-G is necessary for high affinity binding to GABARAP. (a) Ribbon representation of the ankyrin-G/GABARAP complex structure. Key residues critical for the binding are shown in the stick model. Salt bridges and hydrogen bonds are indicated with dashed lines. **(b)** Biochemical analysis of the complex formation between ankyrin-G and GABARAP. Isothermal Titration Calorimetry (ITC)-based mapping of the minimal region of the giant exon of ankyrin-G capable of binding to GABARAP. The minimal and complete fragment identified is highlighted in magenta, and the amino acid sequence of ankyrin-G 1985-2010 is listed at the bottom. "ND" denotes that the construct had no detectable binding to GABARAP. **(c)** ITC-derived binding curves of WT ankyrin-G and W1989R ankyrin-G to GABARAP.

W1989R 480 kDa ankyrin-G maintains WT functionality in assembly of the AIS and nodes of Ranvier *in vivo*

Several mouse models have been generated to evaluate the neuronal role of ankyrin-G *in vivo*, however these mice either die early in development or lack the AIS, nodes of Ranvier, and GABAergic synapses simultaneously, making it difficult to understand the specific role of ankyrin-G-dependent GABAergic circuits (Jenkins et al. 2015; Jenkins et al. 2013; Tseng et al. 2015). To examine the role of 480 kDa ankyrin-G specifically in GABAergic synapse formation and function *in vivo*, we generated a knock-in mouse model expressing the *Ank3* W1989R ((c.5965T>C (p.Trp1989Arg)) mutation within the giant exon of ankyrin-G. Homozygous *Ank3* W1989R mice survive well into adulthood, similar to WT littermate controls, as ~90% (32/36) of *Ank3* W1989R mice live to P250 or longer. Homozygous *Ank3* W1989R mice are similar to WT mice in appearance and grooming behavior, and have no obvious neurological phenotype.

Previous studies demonstrated that expression of the W1989R 480 kDa ankyrin-G in an *Ank3* null background failed to restore $GABA_A$ receptor clustering and mIPSCs in cultured hippocampal neurons (Tseng et al. 2015). However, the W1989R mutant appropriately localized to the AIS and clustered all known binding partners (Tseng et al. 2015). Thus, we expected the knock-in *Ank3* W1989R mutation to function similar to WT at the AIS and nodes of Ranvier *in vivo*. As predicted, immunolabeling of cortical neurons in layer II/III of the somatosensory cortex in coronal brain sections from P30-35 mice with antibodies specific to ankyrin-G revealed that W1989R 480 kDa ankyrin-G appropriately localized to the AIS (Fig. 2.3a and b). In addition, W1989R 480 kDa ankyrin-G clustered all tested ankyrin-G binding partners to the AIS, including βIV-spectrin, neurofascin, KCNQ2 channels, and voltage-gated sodium channels (Fig. 2.4a-h).

In addition to regulating the AIS, 480 kDa ankyrin-G plays a central role in the formation and maintenance of nodes of Ranvier (Jenkins et al. 2015). Analysis of the corpus callosum in homozygous *Ank3* W1989R mice revealed no detectable changes in the total number of nodes of Ranvier (Fig. 2.3c and d) or nodal length (WT: 1.48 ± 0.04 μm, N=3, n=109; W1989R: 1.6 ± 0.03 μm, N=3, n=116) compared to WT mice (Fig. 2.3c). Thus, W1989R 480 kDa ankyrin-G maintains WT functionality in forming the AIS and nodes of Ranvier *in vivo*.

GABAergic synapses and synaptic activity are decreased in Ank3 W1989R forebrain pyramidal neurons *in vivo*

GABAergic interneurons synapse onto the dendrites, soma, and AIS of pyramidal neurons, and regulate excitability, synaptic transmission, and the synchronization of neuronal ensembles (Rudy et al. 2011; Somogyi et al. 2014). To determine the effect of *Ank3* W1989R on GABAergic synapses *in vivo*, we immunostained WT and homozygous mutant P30-35 coronal brain sections with antibodies to the presynaptic inhibitory marker, vesicular GABA transporter (vGAT). *Ank3* W1989R mice showed a ~50-65% reduction in the number of GABAergic synapse clusters on the somatodendritic domain and AIS of cortical pyramidal neurons compared to WT neurons (Fig. 2.5a-c). Moreover, clustering of postsynaptic $GABA_A$ receptors was significantly decreased in dissociated hippocampal neurons from *Ank3* W1989R mice vs. WT (Fig. 2.5d and e). These findings demonstrate that both pre- and postsynaptic structural components of GABAergic synapses are lost when 480 kDa ankyrin-G is unable to interact with GABARAP *in vivo*.

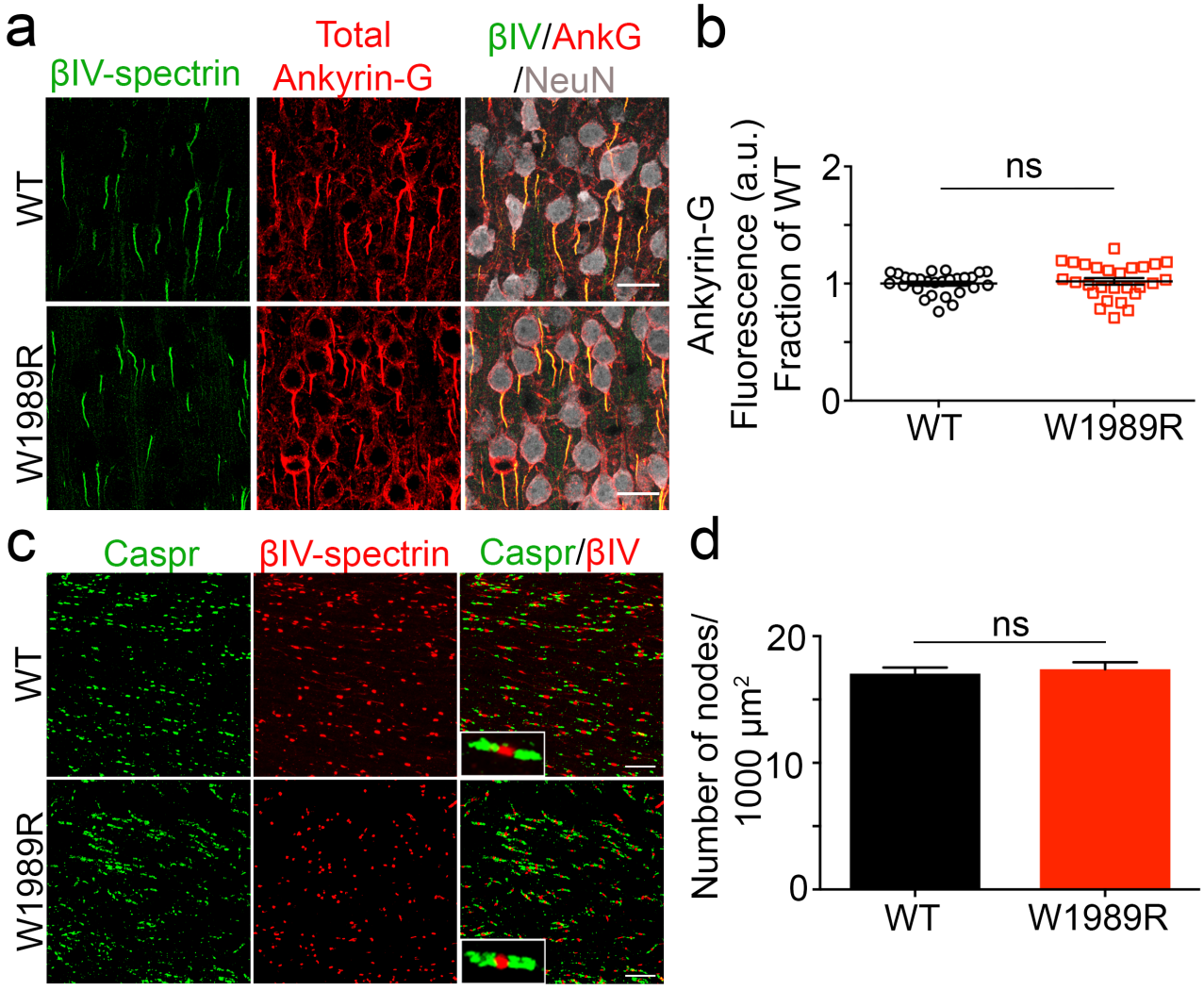

Figure 2.3: AIS and nodes of Ranvier are maintained in the *Ank3* W1989R mouse model. **(a)** Representative images from coronal sections of layer II/III somatosensory cortex of P30-35 WT (top) and *Ank3* W1989R homozygous (bottom) mice. Immunostaining for βIV-spectrin (green), total ankyrin-G (red), and NeuN (white). Scale bar: 20 μm. **(b)** Quantification of ankyrin-G fluorescence intensity (a.u.) as fraction of WT between WT (black circles) and *Ank3* W1989R homozygous (red squares) mice. *t-test* P = 0.5618 (WT: 1 ± 0.02, N=3, n=27; W1989R: 1.02 ± 0.03, N=3, n=27). **(c)** Representative images of nodes of Ranvier from corpus callosum of P30 WT (top) and *Ank3* W1989R homozygous (bottom) mice. Sections immunostained for the paranodal marker Caspr (green) and βIV-spectrin (red). Scale bar: 20μm. **(d)** Quantification of the total number of nodes of Ranvier per 1000 μm^2 from WT (black bar) and *Ank3* W1989R homozygous (red bar) mice. *t-test* P = 0.62, ns: not significant (WT: 17.04 ± 0.5, N=3, n=20; W1989R: 17.4 ± 0.5, N=3, n=18). Data shown as mean ± SEM.

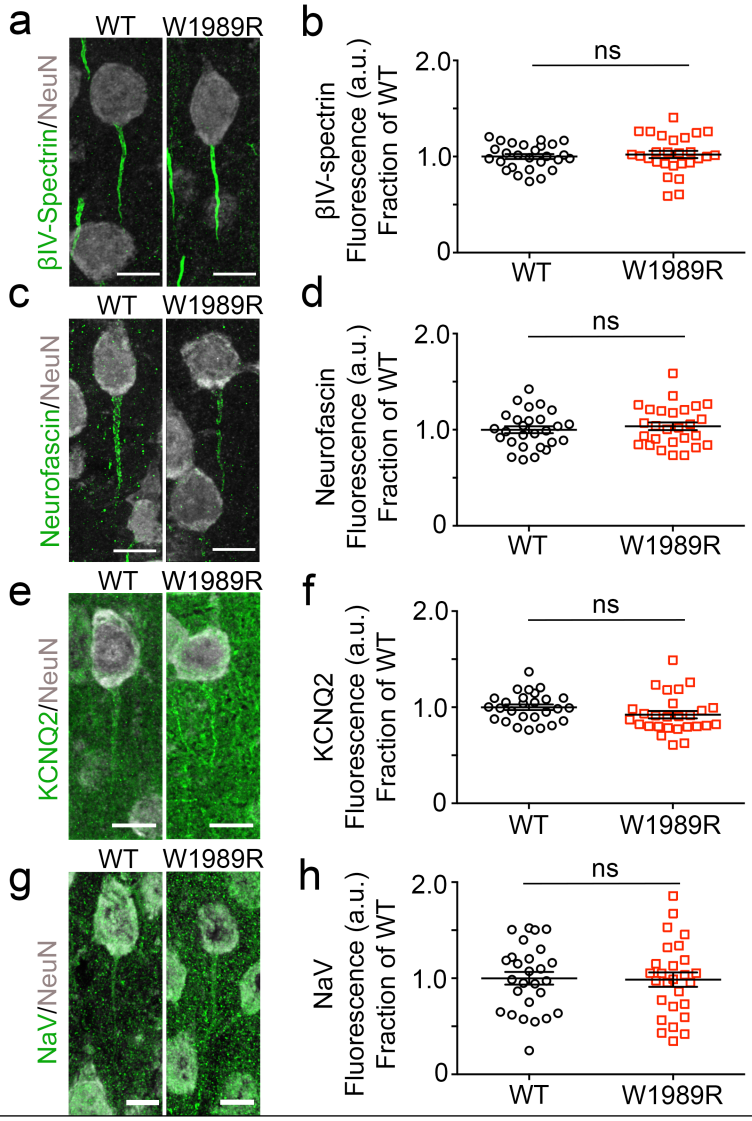

Figure 2.4: W1989R 480 kDa ankyrin-G is capable of clustering all known ankyrin-G binding partners to the AIS. **(a)** Representative images of the AIS of pyramidal neurons in layer II/III of the somatosensory cortex of P30 WT (left) and *Ank3* W1989R homozygous (right) mice. Coronal brain sections immunostained with βIV-spectrin (green) and NeuN (white). Scale bar: 10 μm. **(b)** Quantification of βIV-spectrin fluorescence intensity (a.u.) as fraction of WT between WT (black circles) and *Ank3* W1989R homozygous (red squares) mice. *t-test* P = 0.6375 (WT: 1 ± 0.03, N=3, n=27; W1989R: 1.02 ± 0.04, N=3, n=27). **(c)** Representative images of cortical pyramidal neuron AISs of P30 WT (left) and *Ank3* W1989R homozygous (right) mice immunostained with pan-neurofascin (green) and NeuN (white). Scale bar: 10 μm. **(d)** Quantification of neurofascin fluorescence intensity (a.u.) as fraction of WT between WT (black circles) and *Ank3* W1989R homozygous (red squares) mice. *t-test* P = 0.517 (WT: 1 ± 0.04, N=3, n=27; W1989R: 1.04 ± 0.04, N=3, n=27). **(e)** Representative images of cortical pyramidal neuron AISs of P30 WT (left) and *Ank3* W1989R homozygous (right) mice immunostained with KCNQ2 (green) and NeuN (white). Scale bar: 10 μm. **(f)** Quantification of KCNQ2 fluorescence intensity (a.u.) as fraction of WT between WT (black circles) and *Ank3* W1989R homozygous (red squares) mice. *t-test* P = 0.116 (WT: 1 ± 0.03, N=3, n=27; W1989R: 0.92 ± 0.03, N=3, n=27). **(g)** Representative images of cortical pyramidal neuron AISs of P30 WT (left) and *Ank3* W1989R homozygous (right) mice immunostained with pan-NaV (green) and NeuN (white). Scale bar: 10 μm. **(h)** Quantification of Nav fluorescence intensity (a.u.) as fraction of WT between WT (black circles) and *Ank3* W1989R homozygous (red squares) mice. *t-test* P = 0.89 (WT: 1 ± 0.07, N=3, n=27; W1989R: 0.99 ± 0.07, N=3, n=27). Data shown as mean ± SEM

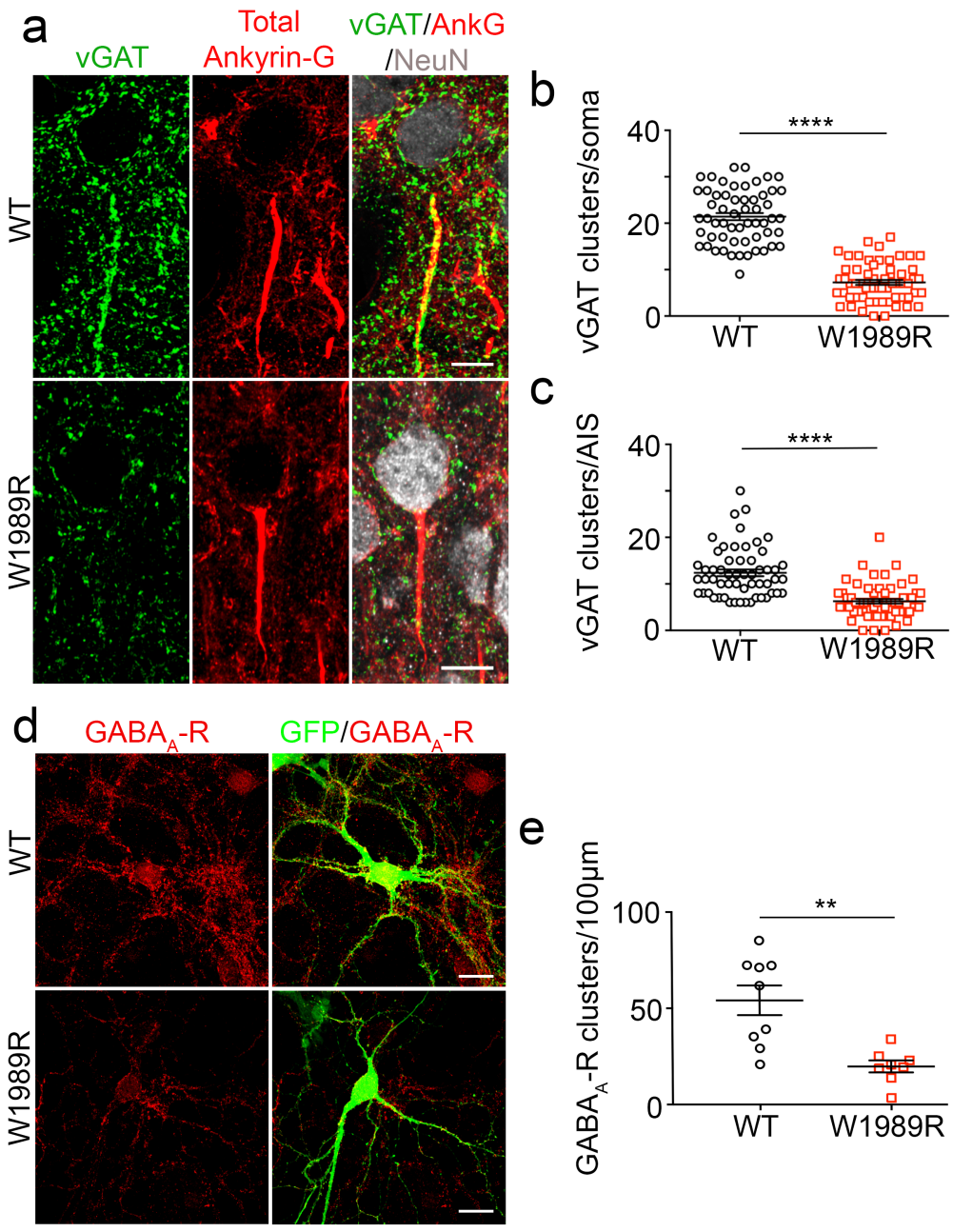

Figure 2.5: Pre- and post- GABAergic synaptic components are reduced in *Ank3* W1989R mice. (a) Representative images of GABAergic synapses from layer II/III somatosensory cortex of P25-48 WT (top) and *Ank3* W1989R homozygous (bottom) mice. Coronal brain sections immunostained with a presynaptic GABAergic marker vGAT (green), total ankyrin-G (red), and NeuN (white). Scale bar: 20 µm. **(b)** Quantification of the total number of vGAT-positive clusters per soma above a set intensity threshold from WT (black circles) and *Ank3* W1989R homozygous (red squares) mice. *t-test* ****P < 0.0001 (WT: 21.42 ± 0.8, N=3, n=57; W1989R: 7.25 ± 0.5, N=3, n=60). **(c)** Quantification of total number of vGAT-positive clusters per AIS from WT (black circles) and *Ank3* W1989R homozygous (red squares) mice. *t-test* ****P < 0.0001 (WT: 12.38 ± 0.7, N=3, n=56; W1989R: 6.27 ± 0.5, N=3, n=60). **(d)** Representative images of dissociated hippocampal cultured neurons at 21 DIV from WT (top) and *Ank3* W1989R homozygous (bottom) mice. Soluble GFP shown in green and immunostaining for GABA$_A$ receptor β2-3 subunit shown in red. Scale bar: 20 µm. **(e)** Quantification of the total number of GABA$_A$ receptor clusters per 100 µm per neuron. *t-test* **P = 0.0013 (WT: 54.1 ± 7.7, N=3, n=9; W1989R: 19.8 ± 3.1, N=3, n=8). Data shown as mean ± SEM.

To evaluate the functional consequences of *Ank3* W1989R on GABAergic signaling, we performed whole-cell patch-clamp recordings in acute brain slices of P25-48 WT and homozygous mutant mice. The frequency and amplitude of spontaneous inhibitory postsynaptic currents (sIPSCs) were significantly reduced in layer II/III cortical neurons as well as CA1 hippocampal neurons of *Ank3* W1989R mice relative to WT (Fig 2.6). The magnitude of reduction in sIPSC frequency (~65%) and amplitude (~40%) were similar between pyramidal neurons in cortical layer II/III and CA1 hippocampal neurons in *Ank3* W1989R mice compared to WT, suggesting that the binding of 480 kDa ankyrin-G to GABARAP may be a common mechanism for stabilizing GABAergic synapses in the forebrain. To address whether the decrease in quantal GABA release observed in *Ank3* W1989R mice is independent of AP firing, we measured mIPSCs in the presence of 1 μM tetrodotoxin (TTX) in acute brain slices of P25-48 mice. Consistent with the sIPSC data, we observed a significant reduction in both the frequency and amplitude of mIPSCs in *Ank3* W1989R cortical neurons versus WT (Fig. 2.7a-c). The iPSC response was completely attenuated following the administration of the $GABA_A$ receptor antagonist bicuculline, confirming that the loss of inhibitory tone in *Ank3* W1989R neurons is specific to $GABA_A$ receptor function rather than to other means of inhibitory synaptic transmission (Fig. 2.7d).

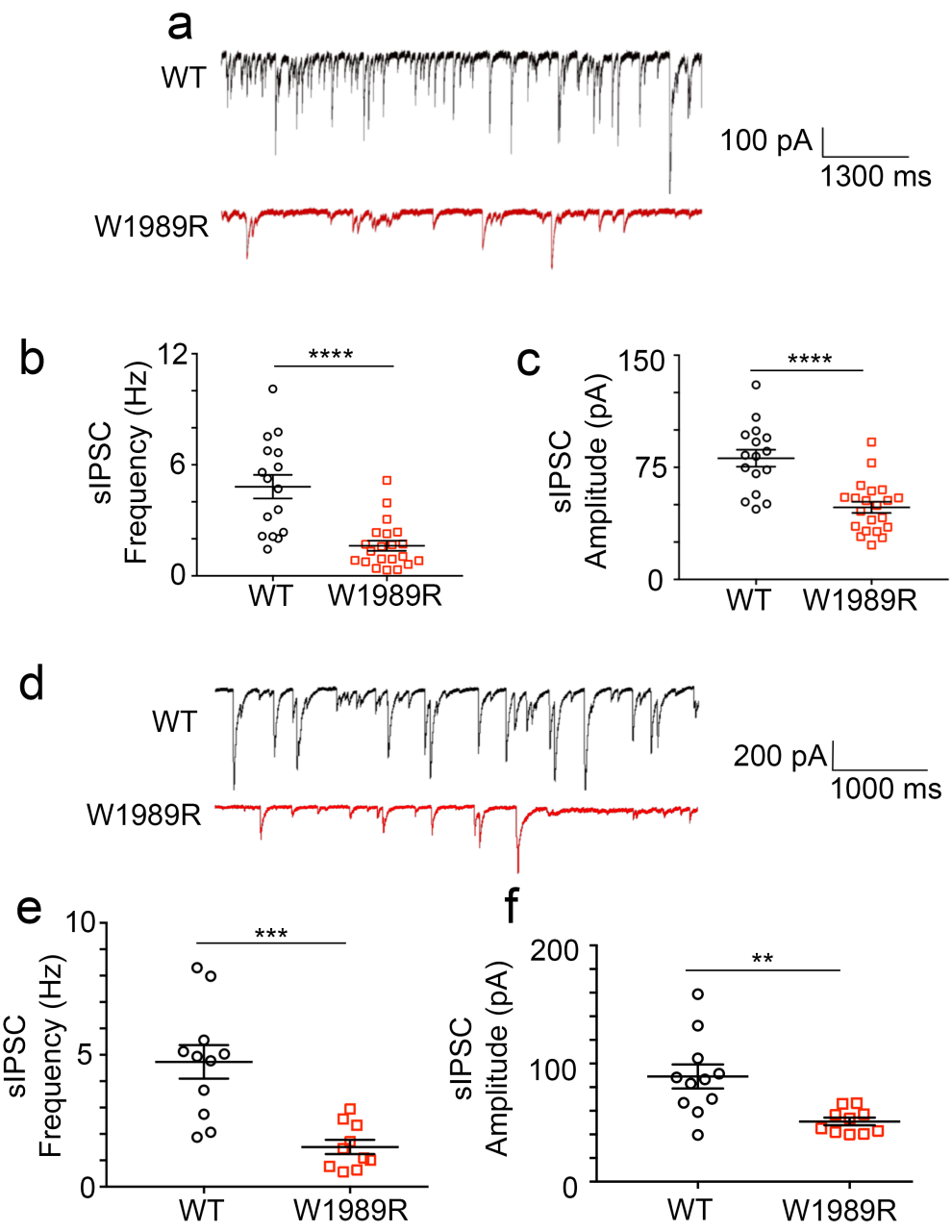

Figure 2.6: Loss of GABAergic synapse function onto *Ank3* W1989R cortical and hippocampal pyramidal neurons. **(a)** Spontaneous inhibitory postsynaptic current (sIPSC) representative traces from layer II/ and III somatosensory cortical neurons in WT (black) and *Ank3* W1989R (red) slices. Scale bars: 100 pA, 1300 ms. **(b)** Quantification of sIPSC frequency from layer II/III somatosensory cortical neurons in WT (black circles) and *Ank3* W1989R (red squares) brain slices. *t-test* ***P < 0.0001 (WT: 4.82 ± 0.6 Hz, n=16; W1989R: 1.63 ± 0.3 Hz, n=21). **(c)** Quantification of sIPSC amplitude from layer II/III somatosensory cortical neurons in WT (black circles) and *Ank3* W1989R (red squares) brain slices. *t-test* ***P < 0.0001 (WT: 81.1 ± 5.7 pA, n=16; W1989R: 48.22 ± 3.7 pA, n=21). **(d)** Spontaneous inhibitory postsynaptic current (sIPSC) representative traces from CA1 hippocampal neurons in WT (black) and *Ank3* W1989R (red) slices. Scale bars: 200 pA, 1000 ms. **(e)** Quantification of spontaneous inhibitory postsynaptic current (sIPSC) frequency in CA1 hippocampal neurons WT (black circles) and *Ank3* W1989R (red squares) brain slices. *t-test* ***P = 0.0002 (WT: 4.7 ± 0.6 Hz, n=11; W1989R: 1.5 ± 0.3 Hz, n=10). **(f)** Quantification of sIPSC amplitude in WT (black circles) and *Ank3* W1989R (red squares) CA1 hippocampal neurons in brain slices. *t-test* ***P = 0.0027 (WT: 89.1 ± 10.1 pA, n=11; W1989R: 51.0 ± 3.3 pA, n=10). Data shown as mean ± SEM.

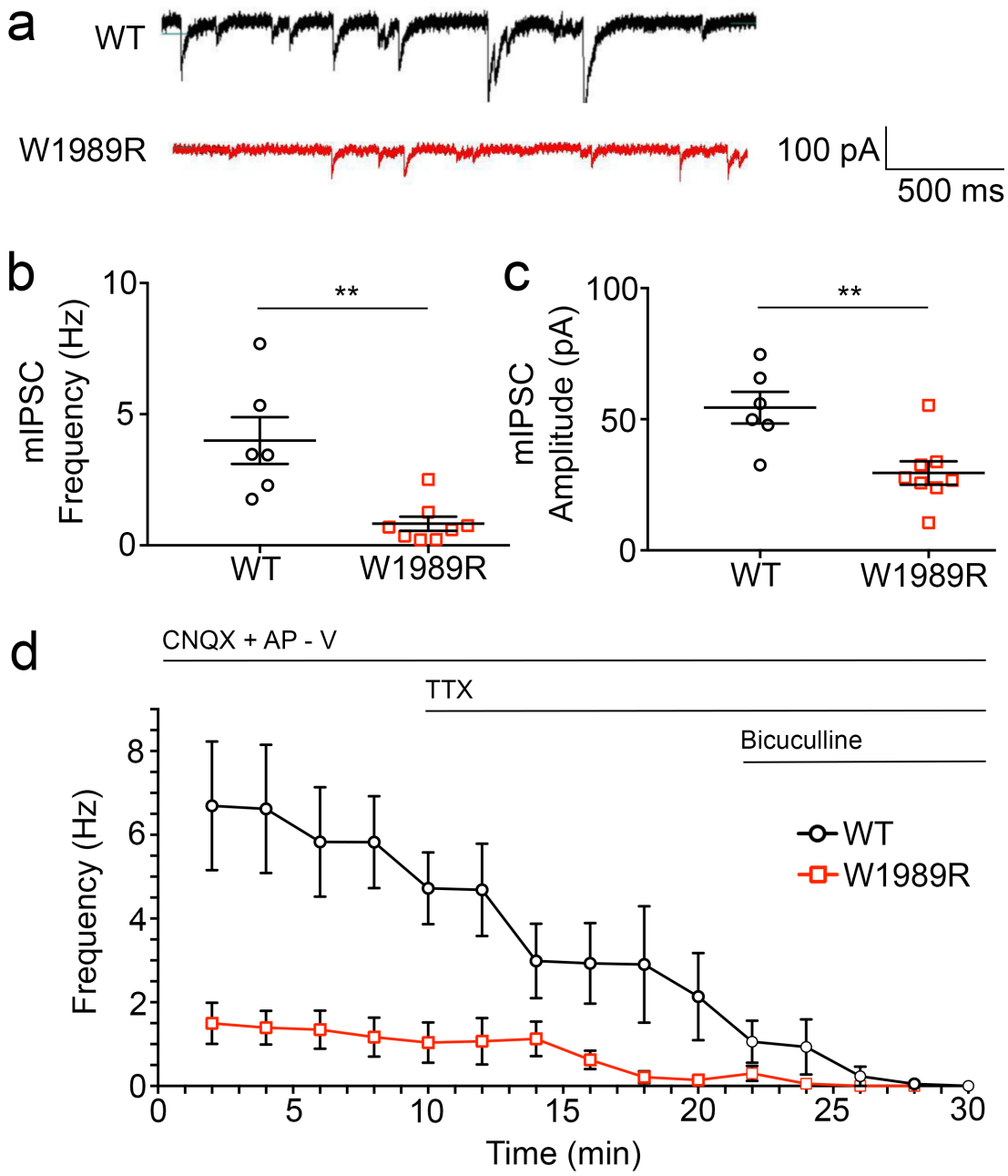

Figure 2.7: Miniature inhibitory postsynaptic currents (mIPSCs) are decreased in *Ank3* W1989R cortical pyramidal neurons. (a) Representative traces of miniature inhibitory postsynaptic currents (mIPSCs) of whole cell voltage-clamp recordings from layer II/III somatosensory cortical neurons in WT (black) and *Ank3* W1989R (red) homozygous brain slices. Scale bar: 100 pA, 500 ms. **(b)** Quantification of mIPSC frequency in WT (black circles) and *Ank3* W1989R homozygous (red squares) brain slices. *t-test* **P = 0.0023 (WT: 4.0 ± 0.9 Hz, n=6; W1989R: 0.83 ± 0.27 Hz, n=8). **(c)** Quantification of mIPSC amplitude in WT (black circles) and W1989R (red squares) brain slices. *t-test* **P = 0.0052 (WT: 54.4 ± 6.0 pA, n=6; W1989R: 29.5 ± 4.5 pA, n=8). **(d)** Quantification of IPSC frequency in response to tetrodotoxin (TTX) and bicuculline between WT (black circles) and *Ank3* W1989R homozygous (red squares). Data shown as mean ± SEM.

To determine whether the 480 kDa ankyrin-G interaction with GABARAP is specific to stabilizing forebrain GABAergic synapses, we immunostained Purkinje neurons in the cerebellum and thalamic neurons of P30-35 mice with antibodies to vGAT. We found that W1989R 480 kDa ankyrin-G is capable of stabilizing pinceau synapses at the AIS as well as somatodendritic GABA synapses on Purkinje neurons (Fig. 2.8a-c). The frequency and amplitude of sIPSCs and mIPSCs of Purkinje neurons were unchanged in *Ank3* W1989R mice relative to WT (Fig. 2.8d-h). We found no difference in the number of vGAT-positive puncta on the soma or AIS of thalamic neurons in *Ank3* W1989R mice as compared to WT (Fig. 2.9a-c). The function of GABA-mediated currents was also unchanged in *Ank3* W1989R thalamic neurons, as sIPSC and mIPSC frequency and amplitude were not significantly different than WT thalamic neurons (Fig. 2.9d-h). Overall, these results demonstrate that stabilization of cell surface $GABA_A$ receptors mediated by 480 kDa ankyrin-G and GABARAP is a cell type- and brain region-specific mechanism for the proper formation and function of GABAergic synapses *in vivo.*

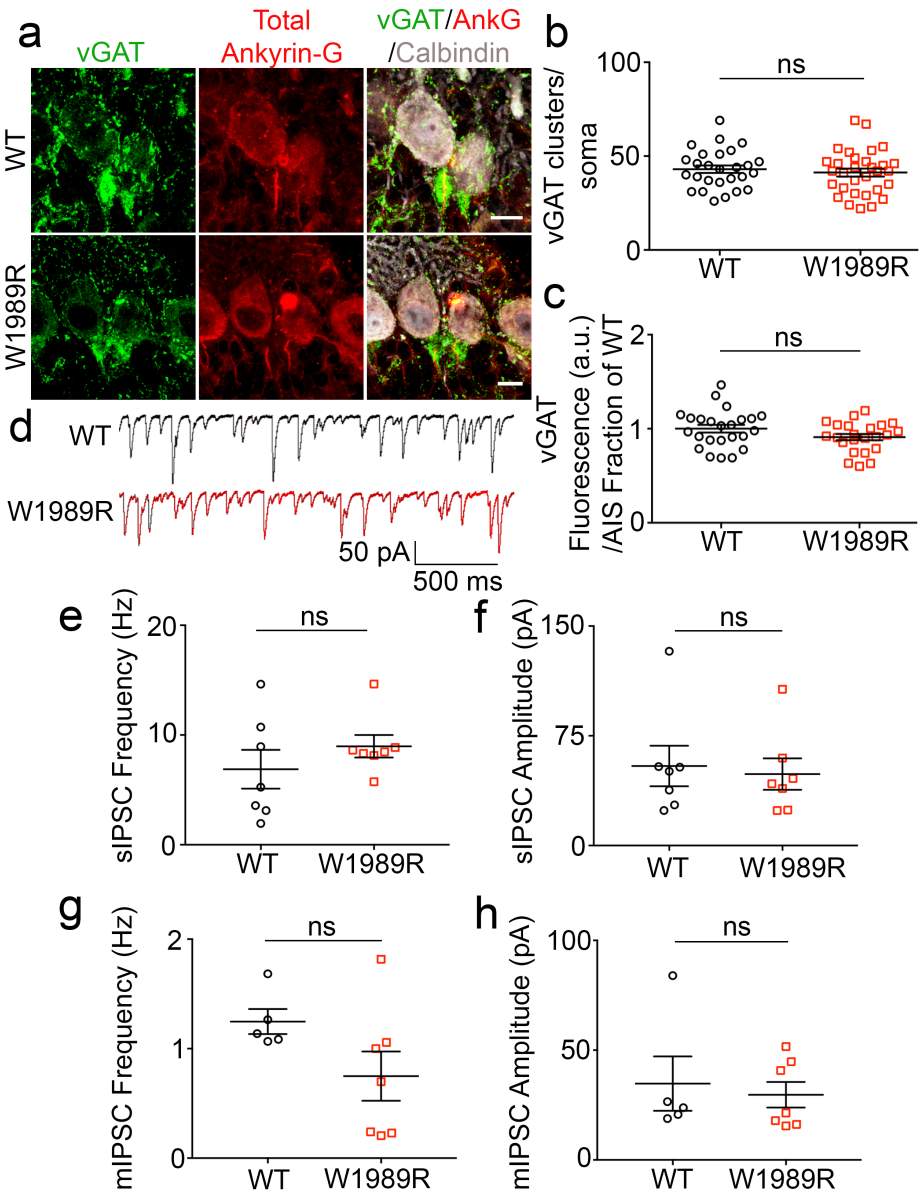

Figure. 2.8: GABAergic synapses are maintained in the cerebellum of *Ank3* W1989R mice. (a) Representative images of GABAergic synapses from cerebellar Purkinje neurons of P30 WT (top) and *Ank3* W1989R homozygous (bottom) mice. Sagittal brain sections immunostained for vGAT (green), total ankyrin-G (red), and calbindin (white). Scale bar: 10 µm. **(b)** Quantification of the total number of vGAT-positive clusters per soma above a set intensity threshold from WT (black circles) and *Ank3* W1989R homozygous (red squares) mice. *t-test* P = 0.54 (WT: 43.07 ± 2.0, N=3, n=27; W1989R: 41.3 ± 2.1, N=3, n=31). **(c)** Quantification of vGAT fluorescence intensity (a.u.) as fraction to WT between WT (black circles) and *Ank3* W1989R homozygous (red squares) mice. *t-test* P = 0.1 (WT: 1 ± 0.04, N=3, n=24; W1989R: 0.91 ± 0.03, N=3, n=23). **(d)** Spontaneous inhibitory postsynaptic current (sIPSC) representative traces from cerebellar Purkinje neurons in WT (black) and *Ank3* W1989R (red) slices. Scale bars: 50 pA, 500 ms. **(e)** Quantification of sIPSC frequency in WT (black circles) and *Ank3* W1989R (red squares) brain slices. *t-test* P = 0.33 (WT: 6.9 ± 1.8 Hz, n=7; W1989R: 8.9 ± 1.0 Hz, n=7). **(f)** Quantification of sIPSC amplitude in WT (black circles) and *Ank3* W1989R (red squares) brain slices. *t-test* P = 0.76 (WT: 54.4 ± 13.9 pA, n=7; W1989R: 48.8 ± 10.74 pA, n=7). **(g)** Quantification of mIPSC frequency in WT (black circles) and *Ank3* W1989R (red squares) brain slices. *t-test* P = 0.11 (WT: 1.23 ± 0.1 Hz, n=5; W1989R: 0.75 ± 0.2 Hz, n=7). **(h)** Quantification of mIPSC amplitude in WT (black circles) and *Ank3* W1989R (red squares) brain slices. *t-test* P = 0.69 (WT: 34.78 ± 12.4 pA, n=5; W1989R: 29.71 ± 5.8 pA, n=7). Data shown as mean ± SEM.

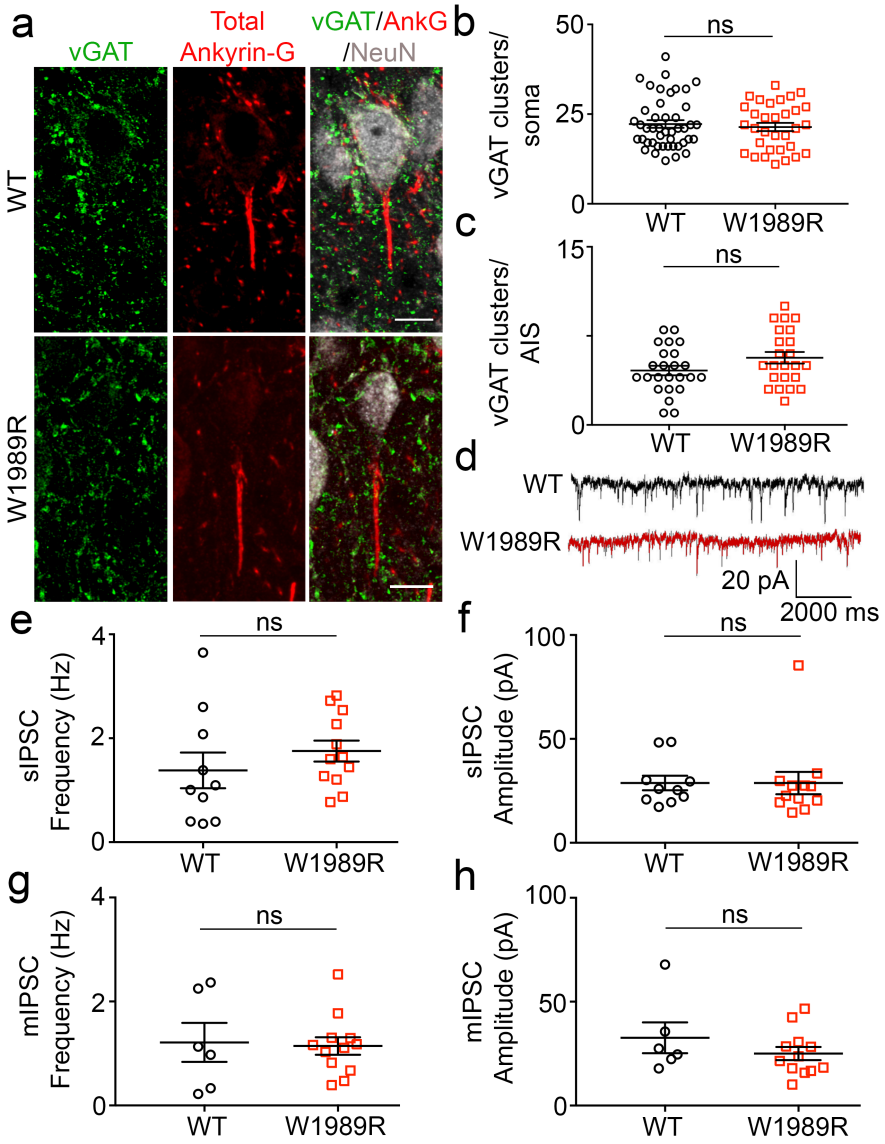

Figure 2.9: Thalamic neurons display normal GABAergic signaling in *Ank3* W1989R mice. (a) Representative images of GABAergic synapses on thalamic neurons of P30 WT (top) and *Ank3* W1989R homozygous (bottom) mice. Coronal brain sections immunostained for vGAT (green), total ankyrin-G (red), and NeuN (white). Scale bar: 10 µm. **(b)** Quantification of the total number of vGAT-positive clusters per soma above a set intensity threshold from WT (black circles) and *Ank3* W1989R homozygous (red squares) mice. *t-test* P = 0.6 (WT: 22.24 ± 1.1, N=3, n=45; W1989R: 21.41 ± 1.2, N=3, n=32. **(c)** Quantification of total number of vGAT-positive clusters per AIS from WT (black circles) and *Ank3* W1989R homozygous (red squares) mice. *t-test* P = 0.09 (WT: 4.6 ± 0.4, N=3, n=24; W1989R: 5.7 ± 0.5, N=3, n=23). **(d)** Spontaneous inhibitory postsynaptic current (sIPSC) representative traces from thalamic neurons in WT (black) and *Ank3* W1989R (red) slices. Scale bars: 20 pA, 2000 ms. **(e)** Quantification of sIPSC frequency in WT (black circles) and *Ank3* W1989R (red squares) brain slices. *t-test* P = 0.34 (WT: 1.38 ± 0.3 Hz, n=10; W1989R: 1.75 ± 0.2 Hz, n=12). **(f)** Quantification of sIPSC amplitude in WT (black circles) and *Ank3* W1989R (red squares) brain slices. *t-test* P = 0.99 (WT: 28.8 ± 3.5 pA, n=10; W1989R: 28.8 ± 5.4 pA, n=12). **(g)** Quantification of mIPSC frequency in WT (black circles) and *Ank3* W1989R (red squares) brain slices. *t-test* P = 0.84 (WT: 1.2 ± 4 Hz, n=6; W1989R: 1.1 ± 0.2 Hz, n=12). **(h)** Quantification of mIPSC amplitude in WT (black circles) and *Ank3* W1989R (red squares) brain slices. *t-test* P = 0.28 (WT: 32.6 ± 7.4 pA, n=6; W1989R: 25.0 ± 3.2 pA, n=12). Data shown as mean ± SEM.

Homozygous *Ank3* W1989R mice show altered network synchronization

Parvalbumin-positive (PV+) GABAergic interneurons are critical for the synchronization of forebrain networks due to their rhythmic, fast-spiking electrophysiological properties, and because a single PV+ interneuron can synapse onto hundreds or thousands of pyramidal neurons simultaneously (Sohal et al. 2009; Tamas et al. 2000). There are two main subtypes of PV+ interneurons: the PV+ basket cells, which synapse onto the soma and proximal dendrites of pyramidal neurons, and PV+ chandelier cells, which innervate the AIS. Decreased GABAergic synapses and sIPSC frequency observed in the *Ank3* W1989R mouse model (Fig. 2.5 and Fig 2.6) suggested a reduction in presynaptic connectivity or reduced density of PV+ interneurons. To test this hypothesis, we measured PV+ cell number and function in layer II/III of the somatosensory cortex. Immunostaining of coronal brain sections with anti-PV antibodies revealed no detectable changes in the density of PV+ interneurons in *Ank3* W1989R mice compared to WT (Fig. 2.10a and b). To evaluate the firing properties of PV+ interneurons, we evoked AP firing by injecting somatic current in acute brain slices of P25-48 homozygous *Ank3* W1989R or WT mice. *Ank3* W1989R PV+ interneurons maintained their fast-spiking electrophysiological properties and demonstrated similar AP frequency and amplitude compared to WT PV+ neurons (Fig. 2.10c, e, and f). We observed a significant increase in the membrane resistance in *Ank3* W1989R PV+ interneurons compared to WT (2.10d), suggesting decreased ion channel expression at the plasma membrane.

PV+ interneurons comprise approximately 40% of the total number of interneurons in the somatosensory cortex (Fogarty et al. 2007). To examine the effect of the *Ank3* W1989R mutation on two additional subclasses of GABAergic interneurons, we performed whole-cell patch clamp recording on regular spiking non-pyramidal interneurons (RSNP) and irregular spiking

interneurons (IS). Despite a large decrease in detectable GABAergic synapse connectivity, there was no significant difference in action potential frequency or amplitude of RSNP interneurons or IS interneurons in *Ank3* W1989R mice compared to WT (Table 2.1). Moreover, there was significant reduction in AP threshold from RSNP and IS interneurons between WT and *Ank3* W1989R mice; however, the input resistance, resting membrane potential, AP amplitude, and AP τ were unchanged (Table 2.1). These data suggest that loss-of-function of the 480 kDa isoform of ankyrin-G results in decreases in GABAergic synaptic connectivity; however, GABAergic inhibitory interneurons are present at normal density and maintain function.

PV+ interneurons are responsible for the synchronization of neuronal networks, which results in the generation of gamma oscillations (Tamas et al. 2000). Gamma oscillations reflect the synchronization of local neuronal network activity providing a "temporal framework" for proper information processing, sensory integration, and cognitive function (Buzsaki and Wang 2012; Cardin et al. 2009; Sohal et al. 2009). We hypothesized that, because *Ank3* W1989R mice exhibit reductions in somatodendritic and AIS GABAergic synapses, network synchronization would be decreased resulting in a reduction in the power of gamma oscillations. To evaluate the synchronization of neuronal ensembles, we used planar multi-electrode arrays to record kainate-induced gamma oscillations in acute slices of hippocampus from WT and homozygous *Ank3* W1989R mice (Fisahn et al. 2004) (Fig. 2.11a and b). The power of the kainate-induced gamma oscillations was ~30% decreased in CA1 and CA3 hippocampal regions in *Ank3* W1989R mice compared to WT (Fig 2.11 c and d and Fig. 2.12a-d). This significant reduction in gamma oscillations in *Ank3* W1989R mouse hippocampus suggests disruptions in network synchrony, consistent with reduced connectivity of PV+ interneurons.

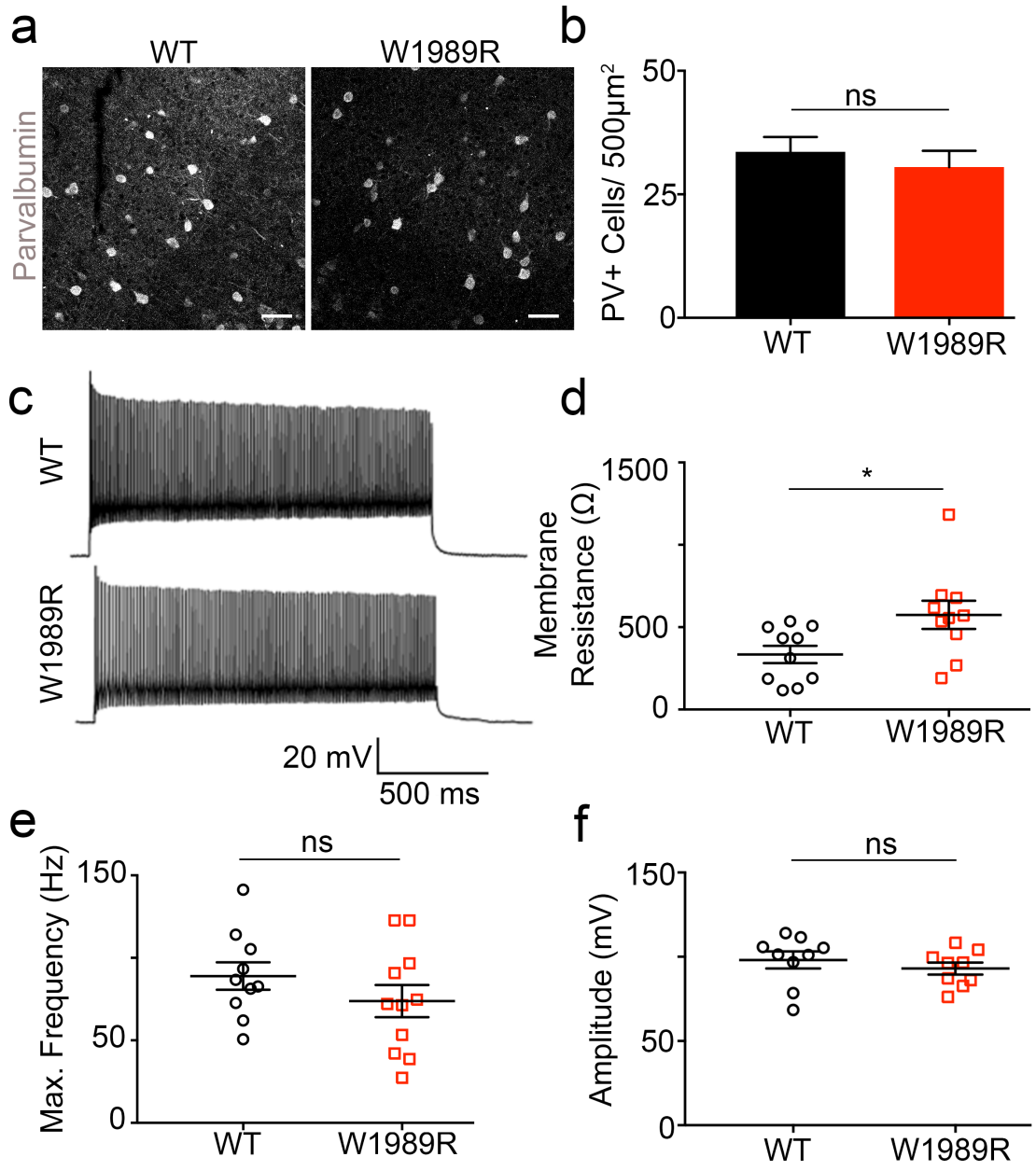

Figure 2.10: **Normal density and fast-spiking properties of *Ank3* W1989R PV+ GABAergic interneurons. (a)** Representative images of parvalbumin-positive (PV+) interneurons in layer II/III somatosensory cortex of P30 WT (left) and *Ank3* W1989R homozygous (right) mice. Coronal brain sections immunostained with PV (white). Scale bar: 50 µm. **(b)** Quantification of total number of PV-positive cells per 500 µm^2 from WT (black bar) and *Ank3* W1989R homozygous (red bar) sections. *t-test* P = 0.497, ns, not significant (WT: 33.59 ± 3.0, N=3, n=15; W1989R: 30.53 ± 3.3, N=3, n=14). **(c)** Representative traces of evoked firing patterns and AP frequencies of fast-spiking PV+ interneurons in layer II/III somatosensory cortex from WT (top) and *Ank3* W1989R homozygous (bottom) brain slices. Scale bar: 20 mV, 500 ms. **(d)** Quantification of membrane resistance of PV+ cells in WT (black circles) and *Ank3* W1989R homozygous (red squares). *t-test* *P = 0.0276 (WT: 334.5 ± 52.8, n=10; W1989R: 574.9 ± 85.31, n=10). **(e)** Quantification of PV+ cell maximum frequency in WT (black circles) and *Ank3* W1989R homozygous (red squares). *t-test* P = 0.256 (WT: 88.99 ± 8.3, n=10; W1989R: 73.83 ± 9.7, n=11). **(f)** Quantification of single AP amplitude of PV+ in WT (black circles) and *Ank3* W1989R homozygous (red squares). *t-test* P = 0.422 (WT: 98.09 ± 5.0, n=9; W1989R: 93.02 ± 3.5, n=10). Data shown as mean ± SEM.

		Membrane Resistance (MΩ)	Membrane Potential (mV)	AP Threshold (mV)	AP Amplitude (mV)	AP Peak Time (ms)	AP Width (ms)	AP Tau (ms)
Pyramidal	WT	228.3 ± 121 (n=27)	-67.5 ± 4 (n=22)	-40.7 ± 20 (n=22)	113.7 ± 13 (n=22)	2.6 ± 0.5 (n=22)	2.6 ± 0.6 (n=22)	25 ± 10 (n=22)
	W1989R	159.9 ± 66* (n=33)	-66.3 ± 5 (n=29)	-36.1 ± 30 (n=29)	111 ± 14 (n=29)	2.7 ± 1 (n=29)	2.8 ± 1 (n=29)	21.6 ± 10 (n=25)
Fast-Spiking	WT	334.6 ± 167 (n=10)	-62.1 ± 5 (n=9)	-46.3 ± 2 (n=9)	98.1 ± 15 (n=9)	2.1 ± 0.4 (n=9)	0.8 ± 0.1 (n=9)	0.9 ± 0.3 (n=9)
	W1989R	574.3 ± 269* (n=9)	-61.6 ± 6 (n=9)	-46.3 ± 2 (n=9)	93 ± 11 (n=9)	2.2 ± 0.4 (n=9)	1.0 ± 0.4 (n=9)	1.2 ± 0.8 (n=9)
Regular Spiking Nonpyramidal	WT	363.9 ± 108 (n=13)	-64.8 ± 5 (n=13)	-41 ± 10 (n=9)	110.2 ± 9 (n=9)	2.4 ± 0.2 (n=13)	2.5 ± 0.7 (n=13)	17.5 ± 11 (n=13)
	W1989R	284.3 ± 125 (n=17)	-57.5 ± 28 (n=18)	-47 ± 6* (n=18)	101.4 ± 15 (n=18)	2.6 ± 0.9 (n=18)	2.4 ± 0.2 (n=18)	12.4 ± 11 (n=17)
Irregular Spiking	WT	227.03 (n=1)	-60.9 ± 5 (n=3)	-43.9 ± 2 (n=3)	88.3 ± 5.6 (n=3)	3.1 ± 0.4 (n=3)	3.0 ± 0.5 (n=3)	9.5 ± 0.7 (n=3)
	W1989R	156.2 ± 14 (n=4)	-64.2 ± 4 (n=4)	-49.4 ± 1* (n=4)	107.4 ± 12 (n=4)	2.7 ± 0.2 (n=4)	3.1 ± 0.3 (n=4)	9.1 ± 1 (n=4)

Table 2.1: Comparison of cell-type specific electrophysiological properties between WT and *Ank3* W1989R mice. Quantification of various electrophysiology measurements of layer II/III cortical pyramidal neurons and the main classes of inhibitory interneurons following evoked APs in acute brain slices from WT and *Ank3* W1989R homozygous mice. Yellow/asterisk indicates significantly different from WT.

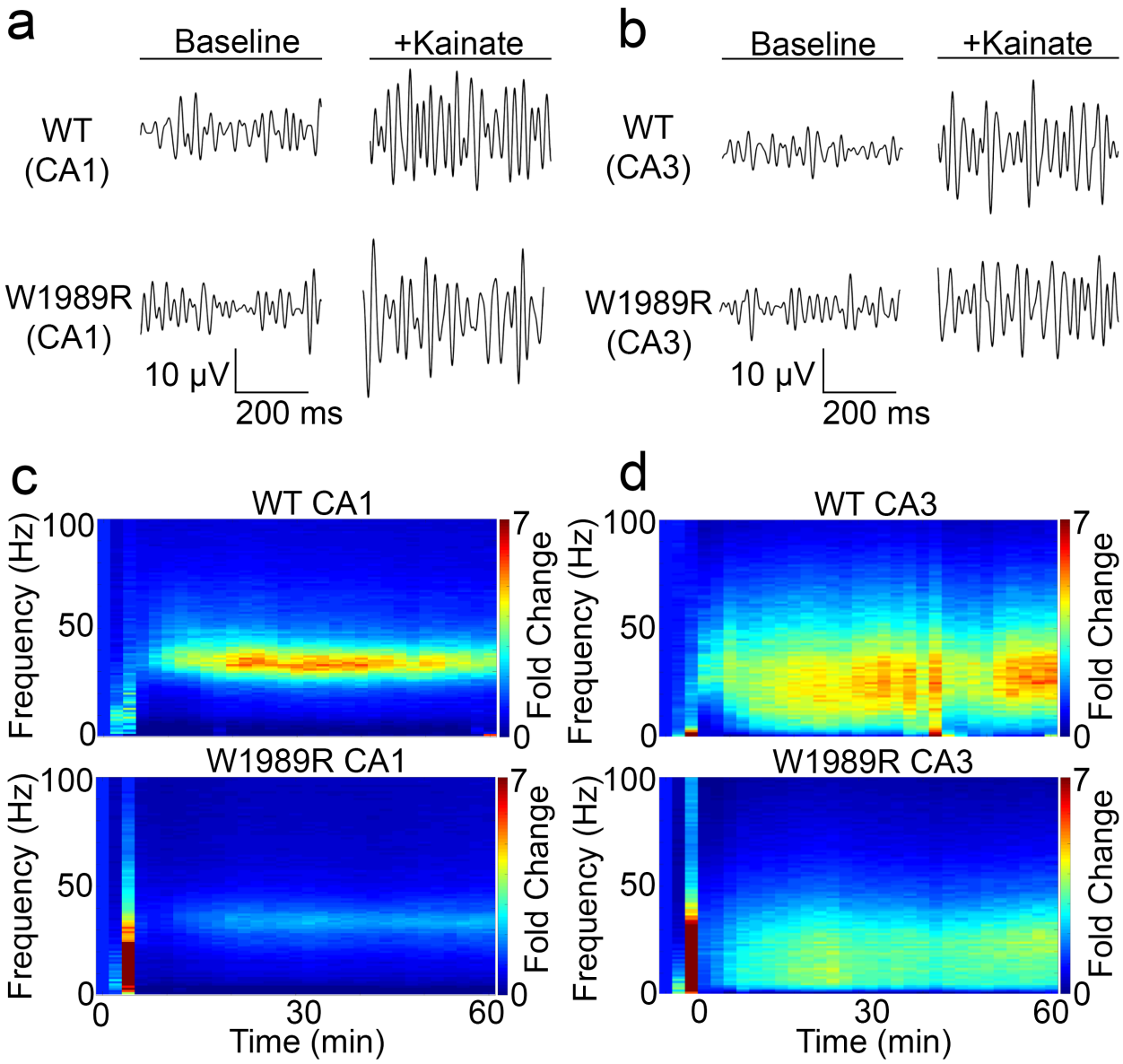

Figure 2.11: Reduced gamma oscillations in the hippocampus of *Ank3* W1989R mice. (a) Representative traces of kainate-induced gamma oscillations from local field potential (LFP) recordings in CA1 hippocampal neurons and **(b)** CA3 hippocampal neurons of WT (top) or *Ank3* W1989R homozygous (bottom) mice in acute brain slices. **(c)** Representative time-frequency sonograms of CA1 hippocampal neurons from WT (top) and W1989R homozygous (bottom) mice. **(d)** Representative time-frequency sonograms of CA3 hippocampal neurons from WT (top) and W1989R homozygous (bottom) mice.

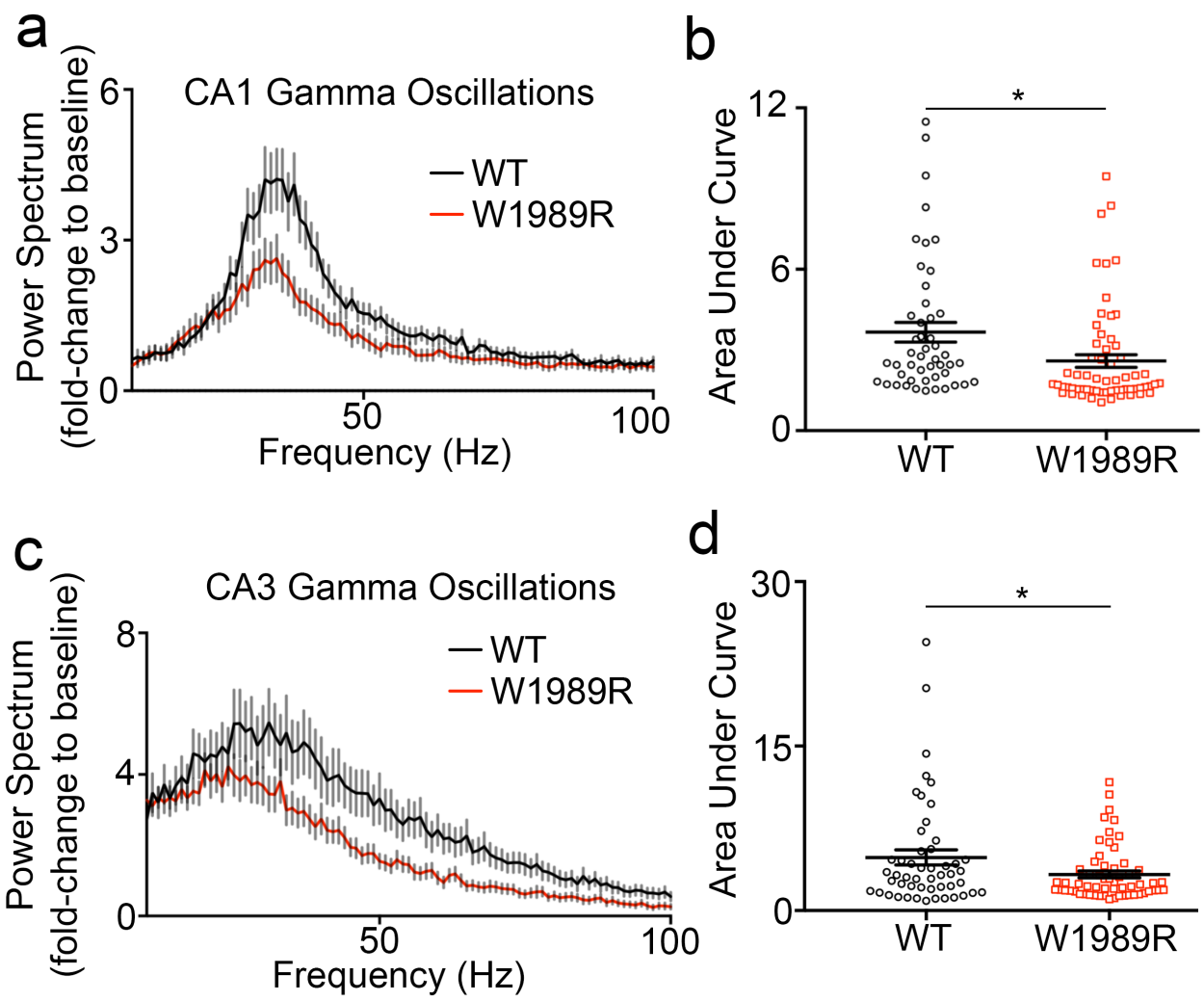

Figure 2.12: Reduced gamma oscillations as local field potential power in the hippocampus of *Ank3* W1989R mice. (a) Power spectral analysis from CA1 hippocampus in acute brain slices of P24-40 WT (black circles) and *Ank3* W1989R homozygous (red squares) mice plotted as fold-change to baseline signal. **(b)** Quantification of the area under the curve for gamma band (30-60Hz) from CA1 hippocampus in WT (black circles) and *Ank3* W1989R homozygous (red squares). *t-test* *P = 0.0118 (WT: 3.66 ± 0.4, N=3, n=48; W1989R: 2.59 ± 0.2, N=3, n=62). **(c)** Power spectral analysis from CA3 hippocampus WT (black circles) and *Ank3* W1989R homozygous (red squares) mice. **(d)** Quantification of the area under the curve for gamma band (30-60Hz) from WT (black circles) and *Ank3* W1989R homozygous (red squares). *t-test* *P=0.0343 (WT: 4.85 ± 0.7, N=5, n=50; W1989R: 3.3 ± 0.3, N=5, n=59). Data shown as mean ± SEM.

Dendritic spine density and function are reduced in *Ank3* W1989R neurons

GABAergic interneurons control the excitability of glutamatergic pyramidal neurons by modulating their spike timing and firing rate. The loss of inhibitory tone, similar to that observed here in *Ank3* W1989R mice, has been linked to pathological neuronal hyperexcitability (Marin 2012). To address the effect of decreases in GABAergic synapses on AP firing rates, we compared evoked APs in acute brain slices of P25-48 homozygous *Ank3* W1989R and WT mice. The frequency of AP firing was significantly increased in *Ank3* W1989R cortical and CA1 hippocampal neurons compared to WT (Fig. 2.13a, c, d, and f). Moreover, the maximum firing rate per neuron was two-fold higher in *Ank3* W1989R neurons versus WT (Fig. 2.13b and e). These data demonstrate that cortical and hippocampal pyramidal neurons are hyperexcitable *in vivo* following 480 kDa ankyrin-G loss-of-function at GABAergic synapses.

Neurons have developed multiple intrinsic mechanisms to maintain excitability homeostasis and stabilize network activity. The AIS has been proposed to participate in activity-dependent plasticity and decreasing AIS length may be one mechanism to reduce excitability. We measured AIS length of layer II/III somatosensory cortical neurons in coronal brain sections in P30 mice and in dissociated hippocampal neurons at 21 DIV from WT and mutant mice. We found that AIS length was approximately 30% shorter in *Ank3* W1989R mice compared to WT (Fig. 2.14a-d)). Consistent with no change in inhibitory tone (Fig. 2.8 and 2.9), there was no detectable difference in AIS length of cerebellar Purkinje neurons (WT: 15.3 ± 1.2 μm, N=3, n=12; W1989R: 14.9 ± 0.6 μm, N=3, n=14 *t-test* P = 0.72) or thalamic neurons (WT: 21.8 ± 0.7 μm, N=3, n=34; W1989R: 21.6 ± 0.9 μm, N=3, n=29 *t-test* P = 0.88) compared to WT mice.

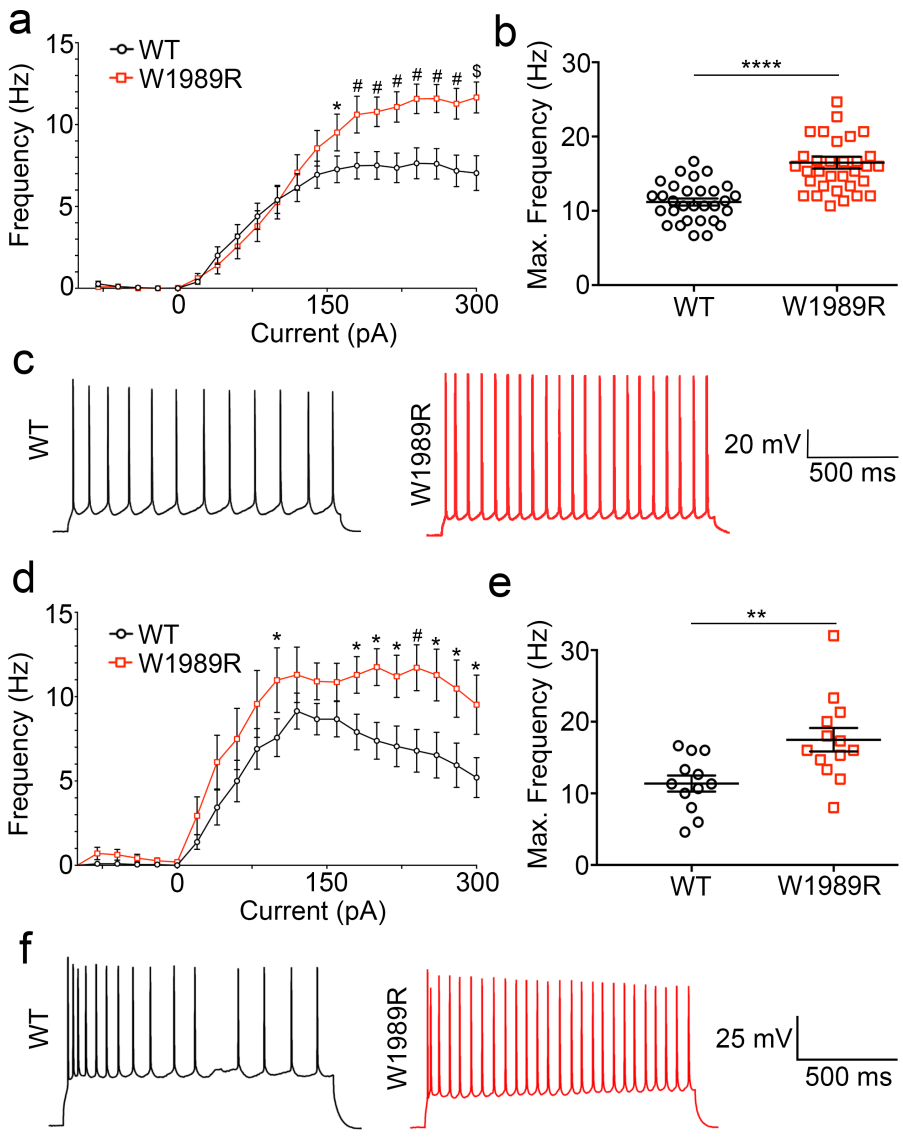

Figure 2.13: Increased firing rate of *Ank3* W1989R cortical and CA1 hippocampal pyramidal neurons. (a) Evoked AP frequency from cortical neurons for WT (black circles) or *Ank3* W1989R homozygous (red squares) in acute brain slices. *Two-way ANOVA, Tukey's post hoc* *P < 0.05, #P <0.001, $P <0.001 (WT: n=40; W1989R: n=40). **(b)** Quantification of average maximum frequency of pyramidal neurons in layer II/III somatosensory cortex in WT (black circles) and *Ank3* W1989R homozygous (red squares) mice. *t-test* ****P < 0.0001 (WT: 11.18 ± 0.5, n=30; W1989R: 16.49 ± 0.8, n=33). **(c)** Representative AP traces from cortical pyramidal neurons of WT (left, black) and *Ank3* W1989R homozygous (right, red) mice. Scale bar: 500 ms. **(d)** Evoked AP frequency from CA1 hippocampal neurons for WT (black circles) or *Ank3* W1989R homozygous (red squares) in acute brain slices. *Two-way ANOVA, Tukey's post hoc* *P < 0.05, #P <0.001 (WT: n=27; W1989R: n=27). **(e)** Quantification of average maximum frequency of pyramidal neurons in CA1 hippocampus of WT (black circles) and *Ank3* W1989R homozygous (red squares) mice. *t-test* **P = 0.0061 (WT: 11.38 ± 1.1, n=12; W1989R: 17.49 ± 1.6, n=13). **(f)** Representative traces from CA1 hippocampal pyramidal neurons of WT (left) and *Ank3* W1989R homozygous (right) mice. Scale bar: 500 ms. Data shown as mean ± SEM.

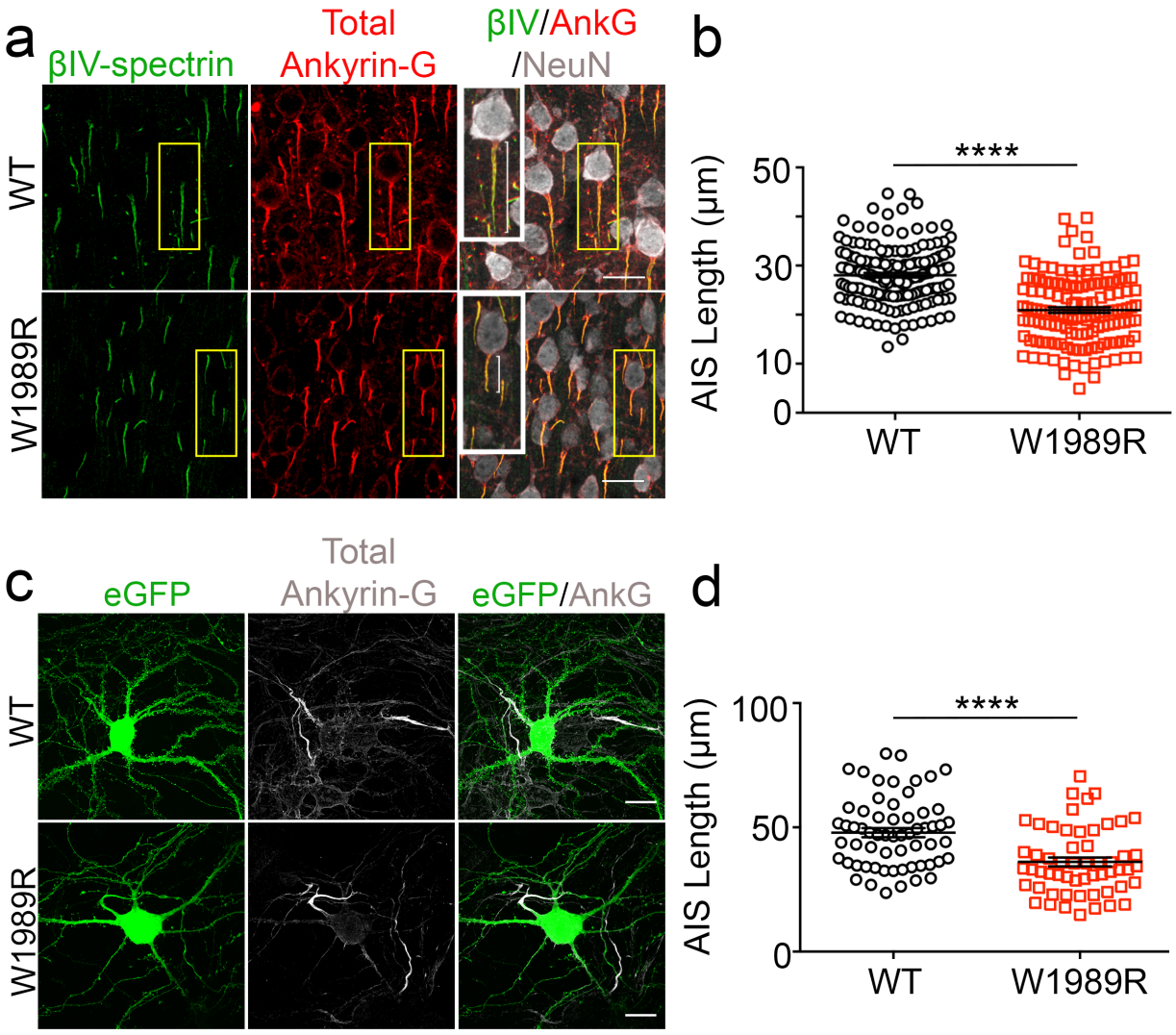

Figure 2.14: Cortical and hippocampal pyramidal neurons have decreased AIS length in *Ank3* W1989R mice. (a) Representative images from coronal sections of layer II/III somatosensory cortex of P30 WT (top) and *Ank3* W1989R homozygous (bottom) mice. Immunostaining for βIV-spectrin (green), total ankyrin-G (red), and NeuN (white). Scale bar: 20 μm. **(b)** Quantification of AIS length between WT (black circles) and W1989R homozygous (red squares) mice. *t-test* ****P < 0.0001 (WT: 28.03 ± 0.5, N=3, n=156; W1989R: 20.94 ± 0.6, N=3, n=140). **(c)** Representative images of dissociated hippocampal cultured neurons from WT (left) and *Ank3* W1989R homozygous (right) mice at 21DIV filled with soluble eGFP. Scale bar: 20 μm. **(d)** Quantification of the AIS length between WT (black circles) and *Ank3* W1989R homozygous (red squares) neurons. *t-test* ****P < 0.0001 (WT: 47.87 ± 1.8, N=3, n=61; W1989R: 36.11 ± 1.8, N=3, n=56). Data shown as mean ± SEM.

Another neuronal mechanism to compensate for the lack of inhibitory tone is to decrease AMPA receptor surface expression and decrease dendritic spine density (Lin and Koleske 2010). We therefore examined dendritic spine density in dissociated hippocampal neurons and CA1 hippocampal neurons *in vivo* from *Ank3* W1989R mice and observed a significant decrease in the total number of dendritic spines compared to WT (Fig. 2.15a and b and 2.16a and b). Consistent with this result, whole-cell patch clamp recordings from CA1 hippocampal neurons in brain slices showed significant decreases in mEPSC amplitude in *Ank3* W1989R mice compared to WT, suggesting a reduction in dendritic AMPARs (Fig. 2.15c and e). Moreover, mEPSC frequency was increased in *Ank3* W1989R neurons (Fig. 2.15e). A previous study showed that 190 kDa ankyrin-G plays a critical role in modulation of dendritic spine morphology and AMPA receptor postsynaptic stability (Smith et al. 2014). Western blot analysis of hippocampal and cortical lysates from *Ank3* W1989R mice showed a 50% decrease in 190 kDa ankyrin-G expression, with no change in the expression of the 270- or 480 kDa splice variants, compared to WT lysates (Fig. 2.15f and g and Fig. 2.17). Overall, these data suggest a novel intrinsic mechanism to compensate for neuronal hyperexcitability by decreasing the expression of 190 kDa ankyrin-G and subsequently dendritic spine density and function in neurons with reduced inhibitory tone.

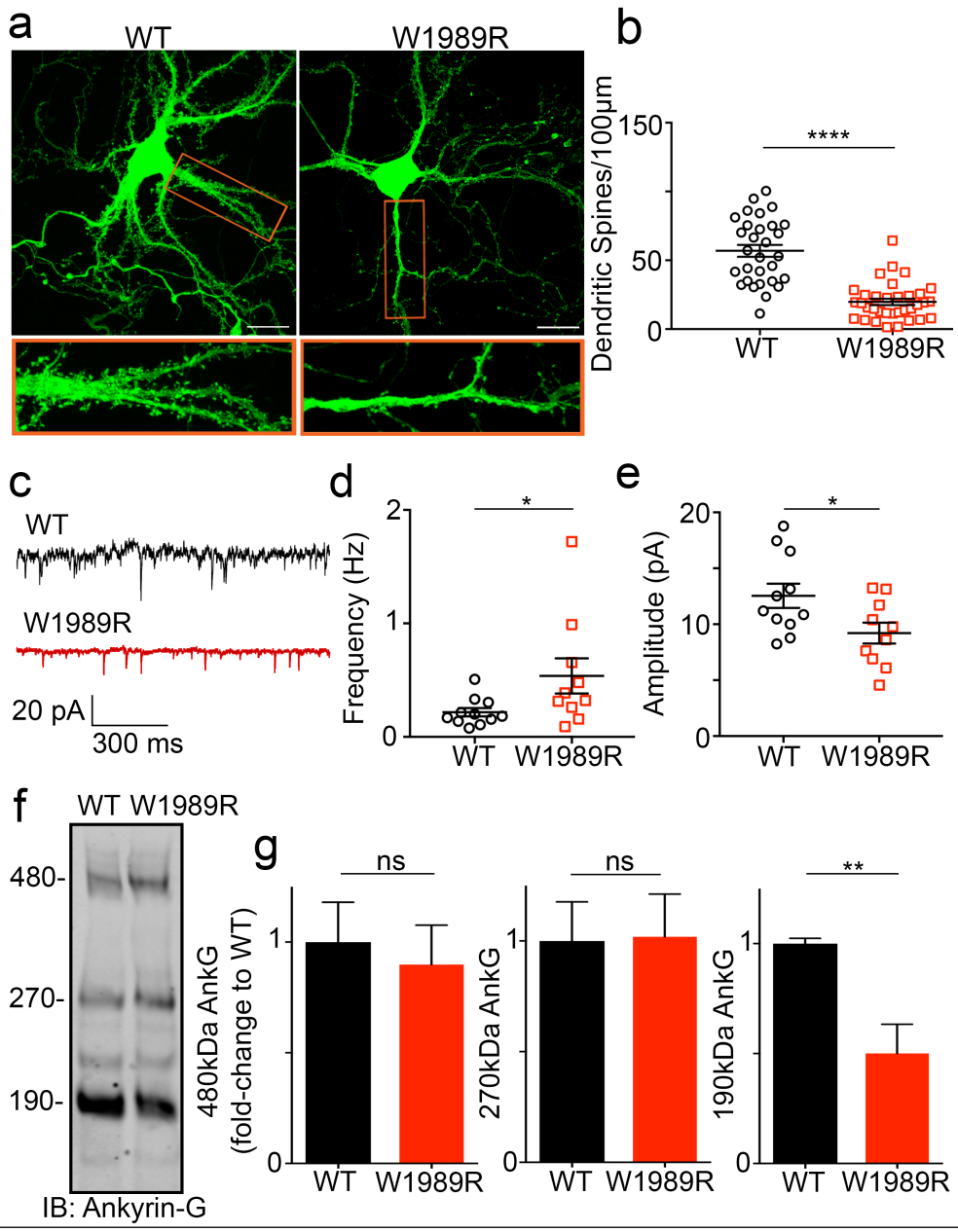

Figure 2.15: Decreased spine density and function and reduced 190 kDa ankyrin-G expression levels in *Ank3* W1989R neurons. (a) Representative images of dissociated hippocampal cultured neurons from WT (left) and *Ank3* W1989R homozygous (right) mice at 21DIV filled with soluble eGFP. Scale bar: 20 µm. **(b)** Quantification of the total number of dendritic spines per 100 µm per neuron. *t-test* ****P < 0.0001 (WT: 56.91 ± 4.3, N=3, n=30; W1989R: 19.78 ± 2.3, N=3, n=34). **(c)** Representative traces of spontaneous excitatory postsynaptic currents (sEPSCs) from CA1 hippocampal neurons in WT (top) and *Ank3* W1989R (bottom) slices. Scale bar: 300 ms. **(d)** Quantification of mEPSC frequency in WT (black circles) and *Ank3* W1989R (red squares) brain slices. *t-test* *P = 0.049 (WT: 0.22 ± 0.04 Hz, n=11; W1989R: 0.54 ± 0.15 Hz, n=10). **(e)** Quantification of mEPSC amplitude in WT (black circles) and *Ank3* W1989R (red squares) brain slices. *t-test* *P = 0.032 (WT: 12.5 ± 1.1 pA, n=11; W1989R: 9.21 ± 0.9 pA, n=10). **(f)** Western blot analysis from hippocampal lysates of P30 WT (left) and *Ank3* W1989R homozygous (right) mice. Blots were probed with antibodies to total ankyrin-G. **(g)** Quantification of relative expression levels of 480 kDa ankyrin-G *t-test* P = 0.71 (WT: 1.0 ± 0.2, N=3; W1989R: 0.9 ± 0.2, N=3), 270 kDa ankyrin-G *t-test* P = 0.95 (WT: 1.0 ± 0.2, N=3; W1989R: 1.019 ± 0.2, N=3), and 190 kDa ankyrin-G *t-test* *P = 0.02 (WT: 1 ± 0.02 N=3; W1989R: 0.5 ± 0.1, N=3). Data normalized to WT controls. Data shown as mean ± SEM.

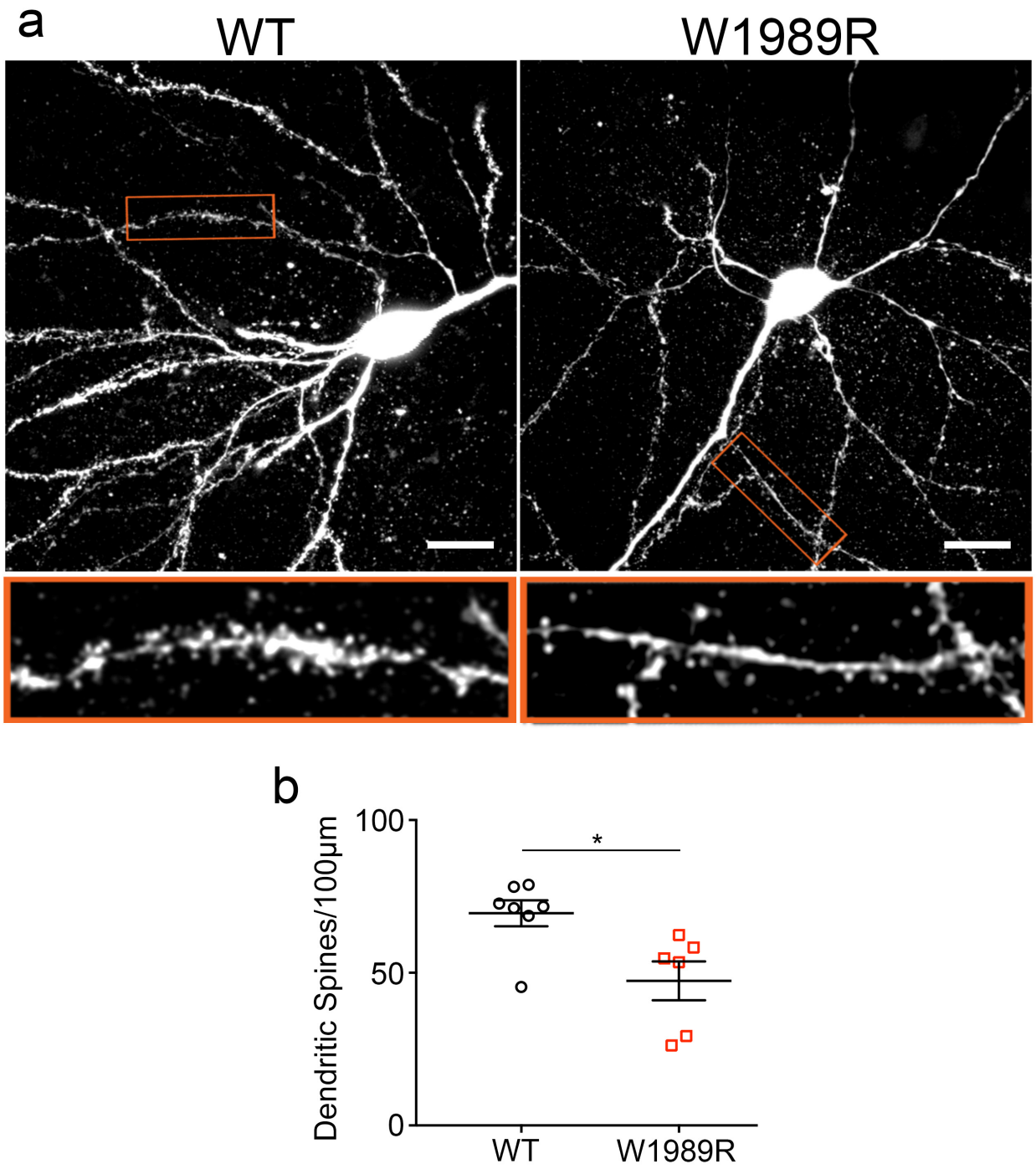

Figure 2.16: Decreased dendritic spine density in CA1 hippocampal pyramidal neurons in *Ank3* W1989R mice *in vivo*. **(a)** Representative images of biocytin-filled CA1 hippocampal pyramidal neurons of P30 WT (left) and *Ank3* W1989R homozygous (right) mice. Images were pseudocolored white. Scale bar: 20 µm. **(b)** Quantification of the total number of dendritic spines per 100 µm per neuron. *t-test* *P < 0.01 (WT: 69.48 ± 4.3, N=3, n=7; W1989R: 47.37 ± 6.3, N=3, n=6). Data shown as mean ± SEM.

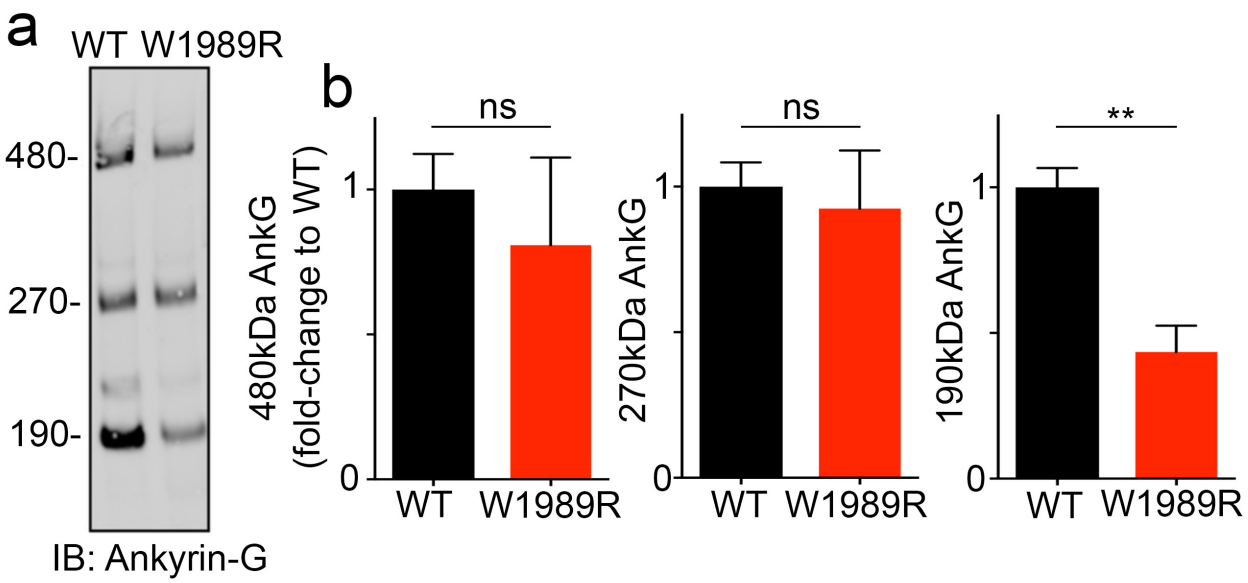

Figure 2.17: 190 kDa ankyrin-G expression levels are reduced in cortex of *Ank3* W1989R mice. (a) Western blot analysis from cortical lysates of P30 WT (left) and *Ank3* W1989R homozygous (right) mice. Blots were probed with antibodies to total ankyrin-G. **(b)** Quantification of relative expression levels of 480 kDa ankyrin-G *t-test* P = 0.59 (WT: 1.0 ± 0.1, N=3; W1989R: 0.81 ± 0.3, N=3), 270 kDa ankyrin-G *t-test* P = 0.75 (WT: 1.0 ± 0.1, N=3; W1989R: 0.92 ± 0.2, N=3), and 190 kDa ankyrin-G *t-test* **P = 0.0073 (WT: 1 ± 0.1 N=3; W1989R: 0.43 ± 0.1, N=3). Data normalized to WT controls. Data shown as mean ± SEM.

Identification of *ANK3* W1989R in a family with BD

Disruptions in forebrain circuitry and network-level activity observed in *Ank3* W1989R mice predict that patients expressing this variant may experience altered brain activity and mood-related behaviors. According to the most recent data from the gnomAD project, the *ANK3* W1989R variant (rs372922084, c.5965T>C (p.Trp1989Arg)) is found in approximately 1: 10,000 European Americans (Lek et al. 2016). We used whole-genome and exome sequencing on blood samples obtained through the Heinz C. Prechter Bipolar Research Program at the University of Michigan to identify a patient expressing the *ANK3* W1989R variant (Fig. 2.18a and b). We confirmed the presence of the variant by extracting DNA from fibroblasts derived from the proband and performing nested PCR followed by Sanger sequencing. The proband (II:2, age 45) was diagnosed with BD type I characterized by recurrent mania and depression with an age of onset of 17 years, with current successful maintenance on lithium (1200 mg daily) and a benzodiazepine (pro re nata) PRN at bedtime. The proband had a brief (<3 months) exposure to antipsychotic medication (chlorpromazine), but no history of treatment with antidepressant medication. To determine whether other family members also carried the *ANK3* W1989R variant, we expanded our studies to include the proband's parents (I:1, I:2), sister (II:1), and daughter (III:1). We extracted DNA from whole blood and performed nested PCR of the region flanking *ANK3* W1989 followed by Sanger sequencing. The proband (II:2), the mother (I:2), the sister (II:1), and the daughter were heterozygous for the *ANK3* W1989R variant (Fig. 2.18a and b). The mother (age 73) was diagnosed with BD type I with age of onset in her mid-30's. She is currently treated in the community with lamotrigine (50 mg daily), clomipramine (50 mg daily) and lorazepam (1-3 mg daily), as needed, for anxiety. Lamotrigine was given for mood stabilization. The proband's sister (age 50) was diagnosed with BD type II, with a prepubertal onset of mood instabilities and

multipleepisodes of depression and hypomania with mixed affective features. Her treatment currently includes antidepressants (fluoxetine 60 mg and buproprion 300 mg daily), an anticonvulsant (lamotrigine 400 mg daily), a stimulant (amphetamine 60 mg daily), and a hypnotic (temazepam 30 mg at bedtime). The proband's daughter (age 19) was diagnosed with major depression. The father (I:1) is WT for W1989 and has no history of depression or treatment of any psychiatric disorder (Fig. 2.18b). This is the first reported characterization of the *ANK3* W1989R human variant (c.5965T>C (p.Trp1989Arg)) (Fig. 2.18c and d). Similar to results from *Ank3* W1989R mutant mice, patients carrying the *ANK3* W1989R variant have survived into adulthood, demonstrating that this variant is compatible with normal lifespan in humans. However, the presence of the *ANK3* W1989R variant in four affected patients is consistent with a potential effect of this variant on neuronal activity and mood-related behaviors.

The individuals in the family diagnosed with BD are all heterozygous for *ANK3* W1989R variant. To test the effect of the *Ank3* W1989R variant on GABAergic circuitry in heterozygous mice, we measured sIPSCs and mIPSCs in layer II/III somatosensory cortical neurons of P30 mice. Heterozygous *Ank3* W1989R mice showed a significant reduction in sIPSC frequency (~50%) and amplitude (~40%) compared to WT mice (Fig. 2.19a, b, and e). The frequency of mIPSCs was also significantly reduced in heterozygous *Ank3* W1989R compared to WT mice, with no change in mIPSC amplitude (Fig. 2.19c, d, and f). These results show that the presence of a single copy of *Ank3* W1989R is sufficient to significantly impact inhibitory signaling in forebrain and suggest that the presence of this variant could contribute to the pathophysiology of BD.

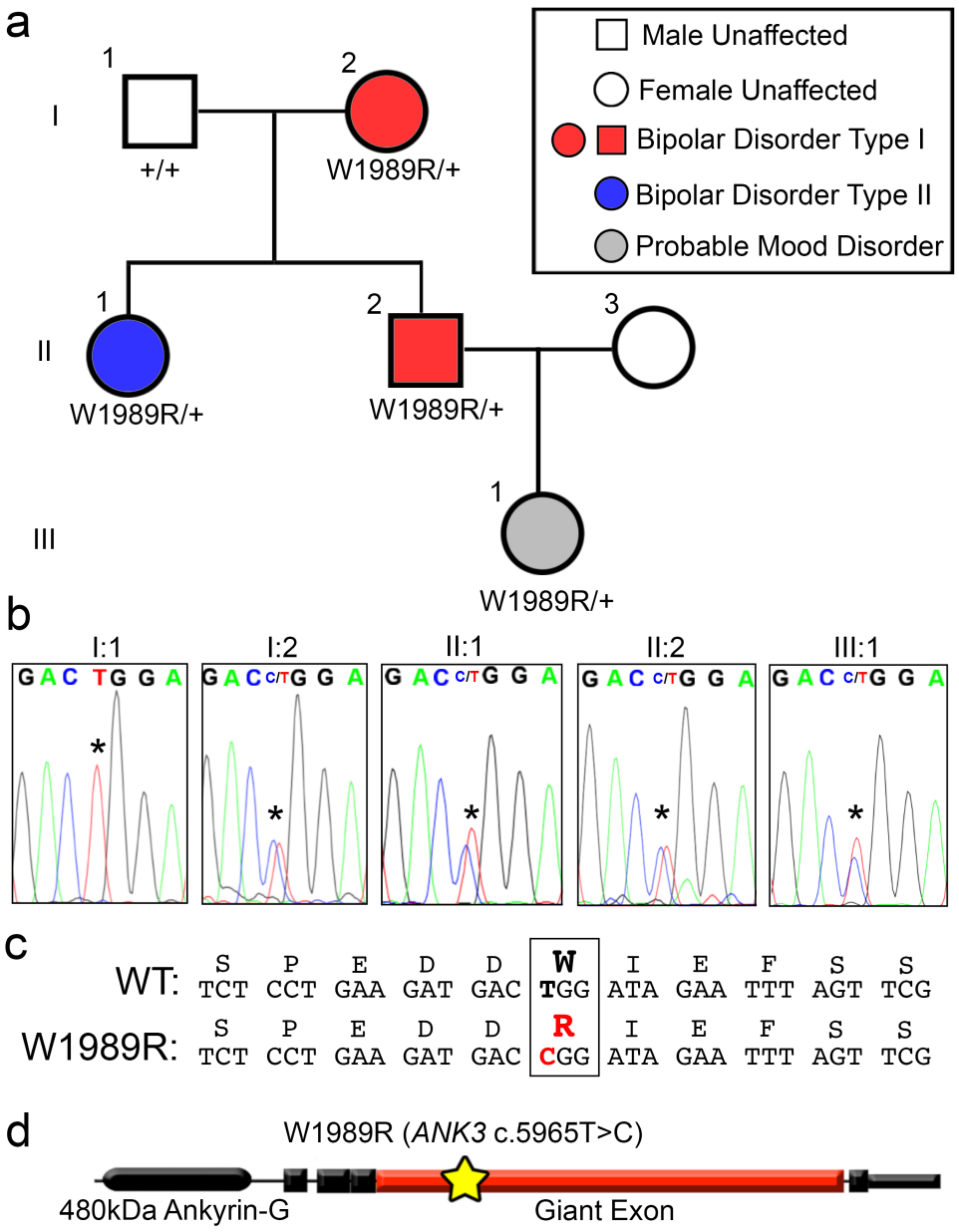

Figure 2.18: *ANK3* W1989R variant identified in a family with bipolar disorder. **(a)** Pedigree of individuals heterozygous for *ANK3* W1989R mutation diagnosed with BD. Red: diagnosis of BD type I. Blue diagnosis of BD type II. Gray: individuals with signs and symptoms of mood disorders. White: neurotypical individuals. Circles: female. Squares: male. The affected proband is individual II:2 represented by a red square. **(b)** Chromatogram from Sanger sequencing confirming presence of *ANK3* W1989R heterozygous mutation in affected mother I:2, affected proband II:2, proband's affected sister II:1, and proband's affected daughter III:1. Asterisk: site of missense mutation in affected individuals I:2, II:1, II:2, and III:1 or wild-type allele in I:1. **(c)** The nucleotide sequence alignment and single-letter amino acid translation of the coding non-synonymous heterozygous W1989R mutation. The W1989R missense mutation c.5965T>C (p.Trp1989Arg) identified in the individuals with BD is highlighted in red. **(d)** Schematic of the 480 kDa splice variant of ankyrin-G. Yellow star: site of W1989R variant (c.5965T>C)((p.Trp1989Arg)) within the giant exon (red) of ankyrin-G.

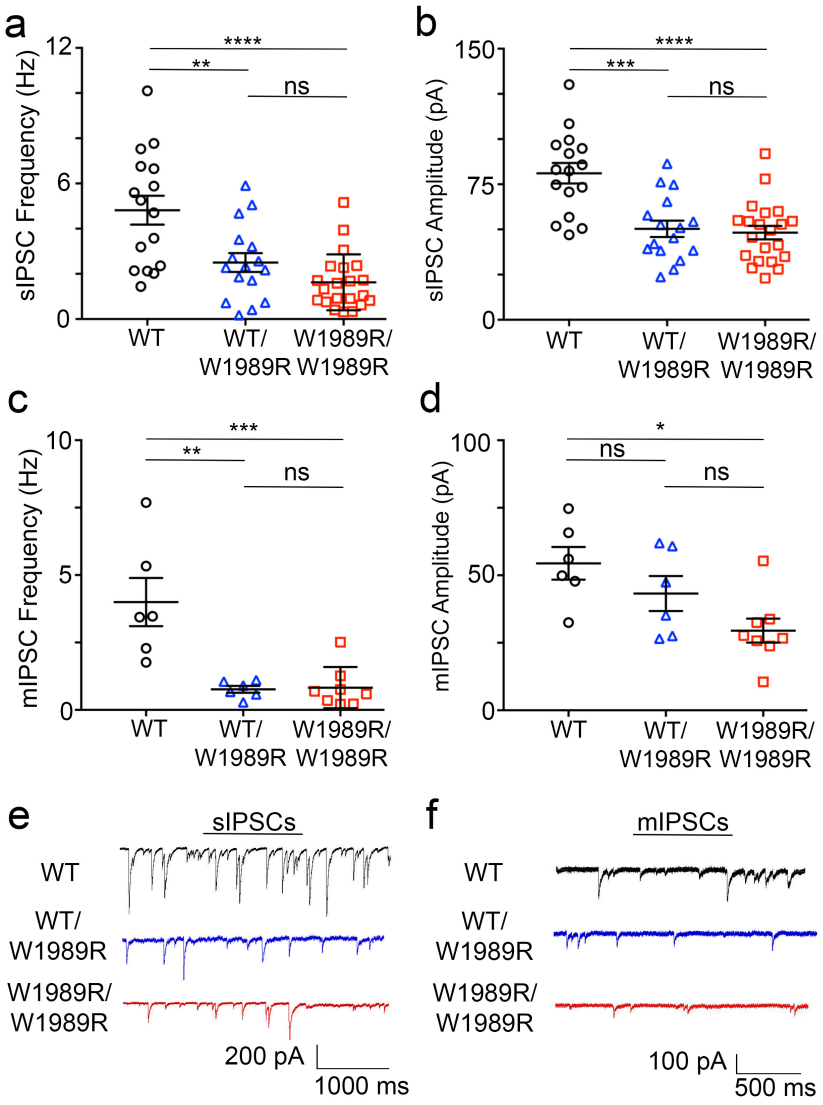

Figure 2.19: Heterozygous *Ank3* W1989R mice have reduced GABAergic synapse function. (a) Quantification of sIPSC frequency in WT (black circles), heterozygous *Ank3* WT/W1989R (blue triangles), and homozygous *Ank3* W1989R/W1989R (red squares) brain slices. *One-way ANOVA, Tukey's post hoc.* WT vs. WT/W1989R **P = 0.0023, WT vs. W1989R/W1989R ****P < 0.0001, WT/W1989R vs. W1989R/W1989R P = 0.33 (WT: n=16; WT/W1989R: n=16; W1989R/W1989R n=21). **(b)** Quantification of sIPSC amplitude in WT (black circles), heterozygous *Ank3* WT/W1989R (blue triangles), and homozygous *Ank3* W1989R/W1989R (red squares) slices. *One-way ANOVA, Tukey's post hoc.* WT vs. WT/W1989R ***P = 0.0001, WT vs. W1989R/W1989R ****P < 0.0001, WT/W1989R vs. W1989R/W1989R P = 0.94 (WT: n=16; WT/W1989R: n=16; W1989R/W1989R n=21). **(c)** Quantification of mIPSC frequency in WT (black circles), heterozygous *Ank3* WT/W1989R (blue triangles), and homozygous *Ank3* W1989R/W1989R (red squares) slices. *One-way ANOVA, Tukey's post hoc.* WT vs. WT/W1989R **P = 0.001, WT vs. W1989R/W1989R ***P = 0.0008, WT/W1989R vs. W1989R/W1989R P = 0.99 (WT: n=6; WT/W1989R: n=6; W1989R/W1989R n=8). **(d)** Quantification of mIPSC amplitude in WT (black circles), heterozygous *Ank3* WT/W1989R (blue triangles), and homozygous *Ank3* W1989R/W1989R (red squares) slices. *One-way ANOVA, Tukey's post hoc.* WT vs. WT/W1989R P = 0.38, WT vs. W1989R/W1989R *P = 0.01, WT/W1989R vs. W1989R/W1989R P = 0.21 (WT: n=6; WT/W1989R: n=6; W1989R/W1989R n=8). **(e)** Representative traces of spontaneous inhibitory postsynaptic currents (sIPSCs) of layer II/III somatosensory cortical neurons in WT (black circles), heterozygous *Ank3* WT/W1989R (blue triangles), and homozygous *Ank3* W1989R/W1989R (red squares) slices. Scale bars: 200 pA, 1000 ms. **(f)** Representative traces of miniature inhibitory postsynaptic currents (mIPSCs) from layer II/III somatosensory cortical neurons in WT (black), and *Ank3* W1989R (red) homozygous brain slices. Scale bar: 100 pA, 500 ms. Data shown as mean ± SEM.

	vGAT (+) GABAergic Synapses	Inhibitory Post-synaptic Currents	Action Potential Firing Rate	Dendritic Spine Density	AIS Length
Layer II/III Somatosensory Cortical Pyramidal Neurons	↓	↓	↑	N.D.	↓
CA1 Hippocampal Pyramidal Neurons	↓	↓	↑	↓	↓
Thalamic Neurons	—	—	N.D.	N.D.	—
Cerebellar Purkinje Neurons	—	—	N.D.	N.D.	—

Table 2.2: Summary of cell-type specific morphological and functional differences in *Ank3* W1989R mice compared to WT. Summary of results demonstrating differences in GABAergic synapse number, GABA-mediated currents, action potential firing rate, dendritic spine density, and AIS length of layer II/III cortical and hippocampal pyramidal neurons, thalamic neurons, and cerebellar Purkinje neurons in *Ank3* W1989R mice compared to WT mice. Blue arrows indicate significantly decreased from WT, red arrows indicate significantly increased from WT, line indicated no difference from WT. N.D. represents not determined.

Discussion

Neuropsychiatric diseases, such as BD and schizophrenia, are highly heritable. Significant progress has been made in the past decade identifying genetic risk factors associated with neuropsychiatric diseases including common single nucleotide polymorphisms (SNPs) through GWAS, copy number variants, and rare inherited and *de novo* variants(Goes et al. 2016). For many neurological diseases, common genetic variants have minimal impact on disease susceptibility, thus it is important to understand how rare genetic variants impact brain function and underlie the pathophysiology of neuropsychiatric disease. *ANK3* is among the most consistent and significant genes associated with BD (Harrison, Geddes, and Tunbridge 2018; Hatzimanolis et al. 2012; Leussis, Madison, and Petryshen 2012; Schulze et al. 2009); however, the mechanisms by which *ANK3* variants contribute to pathophysiology are not known. Although *ANK3* has been associated with multiple neurological disorders, the cellular and molecular mechanisms by which its loss-of-function contributes specifically to BD are poorly understood.

In this study, we generated homozygous *Ank3* W1989R knock-in mice to investigate ankyrin-G/GABARAP interactions and to understand the effects of 480 kDa ankyrin-G loss-of-function at GABAergic synapses *in vivo* (Table 2.2). We found that *Ank3* W1989R mice have reduced GABAergic synapses on the AIS and somatodendritic domain of cortical and hippocampal pyramidal neurons, while the density and function of PV+ GABAergic interneurons are maintained. Gamma oscillations were reduced in *Ank3* W1989R hippocampus, suggesting disruptions in network synchrony, consistent with reduced connectivity of PV+ interneurons. We found that AIS length and dendritic spine density and function were reduced in *Ank3* W1989R cortical and hippocampal neurons, suggesting that regulation of ankyrin-G-dependent domains may be a neuronal mechanism of homeostasis. Finally, we identified the *ANK3* W1989R variant

rs372922084 (c.5965T>C (p.Trp1989Arg)) in a family with BD, suggesting that *ANK3* W1989 is a critical residue involved in disease mechanisms in human patients.

The decrease in AIS length in *Ank3* W1989R mice may be due to neural plasticity changes, as recent reports have shown that alterations in AIS length, location, and/or ion channel surface expression may occur following fluctuations in neuronal activity in an attempt to maintain homeostasis of intrinsic excitability(Yamada and Kuba 2016). Further, we propose that the decreased dendritic spine density and function observed in *Ank3* W1989R mice may be an additional compensatory mechanism to modulate neuronal hyperexcitability. The W1989R mutation is specific to the giant exon, only included in the 270 kDa and 480 kDa splice variants of ankyrin-G, which suggests that the observed decrease in 190 kDa ankyrin-G expression may be a compensatory effect to maintain excitatory/inhibitory balance. It is possible that changes in expression levels of the 190 kDa ankyrin-G may be a common mechanism for modulating dendritic spine morphology and function to compensate for altered neuronal excitability. Future experiments will be necessary to understand the mechanisms by which genetic or pharmacological manipulation of neuronal excitability changes expression of 190 kDa ankyrin-G and dendritic spines. Further, the observed increase in mEPSC frequency may be explained by hyperexcitability of upstream glutamatergic neurons due to the decrease in inhibitory synapses.

Our work shows that the interaction between 480 kDa ankyrin-G and GABARAP is necessary for stabilizing forebrain GABAergic synapses, while additional mechanisms are involved in the formation of GABAergic synapses in the cerebellum and thalamus. Previous studies have shown that deletion of 480 kDa ankyrin-G *in vivo* results in the loss of GABAergic synapses at the AIS of cerebellar Purkinje neurons (Jenkins et al. 2015; Tseng et al. 2015). Further, a study by Ango et al. showed an ankyrin-G-dependent subcellular gradient of neurofascin-186 at

the AIS of Purkinje neurons is necessary for organizing GABAergic synapses (Ango et al. 2004). These findings suggest that, while the formation of GABAergic synapses onto the AIS of cerebellar Purkinje neurons is mediated through 480kDa ankyrin-G, this mechanism requires the clustering of neurofascin-186 and is independent of the ankyrin-G/GABARAP mechanism (Ango et al. 2004). In addition, abolishing the interaction between 480 kDa ankyrin-G and GABARAP did not affect the number or function of thalamic neuron GABAergic synapses, suggesting the formation of thalamic inhibitory synapses is mediation through an alternative mechanism than 480 kDa ankyrin-G/GABARAP. Future studies are needed to understand the postsynaptic mechanisms underlying GABAergic synapse formation in thalamic neurons. Our results demonstrate that ankyrin-G plays a critical role in stabilizing GABAergic synapses through brain region- and cell type-specific mechanisms. Furthermore, the 480 kDa ankyrin-G/GABARAP interaction is unique for stabilizing GABAergic synapses onto cortical and hippocampal pyramidal neurons.

Several mouse models have been generated to understand how *Ank3* contributes to neuronal development and function. Specific deletion of the exon encoding the giant 270- and 480 kDa isoforms of ankyrin-G results in the loss of all known AIS components, gross malformations in the morphology and total number of nodes of Ranvier, and decreased GABAergic inhibitory synapses. This genetic manipulation also results in lethality at P20, preventing the study of mature animals (Jenkins et al. 2015). A recent study generated a mouse model with forebrain-specific deletion of all splice variants of ankyrin-G (Zhu et al. 2017). These ankyrin-G conditional null mice demonstrate “mania-like” behaviors including hyperactivity, decreased anxiety and exploratory behavior, as well as depressive-like behaviors following social defeat stress (Zhu et al. 2017). The behavioral phenotypes identified in this model were rescued following administration of lithium and valproic acid (Zhu et al. 2017). Although the animals survived well

into adulthood, the loss of the AIS, nodes of Ranvier, and GABAergic synapses simultaneously made it difficult to determine which ankyrin-G-dependent domain underlies the observed behavioral phenotypes related to BD. A study by Lopez et al. showed that deletion of *Ank3* exon 1b, which affects ankyrin-G splice variants encoded by alternative first exon and N-termini splicing, results in decreased ankyrin-G expression at the AIS of PV+ interneurons (Lopez et al. 2017). These investigators found that gene dosage-dependent reductions in expression of ankyrin-G corresponded to disease severity. Heterozygous mice displayed behavioral phenotypes representative of BD, whereas homozygous mice demonstrated epilepsy and sudden death (Lopez et al. 2017). In contrast to the *Ank3* W1989R mice, which display no change in the expression of 480 kDa ankyrin-G at the AIS, *Ank3* exon 1b mice show decreased expression of ankyrin-G at the AIS of PV+ interneurons. Reduced ankyrin-G expression at the AIS results in reduced inhibitory conductance due to changes in PV+ interneuron intrinsic excitability in *Ank3* exon 1b mice compared to the loss of GABAergic connectivity as seen in the *Ank3* W1989R mice. Intriguingly, despite the differences in mechanisms, both models result in reduced inhibitory tone and altered excitation/inhibition balance. Another study compared the behaviors of *Ank3* heterozygous null mice with mice in which ankyrin-G was deleted specifically in the hippocampal dentate gyrus using short hairpin RNA (shRNA) viral vectors (Leussis et al. 2013). Both models demonstrated reduced anxiety and increased impulsivity, behavioral phenotypes related to BD (Leussis et al. 2013). These behaviors were reversed following chronic lithium treatment (Leussis et al. 2013). Taken together, these studies, along with the present work, provide evidence that *ANK3* is critical for normal brain function.

Abnormalities in excitatory/inhibitory circuit balance have been implicated in the pathophysiology of BD and schizophrenia (Benes et al. 2007; Glantz and Lewis 2000; Konopaske

et al. 2014; Lee et al. 2018; Ohgi, Futamura, and Hashimoto 2015; Penzes et al. 2013; Penzes et al. 2011). Postmortem brains of BD patients revealed decreased expression of the GABAergic synapse marker GAD_{67}, the GABA transporter GAT1, and various $GABA_A$ receptor subunits (Chattopadhyaya and Cristo 2012; Konradi et al. 2011; Lazarus, Krishnan, and Huang 2015). We found morphological and functional reductions in cortical and hippocampal GABAergic synapses in our mouse model, consistent with GABAergic dysfunction reported in patients with BD (Benes et al. 2007). Cortex and hippocampus are key brain regions associated with the cognitive, emotional, and mood-related behaviors characteristic of BD (Benes 2010). Further, abnormalities in dendritic spines have been associated with neuropsychiatric diseases including BD, schizophrenia, autism spectrum disorders, and intellectual disability (Glantz and Lewis 2000; Konopaske et al. 2014; Ohgi, Futamura, and Hashimoto 2015; Penzes et al. 2013; Penzes et al. 2011). We found reduced density and function of dendritic spines in our mouse model and proposed that these effects act to reduce hyperexcitability and compensate for the lack of inhibitory input. Previous studies have observed impairments in gamma oscillations in patients with neuropsychiatric disease, including BD and schizophrenia (Benes and Berretta 2001; Marin 2012; Schubert, Focking, and Cotter 2015; Sohal 2012; Torrey et al. 2005). Further, recent reports have suggested that gamma oscillations may serve as biomarkers for diagnosing and tracking treatment response in individuals with BD (Ozerdema et al. 2013). Consistent with these studies, we found significant decreases in hippocampal gamma oscillations in the *Ank3* W1989R mice. A study by Ozerdema et al. showed a ~35% reduction in gamma oscillations in patients with BD, which is similar in magnitude to that seen in our mouse model, suggesting that even modest defects in network synchronization can have significant clinical effects (Ozerdem et al. 2010). Thus, our cellular and functional characterization of inhibitory and excitatory synaptic dysfunction in the

Ank3 W1989R mouse model may inform the future development of novel therapeutics for the treatment of BD and other neurological diseases involving altered excitatory/inhibitory balance.

ANK3 variants have been associated with schizophrenia (Wirgenes et al. 2014), autism (Kloth et al. 2017), epilepsy (Lopez et al. 2017), and intellectual disability in addition to BD (Iqbal et al. 2013). Variants in *ANK3* may contribute to these neurological diseases by affecting ankyrin-G expression levels, disrupting protein folding, impacting specific splice variants, or preventing ankyrin-G from interacting with critical binding partners, as observed for GABARAP in the *Ank3* W1989R mouse model. Thus, it remains important to understand how disease-associated variants in *ANK3* affect ankyrin-G function and contribute to disease pathology. Although *ANK3* W1989R is a rare variant, the data reported in this work may have broader impacts on BD patients carrying other variants that reduce ankyrin-G expression. Several independent GWAS studies revealed *ANK3* BD-associated SNPs near the 5' non-coding region, which could potentially lead to altered expression levels of different isoforms of ankyrin-G (Craddock and Sklar 2009; Ferreira et al. 2008; Muhleisen et al. 2014; Schulze et al. 2009). Moreover, studies using postmortem brains from BD patients found reduced *ANK3* mRNA expression (Roussos et al. 2012; Rueckert et al. 2013) Alternatively, a recent study also identified a SNP (rs41283526) in *ANK3* with a strong protective effect against BD (Hughes et al. 2016). Consistent with the *ANK3* W1989R variant, BD-associated rare variants have been detected within alternatively spliced exons of ankyrin-G (Doyle et al. 2012). One potential explanation to describe the genetic etiology of BD is that rare variants in *ANK3* have a high penetrance due to dysfunction of the gene or encoded splice variant. Alternatively, multiple common variants with low penetrance may lead to BD due to the polygenic nature of disease inheritance. In support of this hypothesis, rare variants in several genes involved in GABAergic and glutamatergic neurotransmission as well as voltage-gated calcium channels

contribute to increased risk of BD, as they may result in similar endophenotypes as individuals with *ANK3* mutations (Ament et al. 2015). Ultimately, it will be important to continue to evaluate how patient-specific rare variants affect the expression and function of the different splice variants of ankyrin-G to provide insight on additional pathways that may contribute to BD and other neurological diseases.

Materials and Methods

Constructs, Protein Expression, and Purification: The coding sequence of the GABARAP (UniProt: Q9DCD6) construct was PCR amplified from a mouse brain cDNA library. The coding sequence of ankyrin-G construct was PCR amplified from the full-length rat 270 kDa ankyrin-G (UniProt: O70511) template. All point mutations were generated using the Quikchange II XL site-directed mutagenesis kit and confirmed by DNA sequencing. All of the constructs used for protein expression were cloned into a home-modified pET32a vector. Recombinant proteins were expressed in BL21 (DE3) *E. coli* cells with induction of 0.25 mM IPTG at 16°C. The N-terminal Trx-His_6-tagged proteins were purified using Ni^{2+}-NTA agarose affinity columns followed by size-exclusion chromatography (Superdex 200 column from GE Healthcare) in the final buffer containing 50 mM Tris-HCl, 1 mM DTT, and 1 mM EDTA, pH 7.8 with 100 mM NaCl. The Trx-His_6 tag was removed by incubation with HRV 3C protease and separated by size exclusion columns or reverse usage of Ni^{2+}-NTA columns when needed.

Crystallography: Crystallization of the ankyrin-G/GABARAP complex was performed using the sitting drop vapor diffusion method at 16 °C. Crystals of ankyrin-G/GABARAP were grown in solution containing 2.0 M ammonium citrate tribasic and 0.1 M BIS-TRIS propane buffer (pH

7.0). Crystals were soaked in crystallization solution with higher salt concentration (3 M ammonium citrate) for dehydration and cryoprotection. All datasets were collected at the Shanghai Synchrotron Radiation Facility BL17U1 or BL19U1 beamline at 100 K. Data were processed and scaled using HKL2000 or HKL3000. Structure was solved by molecular replacement using PHASER with apo form structure of GABARAP (PDB: 1KJT) as the searching model. The ankyrin-G peptide was manually built according to the F_o-F_c difference maps in COOT. Further manual model adjustment and refinement were completed iteratively using COOT and PHENIX. The final model was validated by MolProbity and statistics are summarized in Table 1. All structure figures were prepared by PyMOL (http://www.pymol.org).

Isothermal Titration Calorimetry Assay: Isothermal titration calorimetry (ITC) measurements were carried out on a VP-ITC Microcal calorimeter at 25 °C with the titration buffer containing 50 mM Tris-HCl, pH 7.8, 100 mM NaCl, 1 mM DTT, and 1 mM EDTA. For a typical experiment, each titration point was performed by injecting a 10 μL aliquot of protein sample (200 μM) into the cell containing another reactant (20 μM) at a time interval of 120 seconds to ensure that the titration peaks returned to the baseline. 27 aliquots were titrated in each individual experiment. The titration data were analyzed using the program Origin 7.0 and fitted by the one-site binding model.

Generation of W1989R Mouse Model*:* A knock-in mouse was generated by inserting the tryptophan to arginine mutation corresponding to human W1989R within the neuronal-specific giant exon of the mouse *Ank3* gene, which corresponds to exon 37 of human *ANK3*, ENST00000280772. The exon 37 plasmid contained the W1989R mutation and a neomycin

resistance cassette. The neomycin resistance cassette was flanked by LoxP sites containing flippase recognition target (FRT) sites. The linearized construct was introduced into 129S6/SvEvTac-derived TL1 embryonic stem (ES) cells by electroporation. ES cells selected for the W1989R mutation using neomycin were injected into C57BL/6NHsd blastocysts. High percentage chimeric animals were obtained and bred to C57BL/6NHsd mice to produce heterozygous animals. The neo cassette was excised by crossing with the W1989R *Ank3* mouse containing a floxed neo cassette with a Sox2-Cre mouse [B6.Cg-Tg(Sox-cre)1Amc/J, stock number 008454; The Jackson Laboratory]. Mutant mice were backcrossed for at least six generations to C57BL6/J mice from the Jackson Laboratory and were compared to C57BL/6J mice as WT controls. All mouse production was provided by the Duke Cancer Institute Transgenic Mouse Facility. All experiments were performed in accordance with the guidelines for animal care of the Institutional Animal Care and Use Committee (IACUC) and University Laboratory Animal Management (ULAM) at the University of Michigan.

Immunocytochemistry of Brain Sections: For immunohistochemistry, P30-35 mice were administered a ketamine/xylazine mixture (80 mg/kg body weight ketamine and 10 mg/kg xylazine) via intraperitoneal injection. The mice were sacrificed by cardiac perfusion of PBS followed by 4% paraformaldehyde and the brain was immediately removed and fixed overnight in 4% paraformaldehyde. The next day, the brains were processed using a standard single-day paraffin preparation protocol (PBS wash followed by dehydrations through 70, 95, and 100% ethanol with final incubations in xylene and hot paraffin under vacuum) using a Leica ASP 300 paraffin tissue processor. Paraffin sections were cut 7 μm thick using a Leica RM2155 microtome and placed on glass slides. Sections were deparaffinized and rehydrated using a standard protocol of washes: 3 × 4-min xylene washes, 2 × 2-min 100% ethanol washes, and 1 × 2-min 95%, 80%,

and 70% ethanol washes followed by at least 5 min in ddH_2O. Antigen retrieval was then conducted by microwaving the deparaffinized brain sections for 20 min in 10 μM sodium citrate. Sections were cooled, washed for 15 min in ddH_2O, rinsed in PBS for 5 min, and blocked using blocking buffer (5% BSA, 0.2% Tween 20 in PBS) for 1 hour at room temperature. Slides were incubated overnight at 4°C with primary antibodies diluted in blocking buffer. On the following day, slides were washed 3 times for 15 min with PBS containing 0.2% Tween 20, incubated with secondary antibodies diluted in blocking buffer for 1 hour at room temperature, washed 3 times for 15 min, and mounted with Prolong Gold. AIS length was measured using maximum intensity projections of z-stacks. We only quantified AISs which were entirely contained within the bounds of the Z-stack. N refers to the number of mice used in the experiment, whereas n refers to the total number of AISs measured. To measure dendritic spine density *in vivo*, we used coronal brain slices (300-350 μm thick) and filled 1-2 CA1 hippocampal neurons/slice using whole-cell patch clamp with 2% biocytin in the internal solution. The brain slices were then incubated in 4% paraformaldehyde at 4°C for 48 hours, washed 3 times for 15 min with 0.1M PBS at room , and blocked using 10% blocking serum (0.3% Triton X-100 and 10% of 5% BSA + 0.2% Tween in 0.1M PBS) for 1 hour at room temperature. The brain slices were then incubated in Streptavidin-594nm (1:1000 dilution in blocking serum) overnight at 4°C. The next day slices were washed 3 times for 15 min at room temperature, mounted on glass slides with Prolong Gold, and imaged on a Zeiss LSM 880 with a 63X NA1.4 Oil/DIC Plan-Apochromat objective and 561 nm lasers. Images were pseudocolored white.

Neuronal Culture and Transfection: Hippocampi were dissected from postnatal day 0 (P0) mice, treated with 0.25% trypsin and 100 μg/ml DNase in 2 mL HBSS with 10 mM HEPES, and then

gently triturated through a glass pipette with a fire-polished tip. The dissociated neurons were then plated on poly-D-lysine and laminin-coated 35 mm MatTek dishes in 0.5 mL of Neurobasal-A medium containing 10% (vol/vol) FBS, B27 supplement, 2 mM glutamine, and penicillin/streptomycin. On the following day, 2.5 mL of fresh Neurobasal-A medium containing 1% FBS, B27, glutamine, and penicillin/streptomycin was added to the dish. AraC was added at 1:1000 to protect against glial and fibroblast overgrowth. Plates were returned to incubation at 37°C until experimentation. To fill the cells with soluble GFP, the dissociated hippocampal cultures were transfected with eGFPN1 plasmid. Briefly, 1 μg eGFPN1 plasmid was added to 100 μl of Neurobasal-A and, in a second tube, 3 μl of Lipofectamine 2000 was added to 100 μL of Neurobasal-A. The two tubes were mixed and incubated for 15 min at room temperature. The neuronal growth media was then aspirated from the dishes and saved, the transfection was added dropwise to 14 DIV neurons, and the transfected cells were incubated at 37°C for 1 hr. The transfection mixture was aspirated and the original neuronal growth media was added. The cells were maintained in culture until 21 DIV and fixed for immunofluorescence as described below.

Immunofluorescence of Cultured Neurons: Dissociated hippocampal neurons were fixed for 15 min at room temperature with 4% paraformaldehyde, followed by methanol for 10 min at -20°C, and blocked with blocking buffer (5% BSA, 0.2% Tween 20 in PBS). Primary antibodies were diluted in blocking buffer and incubated at 4°C overnight. The following day, cells were washed 3 x 15 min with PBS containing 0.2% Tween 20, incubated with secondary antibodies diluted in blocking buffer for 1 hour at room temperature, washed 3 x 15 min, and mounted with Prolong Gold.

Confocal Microscopy: Samples were imaged on a Zeiss LSM 880 with a 63X NA1.4 Oil/DIC Plan-Apochromat objective and excitation was accomplished using 405, 488, 561, and 633 nm lasers.

In Vitro Electrophysiology Recordings and Analysis: Brains were obtained from WT C57BL/6J or *Ank3* W1989R mutant mice between P25-48. The animals were decapitated under isoflurane and USP anesthesia, the brain was then quickly removed from the skull and placed in 4°C slicing solution containing 62.5 mM NaCl, 2.5 mM KCl, 1.25 mM KH_2PO_4, 26 mM $NaHCO_3$, 5 mM $MgCl_2$, 0.5 mM $CaCl_2$, 20 mM glucose and 100 mM sucrose (pH maintained at 7.4 by saturation with O_2/CO_2, 95/5% respectively). Coronal brain slices (300-350 μm thick) containing layers II/III somatosensory cortex and hippocampus were cut with a microtome (VF-300, Compresstome). The slices were then transferred to a holding chamber and maintained at room temperature in artificial cerebrospinal fluid (ACSF) containing 125 mM NaCl, 2.5 mM KCl, 1.25 mM KH_2PO_4, 26 mM $NaHCO_3$, 1 mM $MgCl_2$, 2 mM $CaCl_2$ and 20 mM glucose, pH 7.4 (with 95%O_2 and 5%CO_2 bubbling through the solution) for at least 1 hour prior to recording. After equilibration, individual slices were transferred to the recording chamber continuously perfused with ACSF (1-2 mL/min). Recording micropipettes were pulled from borosilicate glass capillaries (1.5 mm O.D. HARVARD APPARATUS) for a final resistance of 3-6 MΩ and filled with a solution containing 135 mM K-Gluconate, 4 mM NaCl, 0.4 mM GTP, 2 mM Mg-ATP,0.5mM CaCl2, 5 mM EGTA and 10 mM HEPES. The signals were recorded with an Axoclamp 700B amplifier (Axon Instruments, Union City, CA), low pass filtered at 10 kHz. Current clamp recordings were obtained from neurons in layers II/III of somatosensory cortex, CA1 hippocampus, the thalamus, and the cerebellum; the cells in these brain regions were identified using a Nikon Eclipse FN-1 microscope with a 40X

water-immersion objective and a DAGE-MTI IR-1000 video camera. Neurons were characterized using IR-DIC to evaluate their orientation, morphology, and spiking properties. Pyramidal neurons used for action potential recordings exhibited prominent spike frequency patterns. We also recorded from fast-spiking, irregular spiking, and regular spiking non-pyramidal neurons as previously described (Cauli et al. 2000). Whole-cell patch-clamp recordings with a high cell resistance (greater than 8 GΩ before break-in) were obtained for cells according to the availability. The neurons were characterized electrophysiologically by applying negative and positive current pulses of 20 pA and 1500 ms to calculate the maximum frequency and positive pulses of 50 ms to measure the features for the single AP. For sIPSC and mIPSC recordings in voltage-clamp configuration, the K-gluconate in the internal solution was replaced by CsCl and the recordings were acquired at 2 kHz fixing the voltage at -80 mV. The IPSCs were recorded in the presence of the N-methyl-D-aspartate receptor blockers and non-N-methyl-D-aspartate glutamate receptors, AP-5 (50 mM) and CNQX (10 μM). For measurement of mIPSCs, 1 μM tetrodotoxin (TTX) was added to the superfusion to block synaptic responses dependent on the AP. Access resistance was monitored throughout the experiment and experiments were canceled if changes greater than 20% occurred. The mEPSCs were measured in the presence of bicuculline (10 μM) and TTX (1 μM) while holding the resting membrane potential at -70 mV using K-gluconate internal solution. The peak events were searched automatically using Minianalysis (Synaptosoft Inc.) and visually monitored to exclude erroneous noise. Both the frequency and amplitude of the events and their distribution were analyzed. Mean values were compared using the student's *t*-test. All data are presented as mean ± SEM.

In Vitro Kainate-Induced Oscillations: WT C57BL/6J or *Ank3* W1989R mice between P25-40 were anesthetized with isoflurane. Mice were perfused intracardially with ice cold (4°C) modified N-methy-D-glucamine (NMDG) HEPES artificial cerebrospinal fluid (aCSF) consisting of: 93 mM NMDG 2.5 mM KCl, 0.5 mM $CaCl_2$, 10 mM $MgCl_2$, 1.2 mM NaH_2PO_4, 20 mM HEPES, 25 mM dextrose, 5 mM ascorbic acid, 2mM thiourea and 3 mM Na-pyruvate. pH was maintained at 7.4 by saturation with O_2/CO_2, (95/5%, respectively). Horizontal hippocampal sections (300 μm thick) were prepared with a Leica VT1200 vibratome. Sections were bi-laterally hemisected and transferred to a holding chamber maintained at 33° C for 10-12 min, and then transferred to a holding chamber with aCSF consisting of: 126 mM NaCl, 3 mM KCl, 2 mM $CaCl_2$, 1 mM $MgCl_2$, 1.25 mM NaH_2PO_4, 25 mM $NaHCO_3$ and 10 mM dextrose. pH was maintained at 7.4 by saturating aCSF with 95%O_2/5% CO_2 at 33° C for 35 min. Sections were then transferred to room temperature for 15 min and were mounted on perforated multi-electrode array (pMEAs) (Multichannel Systems, Reutlingen, Germany). Sections were secured to the surface of the pMEA surface by using a peristaltic perfusion system (PPS2, Multichannel Systems, Reutlingen, Germany) to create a slight vacuum through the perforations. The secured sections remained submerged in aCSF (29 -31° C, 95% O_2/5CO^2%) and were superfused at a rate of 5-7 ml/min. Local field potentials were recorded at 20 kHz. Baseline recordings were obtained for 1 hour. Chemically-induced oscillations were evoked by bath application of 400 nM Kainic Acid (KA) for 1 hour. LFP data were imported into MATALAB, downsampled to 10 kHz and low pass filtered at 400 Hz for analysis. Fast Fourier Transformation (FFT) of LFP data was done in 1 sec bins to calculate the power of oscillations. Sonograms are plotted as the average power in a 2 min window and the last 2 min of each bath condition were used for further analysis. Change in oscillatory

power was defined as ($Power_{KA}$ -$Power_{aCSF}$)/$Power_{aCSF}$. Peak frequency and the area under the curve for gamma band (30 – 60 Hz) were calculated using custom written MATLAB scripts.

Western Blot: Homogenization buffer consisting of 8M urea, 5% SDS, and 5 mM N-ethylmaleimide was heated to 65°C. Whole brains were dissected from P30-35 mice and immediately frozen in liquid nitrogen. Frozen brains were then ground into a powder using a mortar and pestle. The powder was scraped into a 1.5 mL microcentrifuge tube and hand-dounced in 10 volumes/weight of 65°C homogenization buffer (i.e. 1.5 mL for 150 mg powder). The homogenate was incubated at 65°C for 20 min and then mixed 1:1 with 5× PAGE buffer (5% (wt/vol) SDS, 25% (wt/vol) sucrose, 50 mM Tris, pH 8, 5 mM EDTA, bromophenol blue). The lysates were stored at -80°C until use. The samples (10 μL-volume) were separated on a 3.5-17% gradient gel in 1X Tris buffer, pH 7.4 (40 mM Tris, 20 mM NaOAc, and 2 mM NaEDTA) with 0.2% SDS. Transfer to nitrocellulose was performed overnight at 300 mA at 4°C in 0.5X Tris buffer with 0.01% SDS. Membranes were blocked with 5% bovine serum albumin (BSA) and incubated overnight at 4°C with primary antibodies (rabbit total ankyrin-G 1:5,000) diluted in blocking buffer. Membranes were washed 3 x 15 min with TBS-T and incubated for 1 hour with LiCor fluorescent secondaries (1:50,000) in blocking buffer. Membrane were then washed 3 x 15 min in TBS-T, 1 x 5 min TBS, and 1 x 5 min in ddH_2O before being imaged on LiCor Odyssey Clx imager.

***Antibodies and Reagents*:** The following antibodies and dilutions were used: rabbit anti-βIV-spectrin (1:1000, lab-generated (Jenkins et al. 2015)), rabbit anti-total ankyrin-G (1:1000, lab-generated (Kizhatil et al. 2007)), goat anti-total ankyrin-G (1:1000, lab-generated (Jenkins et al.

2015)), rabbit anti-KCNQ2N1 (1:500 (Cooper et al. 2001)), rabbit anti-NaV (1:500, Sigma S6936), rabbit anti-neurofascin FNIII (1:500, lab generated (Davis, Lambert, and Bennett 1996)), mouse anti-NeuN (1:1000, Sigma MAB377), mouse anti-caspr (1:1000, Neuromab 75-001), guinea pig anti-vGAT (1:1000, Synaptic Systems 131004), mouse anti-$GABA_A$ receptor β2-3 (1:1000, Sigma, MAB341), mouse anti-parvalbumin (1:1000, Sigma P3088), rabbit anti-calbindin (1:1000, Swant CB-38a). Antibodies against KCNQ2 were used to label heteromeric KCNQ2/3 channels at the AIS (Cooper et al. 2001). Fluorescently conjugated secondary antibodies Alexa Fluor 488, 568, or 647 (1:250, Life Technologies) and Alexa Fluor 594-Streptavidin (1:1000, Jackson ImmunoResearch 016-580-084). The following reagents were used: FBS, Poly-D-lysine, Laminin, Paraformaldehyde, DNase, Urea, and N-ethylmaleimide were from Sigma-Aldrich. B27 supplement, GlutaMAX, Penicillin-Streptomycin, Neurobasal-A, Hank's Balanced Salt Solution, Trypsin, Hepes, Lipofectamine 2000 and Prolong Gold Antifade Reagent were from Life Technologies. Bovine serum albumin was from Gemini Bioproducts. Tween 20 was from Calbiochem.

Image acquisition and Statistical analysis: Multi-color imaging was performed as previously described using a Zeiss 880 confocal microscope (Jenkins et al. 2015). All images were further processed in Adobe Photoshop CC 2018 software. Statistical analyses were performed using Microsoft Excel and GraphPad Prism 7. A confidence interval of 95% ($P<0.05$) was required for values to be considered statistically significant. All data are presented as mean ± SEM.

Subjects, Sequencing, and Genotyping: All subjects were identified with IRB approval through the Heinz C. Prechter Bipolar Research Program at the University of Michigan. This program is

the largest privately-funded longitudinal study of BD, which monitors BD patients for ten years and beyond following an initial evaluation, bi-monthly questionnaires, and neuropsychological testing by a clinical psychiatrist. The proband (II:1) was initially identified using whole-genome and exome sequencing of blood samples from the Prechter Bipolar Genetics Repository at the University of Michigan. We confirmed the *ANK3* W1989R variant (rs372922084, c.5965T>C (p.Trp1989Arg) by extracting DNA from a fibroblast biopsy under IRB from the proband and performing a nested PCR initially using the primer pair 5'-GTAGCTGAAATGAAAGAGGACCT-3' and 5'-TCTCAGAGGTGGAAGTCCTC-3' then 5'-GATGATGAAGAACCTTTCAAAATTG-3' and 5'-GAGGCATTTTGAGTTTGTGTTC-3'. Blood was then drawn from the mother (I:2) and father (I:1) under IRB. We extracted the DNA and performed a nested PCR using the same primers listed above. DNA from the sister (II:1) was provided from the University of Michigan Central Biorepository as part of the Heinz C. Prechter Bipolar Research Program. The 500 bp PCR fragments were purified following gel electrophoresis using a gel extraction kit and sent for sequencing at the University of Michigan DNA sequencing core. All subjects reported Caucasian ancestry. The clinical data is from a detailed clinical interview using an established instrument, the Diagnostic Interview for Genetics Studies (DIGS) (Nurnberger et al. 1994). The interview was conducted by a PhD or MD level clinician and reviewed by two independent MD/PhD level faculty who had access to all available medical records, including those from treating physicians.

Data Availability: Atomic coordinates and structure factors are available from the Protein Data Bank under accession code PDB A9X (AnkG/GABARAPL).

CHAPTER 3

Ankyrin-G Mediates Homeostatic Scaling of Dendritic Spines

Summary

The ability of neurons to maintain their excitability within a proper dynamic range is fundamental for normal brain function. One homeostatic process is synaptic scaling, which is a process by which neurons scale the strength of dendritic spines to compensate for increased or decreased overall input to prevent neuronal network dysfunction. The 190 kDa ankyrin-G has been shown to be regulate spine morphology, density, and function; however, the role of the 190 kDa ankyrin-G in activity-dependent spine plasticity has not been fully elucidated. Here, we showed that *Ank3* W1989R hyperexcitable pyramidal neurons have reduced 190 kDa ankyrin-G expression in hippocampal synaptosomes and fewer dendritic spines. Re-expression with the 190 kDa ankyrin-G partially restored dendritic spine density in *Ank3* W1989R cultured neuron, suggesting a mechanistic link between 190 kDa ankyrin-G and spine scaling. Expression of the 190 kDa ankyrin-G is reduced in *Ank3* W1989R mice at the mRNA level as well as palmitoylation levels of the protein, demonstrating multiple stages of regulation in response to altered neuronal activity. We identified no change in 190 kDa ankyrin-G protein after short-term treatment (48hrs) or mRNA expression after long-term treatment (18 days) by pharmacologically inducing homeostatic scaling in WT neurons using TTX and bicuculline. However, modulating intrinsic neuron excitability with KCl resulted in reduced spine density and faster rates of 190 kDa ankyrin-G turnover. This is the

first demonstration that the 190 kDa ankyrin-G plays a role in homeostatic plasticity of dendritic spines.

Introduction

Pyramidal neurons are the main excitatory cells in the neocortex and are critical for a myriad of brain functions through the release of the neurotransmitter glutamate (Sekino, Kojima, and Shirao 2007; Spruston 2008). Glutamatergic synapses occur mainly on dendritic spines, mushroom-shaped protrusions on the dendrites characterized by the postsynaptic density (PSD). The PSD consists of a number of critically important receptors, scaffolding and trafficking proteins, and signaling pathways important for transmission of neuronal signals (Chen et al. 2011; Chen et al. 2008). Dendritic spines are highly dynamic and have the capacity to undergo rapid structural changes that affect spine shape, density, and function. Spine plasticity is important to regulate synaptic efficacy and neuronal excitability. One form of plasticity known as "Hebbian plasticity" includes long-term potentiation (LTP) and depression (LTD), which underlies synapse strengthening and weakening, and is important for learning and memory (Andersen et al. 1977; Bi and Poo 2001; Bliss and Collingridge 1993; Collingridge et al. 2010). Another mechanism of spine plasticity, referred to as "homeostatic synaptic scaling", is a compensatory form of plasticity by which neurons continuously tune the PSD to maintain neuron firing following changes in upstream input (Chowdhury and Hell 2018; Pozo and Goda 2010; Turrigiano 2008; Turrigiano and Nelson 2000). Homeostatic plasticity is achieved by upregulating (upscaling) or downregulating (downscaling) the number of functional glutamatergic AMPA receptors at the PSD, which corresponds with spine size (Chowdhury and Hell 2018). While synaptic scaling is a well-

established phenomenon, the molecular mechanisms that underlie this process in response to changes in neuronal activity are not completely understood.

Abnormalities in glutamatergic synapses and dendritic spines have been associated with multiple neuropsychiatric disorders including schizophrenia, bipolar disorder (BD), intellectual disability (ID), and autism spectrum disorder (ASD) (Garey et al. 1998; Glantz and Lewis 2000; Konopaske et al. 2014; Nimchinsky, Sabatini, and Svoboda 2002). Further, genetic studies revealed that a number of genes involved in PSD maintenance and spine plasticity are linked to neuropsychiatric disease etiology (Hall et al. 2015; Hamdan, Gauthier, Araki, Lin, Yoshizawa, Higashi, Park, Spiegelman, Dobrzeniecka, Piton, Tomitori, Daoud, Massicotte, Henrion, Diallo, Group, et al. 2011; Kirov et al. 2012; Sanders et al. 2015). Identifying the role of these implicated genes and key substrates in spine organization, function, and plasticity may significantly advance our understanding of neuropsychiatric disease pathophysiology and reveal new molecular targets for investigation.

The *ANK3* gene, which encodes the protein ankyrin-G, is associated with multiple neuropsychiatric diseases including BD (Ferreira et al. 2008; Harrison, Geddes, and Tunbridge 2018; Hatzimanolis et al. 2012; Leussis, Madison, and Petryshen 2012; Schulze et al. 2009; Stahl et al. 2019), schizophrenia (Wirgenes et al. 2014), epilepsy (Lopez et al. 2017), ID (Iqbal et al. 2013), and autism (Kloth et al. 2017). However, the mechanisms by which disease-causing mutations in *ANK3* affect protein function and/or expression and contribute to disease pathophysiology remain unknown. Alternative splicing of *ANK3* gives rise to three main classes of ankyrin-G isoforms – the canonical 190 kDa isoform, and a 270 kDa and giant 480 kDa isoform that utilize part or all of a giant, 7.8 kb exon (Bennett and Lorenzo 2013; Kordeli, Lambert, and Bennett 1995; Nelson and Jenkins 2017). These different splice variants of ankyrin-G display

distinct tissue-specific expression patterns and unique cellular functions. The 480 kDa ankyrin-G organizes the axon initial segment (AIS) and nodes of Ranvier by localizing voltage-gated sodium and KCNQ2/3 potassium channels, the cell adhesion molecule neurofascin-186, and the cytoskeletal protein βIV-spectrin (Jenkins et al. 2015). The 480 kDa ankyrin-G also stabilizes GABAergic synapses on the AIS and somatodendritic domain of cortical and hippocampal pyramidal neurons by inhibiting the endocytosis of $GABA_A$ receptors (Nelson et al. 2018; Tseng et al. 2015). The 270 kDa isoform is suggested play a role in oligodendrocyte function and the enrichment of myelin sheaths surrounding the nodes of Ranvier (Chang et al. 2014). The canonical 190 kDa isoform of ankyrin-G is found in most cell types and tissues throughout the body, and plays a central role in the localization of key signaling proteins to the cardiac intercalated disc and transverse tubule (Cunha and Mohler 2006; Lowe et al. 2008; Makara et al. 2014; Mohler et al. 2004), epithelial lateral membrane (Bennett and Healy 2009; He, Abdi, and Bennett 2014; Jenkins, He, and Bennett 2015; Kizhatil et al. 2007), and photoreceptor outer segment (Kizhatil et al. 2009).

Recent work by Smith et al. identified a neuronal role for the 190 kDa ankyrin-G in dendritic spine morphology and function (Smith et al. 2014). Specifically, the 190 kDa ankyrin-G is localized to distinct nanodomains within the spine head and neck (Smith et al. 2014). Knockdown of 190 kDa ankyrin-G in cultured cortical neurons resulted in fewer spines, reductions in spine size, and smaller miniature postsynaptic current (mEPSC) amplitude (Smith et al. 2014). In contrast, overexpression of 190 kDa ankyrin-G resulted in increased spine density, greater spine size, and larger mEPSC amplitude (Smith et al. 2014). While these findings demonstrate that the 190 kDa ankyrin-G plays a role in AMPA receptor-mediated synaptic transmission and spine morphology, how the 190 kDa ankyrin-G regulates spine density, morphology, and function in response to changes in neuronal activity has yet to be explored.

Previous work from our lab evaluated a mouse model expressing a W1989R mutation within the giant exon of ankyrin-G that abolishes the interaction between ankyrin-G and the $GABA_A$ receptor-associated protein (GABARAP) (Nelson et al. 2018). The *Ank3* W1989R variant is found within a family with BD suggesting this variant may be important to understand pathological changes of brain diseases involving altered inhibitory circuitry (Nelson et al. 2018). *Ank3* W1989R mice demonstrated a striking reduction in GABAergic synapses on the AIS and somatodendritic domain of layer II/III and CA1 hippocampal pyramidal neurons (Nelson et al. 2018). The loss of inhibitory input led to neuron hyperexcitability, shifting the balance between excitatory and inhibitory signaling (Nelson et al. 2018). Interestingly, *Ank3* W1989R mice show reduced expression of the 190 kDa ankyrin-G, with no change in 270 or 480 kDa isoforms in the cortex and hippocampus, as well as reduced dendritic spine density (Nelson et al. 2018). The W1989R mutation is specific to the giant exon, only included in the 270 kDa and 480 kDa splice variants, which suggests that the observed decrease in 190 kDa ankyrin-G expression may be a compensatory effect in an attempt to maintain excitatory/inhibitory balance by reducing dendritic spine density and function. We hypothesized that activity-dependent modulation of 190 kDa ankyrin-G regulates dendritic spine density and AMPA receptor-mediated transmission and this may be a novel intrinsic mechanism to maintain neuronal homeostasis and network balance.

Here, we investigated the role of 190 kDa ankyrin-G in homeostatic synaptic scaling in both the *Ank3* W1989R mouse model and in response to alterations in neuronal activity in wild-type (WT) neurons. We initially found the reduction in 190 kDa ankyrin-G expression in *Ank3* W1989R mouse brains occurs in synaptosomes, suggesting that the loss of 190 kDa occurs in the synapse. We demonstrated that rescue with 190 kDa ankyrin-G in *Ank3* W1989R neurons partially restored dendritic spine density, supporting a cell-autonomous role for 190 kDa ankyrin-G in

regulating spine density. The 190 kDa ankyrin-G expression is reduced in *Ank3* W1989R at the developmental time point when GABAergic synapses reach functional maturity, indicating compensatory regulation of 190 kDa ankyrin-G to maintain neuron excitability. Pharmacological manipulation of neuronal activity in WT neurons with tetrodotoxin (TTX) (promotes upscaling) and bicuculline (promotes downscaling) had no effect on ankyrin-G protein expression or mRNA levels; however, depolarization-induced downregulation of dendritic spine density with KCl (Evans et al. 2013) corresponded with reduced 190 kDa ankyrin-G expression. These findings are the first demonstration of ankyrin-G-dependent regulation of homeostatic plasticity following changes in neuronal activity and may provide insight into mechanisms of neuropsychiatric diseases.

Results

190 kDa ankyrin-G is expression is reduced in synaptosomes of *Ank3* W1989R mice

Pyramidal neurons in layer II/III somatosensory cortex and CA1 hippocampus of *Ank3* W1989R mice are hyperexcitable due to the loss of GABAergic synapse innervation on the soma and AIS (Nelson et al. 2018). GABAergic deficits have been reported to result in pathological hyperexcitability (Butt et al. 2008; Kitamura et al. 2002); however, in an attempt to reduce excitability and return to homeostasis, neurons remove AMPA receptors from the PSD and reduce spine density (O'Brien et al. 1998; Turrigiano 2011). Further, the 190 kDa ankyrin-G has been proposed to play a role in dendritic spine density and AMPA receptor-mediated transmission (Smith et al. 2014). Previous studies showed a reduction in dendritic spine density in hippocampal neurons in *Ank3* W1989R mice (Nelson et al. 2018). Further, cortical and hippocampal lysates from *Ank3* W1989R mice showed a 50% reduction in expression of 190 kDa ankyrin-G, with no

change in the 270- or 480- kDa ankyrin-G (Fig. 3.1a and c) (Nelson et al. 2018). To evaluate whether the 190 kDa ankyrin-G is reduced in the synapse, we isolated synaptosomes from WT and *Ank3* W1989R mice. Western blot analysis revealed a 50% reduction in 190 kDa ankyrin-G in synaptosomes from *Ank3* W1989R mice versus WT mice (Fig. 3.1b and d). These data demonstrate that the 190 kDa isoform of ankyrin-G is localized to synaptosomes, consistent with its reported function in dendritic spines (Smith et al. 2014). In addition, the magnitude of reduction in 190 kDa ankyrin-G protein levels in *Ank3* W1989R synaptosomes is similar to the expression changes in cortical and hippocampal lysates, which suggests that the loss of 190 kDa ankyrin-G observed in *Ank3* W1989R mice is occurring, at least in part, within the synapse.

Re-expression of 190 kDa ankyrin-G partially rescues dendritic spine density in *Ank3* W1989R neurons

To determine whether reduced 190 kDa ankyrin-G expression observed in *Ank3* W1989R synaptosomes is a homeostatic mechanism to decrease dendritic spine density, we transiently transfected 190 kDa ankyrin-G-GFP into *Ank3* W1989R cultured hippocampal neurons and compared spine density versus WT and *Ank3* W1989R neurons filled with soluble GFP. *Ank3* W1989R neurons showed a 65% reduction in dendritic spine density versus WT neurons (Fig. 3.2a and b). Rescue with 190 kDa ankyrin-G-GFP partially restored dendritic spine density in *Ank3* W1989R neurons (Fig. 3.2a and b). These findings demonstrate that the 190 kDa ankyrin-G plays a role in dendritic spine density and suggests the 190 kDa ankyrin-G is being modulated to decrease neuronal excitability to homeostasis.

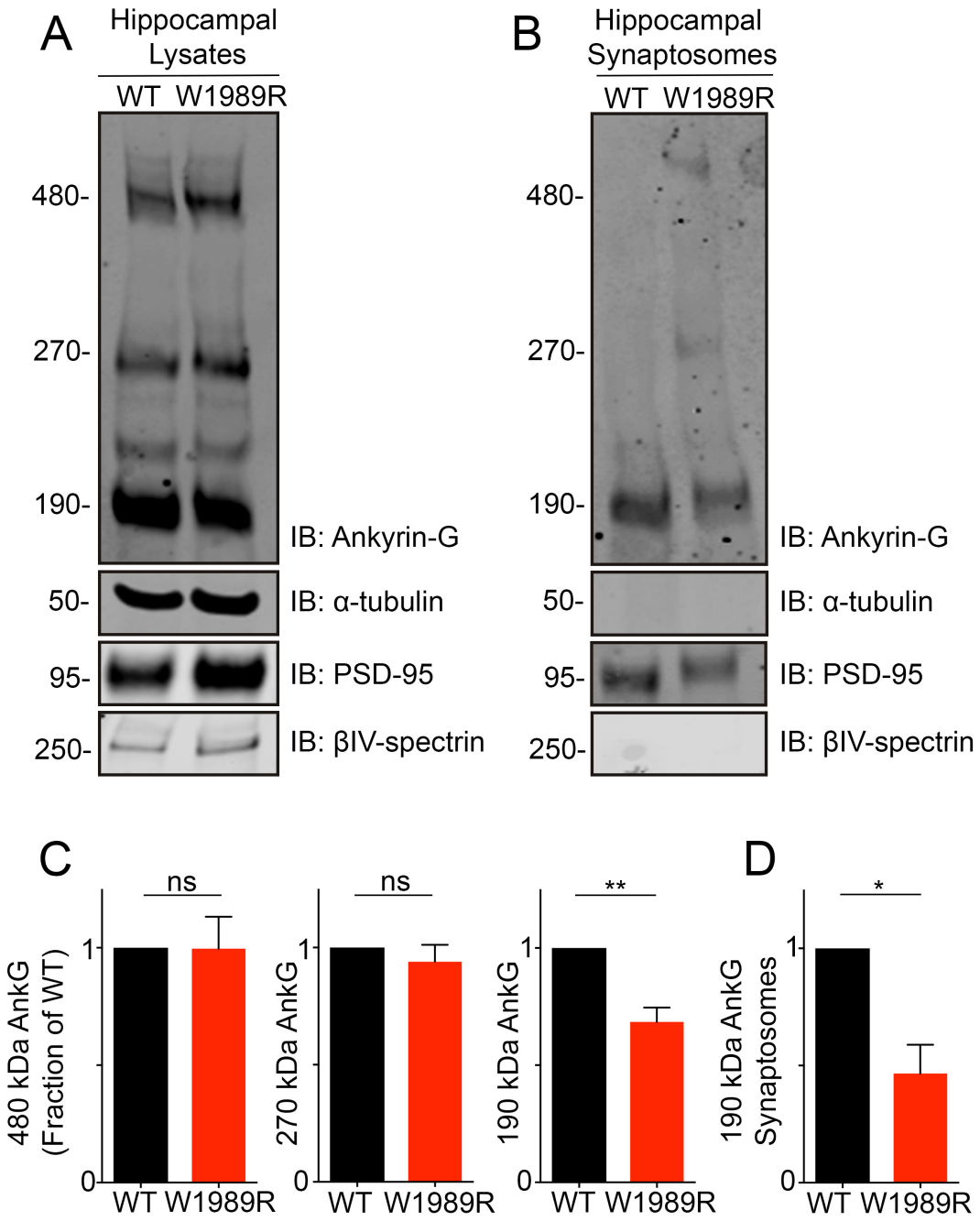

Figure 3.1: 190 kDa ankyrin-G expression is reduced in synaptosomes of *Ank3* W1989R hippocampal lysates. (a) Western blot analysis from hippocampal lysates of P30 WT (left) and *Ank3* W1989R homozygous (right) mice. Blots were probed with antibodies to total ankyrin-G and α-tubulin, PSD-95, and βIV-spectrin. **(b)** Western blot analysis from synaptosome lysates of P30 WT (left) and *Ank3* W1989R homozygous (right) mice. Blots were probed with antibodies to total ankyrin-G, PSD-95, βIV-spectrin, and α-tubulin. **(c)** Quantification of (a) relative expression levels of 480 kDa ankyrin-G *t-test* P = 0.98 (WT: 1.0 ± 0.0, N=3; W1989R: 0.99 ± 0.1, N=3), 270 kDa ankyrin-G *t-test* P = 0.45 (WT: 1.0 ± 0.0, N=3; W1989R: 0.94 ± 0.1, N=3), and 190 kDa ankyrin-G *t-test* **P = 0.0066 (WT: 1.0 ± 0.0, N=3; W1989R: 0.68 ± 0.1, N=3). Data normalized to WT controls. **(d)** Quantification of (b) relative expression levels of 190 kDa ankyrin-G from synaptosomes. *t-test* **P = 0.012 (WT: 1 ± 0.0, N=3; W1989R: 0.47 ± 0.12, N=3). Data normalized to WT controls. Data shown as mean ± SEM.

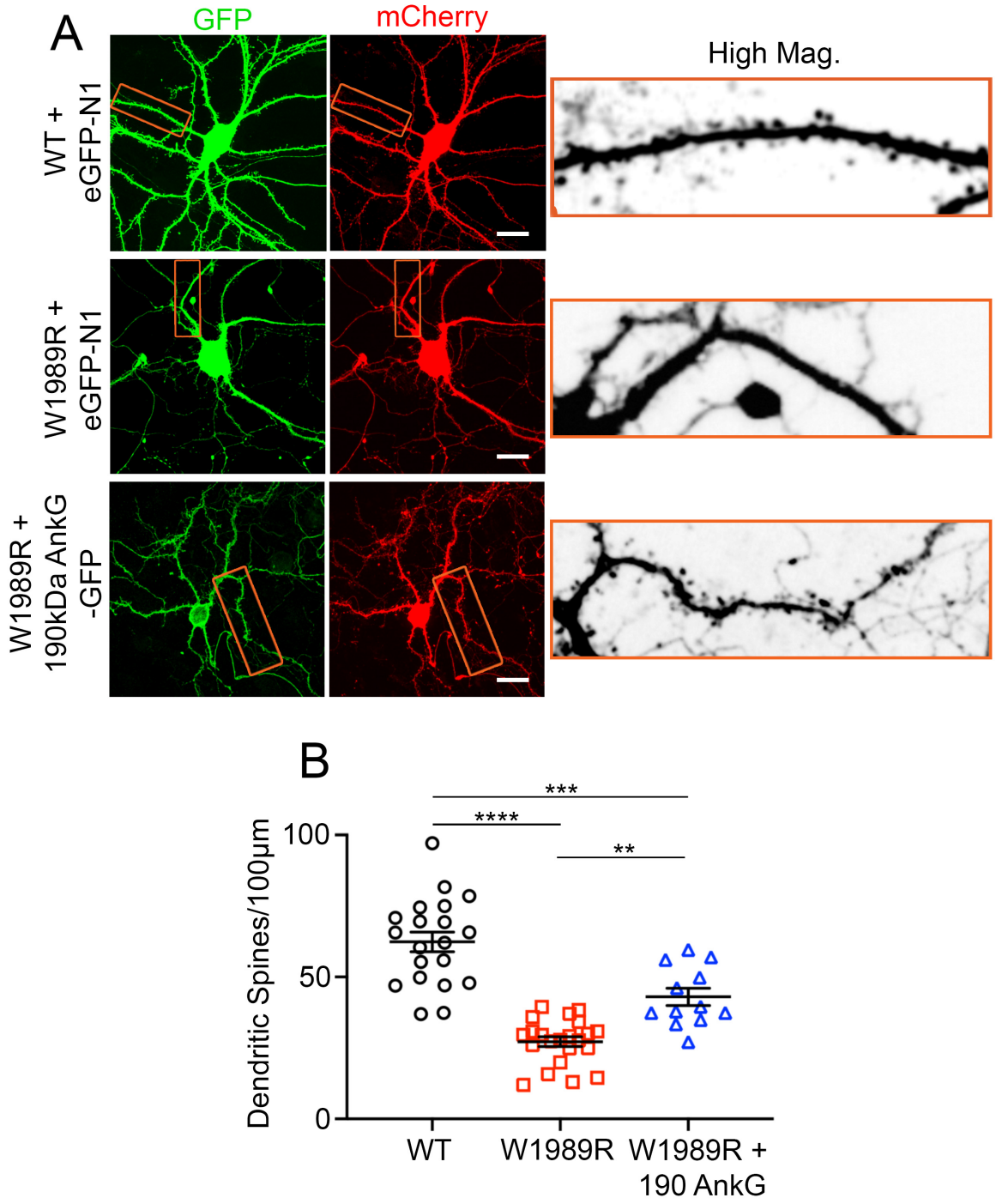

Figure 3.2: Dendritic spine density is partially rescued in *Ank3* W1989R cultured hippocampal neurons by 190 kDa ankyrin-G. (a) Representative images of dissociated cultured hippocampal neurons at 21 DIV from WT (top) and *Ank3* W1989R homozygous mice (middle/bottom). Neurons filled with soluble GFP or 190 kDa ankyrin-G shown in green and mCherry shown in red. High magnification images (right) of orange rectangles from mCherry-filled images. Scale bar: 20 µm. **(b)** Quantification of the total number of dendritic spines per 100 µm per neuron. *One-way ANOVA*, *Tukey's multiple comparisons test* ****P < 0.0001, ***P = 0.0001, **P = 0.0014 (WT: 62.39 ± 3.5, N=3, n=20; W1989R: 27.21 ± 1.7, N=3, n=22; W1989R + 190 kDa ankyrin-G-GFP: 42.99 ± 3.0 N=3, n=13). Data shown as mean ± SEM.

Ank3 W1989R mice have reduced transcription and palmitoylation of 190 kDa ankyrin-G

Decreased 190 kDa ankyrin-G expression observed in the *Ank3* W1989R mice could be due to changes in gene expression, changes in translation, or post-translational modifications to the protein. Gene products that play a role in synaptic plasticity can be controlled through activity-dependent transcriptional regulation (Ibata, Sun, and Turrigiano 2008; Mao et al. 2018). In fact, a number of molecules involved in homeostatic synaptic scaling display altered expression patterns upon increased neuronal activity (Mao et al. 2018). Chronic excitability of *Ank3* W1989R neurons could lead to reduced 190 kDa ankyrin-G expression by modulating transcription of 190 kDa ankyrin-G mRNA. To test this, total RNA was extracted from the hippocampus of P30 WT and *Ank3* W1989R mice and qRT-PCR was performed on the three main splice variants of ankyrin-G as well as GAPDH as a loading control. The expression of the 190 kDa *Ank3* mRNA levels was decreased approximately 50% in *Ank3* W1989R mice compared to WT mice, whereas there was no change in the expression levels of the 270- and 480 kDa ankyrin-G isoforms (Fig. 3.3a). This is consistent with the previous findings of 50% reduction on 190 kDa ankyrin-G protein in *Ank3* W1989R cortical and hippocampal lysates and synaptosomes, suggesting a possible role for transcriptional regulation of activity-dependent expression of 190 kDa *Ank3* mRNA in response to neuronal hyperexcitability.

Post-translational modifications of the 190 kDa ankyrin-G could provide an additional level of regulation of spine density and function. Palmitoylation is a common mechanism for regulating a large number of synaptic proteins, including PSD-95 and AMPA receptors, by promoting protein stability, trafficking, and localization to the PSD in an activity-dependent manner (Fukata et al. 2015; Jeyifous et al. 2016; Kaur et al. 2016). Ankyrin-G is membrane-associated through *S*-palmitoylation, the reversible addition of a 16-carbon fatty acid palmitate, to

the cysteine 70 residue (C70) within the ANK repeats domain (He, Abdi, and Bennett 2014; He, Jenkins, and Bennett 2012). Further, mutation of the C70 residue to alanine prevents association of 190 kDa ankyrin-G with the membrane and renders ankyrin-G completely non-functional in epithelial cells and neurons (He, Jenkins, and Bennett 2012; Tseng et al. 2015). We evaluated palmitoylation of 190 kDa ankyrin-G in *Ank3* W1989R mice using acyl resin-assisted capture (acyl-RAC) (Fig. 3.3b). After normalizing to basal expression levels of 190 kDa ankyrin-G in the starting material, we identified a ~65% reduction in palmitoylation of the remaining 190 kDa ankyrin-G in *Ank3* W1989R mice compared to WT (Fig. 3.3c). *S*-palmitoylation of ankyrin-G is necessary for its targeting and function to the membrane and domain biogenesis. Removal of the palmitate from ankyrin-G in *Ank3* W1989R neurons would be expected to dissociate ankyrin-G from the membrane and potentially degraded to reduce spine size and density. Taken together, these findings suggest ankyrin-G may be regulated at multiple levels, including gene expression changes and post-translational modifications, to regulate dendritic spines in response to changes in neuronal excitability.

Reduced 190 kDa ankyrin-G expression corresponds with GABAergic synapse development

Our data demonstrate a reduction in 190 kDa ankyrin-G in synaptosomes of P30 *Ank3* W1989R mice (Fig. 1b and d). These changes may be compensatory to normalize neuronal activity following the loss of inhibitory tone. GABAergic synapses being to develop between 3-8 DIV with $GABA_A$ receptors first appearing at the postsynaptic membrane (Kato-Negishi et al. 2004). This is followed by emergence of the pre-synaptic GABAergic marker GAD_{65} at 14 DIV and fully functional GABAergic synapses at 21 DIV (Kato-Negishi et al. 2004; Swanwick et al. 2006).

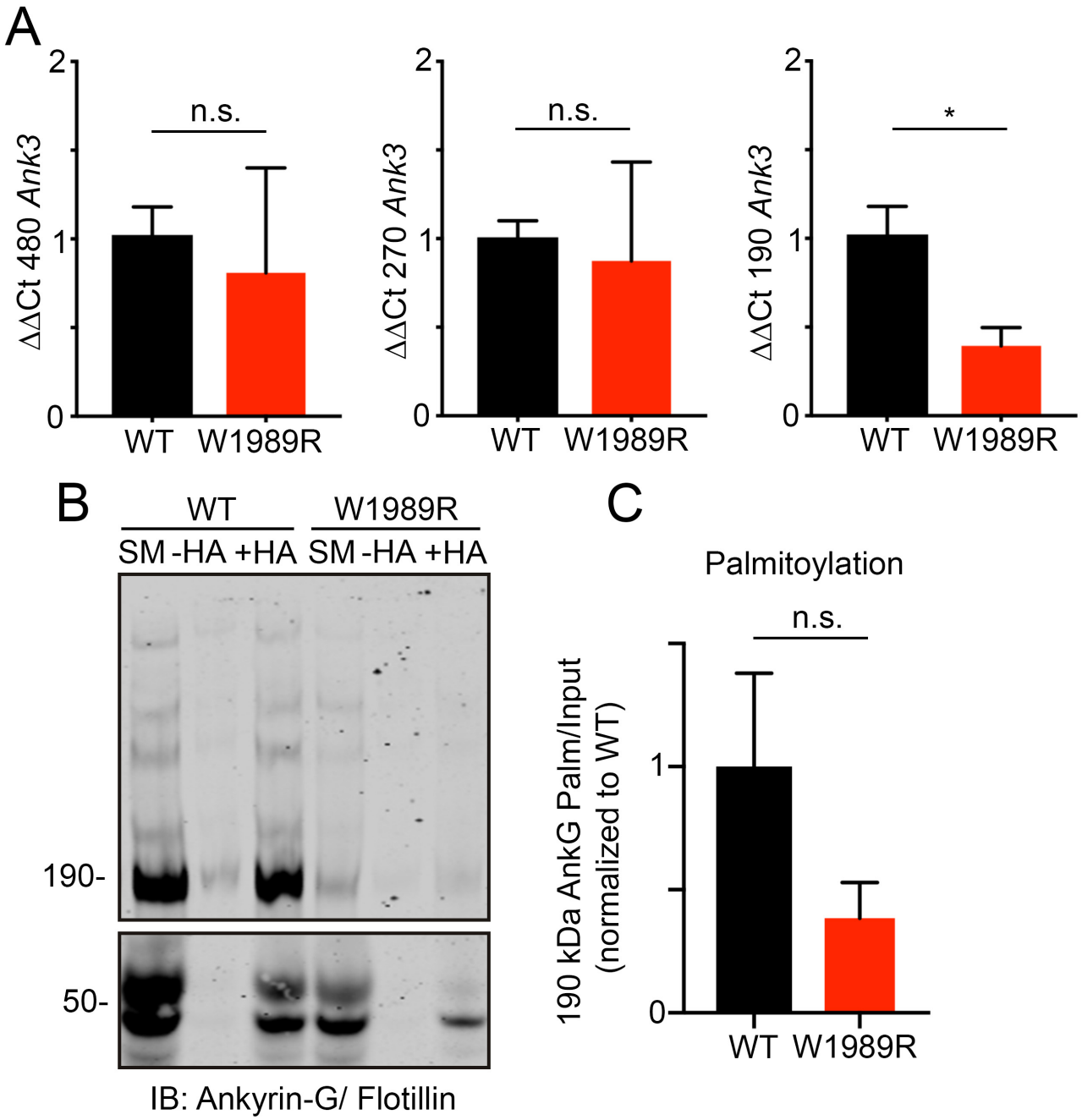

Figure 3.3. Decreased 190 *Ank3* mRNA expression and palmitoylation levels in *Ank3* W1989R mice. (a) qRT-PCR analysis of P30 cortex showing relative transcripts levels of WT (black) and *Ank3* W1989R (red) for 480 kDa ankyrin-G *t-test* P = 0.75 (WT: 1.023 ± 0.2, N=3; W1989R: 0.81 ± 0.6, N=3), 270 kDa ankyrin-G *t-test* P = 0.83 (WT: 1.008 ± 0.1, N=3; W1989R: 0.87 ± 0.6, N=3), 190 kDa ankyrin-G *P = 0.03 (WT: 1.023 ± 0.2, N=3; W1989R: 0.39 ± 0.1, N=3) after normalization to GAPDH as the internal control. Data normalized to WT controls. Data shown as mean ± SEM. **(b)** Western blot analysis of acyl rac of P30 WT and *Ank3* W1989R mice showing starting material (SM), -HA, and +HA samples. **(c)** Quantification of (b) relative 190 kDa ankyrin-G palmitoylation levels (+HA – (-HA))/(SM) and normalized to WT controls: *t-test* P = 0.2 (WT: 1.0 ± 0.4, N=3; W1989R: 0.39 ± 0.2, N=3). Data shown as mean ± SEM.

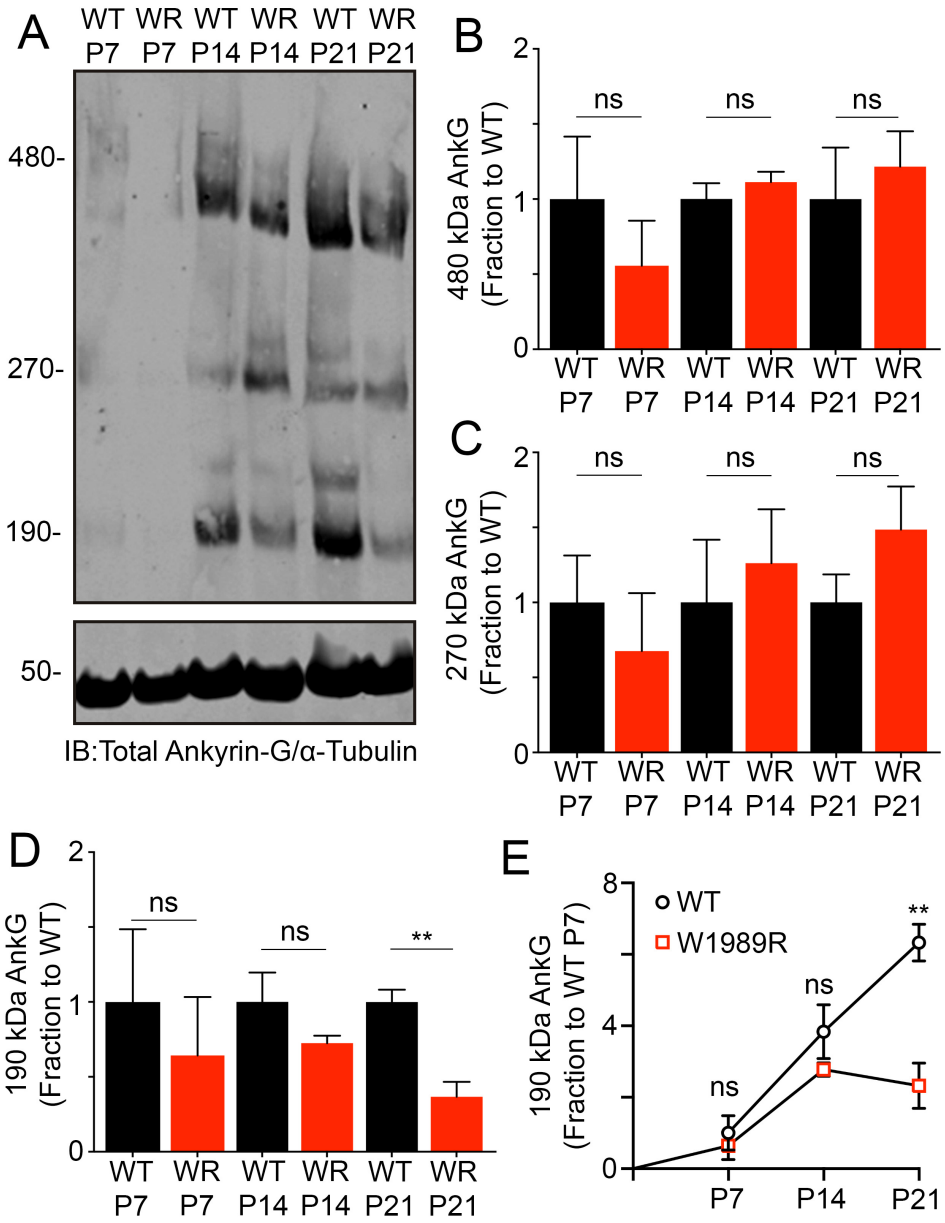

Figure 3.4. 190 kDa ankyrin-G expression is reduced at time of GABAergic synapse maturity in *Ank3* W1989R mice. (a) Western blot analysis from cortical lysates of WT and *Ank3* W1989R homozygous mice at P7, P14, and P21. Blots were probed with antibodies against total ankyrin-G and α-tubulin. **(b)** Quantification of (a) relative expression levels of 480 kDa ankyrin-G at P7: *t-test* P = 0.44 (WT: 1.0 ± 0.4, N=3; W1989R: 0.56 ± 0.3, N=3), P14: *t-test* P = 0.42 (WT: 1.0 ± 0.1, N=3; W1989R: 1.11 ± 0.1, N=3), and P21: *t-test* P = 0.63 (WT: 1.0 ± 1.2, N=3; W1989R: 1.2 ± 0.2, N=3). Data normalized to WT controls at each age. **(c)** Quantification of (a) relative expression levels of 270 kDa ankyrin-G at P7: *t-test* P = 0.55 (WT: 1.0 ± 0.3, N=3; W1989R: 0.68 ± 0.4, N=3), P14: *t-test* P = 0.66 (WT: 1.0 ± 1.3, N=3; W1989R: 1.0 ± 0.4, N=3), and P21: *t-test* P = 0.23 (WT: 1.0 ± 0.2, N=3; W1989R: 1.5 ± 0.3, N=3). Data normalized to WT controls at each age. **(d)** Quantification of (a) relative expression levels of 190 kDa ankyrin-G at P7: *t-test* P = 0.6 (WT: 1.0 ± 0.5, N=3; W1989R: 0.64 ± 0.4, N=3), P14: *t-test* P = 0.25 (WT: 1.0 ± 0.2, N=3; W1989R: 0.73 ± 0.1, N=3), and P21: *t-test* **P = 0.008 (WT: 1.0 ± 0.1, N=3; W1989R: 0.36 ± 0.1, N=3). **(e)** Quantification of (a) relative expression levels of 190 kDa ankyrin-G across development. Data normalized to P7 WT for each group. P7: *t-test* P = 0.6 (WT: 1.0 ± 0.5, N=3; W1989R: 0.6 ± 0.4, N=3), P14: *t-test* P = 0.25 (WT: 3.8 ± 0.8, N=3; W1989R: 2.8 ± 0.2, N=3), P21: *t-test* **P = 0.008 (WT: 6.3 ± 0.5, N=3; W1989R: 2.3 ± 0.6, N=3). Data shown as mean ± SEM.

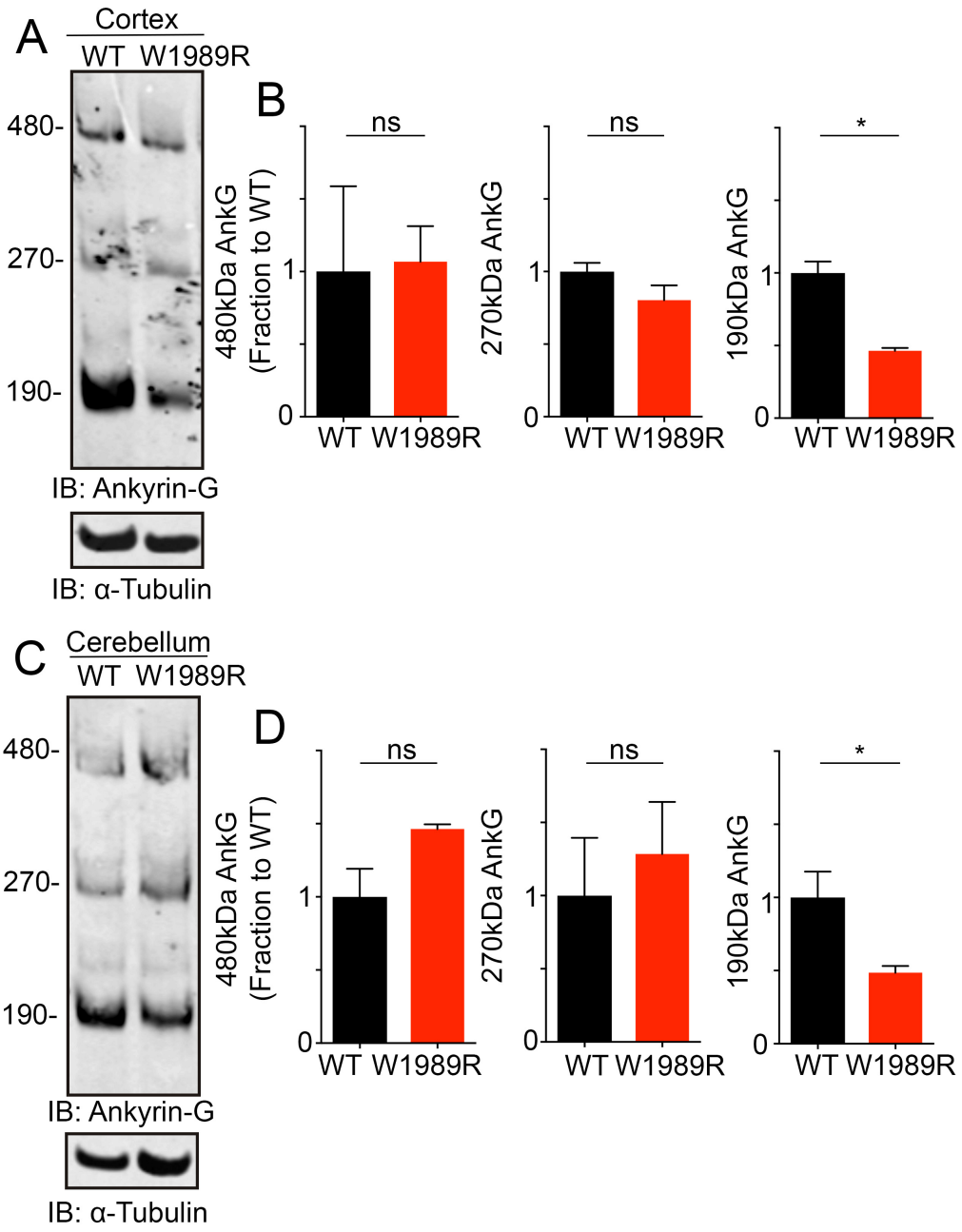

Figure 3.5. ***Ank3*** **W1989R mice demonstrate decreased 190 kDa ankyrin-G expression in cortex and cerebellum. (a)** Western blot analysis from cortical lysates of P30 WT (left) and *Ank3* W1989R homozygous (right) mice. Blots were probed with antibodies against total ankyrin-G and α-tubulin. **(b)** Quantification of (a) relative expression levels of cortical 480 kDa ankyrin-G *t-test* P = 0.92 (WT: 1.0 ± 0.6, N=3; W1989R: 1.07 ± 0.2, N=3), 270 kDa ankyrin-G *t-test* P = 0.17 (WT: 1.0 ± 0.1, N=3; W1989R: 0.80 ± 0.2, N=3), and 190 kDa ankyrin-G *t-test* **P = 0.0026 (WT: 1.0 ± 0.8 N=3; W1989R: 0.46 ± 0.02, N=3). Data normalized to WT controls. **(c)** Western blot analysis from cerebellum lysates of P30 WT (left) and *Ank3* W1989R homozygous (right) mice. Blots were probed with antibodies against total ankyrin-G and α-tubulin. **(d)** Quantification of (a) relative expression levels of cerebellar 480 kDa ankyrin-G *t-test* P = 0.16 (WT: 1.0 ± 0.2, N=3; W1989R: 1.46 ± 0.03, N=3), 270 kDa ankyrin-G *t-test* P = 0.62 (WT: 1.0 ± 0.4, N=3; W1989R: 1.29 ± 0.4, N=3), and 190 kDa ankyrin-G *t-test* **P = 0.0026 (WT: 1.0 ± 0.2, N=3; W1989R: 0.49 ± 0.04, N=3). Data normalized to WT controls. Data shown as mean ± SEM.

The number of functional synapses increases gradually from 7 DIV to 14 DIV and becomes mature at 21 DIV in cultured cortical and hippocampal neurons (Kato-Negishi et al. 2004; Swanwick et al. 2006) and *in vivo* at P21 in mice (Insel 2010). If reduction in 190 kDa ankyrin-G expression was in response to decreased GABAergic synaptic function, one would expect that 190 kDa ankyrin-G would be normal in *Ank3* W1989R mice prior to formation of fully functional GABAergic synapses, then reduced at P21 to adapt for hyperexcitability. To test this, we evaluated ankyrin-G expression levels in the cortical lysates at P7, P14, and P21 in *Ank3* W1989R mice versus WT. Western blot analysis revealed no change in the 270- or 480- kDa ankyrin-G in *Ank3* W1989R versus WT mice all tested developmental ages (Fig. 3.4a, b, and C). Levels of 190 kDa ankyrin-G are similar between *Ank3* W1989R and WT mice at P7 and P14; however, the expression of 190 kDa ankyrin-G is significantly reduced by P21 in *Ank3* W1989R mice (Fig. 3.4a, d, and e). These data demonstrate 190 kDa ankyrin-G protein levels are similar in *Ank3* W1989R mice compared to WT controls early in development; however, consistent with an attempt at homeostatic plasticity, 190 kDa ankyrin-G protein levels are significantly reduced at P21, at the time when GABAergic synapses are reaching maturity.

Expression of 190 kDa ankyrin-G is reduced in multiple brain regions of *Ank3* W1989R mice

Previous work demonstrated the loss of GABAergic synapse connectivity and function in layer II/III somatosensory cortex and CA1 hippocampus leading to pyramidal cell hyperexcitability (Nelson et al. 2018). In contrast, 480 kDa ankyrin-G-dependent pinceau synapses at the AIS and somatodendritic GABA synapses on Purkinje neurons in the cerebellum as well as GABAergic synapses onto thalamic neurons are unaffected in *Ank3* W1989R mice (Nelson et al. 2018). We hypothesize that the changes in expression of 190 kDa ankyrin-G modulates spine

density and function to compensate for hyperexcitability caused by the lack of GABAergic synapses. Since GABAergic synapses are maintained in the cerebellum of *Ank3* W1989R mice, we expected expression of 190 kDa ankyrin-G would be unchanged. Surprisingly, western blot analysis of *Ank3* W1989R cerebellum lysates demonstrated a 50% reduction in expression of 190 kDa ankyrin-G compared to WT cerebellum lysates, but no change in the 270- or 480- kDa ankyrin-G isoforms (Fig. 3.5c and d). These changes in 190 kDa ankyrin-G expression in the cerebellum of *Ank3* W1989R mice are consistent with changes identified in the cortex (Fig. 3.5a and b) and hippocampus (Fig. 3.1a and b). These findings indicate that there may be altered neuronal excitability and changes in 190 kDa ankyrin-G expression in brain regions outside the forebrain *in Ank3* W1989R mice, such as the cerebellum, perhaps due to functional and spatial interactions between the hippocampus and the cerebellum (Yu and Krook-Magnuson 2015).

Pharmacological induction of homeostatic scaling with bicuculline and TTX did not affect 190 kDa ankyrin-G expression in WT neurons

Our data demonstrate that 190 kDa ankyrin-G regulates dendritic spine density and mEPSC amplitude likely to compensate for hyperexcitability in *Ank3* W1989R neurons that exhibit reduced inhibitory tone (Fig. 3.2a and b) (Nelson et al. 2018). We hypothesized that 190 kDa ankyrin-G modulates spine density and function through homeostatic synaptic scaling. Multiple studies have mimicked homeostatic AMPA receptor upscaling in cultured neurons by treating with TTX, which blocks voltage-gated sodium channels and decreases neuronal activity,

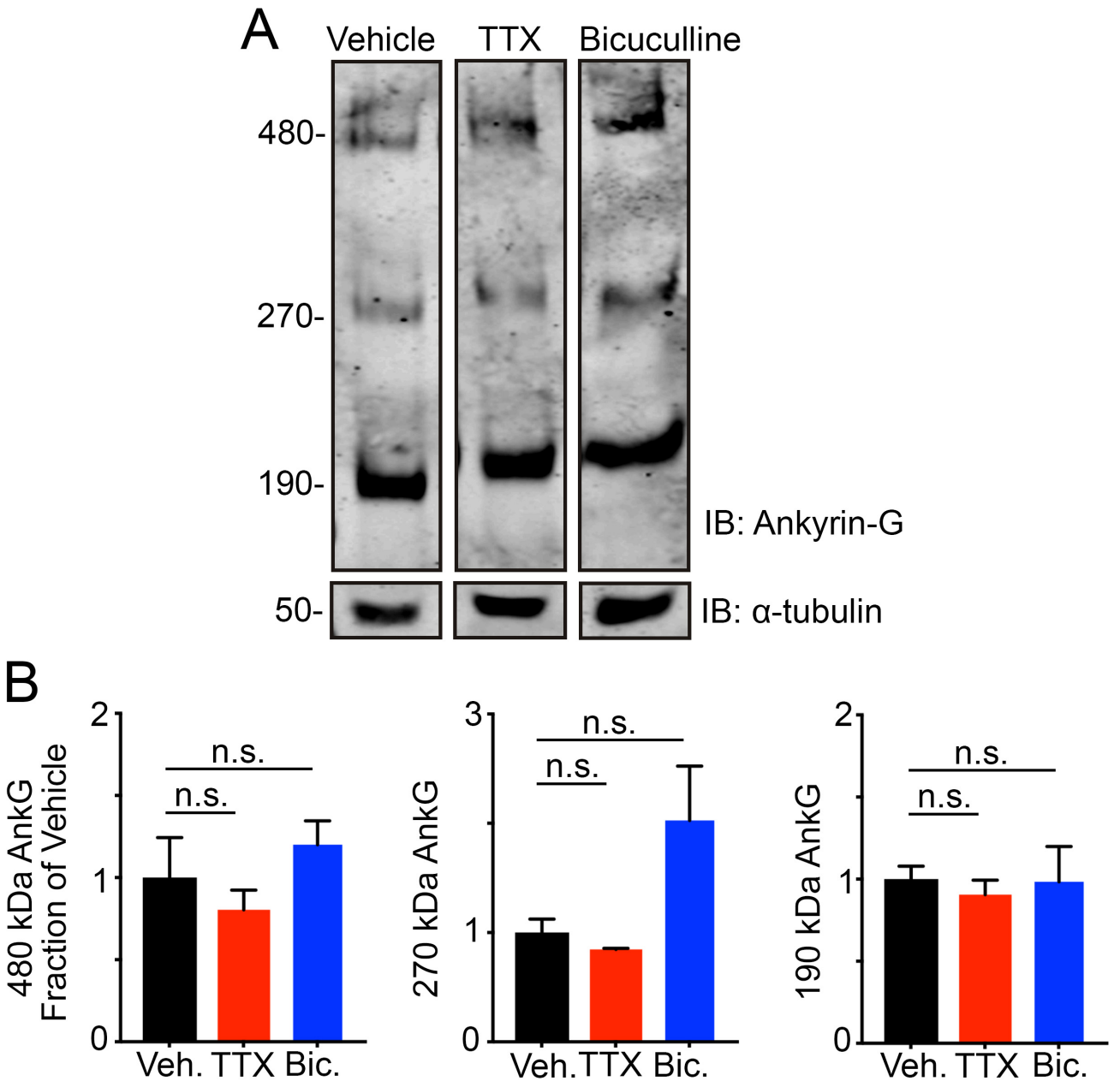

Figure 3.6. Acute pharmacological manipulation of neuron excitability with TTX and bicuculline had no effect on ankyrin-G expression in WT cultured neurons. (a) Western blot analysis of cultured WT hippocampal neurons at 21 DIV treated with vehicle (ddH_2O) (left), 1 μM TTX (middle), or 40 μM bicuculline (right) for 48hrs. Blots were probed with antibodies against total ankyrin-G and α-tubulin. **(b)** Quantification of (a) relative expression levels of 480 kDa ankyrin-G *t-test* P = 0.51 (vehicle: 1.0 ± 0.2, n=3; TTX: 0.8 ± 0.1, n=3), P = 0.52 (vehicle: 1.0 ± 0.3, n=3; bicuculline: 1.2 ± 0.2, n=3), 270 kDa ankyrin-G *t-test* P = 0.29 (vehicle: 1.0 ± 0.1, n=3; TTX: 0.85 ± 0.01, n=3), P = 0.12 (vehicle: 1.0 ± 0.1, n=3; bicuculline: 2.0 ± 0.5, n=3), and 190 kDa ankyrin-G *t-test* P = 0.47 (vehicle: 1.0 ± 0.1, n=3; TTX: 0.91 ± 0.1, n=3), P = 0.95 (vehicle: 1.0 ± 0.1, n=3; bicuculline: 0.98 ± 0.2, n=3). Data normalized to WT controls. Data shown as mean ± SEM.

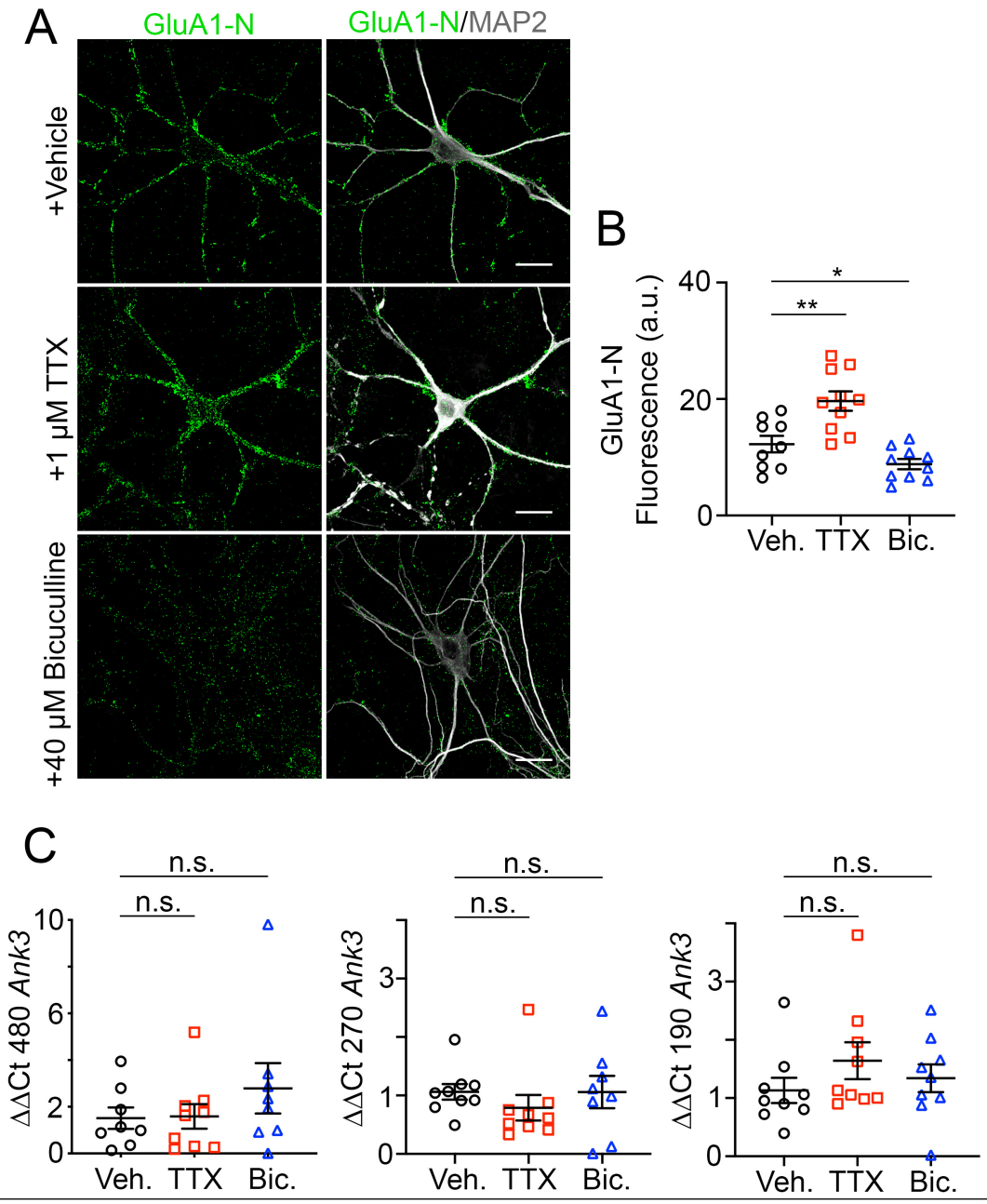

Figure 3.7: Homeostatic scaling with TTX and bicuculline did not affect *Ank3* mRNA expression levels in WT cultured neurons. (a) Representative images of dissociated hippocampal neurons at 21 DIV from WT mice treated with vehicle (ddH_2O) (top), 1 µM TTX (middle), or 40 µM bicuculline (bottom) every 5 days for 18 days. Surface GluA1-N is shown in green and MAP2 is shown in white. Scale bar: 20 µm. **(b)** Quantification of fluorescence intensity of surface GluA1 per neuron between vehicle and TTX: *t-test* **P = 0.004 (vehicle: 12.27 ± 1.4, n=9; TTX: 19.64 ± 1.7, n=10) and vehicle and bicuculline: *t-test* *P = 0.049 (vehicle: 12.27 ± 1.4, n=9; bicuculline: 8.83 ± 0.9, n=10) **(c)** qRT-PCR analysis of 21 DIV cultured hippocampal neurons from WT mice treated with vehicle (ddH_2O) (black), 1 µM TTX (red), or 40 µM bicuculline (blue) every 5 days for 18 days showing relative transcripts levels for 480 kDa ankyrin-G *t-test* P = 0.92 (vehicle: 1.52 ± 0.5, n=8, N=3; TTX: 1.59 ± 0.5, n=9, N=3), P = 0.3 (vehicle: 1.52, n=8, N=3; bicuculline: 2.79 ± 1.1, n=8, N=3), 270 kDa ankyrin-G *t-test* P = 0.3 (vehicle: 1.06 ± 0.1, n=9, N=3; TTX: 0.79 ± 0.2, n=9, N=3), P = 0.99 (vehicle: 1.06 n=9, N=3; bicuculline: 1.06 ± 0.3, n=8, N=3), 190 kDa ankyrin-G *t-tes*t P = 0.2 (vehicle: 1.13 ± 0.2, n=9, N=3; TTX: 1.64 ± 0.3, n=9, N=3), P = 0.53 (vehicle: 1.13 ± 0.2, n=9, N=3; bicuculline: 1.34 ± 0.2, n=9, N=3). Data normalized to GAPDH as the internal control. Data shown as mean ± SEM.

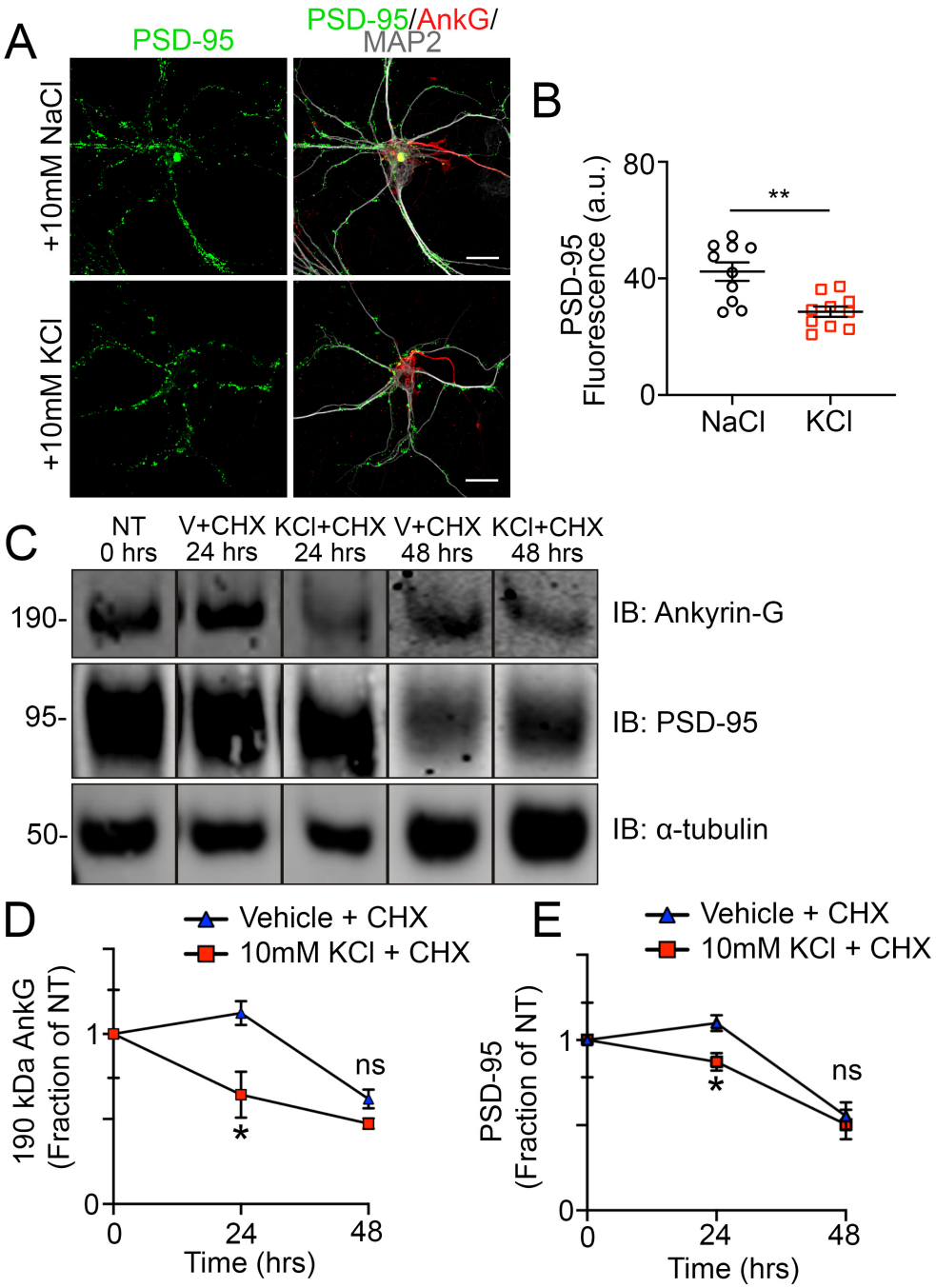

Figure 3.8. Chronic neuron depolarization with KCl leads fewer PSD-95 puncta and reduced 190 kDa ankyrin-G expression. **(a)** Representative images of dissociated hippocampal neurons at 21 DIV from WT mice treated with 10 mM NaCl (top) or 10 mM KCl (bottom) for 48 hrs. Immunostaining for PSD-95 (green), total ankyrin-G (red) and MAP2 (white). Scale bar: 20 µm. **(b)** Quantification of PSD-95 puncta intensity per neuron. *t-test* **P = 0.0013 (NaCl: 42.33 ± 3.17, n=10; KCl: 28.58 ± 1.8, n=10). **(c)** Western blot analysis of cultured hippocampal lysates at 21 DIV with no treatment (NT) or treated with vehicle (V) (ddH_2O) + cycloheximide (CHX) or KCl + CHX at 24 or 48 hrs. **(d)** Quantification of (c) relative expression levels of 190 kDa ankyrin-G at 24 hrs *t-test* *P = 0.03 (vehicle + CHX: 1.1 ± 0.1, n=3; KCl + CHX: 0.64 ± 0.14, n=3); 48hrs *t-test* P = 0.08 (vehicle + CHX: 0.62 ± 0.1, n=3; KCl + CHX: 0.47 ± 0.03, n=3). **(e)** Quantification of (c) relative expression levels of PSD-95 at 24 hrs *t-test* *P = 0.03 (vehicle + CHX: 1.1 ± 0.1, n=3; KCl + CHX: 0.87 ± 0.1, n=3); 48hrs *t-test* P = 0.7 (vehicle + CHX: 0.55 ± 0.1, n=3; KCl + CHX: 0.5 ± 0.1, n=3). Data normalized to NT controls. Data shown as mean ± SEM.

or bicuculline, which is a $GABA_A$ receptor antagonist that increases neuronal excitability (Rabinowitch and Segev 2008; Turrigiano et al. 1998; Wierenga, Ibata, and Turrigiano 2005). TTX induces scaling-up by increasing surface localization of functional GluA1-containing AMPA receptors and spine size, whereas stimulating activity with bicuculline leads to downscaling (Gainey et al. 2009; Turrigiano et al. 1998). To determine if 190 kDa ankyrin-G plays a role in homeostatic synaptic scaling, we treated WT cultured hippocampal neurons at 21 DIV with vehicle, 1 μM TTX, or 40 μM bicuculline for 48 hrs. Given the proposed role of ankyrin-G in regulation of spine size and density, we expected synapse upscaling with TTX would result in elevated 190 kDa ankyrin-G expression after 48 hr treatment and downscaling with bicuculline would have the opposite effect and downregulate 190 kDa ankyrin-G. However, western blot analysis revealed no change 190 kDa ankyrin-G expression following TTX or bicuculline treatment compared to vehicle controls (Fig. 3.6a and b). In addition, there was no change in expression of the 270- or 480- kDa isoforms (Fig. 3.6a and b), suggesting manipulating neuronal activity with TTX or bicuculline does not affect expression any of the ankyrin-G splice variants after 48 hr treatment. However, additional studies need to be conducted to evaluate scaling of AMPA receptors simultaneously with ankyrin-G protein levels following 48 hrs treatment.

To directly assess whether long-term homeostatic scaling of AMPA receptors was regulated by ankyrin-G, we treated cultured WT hippocampal neurons with vehicle, 1 μM TTX, or 40 μM bicuculline every 5 days for 18 days until 21 DIV. We initially examined surface GluA1 levels and found TTX treated neurons exhibited greater GluA1 surface levels when compared to vehicle treated neurons, whereas bicuculline treated neurons exhibited lower GluA1 levels (Fig. 3.7a and b). In contrast to GluA1 surface levels, 190 kDa *Ank3* mRNA levels were not significantly changed following long-term TTX or bicuculline treatment versus vehicle as well as no change in

the expression levels of the 270- and 480 kDa *Ank3* isoforms (Fig. 3.7c). These data suggest pharmacological induction of homeostatic scaling in WT neurons does not affect *Ank3* mRNA expression; however, follow-up experiments should be performed to evaluate changes in ankyrin-G protein expression under these conditions. Thus, 190 kDa ankyrin-G may play an important role in dendritic spine density and function, but perhaps not continuous tuning of AMPA receptor-mediated plasticity following changes in neuronal activity.

Depolarization-induced neuronal activity reduced spine density and 190 kDa ankyrin-G turnover

We next wanted to determine whether other forms of manipulating intrinsic excitability, such as chronic depolarization, affected overall spine density and 190 kDa ankyrin-G expression. Chronic depolarization by KCl has been reported to cause activity-dependent reductions in dendritic spine density (Evans et al. 2013). We treated WT cultured hippocampal neurons with 10 mM KCl and, consistent with previous reports, found a ~30% reduction in PSD-95 fluorescence intensity as compared to neurons treated with 10 mM NaCl (Fig. 3.8a and b) (Evans et al. 2013). To directly examine 190 kDa ankyrin-G protein turnover following depletion of dendritic spines, we treated WT cultured rat hippocampal neurons at 21 DIV with 10 mM KCl and 100 μg/ml cycloheximide (CHX), a protein synthesis inhibitor, for 48 hrs. Western blot showed the levels of 190 kDa ankyrin-G were reduced ~50% after 24 hrs KCl + CHX treatment compared to vehicle + CHX treated neurons (Fig. 3.8c and d). The increase in 190 kDa ankyrin-G turnover corresponded with a reduction in PSD-95 expression at 24 hrs (Fig. 8c and e). After 48hrs, expression levels of 190 kDa ankyrin-G and PSD-95 in vehicle + CHX treated neurons equaled protein levels of KCl + CHX. This is likely because the cultures contain non-neuronal cells such as astrocytes, which

also express 190 kDa ankyrin-G or due to labile pools of 190 kDa ankyrin-G within the neuron. These data demonstrate that a non-synaptic approach of elevated intrinsic neuron activity with KCl increases the rate of 190 kDa ankyrin-G and PSD-95 turnover in cultured WT hippocampal neurons. These findings are consistent with our hypothesis that 190 kDa ankyrin-G is being degraded at a greater rate following sustained depolarization with KCl treatment to reduced dendritic spine density and maintain homeostasis of neuronal excitability.

Discussion

Maintaining the balance between excitation and inhibition is critical for normal function of neuronal networks. This balance is maintained by modulating intrinsic neuron excitability, synaptic strength, and synapse connectivity. Homeostatic synaptic plasticity mechanisms have been shown to stabilize neuron firing rates through a negative feedback response to compensate for changes in neuronal activity (Chowdhury and Hell 2018; Turrigiano and Nelson 2000). The 190 kDa ankyrin-G has been shown to be regulate spine morphology, density, and function (Smith et al. 2014); however, the role of 190 kDa ankyrin-G in activity-dependent spine plasticity is not completely understood. The *Ank3* W1989R mouse model exhibits cortical and hippocampal pyramidal neuron hyperexcitability, decreased 190 kDa ankyrin-G expression, and fewer dendritic spines (Nelson et al. 2018). In this study, we investigated the role of 190 kDa ankyrin-G in homeostatic synaptic scaling to modulate dendritic spine density and function following changes in neuronal activity. We provide evidence that *Ank3* W1989R mice have reduced 190 kDa ankyrin-G expression in hippocampal synaptosomes and re-expression of 190 kDa ankyrin-G partially restored dendritic spine density in *Ank3* W1989R cultured hippocampal neurons. Expression of the 190 kDa ankyrin-G is reduced in *Ank3* W1989R mice due to changes in transcription as well

as less palmitoylation of the protein, presumably rendering it nonfunctional within the spines. We identified no change in 190 kDa ankyrin-G protein or mRNA expression after pharmacologically inducing homeostatic scaling in WT neurons using TTX and bicuculline after short term (48 hrs) or long-term treatment (18 days). However, chronic depolarization of WT neurons with KCl resulted in reduced spine density and increased rate of 190 kDa ankyrin-G turnover, suggesting 190 kDa ankyrin-G plays a critical role in regulating dendritic spine density following changes in neuronal activity.

Our data showed re-expression of 190 kDa ankyrin- G in *Ank3* W1989R mice restored dendritic spine density, suggesting a mechanistic link between reduced 190 kDa ankyrin-G expression and spine density in the *Ank3* W1989R mouse model. These findings demonstrate the 190 kDa ankyrin-G may play a role in homeostatic synaptic scaling to maintain proper neuronal firing. However, the big question that still remains is whether the change in 190 kDa ankyrin-G expression and subsequently spine density normalizes neuron spiking frequency within physiological range. The frequency of action potential (AP) firing is higher in cortical and hippocampal pyramidal neurons from *Ank3* W1989R mice compared to WT (Nelson et al. 2018). In fact, the maximum firing rate per neuron is approximately two-fold greater in *Ank3* W1989R neurons (Nelson et al. 2018). Interestingly, *Ank3* W1989R mice have no obvious behavioral seizure activity (Nelson et al. 2018), perhaps because the neurons compensate for extreme pathological excitability by reducing 190 kDa ankyrin-G expression, dendritic spine density and mEPSC amplitude. Future studies should be conducted to evaluate the spiking property and mEPSCs of *Ank3* W1989R cortical and hippocampal neurons following re-expression of 190 kDa ankyrin-G, which would be expected to return neuron firing rates to a “pre-homeostatic scaling state”. This will allow us to determine the degree by which 190 kDa ankyrin-G scales dendritic

spines and action potential firing frequency in an attempt to maintain homeostasis of neuronal excitability.

Several synaptic components have been shown to regulate the number of AMPA-type glutamate receptors in the PSD in homeostatic scaling. The majority of these molecules are scaffolding proteins, kinases, and phosphatases that directly affect synapse function. These include Arc, GRIP1, PICK1, and PSD-95, as well as protein kinase A (PKA), Ca^{2+}/calmodulin-dependent protein kinase II (CAMKII), and calcineurin (Anggono, Clem, and Huganir 2011; Kim et al. 2007; Kim and Ziff 2014; Oh et al. 2006; Opazo et al. 2010; Shepherd et al. 2006; Tan, Queenan, and Huganir 2015). Our results implicate the 190 kDa ankyrin-G as another regulator of dendritic spines in the *Ank3* W1989R model of hyperexcitability and following chronic depolarization with KCl in WT neurons. Although many molecular mechanisms contribute to synaptic scaling, they all appear to regulate either AMPA receptor trafficking or stabilization of the PSD. A major question that remains is whether all of these components are simultaneously involved in AMPA receptor scaling or whether these molecules operate at distinct phases of spine plasticity in response to different timescales (chronic vs. acute) and intensities in neuronal activity. The latter seems more plausible as some molecular components are involved in only the upscaling phase, the downscaling phase, or both (Chowdhury and Hell 2018). The molecular mechanisms underlying specificity of these molecular events on AMPA receptor plasticity is unclear. Our data show that 190 kDa ankyrin-G protein or mRNA does not respond to TTX or bicuculline treatment. However, although this is a widely accepted method for inducing scaling in WT neurons, future studies need to be performed to evaluate whether 48 hr treatment with TTX and bicuculline changes in AMPA receptor surface localization in our own hands and if this corresponds with altered ankyrin-G expression levels. Chronic depolarization of WT neurons with KCl resulted in a faster rate of 190

kDa ankyrin-G turnover (~50% at 24 hrs) and subsequently reduced PSD-95 labeling within spines. Furthermore, 190 kDa ankyrin-G expression is reduced in the *Ank3* mouse model of hyperexcitability, which correspond to changes in overall dendritic spine density. Taken together, one possible explanation is that 190 kDa ankyrin-G plays a role in overall dendritic spine density, rather than acute changes in AMPA receptor surface levels, under more intense and longer periods of elevated excitability. Our data demonstrate that the190 kDa ankyrin-G downscales dendritic spines in *Ank3* W1989R hyperexcitable neurons; however, the role of 190 kDa ankyrin-G in synaptic upscaling of hypoexcitable neurons is unclear and should be tested in future studies.

Our data suggest that expression of 190 kDa ankyrin-G in *Ank3* W1989R mice is possibly due to reductions in 190 kDa *Ank3* mRNA expression and/or palmitoylation levels of 190 kDa ankyrin-G, which would presumably impact 190 kDa ankyrin-G localization within the spine. The change in 190 kDa *Ank3* mRNA expression is consistent with previous reports highlighting the critical role of activity-dependent transcriptional and translational machineries involved in homeostatic synaptic scaling. Specifically, studies have identified approximately 46 genes as regulators of homeostatic up- and downscaling in hippocampal and cortical neurons (Mao et al. 2018). Further work is needed to is determine the mechanisms involved in 190 kDa *Ank3* mRNA expression changes following altered neuronal activity, such as histone modifications and chromatin regulatory genes. We cannot rule out the possibility that the addition of loxP sites flanking the neo cassette used to generate *Ank3* W1989R mice affects alternative splicing of 190 kDa ankyrin-G. This may explain the decrease in 190 kDa ankyrin-G expression observed in all brain regions, even in regions such as the cerebellum that showed no change in mIPSC frequency or amplitude; however, this seems unlikely as we observed no change in levels of the giant 270- and 480 kDa isoforms. While previous studies found no change in GABAergic synapse function

on Purkinje neurons in the cerebellum (Nelson et al. 2018), the role of the 190 kDa ankyrin-G in spine morphology, maintenance, and function has yet to be explored in these cells. In addition, while previous studies showed no change in mIPSC frequency or amplitude (Nelson et al. 2018), they did not evaluate intrinsic membrane properties or mEPSCs of Purkinje neurons in the cerebellum or thalamic neurons. There is increasing recognition of crosstalk between the hippocampus and cerebellum, in regards to structural connections as well as functional influence from one region to the other (Yu and Krook-Magnuson 2015). It is possible that the changes in inhibitory tone, action potential firing frequency, and dendritic spines observed in *Ank3* W1989R CA1 hippocampal neurons affect excitability and ankyrin-G expression in the cerebellar Purkinje neurons. Future work will be necessary to determine whether the reduction in 190 kDa ankyrin-G expression is due to elevated excitability of Purkinje neurons. Overall, a number of neurodevelopmental disorders have been linked to altered activity-regulated transcription of multiple signaling proteins, indicating that these pathways are critical for cognitive development and function (West and Greenberg 2011).

Activity-dependent palmitoylation regulates the localization and function of many synaptic proteins, most notably PSD-95, SynDig1, GRIP1, and AMPA receptors (Fukata et al. 2015; Han et al. 2015; Hayashi, Rumbaugh, and Huganir 2005; Kaur et al. 2016; Thomas et al. 2012), consistent with reduced palmitoylation levels of 190 kDa ankyrin-G in *Ank3* W1989R brain. Changes in 190 kDa ankyrin-G palmitoylation would be expected to remove 190 ankyrin-G from the membrane within the spine, causing decreased spine density and AMPA receptor function. *S*-palmitoylation is controlled by palmitoyl acyl transferases (PATs), whereas palmitoyl thioesterases catalyze the depalmitoylation of proteins. It would be expected that increased activity of palmitoyl thioesterases in response to hyperexcitability in *Ank3* W1989R neurons underlies the

observed reduction in 190 kDa ankyrin-G palmitoylation levels. Future studies should investigate the palmitoyl thioesterase activity in *Ank3* W1989R neurons, most notably palmitoyl-protein thioesterase-1 (PPT1), acyl-protein thioesterase-1 (APT1) and acyl-protein thioesterase-2 (APT2), and the family of alpha beta hydrolase domain (ABHD) thioesterases, to determine the mechanism of ankyrin-G removal from spine and the degree and time scale by which this occurs. Palmitate turnover on PSD-95, for example, is regulated by neuronal activity (el-Husseini Ael and Bredt 2002; Yokoi et al. 2016). Therefore, additional studies should evaluate palmitoylation levels of 190 kDa ankyrin-G after KCl compared to rates of ankyrin-G depalmitoylation with ankyrin-G turnover at the spines. Understanding the dynamic turnover of ankyrin-G palmitoylation may provide a key mechanism for rapidly changing synaptic strength. Since numerous proteins involved in spine plasticity are regulated by palmitoylation and given that palmitoylation is reversible, PATs and palmitoyl thioesterases could be potential therapeutic targets to restore dendritic spine abnormalities observed in neurological and neuropsychiatric diseases (Penzes et al. 2011).

Previous reports showed the 190 kDa ankyrin-G contributes to LTP-induced spine plasticity using a chemical LTP protocol that promotes rapid activation of NMDA receptors, causing increased spine area and density (Smith et al. 2014). Thus, it is possible that 190 kDa ankyrin-G plays a role in Hebbian plasticity (LTP/LTD), which drives positive feedback processes such as strengthening/weakening of spines, and homeostatic scaling, which is a negative feedback response to maintain homeostatic neuronal activity. The relationship between homeostatic plasticity versus Hebbian plasticity is poorly understood. The effect of LTP on ankyrin-G may be secondary to ankyrin's role in homeostatic scaling or these may be two independent processes. Additional studies will be necessary to tease this apart. Homeostatic adaptation for changes in

neuronal excitability is required to maintain neuronal output in a proper range, but homeostatic scaling must be accomplished without erasing information encoded by Hebbian signaling (Davis and Bezprozvanny, 2001; Turrigiano and Nelson, 2004).

In summary, our findings suggest the 190 kDa ankyrin-G controls dendritic spine density in a homeostatic manner. Mutations in *ANK3* have been associated with numerous neuropsychiatric and neurological disorders. A better understanding ankyrin-G's function and regulated expression in different neuronal domains, such as dendritic spines, may provide insight to molecular mechanisms of disease.

Materials and Methods

Generation of W1989R Mouse Model*:* A knock-in mouse was generated by inserting the tryptophan to arginine mutation corresponding to human W1989R within the neuronal-specific giant exon of the mouse *Ank3* gene, which corresponds to exon 37 of human *ANK3*, ENST00000280772 as previously described (Nelson et al. 2018). Mutant mice were backcrossed for at least six generations to C57BL6/J mice from the Jackson Laboratory and were compared to C57BL/6J mice as WT controls. All mouse production was provided by the Duke Cancer Institute Transgenic Mouse Facility. All experiments were performed in accordance with the guidelines for animal care of the Institutional Animal Care and Use Committee (IACUC) and University Laboratory Animal Management (ULAM) at the University of Michigan.

Neuronal Culture and Transfection: Hippocampi were dissected from postnatal day 0 (P0) mice, treated with 0.25% trypsin and 100 μg/ml DNase in 2 mL HBSS with 10 mM HEPES, and then

gently triturated through a glass pipette with a fire-polished tip. The dissociated neurons were then plated on poly-D-lysine and laminin-coated 35 mm MatTek dishes in 0.5 mL of Neurobasal-A medium containing 10% (vol/vol) FBS, B27 supplement, 2 mM glutamine, and penicillin/streptomycin. On the following day, 2.5 mL of fresh Neurobasal-A medium containing 1% FBS, B27, glutamine, and penicillin/streptomycin was added to the dish. AraC was added at 1:1000 to protect against glial and fibroblast overgrowth. Plates were returned to incubation at 37°C until experimentation. Dissociated hippocampal cultures were transfected with soluble eGFPN1 or 190 kDa ankyrin-G-GFP and empty pLentilox 3.7-mCherry. 1 μg of DNA total (500 ng/plasmid) was added to 100 μl of Neurobasal-A and, in a second tube, 3 μl of Lipofectamine 2000 was added to 100 μL of Neurobasal-A. The two tubes were mixed and incubated for 15 min at room temperature. The neuronal growth media was then aspirated from the dishes and saved, the transfection was added dropwise to 14 DIV neurons, and the transfected cells were incubated at 37°C for 1 hr. The transfection mixture was aspirated and the original neuronal growth media was added. The cells were maintained in culture until 21 DIV and fixed for immunofluorescence as described below.

Immunofluorescence of Cultured Neurons: Dissociated hippocampal neurons were fixed for 15 min at room temperature with 4% paraformaldehyde, followed by methanol for 10 min at -20°C, and blocked with blocking buffer (5% BSA, 0.2% Tween 20 in PBS). Primary antibodies were diluted in blocking buffer and incubated at 4°C overnight. The following day, cells were washed 3 x 15 min with PBS containing 0.2% Tween 20, incubated with secondary antibodies diluted in blocking buffer for 1 hour at room temperature, washed 3 x 15 min, and mounted with Prolong Gold. Soluble eGFP was used as a control in WT and *Ank3* W1989R neurons to evaluate spine

density versus *Ank3* W1989R neurons rescued with 190 kDa ankyrin-G GFP. Dendritic spine density was quantified under each condition using the mCherry cell fill. To label surface AMPA receptors containing GluA1 subunits, 2.5 μg of GluA1-N primary antibody was added to the growth media (2.5 mLs) and incubated at 4°C for 30 min. Neurons were washed 1x with 4°C growth media to remove unbound, excess antibody. Neurons were then fixed in 4% paraformaldehyde, 4% sucrose containing PBS solution for 20 min at 4°C and permeabilized with 0.2% Triton X-100 in PBS for 10 min at RT. Cells were blocked for 1 hr at room temperature in 10% normal goat serum. Primary antibodies (total ankyrin-G and MAP2) were diluted in blocking buffer and incubated overnight at 4°C. Neurons were then washed, incubated in secondary antibodies, washed again, and mounted as described above. Surface GluA1 levels were quantified by tracing MAP2-labeled dendrites of individual neurons and measured at a set intensity threshold using ImageJ software. Background noise was subtracted from mean intensity.

Confocal Microscopy: Samples were imaged on a Zeiss LSM 880 with a 63X NA1.4 Oil/DIC Plan-Apochromat objective and excitation was accomplished using 405, 488, 561, and 633 nm lasers.

Western Blot: Homogenization buffer consisting of 8M urea, 5% SDS, and 5 mM N-ethylmaleimide was heated to 65°C. The desired brain region was dissected from P30-35 mice (P0, P7, P14, and P21 for development experiments), and immediately frozen in liquid nitrogen. Frozen brains were then ground into a powder using a mortar and pestle. The powder was scraped into a 1.5 mL microcentrifuge tube and hand-dounced in 10 volumes/weight of 65°C homogenization buffer (i.e. 1.5 mL for 150 mg powder). The homogenate was incubated at 65°C

for 20 min and then mixed 1:1 with 5× PAGE buffer (5% (wt/vol) SDS, 25% (wt/vol) sucrose, 50 mM Tris, pH 8, 5 mM EDTA, bromophenol blue). The lysates were stored at -80°C until use. The samples (10 μL-volume) were separated on a 3.5-17% gradient gel in 1X Tris buffer, pH 7.4 (40 mM Tris, 20 mM NaOAc, and 2 mM NaEDTA) with 0.2% SDS. Transfer to nitrocellulose was performed overnight at 300 mA at 4°C in 0.5X Tris buffer with 0.01% SDS. Membranes were blocked with 5% bovine serum albumin (BSA) in TBS and incubated overnight at 4°C with primary antibodies (rabbit total ankyrin-G 1:5,000) diluted in blocking buffer. Membranes were washed 3 x 15 min with TBS-T and incubated for 1 hour with LiCor fluorescent secondaries (1:50,000) in blocking buffer. Membrane were then washed 3 x 15 min in TBS-T, 1 x 5 min TBS, and 1 x 5 min in ddH_2O before being imaged on LiCor Odyssey Clx imager.

Synaptosome Purification: WT (C57BL6/J) and *Ank3* W1989R P30 mice were decapitated, and hippocampi were quickly dissected, weighed, and placed in glass hand dounce containing 3 mL/g (wt/vol) of ice-cold homogenization buffer (0.32 M sucrose, 1mM EDTA, pH 7.4, and 1 cOmplete Mini protease inhibitor cocktail tablet (Sigma-Aldrich/10 mLs buffer)). Hippocampi were dissected from other hemisphere and lysates were generated as described above for starting material controls. Dounce tissue exactly 50 times to homogenize and then add homogenate to 1.5 mL microcentrifuge tube. Place sample on ice until all samples are homogenized. Spin samples for 10 mins at 5,650 RCF at 4°C. Remove supernatant in place in a new 1.5 mL microcentrifuge tube and discard pellet. Spin supernatant from 30 mins at 18,400 RCF at 4°C. Discard supernatant (may be beneficial to store at -80°C and run via western blot in case synaptosome fraction is lost). Resuspend pellet in 100 uls of solubilization buffer (10 mM Tris, 150 mM NaCl, 1 mM EDTA, pH 7.5 with protease inhibitors). Place samples on Nutator overnight at 4°C. Spine samples for 30

mins at 21,100 RCF at 4 °C. Mix supernatant 1:1 with 5× PAGE buffer (5% (wt/vol) SDS, 25% (wt/vol) sucrose, 50 mM Tris, pH 8, 5 mM EDTA, bromophenol blue). Run western blot analysis as described above. Store lysates at -80°C indefinitely. Westerns blots of synaptosomes were probed with PSD-95 as a positive control and βIV-spectrin was used as a negative control to assess purity of synaptosome isolation.

Reverse transcription-quantitative polymerase chain reaction (RT-qPCR): RNA was extracted from the cortex of P30 mice or 21 DIV cultured hippocampal neurons using Qiagen RNeasy mini kit (Cat. #74104). 1μg of total RNA was used in 20 μl of reverse transcription reaction with SuperScript III First-Strand Synthesis System (Life Technologies, Cat. #18080-051) with random hexamers and reverse transcription…..The following primer pairs were used in the qPCR reaction: 480 kDa ankyrin-G (forward: 5'-AGTAGGAGGACTGGTCCG-3'; reverse: 5'-AGTTGTGGCATTCTTTCCG-3'), 270 kDa ankyrin-G (forward: 5'-GCCATGTCTCCAGATGTTG; reverse: 5'-TCTGTCCAACTAAGTCCCAG-3'), 190 kDa ankyrin-G (forward: 5'-CTTTGCCTCCCTAGCTTTAC-3'; reverse: same primer as 270 kDa ankyrin-G), and GAPDH (forward: 5'-TCACCACCATGGAGAAGGC -3'; reverse: 5'-GCTAAGCAGTTGGTGGTGCA-3') GAPDH was used as the internal control. The ankyrin-G primer pairs were chosen from (Chang et al. 2014), who evaluated the efficiency of the primer pairs by gel electrophoresis and sequencing the PCR products. Technical triplicates of each set of WT (N=3) or *Ank3* W1989R (N=3) or vehicle (n=9), TTX (n=9), or bicuculline (n=9) and biological replicates (N=3) were performed and analyzed for each experiment.

Acyl Resin Assisted Capture (Acyl RAC): One cortical hemisphere was dissected from P30 WT and *Ank3* W1989R mice and immediately frozen in liquid nitrogen. Frozen brains were ground into a powder using a mortar and pestle. The resulting powder was scraped into a 1.5 mL microcentrifuge tube and homogenized in 500 uL of lysis buffer (100 mM HEPES, 1 mM EDTA, 2.5% SDS, and 2% methyl methanethiosulfonate (MMTS) (Sigma), pH 7.5), using a handheld, battery-operated homogenizer. The samples were sonicated and left to rotate at 40°C overnight. The next day, the samples were transferred into Slide-A-Lyzer Dialysis Cassettes 10,000 MWCO (Thermo Scientific) and left to dialyze at room temperature by rotating overnight in "binding" buffer (100 mM HEPES, 1 mM EDTA, and 1% SDS, pH 7.5). The following day, each dialyzed sample was split into 3 1.5 mL Eppendorf tubes, 1 with 40 uL for "unmanipulated" starting material, and 2 with 220 uL for the palmitoylation assay (one for +HA and one for -HA condition). A 1:1 slurry of pre-activated thiopropyl sepharose beads (GE) was prepared using binding buffer (50 mg beads = 250 uL of binding buffer). 50 uL of the activated bead slurry was added to each 220 uL lysate. 50 uL of freshly prepared 2 M hydroxylamine (HA) (Sigma), adjusted to pH 7.5, were then added to the lysate designated "+HA", while 50 uL of 2 M NaCl were added to the sample designated "-HA". Hydroxylamine/bead/lysate mixtures were left to incubate at room temperature for 2.5 hours, rotating. To wash out the hydroxylamine and NaCl, the beads were spun at 5000x g for 1 min, and the supernatant was removed and discarded. Bead resin was washed 5x with 1 mL of binding buffer, each time spinning at 5000x g for 1 min and discarding the supernatant to recover the beads. Palmitoylated proteins were eluted using 50 uL of 5x sample buffer supplemented with 100 mM DTT. Samples were heated at 65°C for 10 mins and western blot was performed using a 3.5-17% gradient gel. Membranes were probed with antibodies against total ankyrin-G and flotillin-1 as a positive control to confirm efficiency of detecting

palmitoylation levels. Palmitoylation levels were analyzed quantitatively by subtracting the -HA signal intensity from the +HA signal and then dividing by the starting material (N=3 for each genotype). The WT samples were then averaged and palmitoylation levels were calculated for each sample by normalizing to the average WT values.

Protein Stability: Dissociated hippocampal neurons were cultured from postnatal day 1-2 rat pups and grown to 21 DIV as previously described (Henry et al. 2017). At 21 DIV, neurons were treated with vehicle (100% ethanol) plus 100 μg/ml cycloheximide (CHX) or 10 mM KCl and CHX. Lysates were collected from a no treatment (NT) group (referred to as time = 0 hrs) and each treatment condition at 24 and 48 hours with 5× PAGE buffer (5% (wt/vol) SDS, 25% (wt/vol) sucrose, 50 mM Tris, pH 8, 5 mM EDTA, bromophenol blue), sonicated, heated to 65°C for 10 min, and western blot was performed as described above. All conditions were performed in triplicates (n=3 per group). Corresponding dishes of WT neurons at 21 DIV were also treated with 10 mM NaCl or 10 mM KCl, immunostained for PSD-95, total ankyrin-G, and MAP2, and mounted as described above.

***Antibodies, Reagents, Drugs*:** The following antibodies and dilutions were used: rabbit anti-total ankyrin-G (1:1000, lab-generated (Kizhatil et al. 2007)), mouse α-tubulin (1:10,000, Cedarlane Labs (CLT9002)), mouse PSD-95 (1:1000, BioLegend (810401)), rabbit anti-βIV-spectrin (1:1000, lab-generated (Jenkins et al. 2015)), chicken anti-GFP (1:1000, Abcam (ab13970)), goat anti-total ankyrin-G (1:1000, lab-generated (Jenkins et al. 2015)), chicken anti-MAP2 (1:1000, Sigma (AB5543)), mouse anti-GluR1-N (1:500, EMD Millipore (MAB2263)). Fluorescently conjugated secondary antibodies Alexa Fluor 488, 568, or 647 (1:250, Life Technologies) and

Alexa Fluor 594-Streptavidin (1:1000, Jackson ImmunoResearch 016-580-084). The following reagents were used: FBS, Poly-D-lysine, Laminin, Paraformaldehyde, DNase, Urea, and N-ethylmaleimide were from Sigma-Aldrich. B27 supplement, GlutaMAX, Penicillin-Streptomycin, Neurobasal-A, Hank's Balanced Salt Solution, Trypsin, Hepes, Lipofectamine 2000 and Prolong Gold Antifade Reagent were from Life Technologies. Bovine serum albumin was from Gemini Bioproducts. Tween 20 was from Calbiochem. The following drugs were used: 1(S) 9(R)-(-)-Bicuculline Methbromide (Sigma, B7561) and Tetrodotoxin (Biotium, 00061).

Image acquisition and Statistical analysis: Multi-color imaging was performed as previously described using a Zeiss 880 confocal microscope (Jenkins et al. 2015). All images were further processed in Adobe Photoshop CC 2019 software. Statistical analyses were performed using Microsoft Excel and GraphPad Prism 8. A confidence interval of 95% ($P < 0.05$) was required for values to be considered statistically significant. All data are presented as mean ± SEM.

CHAPTER 4

Discussion and Future Directions

Summary and significance

Studies described in this thesis investigated newly identified roles of ankyrin-G in stabilizing GABAergic inhibitory synapses and excitatory dendritic spine plasticity. *ANK3* (encoding the protein ankyrin-G) is among the top genes associated with bipolar disorder and has also been linked to schizophrenia, epilepsy, intellectual disability, and autism, although to a lesser extent. Further, structural and functional abnormalities in both inhibitory and excitatory neurons have been associated with multiple neuropsychiatric and neurodevelopment disorders. Our group is focused on understanding how mutation or loss-of-function of ankyrin-G causes pathological changes in brain circuitry in hopes of elucidating novel targets for drug development.

I have shown ankyrin-G stabilizes GABAergic synapses by interaction with the $GABA_A$ receptor associated protein (GABARAP). I utilized a mouse model expressing a mutation that abolishes the ankyrin-G/GABARAP interaction (*Ank3* W1989R) to understand the effect of loss-of-function ankyrin-G at GABAergic synapses on neuronal circuitry *in vivo*. I have demonstrated that the ankyrin-G/GABARAP interaction is critical for GABAergic synapse connectivity onto excitatory pyramidal neurons in layer II/III of the somatosensory cortex and CA1 hippocampus. I have also shown *Ank3* W1989R mice exhibit a striking reduction in pre- and postsynaptic GABAergic components, which results in pyramidal cell hyperexcitability. I found the interaction between ankyrin-G/GABARAP is important for normal gamma oscillations, which is a measure

of synchronization of neuronal ensembles. I identified reductions in 190 kDa ankyrin-G expression and dendritic spine density in *Ank3* W1989R mice that exhibit pyramidal cell hyperexcitability. This lead us to hypothesize ankyrin-G may play a role in homeostatic synaptic scaling to compensate for changes in inhibitory input to maintain neuronal excitability within a physiological range. We identified the *ANK3* W1989R variant in a family with bipolar disorder, suggesting that understanding the effects of this mutation on brain circuitry may provide insights to the pathophysiology of neuropsychiatric diseases, especially those involving altered inhibitory synapses. Finally, I explored the role of ankyrin-G in dendritic spine plasticity to investigate our hypothesis that ankyrin-G regulates dendritic spine density, morphology, and function to maintain homeostasis of neuronal excitability.

This work provides new insight into how loss-of-function or mutation of ankyrin-G (*ANK3*), one of the genes most highly associated with bipolar disorder, leads to abnormal GABAergic synapse connectivity and function, neuronal excitability and network synchronization, and dendritic spine density. These neuronal changes uncovered in the *Ank3* W1989R mice have previously been linked to patients with neuropsychiatric disease through studies evaluating postmortem brains and electroencephalogram (EEG) recordings. Understanding the source of circuit dysfunction, such as a reduced ankyrin-G-dependent stabilization of GABAergic synapses, may lead to novel therapeutic targets to treat the underlying cause of the disease rather than solely reducing the severity of the psychotic symptoms.

Future directions

While this thesis has answered multiple questions about the role of ankyrin-G on forebrain circuitry and neuropsychiatric disease, it has also raised additional questions, both basic and

translational, regarding ankyrin-G function in the brain that should be the focus of future research. In the following sections, I will discuss these future directions and provide both my hypothesis and possible approaches for addressing them.

Determination of the mechanism underlying GABAergic synapse loss in Ank3 W1989R neurons

Although our understanding of the pathology of neuropsychiatric disorders has improved, limited new neuropsychiatric drugs with improved treatment outcomes have been developed in the past few decades, and most existing treatments were discovered serendipitously. Thus, there remains an unmet need to identify novel therapeutic targets for drug discovery.

One of the most pressing questions of this work is to determine the mechanism of GABAergic synapse loss in the *Ank3* W1989R mouse model. From Chapter 2, we know that abolishing the interaction between ankyrin-G and GABARAP (*Ank3* W1989R) results in reduced $GABA_A$ receptor clustering on the postsynaptic membrane, which subsequently prevents connectivity of the presynaptic terminal. Recent studies have shown that in neurons lacking the 480 kDa ankyrin-G, $GABA_A$ receptors undergo increased rates of endocytosis resulting in loss of both presynaptic and postsynaptic markers (Tseng et al. 2015). Interestingly, treatment of cultured hippocampal neurons with dynasore, a non-specific endocytosis inhibitor, restored $GABA_A$-receptor localization despite the absence of ankyrin-G (Tseng et al. 2015). These findings suggest GABAergic synapse connectivity could potentially be reestablished even in neurons lacking functional ankyrin-G, presumably restoring neuronal excitability, network synchronization, and spine density; however, the endocytic mechanism needs to be elucidated.

I hypothesize that in the absence of ankyrin-G, clathrin heavy chain (CHC) is able to directly interact with GABARAP and promote $GABA_A$-receptor endocytosis (Fig. 4.1). In support

of this hypothesis, normal $GABA_A$-receptor trafficking is mediated by CHC endocytosis (Kittler et al. 2000). Further, a previous study suggested a direct link between CHC and GABARAP, but the functional role of this interaction has not yet been studied (Mohrluder, Hoffmann, et al. 2007). Ankyrin-G has been shown to inhibit the endocytosis of other binding partners at the AIS (Fache et al. 2004). In addition, the 190 kDa isoform of ankyrin-G directly opposes clathrin-mediated endocytosis of E-cadherin in polarized epithelial cells to promote the lateral membrane biogenesis (Jenkins, He, and Bennett 2015; Jenkins et al. 2013). Thus, a critical function of the 480 kDa ankyrin-G may be to inhibit clathrin-mediated endocytosis of the $GABA_A$-receptor to stabilize GABAergic synapses.

To address this question, studies should evaluate the binding between CHC and GABARAP and map the interaction site using coimmunoprecipitation, *in vitro* protein purification and isothermal titration calorimetry, and alanine-scanning mutagenesis. Additional studies should focus on testing the functional role of CHC in $GABA_A$ receptor endocytosis using knockout and rescue experiments with CHC-specific shRNA, dominant-negative fragment of CHC, and endocytosis inhibitors in *Ank3* W1989R mutant neurons. These experiments will answer two key questions: 1) what is the mechanism of synapse loss and are there potential druggable sites? and 2) can GABAergic synapses be rescued in the absence of functional ankyrin-G?

For functional studies, it will be important to make a non-binding mutant of clathrin. High sequence homology (57%-82%) and functional redundancy from other GABARAP isoforms, GABARAPL1/GEC1, GABARAPL2/GATE-16, and GABARAPL3, allow them to interact with the $GABA_A$ receptor (Mansuy-Schlick et al. 2006). This explains why the GABARAP-knockdown mice showed no change in GABAergic synapse transmission compared to the *Ank3* W1989R mouse that express the mutation within the giant exon of ankyrin-G, preventing interaction with

any member of the GABARAP family (O'Sullivan et al. 2005). We can make provisional inferences of the binding site between CHC and GABARAP based on published work. Mohrlüder et al. identified a sequence motif within residues 510-522 (TPD**W**IFLLRNVM) of CHC with peptide binding specificity towards GABARAP (Mohrluder, Hoffmann, et al. 2007). Interestingly, tryptophan has been shown to be a key residue for ligand binding to GABARAP (Thielmann et al. 2008). A conserved tryptophan found in the γ2 subunit of the $GABA_A$ receptor, calreticulin, and the giant exon of the 480 kDa ankyrin-G is necessary for high affinity binding of each of these partners with GABARAP as the tryptophan residue fits precisely into a hydrophobic patch on the conserved face of GABARAP (Knight et al. 2002; Mohrluder, Stangler, et al. 2007; Nelson et al. 2018; Tseng et al. 2015). These findings suggest the W513 residue in CHC may be a critical amino acid necessary for binding to GABARAP. Further, it is possible that the 480 kDa ankyrin-G, CHC, and the γ2 subunit of the $GABA_A$ receptor are all capable of binding to the same conserved surface of GABARAP. Since the 480 kDa ankyrin-G has the highest reported affinity to GABARAP (2.9 nM), versus the estimated k_D of CHC/GABARAP (~1μM), we cannot rule out the possibility that the 480 kDa ankyrin-G saturates GABARAP, which then allows the $GABA_A$ receptor to be properly localized to the postsynaptic membrane. However, in the presence of the *Ank3* W1989R mutation, which prevents 480 kDa ankyrin-G from binding to GABARAP, GABARAP may then interact with the $GABA_A$ receptor (estimated k_D to be > 200 μM) and CHC to drive internalization of the receptor. Future work should investigate the ankyrin-G/GABARAP/$GABA_A$ receptor submolecular organization within the postsynaptic membrane to better understand the mechanisms of GABAergic synapse formation. Overall, identifying the mechanism of endocytosis that underlies GABAergic synapse loss in the *Ank3* W1989R model may lead to new therapeutic targets for drug discovery. Specifically, a small peptide specific to GABARAP that inhibits the

CHC/GABARAP protein-protein interaction would presumably prevent endocytosis of the $GABA_A$ receptor and rescue GABAergic synapses even in the presence of loss-of-function *ANK3* mutations.

Investigate the behavioral consequences of forebrain GABAergic synapse loss in Ank3 W1989R mice

Remarkably, we know little about the underlying neurobiology that contributes to BD or the mechanisms by which effective therapeutics, namely lithium, valproate, carbamazepine, lamotrigine, and other antipsychotics, exert their therapeutic actions. A major reason for this is that there are limited animal models for BD. The available models, which were developed using pharmacological, environmental, and genetic manipulations, allow us to study only the manic or depressive states of the disease, and have numerous additional limitations (Gould and Einat 2007). Previous studies have attempted to study BD in mice by genetically deleting *CLOCK*, *DAT-1*, *NCAN*, *or SHANK3 (Han et al. 2013; Miro et al. 2012; Roybal et al. 2007; Zhuang et al. 2001)*. While many of these models exhibit behavioral phenotypes that resemble BD, *NCAN* is the only gene linked to BD through genome-wide association studies (Cichon et al. 2011). Study of BD susceptibility genes *in vivo* will help define specific pathological processes and associated behaviors involved in the pathways that connect genetic variation to phenotypic symptoms.

Several mouse models have been generated to understand the effects of loss-of-function ankyrin-G on neuronal circuitry and identify a pathological link between *ANK3* mutations and BD. Genetic deletion of all the main classes of ankyrin-G isoforms in the brain results in late embryonic/early postnatal lethality (Jenkins et al. 2013). Knockout of the 480 kDa ankyrin-G splice variant *in vivo* is lethal at P20, preventing the study of circuit development, behavior, and

future pharmacological therapies (Jenkins et al. 2015; Tseng et al. 2015). In addition, knockout of the 480 kDa ankyrin-G causes loss of AISs, nodes of Ranvier, and GABAergic synapses hindering the study of specific phenotypes, such as GABAergic synapse abnormalities, on behavioral outputs and therapeutic mechanisms (Jenkins et al. 2015; Tseng et al. 2015). Recently, we have shown that forebrain-specific knockout of all brain isoforms of ankyrin-G (*Ank3* X CAMKIIα-Cre) late in development (~P30) causes behavioral changes that include hyperactivity and decreased anxiety-like behaviors (Zhu et al. 2017). However, although this animal survives into adulthood, the loss of the AIS, nodes of Ranvier, and GABAergic synapses simultaneously make it difficult to determine which ankyrin-G-dependent domain contributes to the observed behavioral phenotypes. Thus, *Ank3* W1989R mice are useful to understand the specific effects of forebrain GABAergic synapse dysfunction and a BD variant (*ANK3* W1989R) on behavior.

Currently, our lab is working with collaborators to characterize the behavior of the *Ank3* W1989R mouse model. We will investigate a panel of behaviors that will include assays that phenotypically copy aspects of human mania and/or depression. These experiments should include open field tests, elevated plus maze, dark-light box, and social interaction tests to determine whether *Ank3* W1989R mice have reduced anxiety and increased novel exploration, behavioral endophenotypes consistent with BD. Further, the depression facet of BD can be investigated using forced swim test, tail suspension test, and the learned helplessness test. Future studies should also evaluate cortical activity in awake mice using EEG recordings as measurements of cortical oscillations have shown to be altered in patients with BD. Studies have even suggested changes in gamma oscillations in BD patients as potential biomarkers to diagnose and monitor treatment when compared to healthy individuals (Ozerdem et al. 2010; Ozerdema et al. 2013; Sohal 2012). It may be possible to monitor efficacy of potential therapeutics in the *Ank3* W1989R mouse model using

EEG recordings in awake, live mice. Ultimately, adequate animal models for BD will be a useful tool to advance our understanding of the pathophysiology of BD and will allow us to test potential therapeutics to restore neurobiological and behavioral defects.

Evaluate currently used clinical therapeutics in the Ank3 W1989R mouse model

Although the number of pharmacological treatment options available for patients with BD has rapidly increased over the last decade, optimal treatments remain elusive. This is largely due to poor response rates, especially to control the depressive symptoms, and significant side effects, which result in patient noncompliance (Chakrabarti 2016). Understanding the mechanism of action of existing mediations is a major goal of BD research for two main reasons: 1) it can reveal the drug's target(s) to make more specific therapies with fewer side effects and 2) it can lead to personalized treatment regimens, or a more precise approach to treating disease, where molecular diagnosis can result in better-defined, individualized treatment with improved outcomes.

The most commonly prescribed medications approved by the United States Food and Drug Administration (FDA) for at least 1 phase of BD are mood stabilizers that include lithium, valproate, lamotrigine, and carbamazepine, various antipsychotics, and the combination of olanzapine/fluoxetine for depression associated with BD (Ketter, Nasrallah, and Fagiolini 2006). In the family we identified with BD, where affected individuals express the *ANK3* W1989R mutation, the proband is currently prescribed lithium (Nelson et al. 2018). All three family members diagnosed with type I or type II BD are prescribed benzodiazepines, which increase GABA efficacy. In addition, two members are prescribed lamotrigine, which has been shown to increase GABA release. Based on our findings that the W1989R mutation results in reduced GABAergic synapse connectivity and function in *Ank3* W1989R mice, it is interesting that, while

each affected individual in the family is on a different treatment regimen, they are all taking therapeutics that enhance GABA transmission. The *Ank3* W1989R mouse model will be useful to understand the effect of these therapeutics specifically on forebrain inhibitory synapse function, network synchronization, and neuronal excitability. Future studies should evaluate the effects of commonly prescribed therapeutics effective in *ANK3* W1989R patients, namely lithium, valproate, lamotrigine as well as benzodiazepines and antipsychotics, on the molecular, electrophysiological, and network level abnormalities observed in *Ank3* W1989R mice. If administration of these compounds yields rescue of GABAergic synapse function, neuronal excitability, and/or network synchronization, it will be important for follow-up studies to delineate the intracellular signaling pathways that underlie the actions of mood stabilizers and antipsychotics. For example, lithium has been shown to target glycogen synthase kinase-3 (GSK-3) and valproate targets histone deacetylases (HDAC) (Duman and Voleti 2012). GSK3 is at the interaction of several signaling pathways and downstream targets, most notably the protein kinase Akt and β-catenin (Duman and Voleti 2012). Future studies should evaluate the effectiveness of lithium on enhancing GABAergic transmission in *Ank3* W1989R mice. In addition, experiments should determine levels of phosphorylated-GSK3 and Akt (to name a few) in *Ank3* W1989R mice versus controls. Perhaps if lithium treatment reverses GSK3 phosphorylation and enhances GABAergic transmission future studies could focus on developing more specific therapies that target the molecular signaling cascades in the PV+ interneurons. Increasing GABA release from the presynaptic terminal would presumably restore pyramidal cell hyperactivity and network synchronization in *Ank3* W1989R mice since the PV+ interneurons are still present and capable of functioning, but they fail to synapse onto pyramidal neurons. Identifying the lithium targets in the PV+ cells, for example, that promote increased GABA release could lead to development of more specific inhibitors with fewer

side effects than lithium. Furthermore, HDAC inhibitors such as valproate enhance the expression of multiple genes (Williams et al. 1992). RNA-seq could be performed on *Ank3* W1989R mice treated with valproate or lithium, and compared to no treatment controls, to identify genetic changes that may correspond with restoration of synapse function or neuronal excitability. Determining the molecular and electrophysiological effects of commonly prescribed therapeutics in *Ank3* W1989R mice may lead to improved therapeutics with less side effect as well as provide insight into effective treatment regimens for patients with impaired inhibitory circuitry or abnormal EEG recordings of network synchronization.

Investigate induced pluripotent stem cell (iPSCS) function from ANK3 W1989R patients

While we have identified the *ANK3* W1989R mutation in a family with BD, we cannot rule out the possibility that variation in other genes may contribute to disease susceptibility. Especially considering BD, like many other complex diseases, appears to be highly polygenic with many loci having small effect on risk of disease (Calafato et al. 2018; Selzam et al. 2018; Toma et al. 2018). For rare variants, such as *ANK3* W1989R, a very large sample size of unrelated individuals or many related individuals from large, multi-generational families is necessary to unambiguously associate a variant with the disease. However, that is likely unfeasible because of its rarity and because whole-genome sequencing data from all members of the family would be difficult to interpret as it is challenging to identify which of the many single nucleotide polymorphisms (SNPs) uncovered may contribute to disease risk. The recent advancement of iPSCs enables us to study the *ANK3* W1989R mutation in human-specific neurons, on an identical genetic background as the patients.

In collaboration with the Heinz C. Prechter Bipolar Research Fund we have collected fibroblasts from the proband (Chapter 2, Figure 2.18, II:2) and control patients and have successfully reprogrammed these fibroblasts into iPSC-derived pyramidal neurons (Fig. 4.2). We can used electrophysiology and confocal microscopy to evaluate $GABA_A$ receptor surface levels, miniature inhibitory postsynaptic currents (IPSCs), and action potential spiking properties. I hypothesize that *ANK3* W1989R iPSC neurons will display reduced $GABA_A$ receptor densities and $GABA_A$ receptor-mediated currents and higher action potential firing frequency compared to control iPSCs, consistent with single-cell changes observed in *Ank3* W1989R mice. Additional studies should treat iPSC-derived neurons with common BD therapies, such a lithium and valproate, which will allow researchers to correlate cellular phenotypes to individual patient response to treatment. Further, BD iPSCs should also be used to test efficacy of new compounds to restore GABAergic signaling and neuron excitability. CRISPR-Cas9 gene editing on *ANK3* W1989R patient-derived iPSCs and neurotypical controls will allow us to improve our understanding of the genomic variation that contributes to their BD and would shed light on the potential therapeutic application of gene therapy for these individuals. For example, allele-specific correction with a WT copy using CRISPR-Cas9 in patient-derived iPSCs would allow us to estimate the penetrance of the *ANK3* W1989R mutation as a disease-causing variant. If the *ANK3* W1989R variant is a highly penetrant mutation linked to loss-of-function effects on GABAergic synapses, then this would be a useful approach to therapeutically restore GABAergic deficits. Continued work with iPSCs will help understand the genetics and neurobiology of BD and provide more effective treatments for individuals with BD.

Determine the mechanisms by which the 480 kDa ankyrin-G is localized to the somatodendritic domain

Early in development, around P7 in mice, the 480 kDa ankyrin-G localizes specifically to the AIS in cultured hippocampal neurons and coronal brain sections (Tseng et al. 2015). Late in development, around P21, ankyrin-G accumulates on the somatodendritic domain in addition to the AIS (Tseng et al. 2015). The timing of ankyrin-G on the soma corresponds with GABAergic synapse development, which occurs around P21 in mice and the beginning of adolescence (~15 years of age) in humans (Kato-Negishi et al. 2004; Swanwick et al. 2006). Interestingly, the timing of GABAergic synapse development and, presumably ankyrin-G accumulation on the soma, corresponds with appearance of the signs and symptoms in BD patients (Insel 2010).

The molecular mechanisms that regulate localization of the 480 kDa ankyrin-G to the AIS early in development versus the somatodendritic domain late in development remain unknown. Previous studies have shown that ankyrin-G is membrane-associated through *S*-palmitoylation, the reversible addition of a 16-carbon fatty acid palmitate, to the cystine 70 residue (C70) within the ANK repeats domain (He, Abdi, and Bennett 2014; He, Jenkins, and Bennett 2012). In general, *S*-palmitoylation is mediated by a family of 23 palmitoyl acyl transferases (zDHHC PATs) (Korycka et al. 2012). Two of the 23 PATs, zDHHC5 and zDHHC8, have been shown to palmitoylate the 190 kDa ankyrin-G in a functionally redundant manner, which localize it to the lateral membrane of epithelial cells and allow for ankyrin-G to build the lateral membrane (He, Abdi, and Bennett 2014). In ankyrin-G-null neurons, rescue with palmitoylation-resistant 480 kDa ankyrin-G (C70A mutant) results in loss of all AIS components and fails to cluster $GABA_A$ receptors at the somatodendritic membrane (Jenkins et al. 2015; Tseng et al. 2015). Thus, palmitoylation is critical for proper localization and function of the 480 kDa ankyrin-G in neurons. The PATs responsible

for palmitoylating the neuronal classes of ankyrin-G isoforms, the 270- and 480-kDa as well as the 190 kDa ankyrin-G in neurons, have not been identified. I hypothesize that zDHHC5 and zDDHC8 palmitoylate the 480 kDa ankyrin-G in neurons because the palmitoyl site, C70 within the ANK repeats, is conserved between all ankyrin-G splice variants. Future studies could answer this question by co-expressing the 480 kDa ankyrin-G-GFP with each member of the zDHHC family of PATs in heterologous cells and perform acyl resin-assisted capture (acyl-RAC) to identify which PATs enhance the palmitoylation signal of co-expressed ankyrin-G-GFP. Since the 480 kDa ankyrin-G-GFP is difficult to transfect into heterologous cells at high efficiencies, it may be more useful to generate a stable cell line expressing the 480 kDa ankyrin-G-GFP. Furthermore, to validate the PATs responsible for endogenous 480 kDa ankyrin-G, experiments should genetically delete the enzymes using a Cre/loxP system or knockdown using shRNA in cultured hippocampal neurons and immunostain with antibodies against the 480 kDa ankyrin-G.

We cannot rule out the possibility that different zDHHCs palmitoylate the 480 kDa ankyrin-G at the AIS early in development versus the somatodendritic domain late in development. Another possibility could be that zDHHC5 and zDHHC8 palmitoylate the 480 kDa ankyrin-G at both domains, but they themselves are not expressed at the somatodendritic domain until later developmental stages. Experiments could address this question by immunostaining against (or transfecting tagged DHHCs if antibodies are poor) the zDHHCs that are shown to palmitoylate the 480 kDa ankyrin-G at different time points across development. Furthermore, it would be interesting to investigate how the 190 kDa ankyrin-G is localized to dendritic spines, whereas the 480 kDa anykyrin-G is localized to the AIS and somatodendritic domain to stabilize GABAergic synapses, especially if they are palmitoylated by the same zDHHCs. One potential explanation is that the different *Ank3* mRNAs are localized to their respective domains with *ZDHHC* mRNAs

and among these mRNAs are specific transcription factors that promote local translation and subsequently local palmitoylation of the distinct ankyrin isoforms. Neurodevelopment and neuropsychiatric diseases have been linked to palmitoylation and genes encoding zDHHCs, such as zDHHC8 and zDHHC9 (Masurel-Paulet et al. 2014; Mukai et al. 2008; Mukai et al. 2004; Woodin et al. 2001). Loss-of-function mutations in zDHHCs that palmitoylate the neuronal classes of ankyrin-G may lead to disruption in ankyrin-G-dependent functions, such as GABAergic synaptogenesis, dendritic spine scaling, and AIS composition. Multiple perturbations that contribute to neuropsychiatric disorder risk may converge mechanistically and mutations may cause common patterns of neuron dysfunction and disease phenotypes. Thus, mutations in zDHHCs that may regulate distinct localization of the different splice variants of ankyrin-G at the AIS, somatodendritic domain, or dendritic spines may have similar downstream effects as *ANK3* mutations.

Evaluate the effects of additional ANK3 BD variants on GABAergic synapse stability and function, dendritic spine scaling, and AIS composition

We initially developed the *Ank3* W1989R mouse model as a tool to study the effects of loss-of-function ankyrin-G specifically on GABAergic synapses *in vivo,* in a model that survives, and maintains the AIS and nodes of Ranvier. We were fortunate to have identified the *ANK3* W1989R variant in our patient cohort in Heinz C. Prechter Bipolar Research Fund at the University of Michigan, highlighting the importance of understand this mutation in disease (Chapter 2). However, *ANK3* W1989R (rs372922084, c.5965T>C (p.Trp1989Arg)) is a rare variant found in approximately 1: 10,000 European Americans according to the most recent data from the gnomAD project (Lek et al. 2016). It will be important for future studies to evaluate how additional variants

in *ANK3*, both common and rare, may contribute to BD etiology, as well as other *ANK3*-associated neurological diseases, and whether they phenocopy changes in neuronal circuitry uncovered in *Ank3* W1989R mice or lead to new avenues of disease pathology. *ANK3* variants may contribute to disease susceptibility by disrupting protein-protein interactions, causing protein misfolding, altering transcript expression levels, or may affect different splice variants causing protein dysfunction.

BD is a polygenetic disorder, which suggests very large sample sizes will be necessary to detect even a modest effect of allelic variation on BD susceptibility (Schulze 2010). Genome-wide associated studies (GWAS) have uncovered multiple SNPs in *ANK3* with significant allelic association to BD including: rs10994338 ($p = 1.20 \times 10^{-7}$), rs4948418 ($p = 8.93 \times 10^{-9}$) rs10994336 ($p = 9.1 \times 10^{-9}$), rs10994397 ($p = 7.1 \times 10^{-9}$) (Chen et al. 2013; Ferreira et al. 2008; Fiorentino et al. 2014; Lett et al. 2011; Liu et al. 2011; Schulze et al. 2009; Scott et al. 2009; Tesli et al. 2011). GWAS has revealed these SNPs are linked to the 5' region of *ANK3*, which includes the first two exons (exon1b and exon1e), as well as rs9804190 ($p = 1.20 \times 10^{-4}$) at the 3' end of *ANK3*; however, due to linkage disequilibrium of a 250 kb region, these variants may be found within the promoter and intronic region (Rueckert et al. 2013). While these *ANK3* SNPs appear to be strongly associated with BD risk, their functional consequences have not yet been fully investigated. Future studies could perform knockout-and-rescue experiments to determine the impact of these mutations on AIS composition, $GABA_A$ receptor localization, and/or dendritic spine plasticity as well as neuron electrophysiology properties. It is also possible that these BD risk variants display their functional effects by altering *ANK3* expression, perhaps by manipulating regulatory elements, promoter activity, or alternative splicing. This would be consistent with studies demonstrating reduced *ANK3* mRNA levels in postmortem brains from BD patients (Roussos et al. 2012;

Rueckert et al. 2013). To address the impact of *ANK3* SNPs on ankyrin-G expression future studies could utilize CRISPR/Cas9 technology to knock these variants into human embryonic stem cells (ESCs). In addition, experiments could be performed using RNA Ligase-Mediated Rapid Amplification of cDNA Ends (RLM-RACE) to evaluate distinct transcriptional start sites (TSS) of different *ANK3* isoforms to assess the impact of BD SNPs on expression levels of specific mRNA transcripts. This technique could also be used to address how different variants affect expression of the different classes of ankyrin-G isoform, which would provide information on which neuronal domains are affected. For example, variants that alter expression of the 480 kDa ankyrin-G may impact the AIS or GABAergic synapses, whereas altered expression of the 190 kDa ankyrin-G may impact dendritic spines.

Despite substantial evidence linking *ANK3* GWAS susceptibility SNPs to BD, effect sizes of *ANK3* variants are modest with odds ratios less than 1.4 (Craddock and Sklar 2009). Thus it will be important to also study how rare, highly penetrant variants in *ANK3* may contribute to BD etiology. Recently, next generation sequencing revealed 18 novel rare missense and one indel mutation have been identified in the serine-rich domain with in the giant exon (exon 37), which encodes the 270- and 480- kDa splice variants of ankyrin-G, as potentially disease-causing (Doyle et al. 2012). However, the effect of these variants on neuron function has not yet been explored. Additional variants obtained using whole-genome and exome sequencing data from the Heinz C. Prechter Bipolar Research Program should be studied. To date, we have identified *ANK3* variants in at least 10 BD individuals within our patient cohort that include missense and synonymous mutations in the coding sequence, intronic region, and the 5' UTR. It may also be beneficial to explore highly evolutionarily conversed amino acid sequences within protein-coding and non-coding regions of ankyrin-G to identify novel domains critical for ankyrin-G function as well as

regions more likely to be affected by disease-causing mutations (Woolfe et al. 2005). Ultimately, understanding how patient-specific rare variants affect the expression and function of the different splice variants of ankyrin-G may provide insight to common or new pathways by which mutations in *ANK3* contribute to BD and other neurological diseases.

Investigate the ability of the 480 kDa ankyrin-G to bind and localize additional proteins to the somatodendritic domain

Yeast-two hybrid screens from a mouse brain library initially revealed GABARAP as a potential interacting protein of the giant exon (exon 37) that encodes the 480 kDa ankyrin-G (Tseng et al. 2015). This work lead to the discovery that ankyrin-G has critical roles outside of the AIS and nodes of Ranvier to cluster $GABA_A$ receptors within the somatodendritic membrane. These studies were conducted using a fragment of the giant exon of ankyrin-G, therefore it is likely that additional novel interacting partners of the 480 kDa ankyrin-G were not detected in this screen. In addition, the yeast expression system does not have the same components involved in post-translational modifications that regulate ankyrin-G binding to its partners, which reduces the probability of discovering new bindings partners of ankyrin-G. Future studies should determine whether the full length 480 kDa ankyrin-G interacts with and clusters additional proteins to the somatodendritic domain using mammalian cells, particularly neurons. Although various subtypes of calcium, potassium, and sodium channels have been demonstrated to localize to the soma and dendrites (although at significantly lower densities than the AIS and node of Ranvier) (Catterall 2000; Hell et al. 1993; Misonou et al. 2004) the mechanisms by which they are clustered to the membrane are unknown. It is also possible that the 480 kDa is capable of localizing additional ion channels, cell adhesion molecules, and transporters to the somatodendritic domains through

additional adaptor proteins than GABARAP to prevent their endocytosis. To test this, experiments could include using additional fragments of the 480 kDa ankyrin-G in two-hybrid screens of brain libraries that include the giant exon as well as conserved domains between all isoforms. Further studies could utilize co-immunoprecipitation, and fluorescence-based techniques such as FRET and proximity ligation assay although these experiments would be low throughput compared to screening approaches. In addition, since the 480 kDa ankyrin is insoluble and highly prone to proteolysis, a new approach to identify novel binding partners from brain could be to perfuse mice with the reversible, intracellular crosslinking reagent dithiobis[succinimidylpropionate] (DSP), dissect out the brain, and isolate cross-linked proteins with trizole extraction. Subsequently, reconstitute proteins in an aqueous solution and immunoprecipitate (IP) ankyrin-G. Lastly, elute with a reducing agent and send the samples for mass spectrometry. This technique will allow for the identification of novel ankyrin-G binding partners using endogenous protein from mouse brain. It would be interesting to IP with multiple antibodies against different domains of ankyrin-G (i.e. antibodies that recognizes the N-terminus conserved in all isoforms, the giant exon that encodes both the 270- and 480- kDa ankyrin-G isoforms, and the 3' end of the giant exon that encodes only the 480- kDa ankyrin-G) to identify potential binding partners unique to the different splice variants. I expect we have only uncovered a fraction of ankyrin-G binding partners to date and identifying new interacting partners would lead to novel roles of ankyrin-G critical for neuronal function.

Overall Conclusions

As a whole, this thesis describes novel roles of ankyrin-G at GABAergic inhibitory synapses and excitatory dendritic spines outside of its historical roles at the AIs and nodes of

Ranvier. It provides a basis by which loss-of-function ankyrin-G at GABAergic synapses causes neuronal network dysfunction. It sets a framework for future studies to identify novel therapeutic targets for the treatment of neuropsychiatric diseases, especially those involving altered inhibitory circuitry. It establishes an approach for evaluating endophenotypes of neuropsychiatric diseases and highlights how potential-disease causing variation in *ANK3* contributes to disease pathology. Future work will aim to identify novel targets for drug development, improve existing therapies for personalized treatment, and utilize new approaches to assessing efficacy of potential therapeutics.

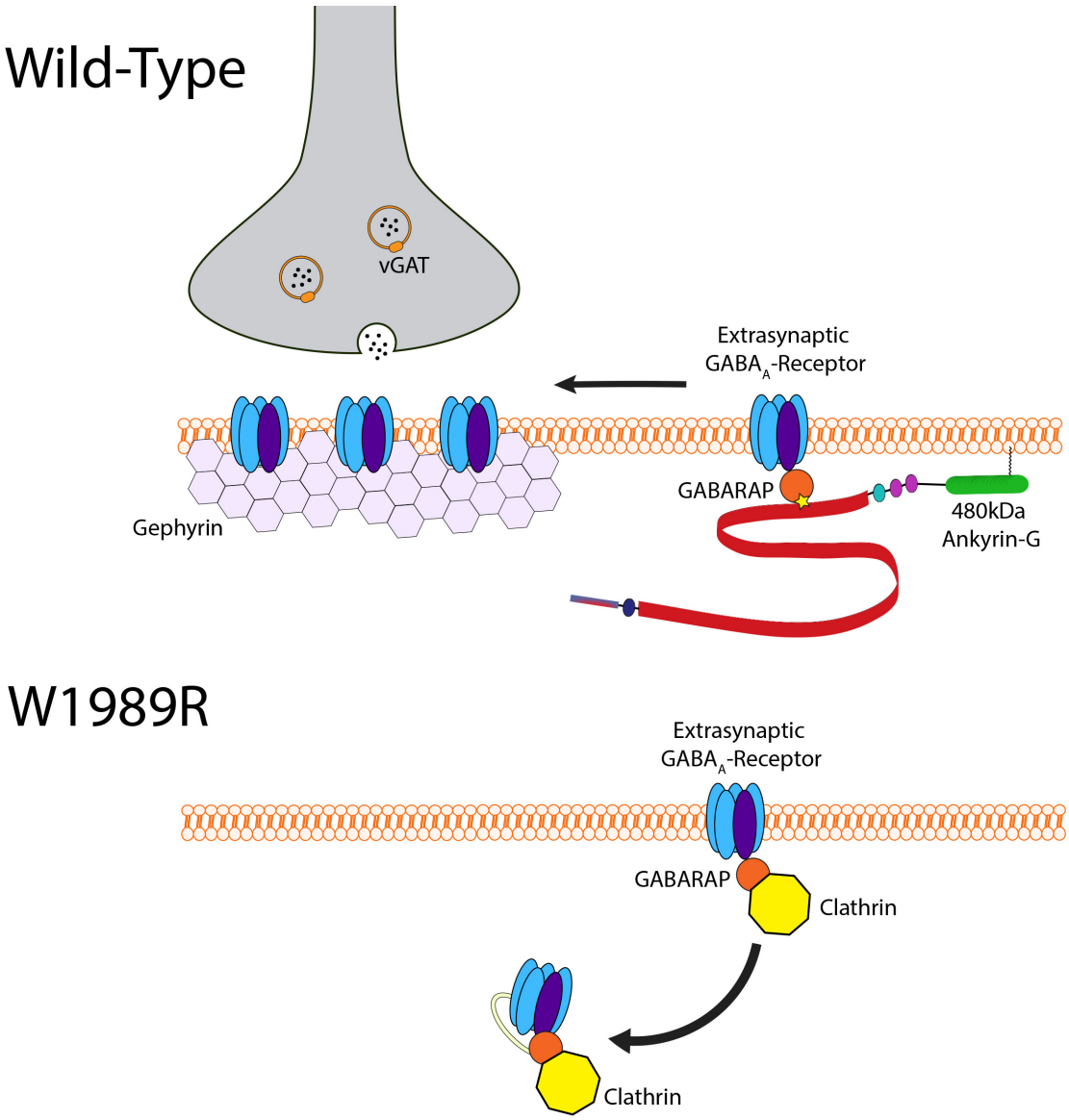

Figure 4.1. Proposed mechanism of GABAergic synapse loss in *Ank3* W1989R mice. In WT neurons, the 480 kDa ankyrin-G binds to the $GABA_A$ receptor-associated protein (GABARAP) to cluster extrasynaptic $GABA_A$ receptors in the postsynaptic membrane. Gephyrin then form a permanent scaffold to stabilize synaptic $GABA_A$ receptors and pre-synaptic GABAergic synapses (identified with the pre-synaptic GABAergic marker, vesicular GABA transporter (vGAT)). I hypothesize that the GABAergic synapses are lost in *Ank3* W1989R neurons due to an increased rate of $GABA_A$ receptor endocytosis. Specifically, in the absence of the 480 kDa ankyrin-G, clathrin heavy chain (CHC) directly interaction with GABARAP to promote $GABA_A$ receptors, resulting in loss of pre- and post- GABAergic components.

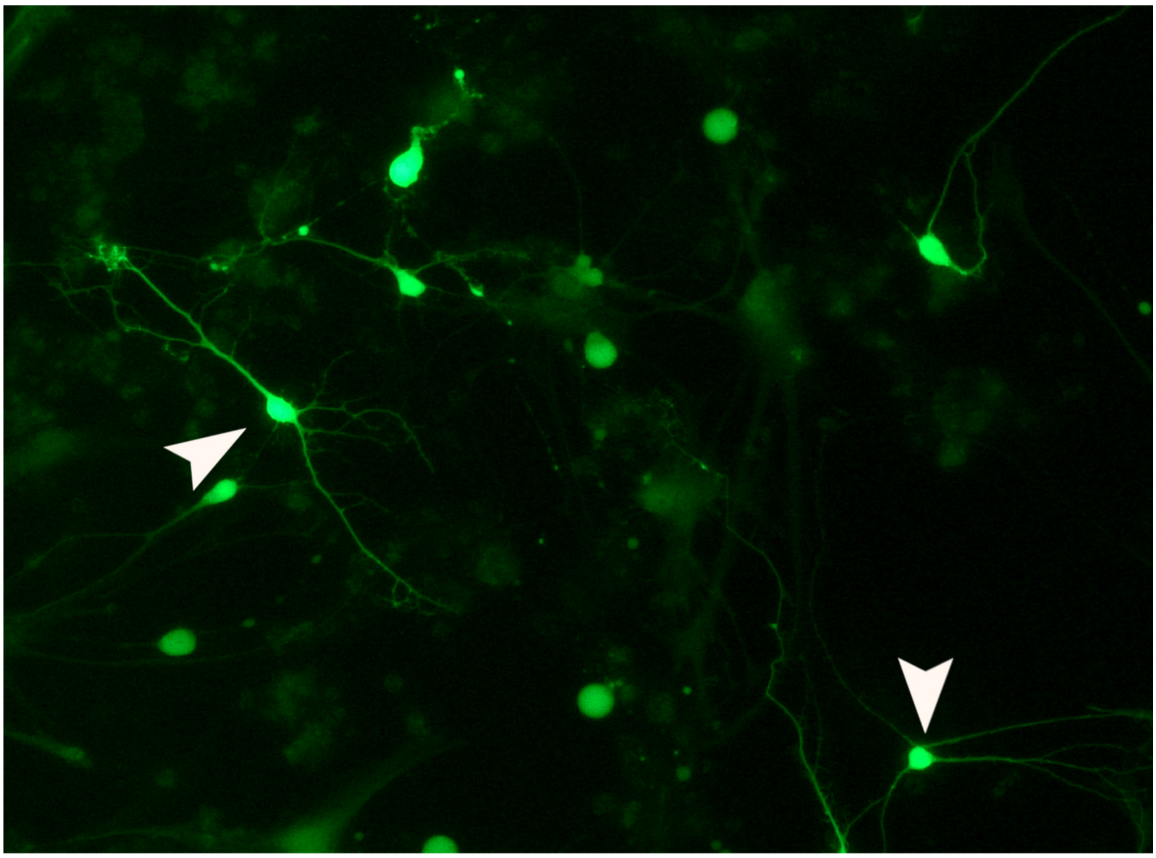

Figure 4.2: iPSC-derived neurons from BD patients heterozygous for the *ANK3* W1989R variant after 3-5 weeks in culture. Neurons were transfected with CAMKII-GFP virus, which is a neuron specific marker. Arrows indicates CAMKII-positive neurons.

BIBLIOGRAPHY

Al-Bassam, S., M. Xu, T. J. Wandless, and D. B. Arnold. 2012. 'Differential trafficking of transport vesicles contributes to the localization of dendritic proteins', *Cell Rep*, 2: 89-100.

Alemu, E. A., T. Lamark, K. M. Torgersen, A. B. Birgisdottir, K. B. Larsen, A. Jain, H. Olsvik, A. Overvatn, V. Kirkin, and T. Johansen. 2012. 'ATG8 family proteins act as scaffolds for assembly of the ULK complex: sequence requirements for LC3-interacting region (LIR) motifs', *J Biol Chem*, 287: 39275-90.

Ament, S. A., S. Szelinger, G. Glusman, J. Ashworth, L. Hou, N. Akula, T. Shekhtman, J. A. Badner, M. E. Brunkow, D. E. Mauldin, A. B. Stittrich, K. Rouleau, S. D. Detera-Wadleigh, J. I. Nurnberger, Jr., H. J. Edenberg, E. S. Gershon, N. Schork, Study Bipolar Genome, N. D. Price, R. Gelinas, L. Hood, D. Craig, F. J. McMahon, J. R. Kelsoe, and J. C. Roach. 2015. 'Rare variants in neuronal excitability genes influence risk for bipolar disorder', *Proc Natl Acad Sci U S A*, 112: 3576-81.

Amor, V., C. Zhang, A. Vainshtein, A. Zhang, D. R. Zollinger, Y. Eshed-Eisenbach, P. J. Brophy, M. N. Rasband, and E. Peles. 2017. 'The paranodal cytoskeleton clusters Na+ channels at nodes of Ranvier', *Elife*, 6.

Andersen, P., S. H. Sundberg, O. Sveen, and H. Wigstrom. 1977. 'Specific long-lasting potentiation of synaptic transmission in hippocampal slices', *Nature*, 266: 736-7.

Anggono, V., R. L. Clem, and R. L. Huganir. 2011. 'PICK1 loss of function occludes homeostatic synaptic scaling', *J Neurosci*, 31: 2188-96.

Ango, F., G. di Cristo, H. Higashiyama, V. Bennett, P. Wu, and Z. J. Huang. 2004. 'Ankyrin-based subcellular gradient of neurofascin, an immunoglobulin family protein, directs GABAergic innervation at Purkinje axon initial segment', *Cell*, 119: 257-72.

Awadalla, P., J. Gauthier, R. A. Myers, F. Casals, F. F. Hamdan, A. R. Griffing, M. Cote, E. Henrion, D. Spiegelman, J. Tarabeux, A. Piton, Y. Yang, A. Boyko, C. Bustamante, L. Xiong, J. L. Rapoport, A. M. Addington, J. L. E. DeLisi, M. O. Krebs, R. Joober, B. Millet, E. Fombonne, L. Mottron, M. Zilversmit, J. Keebler, H. Daoud, C. Marineau, M. H. Roy-Gagnon, M. P. Dube, A. Eyre-Walker, P. Drapeau, E. A. Stone, R. G. Lafreniere, and G. A. Rouleau. 2010. 'Direct Measure of the De Novo Mutation Rate in Autism and Schizophrenia Cohorts', *American Journal of Human Genetics*, 87: 316-24.

Baalman, K. L., R. J. Cotton, S. N. Rasband, and M. N. Rasband. 2013. 'Blast wave exposure impairs memory and decreases axon initial segment length', *J Neurotrauma*, 30: 741-51.

Bartos, M., I. Vida, and P. Jonas. 2007. 'Synaptic mechanisms of synchronized gamma oscillations in inhibitory interneuron networks', *Nature Reviews Neuroscience*, 8: 45-56.

Bekku, Y., U. Rauch, Y. Ninomiya, and T. Oohashi. 2009. 'Brevican distinctively assembles extracellular components at the large diameter nodes of Ranvier in the CNS', *Journal of Neurochemistry*, 108: 1266-76.

Bender, K. J., and L. O. Trussell. 2012. 'The physiology of the axon initial segment', *Annu Rev Neurosci*, 35: 249-65.
Benes, F. M. 2010. 'Amygdalocortical circuitry in schizophrenia: from circuits to molecules', *Neuropsychopharmacology*, 35: 239-57.
Benes, F. M., and S. Berretta. 2001. 'GABAergic interneurons: implications for understanding schizophrenia and bipolar disorder', *Neuropsychopharmacology*, 25: 1-27.
Benes, F. M., B. Lim, D. Matzilevich, J. P. Walsh, S. Subburaju, and M. Minns. 2007. 'Regulation of the GABA cell phenotype in hippocampus of schizophrenics and bipolars', *Proc Natl Acad Sci U S A*, 104: 10164-9.
Bennett, V., and A. J. Baines. 2001. 'Spectrin and ankyrin-based pathways: metazoan inventions for integrating cells into tissues', *Physiol Rev*, 81: 1353-92.
Bennett, V., and J. Healy. 2009. 'Membrane domains based on ankyrin and spectrin associated with cell-cell interactions', *Cold Spring Harb Perspect Biol*, 1: a003012.
Bennett, V., and D. N. Lorenzo. 2013. 'Spectrin- and Ankyrin-Based Membrane Domains and the Evolution of Vertebrates', *Functional Organization of Vertebrate Plasma Membrane*, 72: 1-37.
Berghs, S., D. Aggujaro, R. Dirkx, E. Maksimova, P. Stabach, J. M. Hermel, J. P. Zhang, W. Philbrick, V. Slepnev, T. Ort, and M. Solimena. 2000. 'beta IV spectrin, a new spectrin localized at axon initial segments and nodes of ranvier in the central and peripheral nervous system', *Journal of Cell Biology*, 151: 985-1001.
Bevers, M. B., and R. W. Neumar. 2008. 'Mechanistic role of calpains in postischemic neurodegeneration', *Journal of Cerebral Blood Flow and Metabolism*, 28: 655-73.
Bhat, M. A., J. C. Rios, Y. Lu, G. P. Garcia-Fresco, W. Ching, M. St Martin, J. Li, S. Einheber, M. Chesler, J. Rosenbluth, J. L. Salzer, and H. J. Bellen. 2001. 'Axon-glia interactions and the domain organization of myelinated axons requires neurexin IV/Caspr/Paranodin', *Neuron*, 30: 369-83.
Bi, G., and M. Poo. 2001. 'Synaptic modification by correlated activity: Hebb's postulate revisited', *Annu Rev Neurosci*, 24: 139-66.
Black, J. A., and S. G. Waxman. 2012. 'Sodium channels and microglial function', *Experimental Neurology*, 234: 302-15.
Bliss, T. V., and G. L. Collingridge. 1993. 'A synaptic model of memory: long-term potentiation in the hippocampus', *Nature*, 361: 31-9.
Boiko, T., A. Van Wart, J. H. Caldwell, S. R. Levinson, J. S. Trimmer, and G. Matthews. 2003. 'Functional specialization of the axon initial segment by isoform-specific sodium channel targeting', *J Neurosci*, 23: 2306-13.
Brechet, A., M. P. Fache, A. Brachet, G. Ferracci, A. Baude, M. Irondelle, S. Pereira, C. Leterrier, and B. Dargent. 2008. 'Protein kinase CK2 contributes to the organization of sodium channels in axonal membranes by regulating their interactions with ankyrin G', *Journal of Cell Biology*, 183: 1101-14.
Butt, S. J., V. H. Sousa, M. V. Fuccillo, J. Hjerling-Leffler, G. Miyoshi, S. Kimura, and G. Fishell. 2008. 'The requirement of Nkx2-1 in the temporal specification of cortical interneuron subtypes', *Neuron*, 59: 722-32.
Buzsaki, G., and X. J. Wang. 2012. 'Mechanisms of gamma oscillations', *Annu Rev Neurosci*, 35: 203-25.

Calafato, M. S., J. H. Thygesen, S. Ranlund, E. Zartaloudi, W. Cahn, B. Crespo-Facorro, A. Diez-Revuelta, M. Di Forti, Risk Genetic, consortium Outcome of Psychosis, M. H. Hall, C. Iyegbe, A. Jablensky, R. Kahn, L. Kalaydjieva, E. Kravariti, K. Lin, C. McDonald, A. M. McIntosh, A. McQuillin, M. Picchioni, D. Rujescu, M. Shaikh, T. Toulopoulou, J. V. Os, E. Vassos, M. Walshe, J. Powell, C. M. Lewis, R. M. Murray, and E. Bramon. 2018. 'Use of schizophrenia and bipolar disorder polygenic risk scores to identify psychotic disorders', *Br J Psychiatry*, 213: 535-41.

Cardin, J. A., M. Carlen, K. Meletis, U. Knoblich, F. Zhang, K. Deisseroth, L. H. Tsai, and C. I. Moore. 2009. 'Driving fast-spiking cells induces gamma rhythm and controls sensory responses', *Nature*, 459: 663-7.

Catterall, W. A. 2000. 'From ionic currents to molecular mechanisms: the structure and function of voltage-gated sodium channels', *Neuron*, 26: 13-25.

Cauli, B., J. T. Porter, K. Tsuzuki, B. Lambolez, J. Rossier, B. Quenet, and E. Audinat. 2000. 'Classification of fusiform neocortical interneurons based on unsupervised clustering', *Proc Natl Acad Sci U S A*, 97: 6144-9.

Chakrabarti, S. 2016. 'Treatment-adherence in bipolar disorder: A patient-centred approach', *World J Psychiatry*, 6: 399-409.

Chang, K. J., D. R. Zollinger, K. Susuki, D. L. Sherman, M. A. Makara, P. J. Brophy, E. C. Cooper, V. Bennett, P. J. Mohler, and M. N. Rasband. 2014. 'Glial ankyrins facilitate paranodal axoglial junction assembly', *Nat Neurosci*, 17: 1673-81.

Chattopadhyaya, B., and G. D. Cristo. 2012. 'GABAergic circuit dysfunctions in neurodevelopmental disorders', *Front Psychiatry*, 3: 51.

Chen, C., V. Bharucha, Y. Chen, R. E. Westenbroek, A. Brown, J. D. Malhotra, D. Jones, C. Avery, P. J. Gillespie, 3rd, K. A. Kazen-Gillespie, K. Kazarinova-Noyes, P. Shrager, T. L. Saunders, R. L. Macdonald, B. R. Ransom, T. Scheuer, W. A. Catterall, and L. L. Isom. 2002. 'Reduced sodium channel density, altered voltage dependence of inactivation, and increased susceptibility to seizures in mice lacking sodium channel beta 2-subunits', *Proc Natl Acad Sci U S A*, 99: 17072-7.

Chen, C. L., J. D. Calhoun, Y. Q. Zhang, L. Lopez-Santiago, N. Zhou, T. H. Davis, J. L. Salzer, and L. L. Isom. 2012. 'Identification of the Cysteine Residue Responsible for Disulfide Linkage of Na+ Channel alpha and beta 2 Subunits', *Journal of Biological Chemistry*, 287: 39061-69.

Chen, D. T., X. Jiang, N. Akula, Y. Y. Shugart, J. R. Wendland, C. J. Steele, L. Kassem, J. H. Park, N. Chatterjee, S. Jamain, A. Cheng, M. Leboyer, P. Muglia, T. G. Schulze, S. Cichon, M. M. Nothen, M. Rietschel, BiGs, F. J. McMahon, A. Farmer, P. McGuffin, I. Craig, C. Lewis, G. Hosang, S. Cohen-Woods, J. B. Vincent, J. L. Kennedy, and J. Strauss. 2013. 'Genome-wide association study meta-analysis of European and Asian-ancestry samples identifies three novel loci associated with bipolar disorder', *Mol Psychiatry*, 18: 195-205.

Chen, X., C. D. Nelson, X. Li, C. A. Winters, R. Azzam, A. A. Sousa, R. D. Leapman, H. Gainer, M. Sheng, and T. S. Reese. 2011. 'PSD-95 is required to sustain the molecular organization of the postsynaptic density', *J Neurosci*, 31: 6329-38.

Chen, X., C. Winters, R. Azzam, X. Li, J. A. Galbraith, R. D. Leapman, and T. S. Reese. 2008. 'Organization of the core structure of the postsynaptic density', *Proc Natl Acad Sci U S A*, 105: 4453-8.

Chen, Z. W., and R. W. Olsen. 2007. 'GABAA receptor associated proteins: a key factor regulating GABAA receptor function', *Journal of Neurochemistry*, 100: 279-94.
Chowdhury, D., and J. W. Hell. 2018. 'Homeostatic synaptic scaling: molecular regulators of synaptic AMPA-type glutamate receptors', *F1000Res*, 7: 234.
Cichon, S., T. W. Muhleisen, F. A. Degenhardt, M. Mattheisen, X. Miro, J. Strohmaier, M. Steffens, C. Meesters, S. Herms, M. Weingarten, L. Priebe, B. Haenisch, M. Alexander, J. Vollmer, R. Breuer, C. Schmal, P. Tessmann, S. Moebus, H. E. Wichmann, S. Schreiber, B. Muller-Myhsok, S. Lucae, S. Jamain, M. Leboyer, F. Bellivier, B. Etain, C. Henry, J. P. Kahn, S. Heath, Consortium Bipolar Disorder Genome Study, M. Hamshere, M. C. O'Donovan, M. J. Owen, N. Craddock, M. Schwarz, H. Vedder, J. Kammerer-Ciernioch, A. Reif, J. Sasse, M. Bauer, M. Hautzinger, A. Wright, P. B. Mitchell, P. R. Schofield, G. W. Montgomery, S. E. Medland, S. D. Gordon, N. G. Martin, O. Gustafsson, O. Andreassen, S. Djurovic, E. Sigurdsson, S. Steinberg, H. Stefansson, K. Stefansson, L. Kapur-Pojskic, L. Oruc, F. Rivas, F. Mayoral, A. Chuchalin, G. Babadjanova, A. S. Tiganov, G. Pantelejeva, L. I. Abramova, M. Grigoroiu-Serbanescu, C. C. Diaconu, P. M. Czerski, J. Hauser, A. Zimmer, M. Lathrop, T. G. Schulze, T. F. Wienker, J. Schumacher, W. Maier, P. Propping, M. Rietschel, and M. M. Nothen. 2011. 'Genome-wide association study identifies genetic variation in neurocan as a susceptibility factor for bipolar disorder', *American Journal of Human Genetics*, 88: 372-81.
Clark, K. C., A. Josephson, S. D. Benusa, R. K. Hartley, M. Baer, S. Thummala, M. Joslyn, B. A. Sword, H. Elford, U. Oh, A. Dilsizoglu-Senol, C. Lubetzki, M. Davenne, G. H. DeVries, and J. L. Dupree. 2016. 'Compromised axon initial segment integrity in EAE is preceded by microglial reactivity and contact', *Glia*, 64: 1190-209.
Collingridge, G. L., S. Peineau, J. G. Howland, and Y. T. Wang. 2010. 'Long-term depression in the CNS', *Nature Reviews Neuroscience*, 11: 459-73.
Coman, I., M. S. Aigrot, D. Seilhean, R. Reynolds, J. A. Girault, B. Zalc, and C. Lubetzki. 2006. 'Nodal, paranodal and juxtaparanodal axonal proteins during demyelination and remyelination in multiple sclerosis', *Brain*, 129: 3186-95.
Cooper, E. C. 2011. 'Made for "anchorin": Kv7.2/7.3 (KCNQ2/KCNQ3) channels and the modulation of neuronal excitability in vertebrate axons', *Seminars in Cell & Developmental Biology*, 22: 185-92.
Cooper, E. C., E. Harrington, Y. N. Jan, and L. Y. Jan. 2001. 'M channel KCNQ2 subunits are localized to key sites for control of neuronal network oscillations and synchronization in mouse brain', *J Neurosci*, 21: 9529-40.
Craddock, N., and P. Sklar. 2009. 'Genetics of bipolar disorder: successful start to a long journey', *Trends Genet*, 25: 99-105.
Craner, M. J., J. Newcombe, J. A. Black, C. Hartle, M. L. Cuzner, and S. G. Waxman. 2004. 'Molecular changes in neurons in multiple sclerosis: Altered axonal expression of Na(v)1.2 and Na(v)1.6 sodium channels and Na(+)/Ca(2+) exchanger', *Proceedings of the National Academy of Sciences of the United States of America*, 101: 8168-73.
Cruz, D. A., C. L. Weaver, E. M. Lovallo, D. S. Melchitzky, and D. A. Lewis. 2009. 'Selective alterations in postsynaptic markers of chandelier cell inputs to cortical pyramidal neurons in subjects with schizophrenia', *Neuropsychopharmacology*, 34: 2112-24.

Cunha, S. R., and P. J. Mohler. 2006. 'Cardiac ankyrins: Essential components for development and maintenance of excitable membrane domains in heart', *Cardiovasc Res*, 71: 22-9.
Czogalla, A., and A. F. Sikorski. 2005. 'Spectrin and calpain: a 'target' and a 'sniper' in the pathology of neuronal cells', *Cellular and Molecular Life Sciences*, 62: 1913-24.
D'Este, E., D. Kamin, F. Gottfert, A. El-Hady, and S. W. Hell. 2015. 'STED nanoscopy reveals the ubiquity of subcortical cytoskeleton periodicity in living neurons', *Cell Rep*, 10: 1246-51.
Davis, J. Q., and V. Bennett. 1994. 'Ankyrin Binding-Activity Shared by the Neurofascin/L1/Nrcam Family of Nervous-System Cell-Adhesion Molecules', *Journal of Biological Chemistry*, 269: 27163-66.
Davis, J. Q., S. Lambert, and V. Bennett. 1996. 'Molecular composition of the node of Ranvier: identification of ankyrin-binding cell adhesion molecules neurofascin (mucin+/third FNIII domain-) and NrCAM at nodal axon segments', *Journal of Cell Biology*, 135: 1355-67.
Davis, L., K. Abdi, M. Machius, C. Brautigam, D. R. Tomchick, V. Bennett, and P. Michaely. 2009. 'Localization and structure of the ankyrin-binding site on beta2-spectrin', *J Biol Chem*, 284: 6982-7.
Del Pino, I., B. Rico, and O. Marin. 2018. 'Neural circuit dysfunction in mouse models of neurodevelopmental disorders', *Curr Opin Neurobiol*, 48: 174-82.
Dotti, C. G., C. A. Sullivan, and G. A. Banker. 1988. 'The establishment of polarity by hippocampal neurons in culture', *J Neurosci*, 8: 1454-68.
Dours-Zimmermann, M. T., K. Maurer, U. Rauch, W. Stoffel, R. Fassler, and D. R. Zimmermann. 2009. 'Versican V2 assembles the extracellular matrix surrounding the nodes of ranvier in the CNS', *J Neurosci*, 29: 7731-42.
Doyle, G. A., A. T. Lai, A. D. Chou, M. J. Wang, X. Gai, E. F. Rappaport, and W. H. Berrettini. 2012. 'Re-sequencing of ankyrin 3 exon 48 and case-control association analysis of rare variants in bipolar disorder type I', *Bipolar Disord*, 14: 809-21.
Duflocq, A., B. Le Bras, E. Bullier, F. Couraud, and M. Davenne. 2008. 'Nav1.1 is predominantly expressed in nodes of Ranvier and axon initial segments', *Molecular and Cellular Neuroscience*, 39: 180-92.
Duman, R. S., and B. Voleti. 2012. 'Signaling pathways underlying the pathophysiology and treatment of depression: novel mechanisms for rapid-acting agents', *Trends Neurosci*, 35: 47-56.
Dumitrescu, A. S., M. D. Evans, and M. S. Grubb. 2016. 'Evaluating Tools for Live Imaging of Structural Plasticity at the Axon Initial Segment', *Front Cell Neurosci*, 10: 268.
Dutta, R., and B. D. Trapp. 2007. 'Pathogenesis of axonal and neuronal damage in multiple sclerosis', *Neurology*, 68: S22-31; discussion S43-54.
Dzhashiashvili, Y., Y. Q. Zhang, J. Galinska, I. Lam, M. Grumet, and J. L. Salzer. 2007. 'Nodes of Ranvier and axon initial segments are ankyrin G-dependent domains that assemble by distinct mechanisms', *Journal of Cell Biology*, 177: 857-70.
el-Husseini Ael, D., and D. S. Bredt. 2002. 'Protein palmitoylation: a regulator of neuronal development and function', *Nature Reviews Neuroscience*, 3: 791-802.
Eshed, Y., K. Feinberg, S. Poliak, H. Sabanay, O. Sarig-Nadir, I. Spiegel, J. R. Bermingham, Jr., and E. Peles. 2005. 'Gliomedin mediates Schwann cell-axon interaction and the molecular assembly of the nodes of Ranvier', *Neuron*, 47: 215-29.

Evans, M. D., A. S. Dumitrescu, D. L. H. Kruijssen, S. E. Taylor, and M. S. Grubb. 2015. 'Rapid Modulation of Axon Initial Segment Length Influences Repetitive Spike Firing', *Cell Reports*, 13: 1233-45.

Evans, M. D., R. P. Sammons, S. Lebron, A. S. Dumitrescu, T. B. Watkins, V. N. Uebele, J. J. Renger, and M. S. Grubb. 2013. 'Calcineurin signaling mediates activity-dependent relocation of the axon initial segment', *J Neurosci*, 33: 6950-63.

Fache, M. P., A. Moussif, F. Fernandes, P. Giraud, J. J. Garrido, and B. Dargent. 2004. 'Endocytotic elimination and domain-selective tethering constitute a potential mechanism of protein segregation at the axonal initial segment', *Journal of Cell Biology*, 166: 571-78.

Farias, G. G., C. M. Guardia, D. J. Britt, X. Guo, and J. S. Bonifacino. 2015. 'Sorting of Dendritic and Axonal Vesicles at the Pre-axonal Exclusion Zone', *Cell Rep*, 13: 1221-32.

Feinberg, K., Y. Eshed-Eisenbach, S. Frechter, V. Amor, D. Salomon, H. Sabanay, J. L. Dupree, M. Grumet, P. J. Brophy, P. Shrager, and E. Peles. 2010. 'A glial signal consisting of gliomedin and NrCAM clusters axonal Na+ channels during the formation of nodes of Ranvier', *Neuron*, 65: 490-502.

Ferreira, M. A., M. C. O'Donovan, Y. A. Meng, I. R. Jones, D. M. Ruderfer, L. Jones, J. Fan, G. Kirov, R. H. Perlis, E. K. Green, J. W. Smoller, D. Grozeva, J. Stone, I. Nikolov, K. Chambert, M. L. Hamshere, V. L. Nimgaonkar, V. Moskvina, M. E. Thase, S. Caesar, G. S. Sachs, J. Franklin, K. Gordon-Smith, K. G. Ardlie, S. B. Gabriel, C. Fraser, B. Blumenstiel, M. Defelice, G. Breen, M. Gill, D. W. Morris, A. Elkin, W. J. Muir, K. A. McGhee, R. Williamson, D. J. MacIntyre, A. W. MacLean, C. D. St, M. Robinson, M. Van Beck, A. C. Pereira, R. Kandaswamy, A. McQuillin, D. A. Collier, N. J. Bass, A. H. Young, J. Lawrence, I. N. Ferrier, A. Anjorin, A. Farmer, D. Curtis, E. M. Scolnick, P. McGuffin, M. J. Daly, A. P. Corvin, P. A. Holmans, D. H. Blackwood, H. M. Gurling, M. J. Owen, S. M. Purcell, P. Sklar, N. Craddock, and Consortium Wellcome Trust Case Control. 2008. 'Collaborative genome-wide association analysis supports a role for ANK3 and CACNA1C in bipolar disorder', *Nature Genetics*, 40: 1056-8.

Fiorentino, A., N. L. O'Brien, D. P. Locke, A. McQuillin, A. Jarram, A. Anjorin, R. Kandaswamy, D. Curtis, R. A. Blizard, and H. M. Gurling. 2014. 'Analysis of ANK3 and CACNA1C variants identified in bipolar disorder whole genome sequence data', *Bipolar Disord*, 16: 583-91.

Fisahn, A., A. Contractor, R. D. Traub, E. H. Buhl, S. F. Heinemann, and C. J. McBain. 2004. 'Distinct roles for the kainate receptor subunits GluR5 and GluR6 in kainate-induced hippocampal gamma oscillations', *J Neurosci*, 24: 9658-68.

Fjell, J., P. Hjelmstrom, W. Hormuzdiar, M. Milenkovic, F. Aglieco, L. Tyrrell, S. Dib-Hajj, S. G. Waxman, and J. A. Black. 2000. 'Localization of the tetrodotoxin-resistant sodium channel NaN in nociceptors', *Neuroreport*, 11: 199-202.

Fogarty, M., M. Grist, D. Gelman, O. Marin, V. Pachnis, and N. Kessaris. 2007. 'Spatial genetic patterning of the embryonic neuroepithelium generates GABAergic interneuron diversity in the adult cortex', *J Neurosci*, 27: 10935-46.

Freal, A., C. Fassier, B. Le Bras, E. Bullier, S. De Gois, J. Hazan, C. C. Hoogenraad, and F. Couraud. 2016. 'Cooperative Interactions between 480 kDa Ankyrin-G and EB Proteins Assemble the Axon Initial Segment', *J Neurosci*, 36: 4421-33.

Fukata, M., A. Sekiya, T. Murakami, N. Yokoi, and Y. Fukata. 2015. 'Postsynaptic nanodomains generated by local palmitoylation cycles', *Biochem Soc Trans*, 43: 199-204.
Gainey, M. A., J. R. Hurvitz-Wolff, M. E. Lambo, and G. G. Turrigiano. 2009. 'Synaptic scaling requires the GluR2 subunit of the AMPA receptor', *J Neurosci*, 29: 6479-89.
Galiano, M. R., S. Jha, T. S. Y. Ho, C. S. Zhang, Y. Ogawa, K. J. Chang, M. C. Stankewich, P. J. Mohler, and M. N. Rasband. 2012. 'A Distal Axonal Cytoskeleton Forms an Intra-Axonal Boundary that Controls Axon Initial Segment Assembly', *Cell*, 149: 1125-39.
Garey, L. J., W. Y. Ong, T. S. Patel, M. Kanani, A. Davis, A. M. Mortimer, T. R. Barnes, and S. R. Hirsch. 1998. 'Reduced dendritic spine density on cerebral cortical pyramidal neurons in schizophrenia', *J Neurol Neurosurg Psychiatry*, 65: 446-53.
Gasser, A., T. S. Y. Ho, X. Y. Cheng, K. J. Chang, S. G. Waxman, M. N. Rasband, and S. D. Dib-Hajj. 2012. 'An AnkyrinG-Binding Motif Is Necessary and Sufficient for Targeting Na(v)1.6 Sodium Channels to Axon Initial Segments and Nodes of Ranvier', *Journal of Neuroscience*, 32: 7232-43.
Glantz, L. A., and D. A. Lewis. 2000. 'Decreased dendritic spine density on prefrontal cortical pyramidal neurons in schizophrenia', *Arch Gen Psychiatry*, 57: 65-73.
Goes, F. S., M. Pirooznia, J. S. Parla, M. Kramer, E. Ghiban, S. Mavruk, Y. C. Chen, E. T. Monson, V. L. Willour, R. Karchin, M. Flickinger, A. E. Locke, S. E. Levy, L. J. Scott, M. Boehnke, E. Stahl, J. L. Moran, C. M. Hultman, M. Landen, S. M. Purcell, P. Sklar, P. P. Zandi, W. R. McCombie, and J. B. Potash. 2016. 'Exome Sequencing of Familial Bipolar Disorder', *JAMA Psychiatry*, 73: 590-7.
Gould, T. D., and H. Einat. 2007. 'Animal models of bipolar disorder and mood stabilizer efficacy: a critical need for improvement', *Neurosci Biobehav Rev*, 31: 825-31.
Grubb, M. S., and J. Burrone. 2010. 'Activity-dependent relocation of the axon initial segment fine-tunes neuronal excitability', *Nature*, 465: 1070-U131.
Gutzmann, A., N. Ergul, R. Grossmann, C. Schultz, P. Wahle, and M. Engelhardt. 2014. 'A period of structural plasticity at the axon initial segment in developing visual cortex', *Front Neuroanat*, 8: 11.
Hall, J., S. Trent, K. L. Thomas, M. C. O'Donovan, and M. J. Owen. 2015. 'Genetic risk for schizophrenia: convergence on synaptic pathways involved in plasticity', *Biol Psychiatry*, 77: 52-8.
Hamada, M. S., and M. H. Kole. 2015. 'Myelin loss and axonal ion channel adaptations associated with gray matter neuronal hyperexcitability', *J Neurosci*, 35: 7272-86.
Hamdan, F. F., J. Gauthier, Y. Araki, D. T. Lin, Y. Yoshizawa, K. Higashi, A. R. Park, D. Spiegelman, S. Dobrzeniecka, A. Piton, H. Tomitori, H. Daoud, C. Massicotte, E. Henrion, O. Diallo, S. D. Group, M. Shekarabi, C. Marineau, M. Shevell, B. Maranda, G. Mitchell, A. Nadeau, G. D'Anjou, M. Vanasse, M. Srour, R. G. Lafreniere, P. Drapeau, J. C. Lacaille, E. Kim, J. R. Lee, K. Igarashi, R. L. Huganir, G. A. Rouleau, and J. L. Michaud. 2011. 'Excess of de novo deleterious mutations in genes associated with glutamatergic systems in nonsyndromic intellectual disability', *American Journal of Human Genetics*, 88: 306-16.
Hamdan, F. F., J. Gauthier, Y. Araki, D. T. Lin, Y. Yoshizawa, K. Higashi, A. R. Park, D. Spiegelman, S. Dobrzeniecka, A. Piton, H. Tomitori, H. Daoud, C. Massicotte, E. Henrion, O. Diallo, M. Shekarabi, C. Marineau, M. Shevell, B. Maranda, G. Mitchell, A. Nadeau, G. D'Anjou, M. Vanasse, M. Srour, R. G. Lafreniere, P. Drapeau, J. C. Lacaille,

E. Kim, J. R. Lee, K. Igarashi, R. L. Huganir, G. A. Rouleau, J. L. Michaud, and S2D Grp. 2011. 'Excess of De Novo Deleterious Mutations in Genes Associated with Glutamatergic Systems in Nonsyndromic Intellectual Disability (vol 88, pg 306, 2011)', *American Journal of Human Genetics*, 88: 516-16.

Han, J., P. Wu, F. Wang, and J. Chen. 2015. 'S-palmitoylation regulates AMPA receptors trafficking and function: a novel insight into synaptic regulation and therapeutics', *Acta Pharm Sin B*, 5: 1-7.

Han, K., J. L. Holder, Jr., C. P. Schaaf, H. Lu, H. Chen, H. Kang, J. Tang, Z. Wu, S. Hao, S. W. Cheung, P. Yu, H. Sun, A. M. Breman, A. Patel, H. C. Lu, and H. Y. Zoghbi. 2013. 'SHANK3 overexpression causes manic-like behaviour with unique pharmacogenetic properties', *Nature*, 503: 72-7.

Harada, K., S. Fukuda, M. Kunimoto, and K. Yoshida. 1997. 'Distribution of ankyrin isoforms and their proteolysis after ischemia and reperfusion in rat brain', *Journal of Neurochemistry*, 69: 371-76.

Harrison, P. J., J. R. Geddes, and E. M. Tunbridge. 2018. 'The Emerging Neurobiology of Bipolar Disorder', *Trends Neurosci*, 41: 18-30.

Hatzimanolis, A., N. Smyrnis, D. Avramopoulos, C. N. Stefanis, I. Evdokimidis, and N. C. Stefanis. 2012. 'Bipolar disorder ANK3 risk variant effect on sustained attention is replicated in a large healthy population', *Psychiatr Genet*, 22: 210-3.

Hayashi, T., G. Rumbaugh, and R. L. Huganir. 2005. 'Differential regulation of AMPA receptor subunit trafficking by palmitoylation of two distinct sites', *Neuron*, 47: 709-23.

He, M., K. M. Abdi, and V. Bennett. 2014. 'Ankyrin-G palmitoylation and betaII-spectrin binding to phosphoinositide lipids drive lateral membrane assembly', *Journal of Cell Biology*, 206: 273-88.

He, M., P. Jenkins, and V. Bennett. 2012. 'Cysteine 70 of ankyrin-G is S-palmitoylated and is required for function of ankyrin-G in membrane domain assembly', *J Biol Chem*, 287: 43995-4005.

Hedstrom, K. L., Y. Ogawa, and M. N. Rasband. 2008. 'AnkyrinG is required for maintenance of the axon initial segment and neuronal polarity', *Journal of Cell Biology*, 183: 635-40.

Hell, J. W., R. E. Westenbroek, C. Warner, M. K. Ahlijanian, W. Prystay, M. M. Gilbert, T. P. Snutch, and W. A. Catterall. 1993. 'Identification and differential subcellular localization of the neuronal class C and class D L-type calcium channel alpha 1 subunits', *Journal of Cell Biology*, 123: 949-62.

Henry, F. E., W. Hockeimer, A. Chen, S. P. Mysore, and M. A. Sutton. 2017. 'Mechanistic target of rapamycin is necessary for changes in dendritic spine morphology associated with long-term potentiation', *Mol Brain*, 10: 50.

Henry, M. A., H. J. Sorensen, L. R. Johnson, and S. R. Levinson. 2005. 'Localization of the Na-v 1.8 sodium channel isoform at nodes of Ranvier in normal human radicular tooth pulp', *Neuroscience Letters*, 380: 32-36.

Hill, A. S., A. Nishino, K. Nakajo, G. X. Zhang, J. R. Fineman, M. E. Selzer, Y. Okamura, and E. C. Cooper. 2008. 'Ion Channel Clustering at the Axon Initial Segment and Node of Ranvier Evolved Sequentially in Early Chordates', *Plos Genetics*, 4.

Hirokawa, N., and R. Takemura. 2005. 'Molecular motors and mechanisms of directional transport in neurons', *Nature Reviews Neuroscience*, 6: 201-14.

Ho, T. S., D. R. Zollinger, K. J. Chang, M. Xu, E. C. Cooper, M. C. Stankewich, V. Bennett, and M. N. Rasband. 2014. 'A hierarchy of ankyrin-spectrin complexes clusters sodium channels at nodes of Ranvier', *Nat Neurosci*, 17: 1664-72.

Hoogenraad, C. C., and F. Bradke. 2009. 'Control of neuronal polarity and plasticity--a renaissance for microtubules?', *Trends Cell Biol*, 19: 669-76.

Howell, O. W., A. Palser, A. Polito, S. Melrose, B. Zonta, C. Scheiermann, A. J. Vora, P. J. Brophy, and R. Reynolds. 2006. 'Disruption of neurofascin localization reveals early changes preceding demyelination and remyelination in multiple sclerosis', *Brain*, 129: 3173-85.

Hughes, T., L. Hansson, I. E. Sonderby, L. Athanasiu, V. Zuber, M. Tesli, J. Song, C. M. Hultman, S. E. Bergen, M. Landen, I. Melle, O. A. Andreassen, and S. Djurovic. 2016. 'A Loss-of-Function Variant in a Minor Isoform of ANK3 Protects Against Bipolar Disorder and Schizophrenia', *Biol Psychiatry*, 80: 323-30.

Hund, T. J., O. M. Koval, J. Li, P. J. Wright, L. Qian, J. S. Snyder, H. Gudmundsson, C. F. Kline, N. P. Davidson, N. Cardona, M. N. Rasband, M. E. Anderson, and P. J. Mohler. 2010. 'A beta(IV)-spectrin/CaMKII signaling complex is essential for membrane excitability in mice', *J Clin Invest*, 120: 3508-19.

Ibata, K., Q. Sun, and G. G. Turrigiano. 2008. 'Rapid synaptic scaling induced by changes in postsynaptic firing', *Neuron*, 57: 819-26.

Ikeda, Y., K. A. Dick, M. R. Weatherspoon, D. Gincel, K. R. Armbrust, J. C. Dalton, G. Stevanin, A. Durr, C. Zuhlke, K. Burk, H. B. Clark, A. Brice, J. D. Rothstein, L. J. Schut, J. W. Day, and L. P. Ranum. 2006. 'Spectrin mutations cause spinocerebellar ataxia type 5', *Nature Genetics*, 38: 184-90.

Insel, T. R. 2010. 'Rethinking schizophrenia', *Nature*, 468: 187-93.

Ipsaro, J. J., S. L. Harper, T. E. Messick, R. Marmorstein, A. Mondragon, and D. W. Speicher. 2010. 'Crystal structure and functional interpretation of the erythrocyte spectrin tetramerization domain complex', *Blood*, 115: 4843-52.

Ipsaro, J. J., and A. Mondragon. 2010. 'Structural basis for spectrin recognition by ankyrin', *Blood*, 115: 4093-101.

Iqbal, Z., G. Vandeweyer, M. van der Voet, A. M. Waryah, M. Y. Zahoor, J. A. Besseling, L. T. Roca, A. T. Vulto-van Silfhout, B. Nijhof, J. M. Kramer, N. Van der Aa, M. Ansar, H. Peeters, C. Helsmoortel, C. Gilissen, L. E. Vissers, J. A. Veltman, A. P. de Brouwer, R. Frank Kooy, S. Riazuddin, A. Schenck, H. van Bokhoven, and L. Rooms. 2013. 'Homozygous and heterozygous disruptions of ANK3: at the crossroads of neurodevelopmental and psychiatric disorders', *Hum Mol Genet*, 22: 1960-70.

Iqbal, Z., M. H. Willemsen, M. A. Papon, L. Musante, M. Benevento, H. Hu, H. Venselaar, W. M. Wissink-Lindhout, A. T. Vulto-van Silfhout, L. E. L. M. Vissers, A. P. M. de Brouwer, S. Marouillat, T. F. Wienker, H. H. Ropers, K. Kahrizi, N. N. Kasri, H. Najmabadi, F. Laumonnier, T. Kleefstra, and H. van Bokhoven. 2015. 'Homozygous SLC6A17 Mutations Cause Autosomal-Recessive Intellectual Disability with Progressive Tremor, Speech Impairment, and Behavioral Problems', *American Journal of Human Genetics*, 96: 386-96.

Jacobson, C., B. Schnapp, and G. A. Banker. 2006. 'A change in the selective translocation of the Kinesin-1 motor domain marks the initial specification of the axon', *Neuron*, 49: 797-804.

Jegla, T., M. M. Nguyen, C. Feng, D. J. Goetschius, E. Luna, D. B. van Rossum, B. Kamel, A. Pisupati, E. S. Milner, and M. M. Rolls. 2016. 'Bilaterian Giant Ankyrins Have a Common Evolutionary Origin and Play a Conserved Role in Patterning the Axon Initial Segment', *PLoS Genet*, 12: e1006457.

Jenkins, P. M., M. He, and V. Bennett. 2015. 'Dynamic spectrin/ankyrin-G microdomains promote lateral membrane assembly by opposing endocytosis', *Sci Adv*, 1: e1500301.

Jenkins, P. M., N. Kim, S. L. Jones, W. C. Tseng, T. M. Svitkina, H. H. Yin, and V. Bennett. 2015. 'Giant ankyrin-G: a critical innovation in vertebrate evolution of fast and integrated neuronal signaling', *Proc Natl Acad Sci U S A*, 112: 957-64.

Jenkins, P. M., C. Vasavda, J. Hostettler, J. Q. Davis, K. Abdi, and V. Bennett. 2013. 'E-cadherin polarity is determined by a multifunction motif mediating lateral membrane retention through ankyrin-G and apical-lateral transcytosis through clathrin', *J Biol Chem*, 288: 14018-31.

Jenkins, S. M., and V. Bennett. 2001. 'Ankyrin-G coordinates assembly of the spectrin-based membrane skeleton, voltage-gated sodium channels, and L1 CAMs at Purkinje neuron initial segments', *Journal of Cell Biology*, 155: 739-46.

Jeyifous, O., E. I. Lin, X. Chen, S. E. Antinone, R. Mastro, R. Drisdel, T. S. Reese, and W. N. Green. 2016. 'Palmitoylation regulates glutamate receptor distributions in postsynaptic densities through control of PSD95 conformation and orientation', *Proc Natl Acad Sci U S A*, 113: E8482-E91.

Jones, S. L., F. Korobova, and T. Svitkina. 2014. 'Axon initial segment cytoskeleton comprises a multiprotein submembranous coat containing sparse actin filaments', *Journal of Cell Biology*, 205: 67-81.

Jones, S. L., and T. M. Svitkina. 2016. 'Axon Initial Segment Cytoskeleton: Architecture, Development, and Role in Neuron Polarity', *Neural Plast*, 2016: 6808293.

Kapitein, L. C., and C. C. Hoogenraad. 2011. 'Which way to go? Cytoskeletal organization and polarized transport in neurons', *Molecular and Cellular Neuroscience*, 46: 9-20.

Kato-Negishi, M., K. Muramoto, M. Kawahara, Y. Kuroda, and M. Ichikawa. 2004. 'Developmental changes of GABAergic synapses formed between primary cultured cortical neurons', *Brain Res Dev Brain Res*, 152: 99-108.

Kaur, I., V. Yarov-Yarovoy, L. M. Kirk, K. E. Plambeck, E. V. Barragan, E. S. Ontiveros, and E. Diaz. 2016. 'Activity-Dependent Palmitoylation Controls SynDIG1 Stability, Localization, and Function', *J Neurosci*, 36: 7562-8.

Ketter, T. A., H. A. Nasrallah, and A. Fagiolini. 2006. 'Mood stabilizers and atypical antipsychotics: bimodal treatments for bipolar disorder', *Psychopharmacol Bull*, 39: 120-46.

Kim, M. J., K. Futai, J. Jo, Y. Hayashi, K. Cho, and M. Sheng. 2007. 'Synaptic accumulation of PSD-95 and synaptic function regulated by phosphorylation of serine-295 of PSD-95', *Neuron*, 56: 488-502.

Kim, S., and E. B. Ziff. 2014. 'Calcineurin mediates synaptic scaling via synaptic trafficking of Ca2+-permeable AMPA receptors', *PLoS Biol*, 12: e1001900.

Kirov, G., A. J. Pocklington, P. Holmans, D. Ivanov, M. Ikeda, D. Ruderfer, J. Moran, K. Chambert, D. Toncheva, L. Georgieva, D. Grozeva, M. Fjodorova, R. Wollerton, E. Rees, I. Nikolov, L. N. van de Lagemaat, A. Bayes, E. Fernandez, P. I. Olason, Y. Bottcher, N. H. Komiyama, M. O. Collins, J. Choudhary, K. Stefansson, H. Stefansson,

S. G. Grant, S. Purcell, P. Sklar, M. C. O'Donovan, and M. J. Owen. 2012. 'De novo CNV analysis implicates specific abnormalities of postsynaptic signalling complexes in the pathogenesis of schizophrenia', *Mol Psychiatry*, 17: 142-53.

Kitamura, K., M. Yanazawa, N. Sugiyama, H. Miura, A. Iizuka-Kogo, M. Kusaka, K. Omichi, R. Suzuki, Y. Kato-Fukui, K. Kamiirisa, M. Matsuo, S. Kamijo, M. Kasahara, H. Yoshioka, T. Ogata, T. Fukuda, I. Kondo, M. Kato, W. B. Dobyns, M. Yokoyama, and K. Morohashi. 2002. 'Mutation of ARX causes abnormal development of forebrain and testes in mice and X-linked lissencephaly with abnormal genitalia in humans', *Nature Genetics*, 32: 359-69.

Kittler, J. T., P. Delmas, J. N. Jovanovic, D. A. Brown, T. G. Smart, and S. J. Moss. 2000. 'Constitutive endocytosis of GABAA receptors by an association with the adaptin AP2 complex modulates inhibitory synaptic currents in hippocampal neurons', *J Neurosci*, 20: 7972-7.

Kizhatil, K., S. A. Baker, V. Y. Arshavsky, and V. Bennett. 2009. 'Ankyrin-G promotes cyclic nucleotide-gated channel transport to rod photoreceptor sensory cilia', *Science*, 323: 1614-7.

Kizhatil, K., W. Yoon, P. J. Mohler, L. H. Davis, J. A. Hoffman, and V. Bennett. 2007. 'Ankyrin-G and beta2-spectrin collaborate in biogenesis of lateral membrane of human bronchial epithelial cells', *J Biol Chem*, 282: 2029-37.

Kloth, K., J. Denecke, M. Hempel, J. Johannsen, T. M. Strom, C. Kubisch, and D. Lessel. 2017. 'First de novo ANK3 nonsense mutation in a boy with intellectual disability, speech impairment and autistic features', *Eur J Med Genet*, 60: 494-98.

Knight, D., R. Harris, M. S. McAlister, J. P. Phelan, S. Geddes, S. J. Moss, P. C. Driscoll, and N. H. Keep. 2002. 'The X-ray crystal structure and putative ligand-derived peptide binding properties of gamma-aminobutyric acid receptor type A receptor-associated protein', *J Biol Chem*, 277: 5556-61.

Kobayashi, T., B. Storrie, K. Simons, and C. G. Dotti. 1992. 'A functional barrier to movement of lipids in polarized neurons', *Nature*, 359: 647-50.

Kole, M. H., S. U. Ilschner, B. M. Kampa, S. R. Williams, P. C. Ruben, and G. J. Stuart. 2008. 'Action potential generation requires a high sodium channel density in the axon initial segment', *Nat Neurosci*, 11: 178-86.

Kole, M. H., and G. J. Stuart. 2012. 'Signal processing in the axon initial segment', *Neuron*, 73: 235-47.

Komada, M., and P. Soriano. 2002. 'beta IV-spectrin regulates sodium channel clustering through ankyrin-G at axon initial segments and nodes of Ranvier', *Journal of Cell Biology*, 156: 337-48.

Konopaske, G. T., N. Lange, J. T. Coyle, and F. M. Benes. 2014. 'Prefrontal cortical dendritic spine pathology in schizophrenia and bipolar disorder', *JAMA Psychiatry*, 71: 1323-31.

Konradi, C., E. I. Zimmerman, C. K. Yang, K. M. Lohmann, P. Gresch, H. Pantazopoulos, S. Berretta, and S. Heckers. 2011. 'Hippocampal interneurons in bipolar disorder', *Arch Gen Psychiatry*, 68: 340-50.

Kordeli, E., S. Lambert, and V. Bennett. 1995. 'AnkyrinG. A new ankyrin gene with neural-specific isoforms localized at the axonal initial segment and node of Ranvier', *J Biol Chem*, 270: 2352-9.

Korycka, J., A. Lach, E. Heger, D. M. Boguslawska, M. Wolny, M. Toporkiewicz, K. Augoff, J. Korzeniewski, and A. F. Sikorski. 2012. 'Human DHHC proteins: a spotlight on the hidden player of palmitoylation', *Eur J Cell Biol*, 91: 107-17.

Kuba, H., T. M. Ishii, and H. Ohmori. 2006. 'Axonal site of spike initiation enhances auditory coincidence detection', *Nature*, 444: 1069-72.

Kuba, H., Y. Oichi, and H. Ohmori. 2010. 'Presynaptic activity regulates Na+ channel distribution at the axon initial segment', *Nature*, 465: 1075-U136.

Kuijpers, M., D. van de Willige, A. Freal, A. Chazeau, M. A. Franker, J. Hofenk, R. J. C. Rodrigues, L. C. Kapitein, A. Akhmanova, D. Jaarsma, and C. C. Hoogenraad. 2016. 'Dynein Regulator NDEL1 Controls Polarized Cargo Transport at the Axon Initial Segment', *Neuron*, 89: 461-71.

Lai, H. C., and L. Y. Jan. 2006. 'The distribution and targeting of neuronal voltage-gated ion channels', *Nature Reviews Neuroscience*, 7: 548-62.

Lambert, S., J. Q. Davis, and V. Bennett. 1997. 'Morphogenesis of the node of Ranvier: Co-clusters of ankyrin and ankyrin-binding integral proteins define early developmental intermediates', *Journal of Neuroscience*, 17: 7025-36.

Lazarus, M. S., K. Krishnan, and Z. J. Huang. 2015. 'GAD67 deficiency in parvalbumin interneurons produces deficits in inhibitory transmission and network disinhibition in mouse prefrontal cortex', *Cereb Cortex*, 25: 1290-6.

Le Bras, B., A. Freal, A. Czarnecki, P. Legendre, E. Bullier, M. Komada, P. J. Brophy, M. Davenne, and F. Couraud. 2014. 'In vivo assembly of the axon initial segment in motor neurons', *Brain Struct Funct*, 219: 1433-50.

Lee, Y., Y. Zhang, S. Kim, and K. Han. 2018. 'Excitatory and inhibitory synaptic dysfunction in mania: an emerging hypothesis from animal model studies', *Exp Mol Med*, 50: 12.

Lek, M., K. J. Karczewski, E. V. Minikel, K. E. Samocha, E. Banks, T. Fennell, A. H. O'Donnell-Luria, J. S. Ware, A. J. Hill, B. B. Cummings, T. Tukiainen, D. P. Birnbaum, J. A. Kosmicki, L. E. Duncan, K. Estrada, F. Zhao, J. Zou, E. Pierce-Hoffman, J. Berghout, D. N. Cooper, N. Deflaux, M. DePristo, R. Do, J. Flannick, M. Fromer, L. Gauthier, J. Goldstein, N. Gupta, D. Howrigan, A. Kiezun, M. I. Kurki, A. L. Moonshine, P. Natarajan, L. Orozco, G. M. Peloso, R. Poplin, M. A. Rivas, V. Ruano-Rubio, S. A. Rose, D. M. Ruderfer, K. Shakir, P. D. Stenson, C. Stevens, B. P. Thomas, G. Tiao, M. T. Tusie-Luna, B. Weisburd, H. H. Won, D. Yu, D. M. Altshuler, D. Ardissino, M. Boehnke, J. Danesh, S. Donnelly, R. Elosua, J. C. Florez, S. B. Gabriel, G. Getz, S. J. Glatt, C. M. Hultman, S. Kathiresan, M. Laakso, S. McCarroll, M. I. McCarthy, D. McGovern, R. McPherson, B. M. Neale, A. Palotie, S. M. Purcell, D. Saleheen, J. M. Scharf, P. Sklar, P. F. Sullivan, J. Tuomilehto, M. T. Tsuang, H. C. Watkins, J. G. Wilson, M. J. Daly, D. G. MacArthur, and Consortium Exome Aggregation. 2016. 'Analysis of protein-coding genetic variation in 60,706 humans', *Nature*, 536: 285-91.

Leterrier, C., N. Clerc, F. Rueda-Boroni, A. Montersino, B. Dargent, and F. Castets. 2017. 'Ankyrin G Membrane Partners Drive the Establishment and Maintenance of the Axon Initial Segment', *Front Cell Neurosci*, 11: 6.

Leterrier, C., J. Potier, G. Caillol, C. Debarnot, F. Rueda Boroni, and B. Dargent. 2015. 'Nanoscale Architecture of the Axon Initial Segment Reveals an Organized and Robust Scaffold', *Cell Rep*, 13: 2781-93.

Lett, T. A., C. C. Zai, A. K. Tiwari, S. A. Shaikh, O. Likhodi, J. L. Kennedy, and D. J. Muller. 2011. 'ANK3, CACNA1C and ZNF804A gene variants in bipolar disorders and psychosis subphenotype', *World J Biol Psychiatry*, 12: 392-7.

Leussis, M. P., E. M. Berry-Scott, M. Saito, H. Jhuang, G. de Haan, O. Alkan, C. J. Luce, J. M. Madison, P. Sklar, T. Serre, D. E. Root, and T. L. Petryshen. 2013. 'The ANK3 bipolar disorder gene regulates psychiatric-related behaviors that are modulated by lithium and stress', *Biol Psychiatry*, 73: 683-90.

Leussis, M. P., J. M. Madison, and T. L. Petryshen. 2012. 'Ankyrin 3: genetic association with bipolar disorder and relevance to disease pathophysiology', *Biol Mood Anxiety Disord*, 2: 18.

Lewis, T. L., T. Y. Mao, K. Svoboda, and D. B. Arnold. 2009. 'Myosin-dependent targeting of transmembrane proteins to neuronal dendrites', *Nature Neuroscience*, 12: 568-76.

Li, J., R. Zhu, K. Chen, H. Zheng, H. Zhao, C. Yuan, H. Zhang, C. Wang, and M. Zhang. 2018. 'Potent and specific Atg8-targeting autophagy inhibitory peptides from giant ankyrins', *Nat Chem Biol*, 14: 778-87.

Lin, Y. C., and A. J. Koleske. 2010. 'Mechanisms of synapse and dendrite maintenance and their disruption in psychiatric and neurodegenerative disorders', *Annu Rev Neurosci*, 33: 349-78.

Liu, Y., D. H. Blackwood, S. Caesar, E. J. de Geus, A. Farmer, M. A. Ferreira, I. N. Ferrier, C. Fraser, K. Gordon-Smith, E. K. Green, D. Grozeva, H. M. Gurling, M. L. Hamshere, P. Heutink, P. A. Holmans, W. J. Hoogendijk, J. J. Hottenga, L. Jones, I. R. Jones, G. Kirov, D. Lin, P. McGuffin, V. Moskvina, W. A. Nolen, R. H. Perlis, D. Posthuma, E. M. Scolnick, A. B. Smit, J. H. Smit, J. W. Smoller, D. St Clair, R. van Dyck, M. Verhage, G. Willemsen, A. H. Young, T. Zandbelt, D. I. Boomsma, N. Craddock, M. C. O'Donovan, M. J. Owen, B. W. Penninx, S. Purcell, P. Sklar, P. F. Sullivan, and Consortium Wellcome Trust Case-Control. 2011. 'Meta-analysis of genome-wide association data of bipolar disorder and major depressive disorder', *Mol Psychiatry*, 16: 2-4.

Lopez, A. Y., X. Wang, M. Xu, A. Maheshwari, D. Curry, S. Lam, A. M. Adesina, J. L. Noebels, Q. Q. Sun, and E. C. Cooper. 2017. 'Ankyrin-G isoform imbalance and interneuronopathy link epilepsy and bipolar disorder', *Mol Psychiatry*, 22: 1464-72.

Lorenzo, D. N., A. Badea, J. Davis, J. Hostettler, J. He, G. S. Zhong, X. W. Zhuang, and V. Bennett. 2014. 'A PIK3C3-Ankyrin-B-Dynactin pathway promotes axonal growth and multiorganelle transport', *Journal of Cell Biology*, 207: 735-52.

Lowe, J. S., O. Palygin, N. Bhasin, T. J. Hund, P. A. Boyden, E. Shibata, M. E. Anderson, and P. J. Mohler. 2008. 'Voltage-gated Nav channel targeting in the heart requires an ankyrin-G dependent cellular pathway', *Journal of Cell Biology*, 180: 173-86.

Makara, M. A., J. Curran, S. C. Little, H. Musa, I. Polina, S. A. Smith, P. J. Wright, S. D. Unudurthi, J. Snyder, V. Bennett, T. J. Hund, and P. J. Mohler. 2014. 'Ankyrin-G coordinates intercalated disc signaling platform to regulate cardiac excitability in vivo', *Circ Res*, 115: 929-38.

Mansuy-Schlick, V., F. Tolle, R. Delage-Mourroux, A. Fraichard, P. Y. Risold, and M. Jouvenot. 2006. 'Specific distribution of gabarap, gec1/gabarap Like 1, gate16/gabarap Like 2, lc3 messenger RNAs in rat brain areas by quantitative real-time PCR', *Brain Res*, 1073-1074: 83-7.

Mao, W., A. C. Salzberg, M. Uchigashima, Y. Hasegawa, H. Hock, M. Watanabe, S. Akbarian, Y. I. Kawasawa, and K. Futai. 2018. 'Activity-Induced Regulation of Synaptic Strength through the Chromatin Reader L3mbtl1', *Cell Rep*, 23: 3209-22.

Marin, O. 2012. 'Interneuron dysfunction in psychiatric disorders', *Nature Reviews Neuroscience*, 13: 107-20.

Markram, H., M. Toledo-Rodriguez, Y. Wang, A. Gupta, G. Silberberg, and C. Wu. 2004. 'Interneurons of the neocortical inhibitory system', *Nature Reviews Neuroscience*, 5: 793-807.

Masurel-Paulet, A., V. M. Kalscheuer, N. Lebrun, H. Hu, F. Levy, C. Thauvin-Robinet, V. Darmency-Stamboul, S. El Chehadeh, J. Thevenon, S. Chancenotte, M. Ruffier-Bourdet, M. Bonnet, J. M. Pinoit, F. Huet, V. Desportes, J. Chelly, and L. Faivre. 2014. 'Expanding the clinical phenotype of patients with a ZDHHC9 mutation', *Am J Med Genet A*, 164A: 789-95.

Mathey, E. K., T. Derfuss, M. K. Storch, K. R. Williams, K. Hales, D. R. Woolley, A. Al-Hayani, S. N. Davies, M. N. Rasband, T. Olsson, A. Moldenhauer, S. Velhin, R. Hohlfeld, E. Meinl, and C. Linington. 2007. 'Neurofascin as a novel target for autoantibody-mediated axonal injury', *J Exp Med*, 204: 2363-72.

Miro, X., S. Meier, M. L. Dreisow, J. Frank, J. Strohmaier, R. Breuer, C. Schmal, O. Albayram, M. T. Pardo-Olmedilla, T. W. Muhleisen, F. A. Degenhardt, M. Mattheisen, I. Reinhard, A. Bilkei-Gorzo, S. Cichon, C. Seidenbecher, M. Rietschel, M. M. Nothen, and A. Zimmer. 2012. 'Studies in humans and mice implicate neurocan in the etiology of mania', *Am J Psychiatry*, 169: 982-90.

Misonou, H., D. P. Mohapatra, E. W. Park, V. Leung, D. Zhen, K. Misonou, A. E. Anderson, and J. S. Trimmer. 2004. 'Regulation of ion channel localization and phosphorylation by neuronal activity', *Nat Neurosci*, 7: 711-8.

Mohler, P. J., I. Rivolta, C. Napolitano, G. LeMaillet, S. Lambert, S. G. Priori, and V. Bennett. 2004. 'Nav1.5 E1053K mutation causing Brugada syndrome blocks binding to ankyrin-G and expression of Nav1.5 on the surface of cardiomyocytes', *Proc Natl Acad Sci U S A*, 101: 17533-8.

Mohler, P. J., W. Yoon, and V. Bennett. 2004. 'Ankyrin-B targets beta(2)-spectrin to an intracellular compartment in neonatal cardiomyocytes', *Journal of Biological Chemistry*, 279: 40185-93.

Mohrluder, J., Y. Hoffmann, T. Stangler, K. Hanel, and D. Willbold. 2007. 'Identification of clathrin heavy chain as a direct interaction partner for the gamma-aminobutyric acid type A receptor associated protein', *Biochemistry*, 46: 14537-43.

Mohrluder, J., T. Stangler, Y. Hoffmann, K. Wiesehan, A. Mataruga, and D. Willbold. 2007. 'Identification of calreticulin as a ligand of GABARAP by phage display screening of a peptide library', *FEBS J*, 274: 5543-55.

Muhleisen, T. W., M. Leber, T. G. Schulze, J. Strohmaier, F. Degenhardt, J. Treutlein, M. Mattheisen, A. J. Forstner, J. Schumacher, R. Breuer, S. Meier, S. Herms, P. Hoffmann, A. Lacour, S. H. Witt, A. Reif, B. Muller-Myhsok, S. Lucae, W. Maier, M. Schwarz, H. Vedder, J. Kammerer-Ciernioch, A. Pfennig, M. Bauer, M. Hautzinger, S. Moebus, L. Priebe, P. M. Czerski, J. Hauser, J. Lissowska, N. Szeszenia-Dabrowska, P. Brennan, J. D. Mckay, A. Wright, P. B. Mitchell, J. M. Fullerton, P. R. Schofield, G. W. Montgomery, S. E. Medland, S. D. Gordon, N. G. Martin, V. Krasnow, A. Chuchalin, G.

Babadjanova, G. Pantelejeva, L. I. Abramova, A. S. Tiganov, A. Polonikov, E. Khusnutdinova, M. Alda, P. Grof, G. A. Rouleau, G. Turecki, C. Laprise, F. Rivas, F. Mayoral, M. Kogevinas, M. Grigoroiu-Serbanescu, P. Propping, T. Becker, M. Rietschel, M. M. Nothen, and S. Cichon. 2014. 'Genome-wide association study reveals two new risk loci for bipolar disorder', *Nature Communications*, 5.

Muir, J., and J. T. Kittler. 2014. 'Plasticity of GABA(A) receptor diffusion dynamics at the axon initial segment', *Frontiers in Cellular Neuroscience*, 8.

Mukai, J., A. Dhilla, L. J. Drew, K. L. Stark, L. Cao, A. B. MacDermott, M. Karayiorgou, and J. A. Gogos. 2008. 'Palmitoylation-dependent neurodevelopmental deficits in a mouse model of 22q11 microdeletion', *Nat Neurosci*, 11: 1302-10.

Mukai, J., H. Liu, R. A. Burt, D. E. Swor, W. S. Lai, M. Karayiorgou, and J. A. Gogos. 2004. 'Evidence that the gene encoding ZDHHC8 contributes to the risk of schizophrenia', *Nature Genetics*, 36: 725-31.

Nakada, C., K. Ritchie, Y. Oba, M. Nakamura, Y. Hotta, R. Iino, R. S. Kasai, K. Yamaguchi, T. Fujiwara, and A. Kusumi. 2003. 'Accumulation of anchored proteins forms membrane diffusion barriers during neuronal polarization', *Nat Cell Biol*, 5: 626-32.

Nakata, T., S. Niwa, Y. Okada, F. Perez, and N. Hirokawa. 2011. 'Preferential binding of a kinesin-1 motor to GTP-tubulin-rich microtubules underlies polarized vesicle transport', *Journal of Cell Biology*, 194: 245-55.

Nelson, A. D., R. N. Caballero-Floran, J. C. Rodriguez Diaz, J. M. Hull, Y. Yuan, J. Li, K. Chen, K. K. Walder, L. F. Lopez-Santiago, V. Bennett, M. G. McInnis, L. L. Isom, C. Wang, M. Zhang, K. S. Jones, and P. M. Jenkins. 2018. 'Ankyrin-G regulates forebrain connectivity and network synchronization via interaction with GABARAP', *Mol Psychiatry*.

Nelson, A. D., and P. M. Jenkins. 2017. 'Axonal Membranes and Their Domains: Assembly and Function of the Axon Initial Segment and Node of Ranvier', *Front Cell Neurosci*, 11: 136.

Nicita, F., F. Ulgiati, L. Bernardini, G. Garone, L. Papetti, A. Novelli, and A. Spalice. 2015. 'Early myoclonic encephalopathy in 9q33-q34 deletion encompassing STXBP1 and SPTAN1', *Ann Hum Genet*, 79: 209-17.

Nimchinsky, E. A., B. L. Sabatini, and K. Svoboda. 2002. 'Structure and function of dendritic spines', *Annu Rev Physiol*, 64: 313-53.

Nurnberger, J. I., Jr., M. C. Blehar, C. A. Kaufmann, C. York-Cooler, S. G. Simpson, J. Harkavy-Friedman, J. B. Severe, D. Malaspina, and T. Reich. 1994. 'Diagnostic interview for genetic studies. Rationale, unique features, and training. NIMH Genetics Initiative', *Arch Gen Psychiatry*, 51: 849-59; discussion 63-4.

O'Brien, R. J., S. Kamboj, M. D. Ehlers, K. R. Rosen, G. D. Fischbach, and R. L. Huganir. 1998. 'Activity-dependent modulation of synaptic AMPA receptor accumulation', *Neuron*, 21: 1067-78.

O'Malley, H. A., and L. L. Isom. 2015. 'Sodium channel beta subunits: emerging targets in channelopathies', *Annu Rev Physiol*, 77: 481-504.

O'Sullivan, G. A., M. Kneussel, Z. Elazar, and H. Betz. 2005. 'GABARAP is not essential for GABA receptor targeting to the synapse', *Eur J Neurosci*, 22: 2644-8.

Occhi, S., D. Zambroni, U. Del Carro, S. Amadio, E. E. Sirkowski, S. S. Scherer, K. P. Campbell, S. A. Moore, Z. L. Chen, S. Strickland, A. Di Muzio, A. Uncini, L. Wrabetz,

and M. L. Feltri. 2005. 'Both laminin and Schwann cell dystroglycan are necessary for proper clustering of sodium channels at nodes of Ranvier', *J Neurosci*, 25: 9418-27.
Ogawa, Y., D. P. Schafer, I. Horresh, V. Bar, K. Hales, Y. Yang, K. Susuki, E. Peles, M. C. Stankewich, and M. N. Rasband. 2006. 'Spectrins and ankyrinB constitute a specialized paranodal cytoskeleton', *Journal of Neuroscience*, 26: 5230-39.
Oh, M. C., V. A. Derkach, E. S. Guire, and T. R. Soderling. 2006. 'Extrasynaptic membrane trafficking regulated by GluR1 serine 845 phosphorylation primes AMPA receptors for long-term potentiation', *J Biol Chem*, 281: 752-8.
Ohgi, Y., T. Futamura, and K. Hashimoto. 2015. 'Glutamate Signaling in Synaptogenesis and NMDA Receptors as Potential Therapeutic Targets for Psychiatric Disorders', *Curr Mol Med*, 15: 206-21.
Oohashi, T., S. Hirakawa, Y. Bekku, U. Rauch, D. R. Zimmermann, W. D. Su, A. Ohtsuka, T. Murakami, and Y. Ninomiya. 2002. 'Bral1, a brain-specific link protein, colocalizing with the versican V2 isoform at the nodes of Ranvier in developing and adult mouse central nervous systems', *Molecular and Cellular Neuroscience*, 19: 43-57.
Opazo, P., S. Labrecque, C. M. Tigaret, A. Frouin, P. W. Wiseman, P. De Koninck, and D. Choquet. 2010. 'CaMKII triggers the diffusional trapping of surface AMPARs through phosphorylation of stargazin', *Neuron*, 67: 239-52.
Osorio, N., G. Alcaraz, F. Padilla, F. Couraud, P. Delmas, and M. Crest. 2005. 'Differential targeting and functional specialization of sodium channels in cultured cerebellar granule cells', *J Physiol*, 569: 801-16.
Ozerdem, A., B. Guntekin, E. Saatci, Z. Tunca, and E. Basar. 2010. 'Disturbance in long distance gamma coherence in bipolar disorder', *Prog Neuropsychopharmacol Biol Psychiatry*, 34: 861-5.
Ozerdema, A., B. Guntekind, M. I. Atagune, and E. Basar. 2013. 'Brain oscillations in bipolar disorder in search of new biomarkers', *Suppl Clin Neurophysiol*, 62: 207-21.
Palay, S. L., C. Sotelo, A. Peters, and P. M. Orkand. 1968. 'Axon Hillock and Initial Segment', *Journal of Cell Biology*, 38: 193-&.
Pan, Z., T. Kao, Z. Horvath, J. Lemos, J. Y. Sul, S. D. Cranstoun, V. Bennett, S. S. Scherer, and E. C. Cooper. 2006. 'A common ankyrin-G-based mechanism retains KCNQ and NaV channels at electrically active domains of the axon', *J Neurosci*, 26: 2599-613.
Pedraza, L., J. K. Huang, and D. R. Colman. 2001. 'Organizing principles of the axoglial apparatus', *Neuron*, 30: 335-44.
Penzes, P., A. Buonanno, M. Passafaro, C. Sala, and R. A. Sweet. 2013. 'Developmental vulnerability of synapses and circuits associated with neuropsychiatric disorders', *Journal of Neurochemistry*, 126: 165-82.
Penzes, P., M. E. Cahill, K. A. Jones, J. E. VanLeeuwen, and K. M. Woolfrey. 2011. 'Dendritic spine pathology in neuropsychiatric disorders', *Nat Neurosci*, 14: 285-93.
Petersen, J. D., S. Kaech, and G. Banker. 2014. 'Selective microtubule-based transport of dendritic membrane proteins arises in concert with axon specification', *J Neurosci*, 34: 4135-47.
Pozo, K., and Y. Goda. 2010. 'Unraveling mechanisms of homeostatic synaptic plasticity', *Neuron*, 66: 337-51.
Rabinowitch, I., and I. Segev. 2008. 'Two opposing plasticity mechanisms pulling a single synapse', *Trends Neurosci*, 31: 377-83.

Rasband, M. N. 2010. 'The axon initial segment and the maintenance of neuronal polarity', *Nature Reviews Neuroscience*, 11: 552-62.
Rasband, M. N., E. Peles, J. S. Trimmer, S. R. Levinson, S. E. Lux, and P. Shrager. 1999. 'Dependence of nodal sodium channel clustering on paranodal axoglial contact in the developing CNS', *J Neurosci*, 19: 7516-28.
Ren, Q., and V. Bennett. 1998. 'Palmitoylation of neurofascin at a site in the membrane-spanning domain highly conserved among the L1 family of cell adhesion molecules', *Journal of Neurochemistry*, 70: 1839-49.
Rogov, V. V., A. Stolz, A. C. Ravichandran, D. O. Rios-Szwed, H. Suzuki, A. Kniss, F. Lohr, S. Wakatsuki, V. Dotsch, I. Dikic, R. C. Dobson, and D. G. McEwan. 2017. 'Structural and functional analysis of the GABARAP interaction motif (GIM)', *EMBO Rep*, 18: 1382-96.
Roussos, P., P. Katsel, K. L. Davis, P. Bitsios, S. G. Giakoumaki, J. Jogia, K. Rozsnyai, D. Collier, S. Frangou, L. J. Siever, and V. Haroutunian. 2012. 'Molecular and genetic evidence for abnormalities in the nodes of Ranvier in schizophrenia', *Arch Gen Psychiatry*, 69: 7-15.
Roybal, K., D. Theobold, A. Graham, J. A. DiNieri, S. J. Russo, V. Krishnan, S. Chakravarty, J. Peevey, N. Oehrlein, S. Birnbaum, M. H. Vitaterna, P. Orsulak, J. S. Takahashi, E. J. Nestler, W. A. Carlezon, Jr., and C. A. McClung. 2007. 'Mania-like behavior induced by disruption of CLOCK', *Proc Natl Acad Sci U S A*, 104: 6406-11.
Rudy, B., G. Fishell, S. Lee, and J. Hjerling-Leffler. 2011. 'Three groups of interneurons account for nearly 100% of neocortical GABAergic neurons', *Dev Neurobiol*, 71: 45-61.
Rueckert, E. H., D. Barker, D. Ruderfer, S. E. Bergen, C. O'Dushlaine, C. J. Luce, S. D. Sheridan, K. M. Theriault, K. Chambert, J. Moran, S. M. Purcell, J. M. Madison, S. J. Haggarty, and P. Sklar. 2013. 'Cis-acting regulation of brain-specific ANK3 gene expression by a genetic variant associated with bipolar disorder', *Mol Psychiatry*, 18: 922-9.
Saifetiarova, J., X. Liu, A. M. Taylor, J. Li, and M. A. Bhat. 2017. 'Axonal domain disorganization in Caspr1 and Caspr2 mutant myelinated axons affects neuromuscular junction integrity, leading to muscle atrophy', *J Neurosci Res*.
Saitsu, H., J. Tohyama, T. Kumada, K. Egawa, K. Hamada, I. Okada, T. Mizuguchi, H. Osaka, R. Miyata, T. Furukawa, K. Haginoya, H. Hoshino, T. Goto, Y. Hachiya, T. Yamagata, S. Saitoh, T. Nagai, K. Nishiyama, A. Nishimura, N. Miyake, M. Komada, K. Hayashi, S. Hirai, K. Ogata, M. Kato, A. Fukuda, and N. Matsumoto. 2010. 'Dominant-negative mutations in alpha-II spectrin cause West syndrome with severe cerebral hypomyelination, spastic quadriplegia, and developmental delay', *American Journal of Human Genetics*, 86: 881-91.
Sanders, S. J., X. He, A. J. Willsey, A. G. Ercan-Sencicek, K. E. Samocha, A. E. Cicek, M. T. Murtha, V. H. Bal, S. L. Bishop, S. Dong, A. P. Goldberg, C. Jinlu, J. F. Keaney, 3rd, L. Klei, J. D. Mandell, D. Moreno-De-Luca, C. S. Poultney, E. B. Robinson, L. Smith, T. Solli-Nowlan, M. Y. Su, N. A. Teran, M. F. Walker, D. M. Werling, A. L. Beaudet, R. M. Cantor, E. Fombonne, D. H. Geschwind, D. E. Grice, C. Lord, J. K. Lowe, S. M. Mane, D. M. Martin, E. M. Morrow, M. E. Talkowski, J. S. Sutcliffe, C. A. Walsh, T. W. Yu, Consortium Autism Sequencing, D. H. Ledbetter, C. L. Martin, E. H. Cook, J. D. Buxbaum, M. J. Daly, B. Devlin, K. Roeder, and M. W. State. 2015. 'Insights into Autism

Spectrum Disorder Genomic Architecture and Biology from 71 Risk Loci', *Neuron*, 87: 1215-33.
Schafer, D. P., A. W. Custer, P. Shrager, and M. N. Rasband. 2006. 'Early events in node of Ranvier formation during myelination and remyelination in the PNS', *Neuron Glia Biol*, 2: 69-79.
Schafer, D. P., S. Jha, F. D. Liu, T. Akella, L. D. McCullough, and M. N. Rasband. 2009. 'Disruption of the Axon Initial Segment Cytoskeleton Is a New Mechanism for Neuronal Injury', *Journal of Neuroscience*, 29: 13242-54.
Schubert, K. O., M. Focking, and D. R. Cotter. 2015. 'Proteomic pathway analysis of the hippocampus in schizophrenia and bipolar affective disorder implicates 14-3-3 signaling, aryl hydrocarbon receptor signaling, and glucose metabolism: potential roles in GABAergic interneuron pathology', *Schizophr Res*, 167: 64-72.
Schulze, T. G. 2010. 'Genetic research into bipolar disorder: the need for a research framework that integrates sophisticated molecular biology and clinically informed phenotype characterization', *Psychiatr Clin North Am*, 33: 67-82.
Schulze, T. G., S. D. Detera-Wadleigh, N. Akula, A. Gupta, L. Kassem, J. Steele, J. Pearl, J. Strohmaier, R. Breuer, M. Schwarz, P. Propping, M. M. Nothen, S. Cichon, J. Schumacher, Nimh Genetics Initiative Bipolar Disorder Consortium, M. Rietschel, and F. J. McMahon. 2009. 'Two variants in Ankyrin 3 (ANK3) are independent genetic risk factors for bipolar disorder', *Mol Psychiatry*, 14: 487-91.
Scott, L. J., P. Muglia, X. Q. Kong, W. Guan, M. Flickinger, R. Upmanyu, F. Tozzi, J. Z. Li, M. Burmeister, D. Absher, R. C. Thompson, C. Francks, F. Meng, A. Antoniades, A. M. Southwick, A. F. Schatzberg, W. E. Bunney, J. D. Barchas, E. G. Jones, R. Day, K. Matthews, P. McGuffin, J. S. Strauss, J. L. Kennedy, L. Middleton, A. D. Roses, S. J. Watson, J. B. Vincent, R. M. Myers, A. E. Farmer, H. Akil, D. K. Burns, and M. Boehnke. 2009. 'Genome-wide association and meta-analysis of bipolar disorder in individuals of European ancestry', *Proc Natl Acad Sci U S A*, 106: 7501-6.
Sekino, Y., N. Kojima, and T. Shirao. 2007. 'Role of actin cytoskeleton in dendritic spine morphogenesis', *Neurochem Int*, 51: 92-104.
Selten, M., H. van Bokhoven, and N. Nadif Kasri. 2018. 'Inhibitory control of the excitatory/inhibitory balance in psychiatric disorders', *F1000Res*, 7: 23.
Selzam, S., J. R. I. Coleman, A. Caspi, T. E. Moffitt, and R. Plomin. 2018. 'A polygenic p factor for major psychiatric disorders', *Transl Psychiatry*, 8: 205.
Shepherd, J. D., G. Rumbaugh, J. Wu, S. Chowdhury, N. Plath, D. Kuhl, R. L. Huganir, and P. F. Worley. 2006. 'Arc/Arg3.1 mediates homeostatic synaptic scaling of AMPA receptors', *Neuron*, 52: 475-84.
Sherman, D. L., S. Tait, S. Melrose, R. Johnson, B. Zonta, F. A. Court, W. B. Macklin, S. Meek, A. J. Smith, D. F. Cottrell, and P. J. Brophy. 2005. 'Neurofascins are required to establish axonal domains for saltatory conduction', *Neuron*, 48: 737-42.
Silverman, M. A., S. Kaech, M. Jareb, M. A. Burack, L. Vogt, P. Sonderegger, and G. Banker. 2001. 'Sorting and directed transport of membrane proteins during development of hippocampal neurons in culture', *Proc Natl Acad Sci U S A*, 98: 7051-7.
Singh, N. A., P. Westenskow, C. Charlier, C. Pappas, J. Leslie, J. Dillon, V. E. Anderson, M. C. Sanguinetti, M. F. Leppert, and Bfnc Physician Consortium. 2003. 'KCNQ2 and KCNQ3

potassium channel genes in benign familial neonatal convulsions: expansion of the functional and mutation spectrum', *Brain*, 126: 2726-37.
Smith, K. R., K. J. Kopeikina, J. M. Fawcett-Patel, K. Leaderbrand, R. Gao, B. Schurmann, K. Myczek, J. Radulovic, G. T. Swanson, and P. Penzes. 2014. 'Psychiatric risk factor ANK3/ankyrin-G nanodomains regulate the structure and function of glutamatergic synapses', *Neuron*, 84: 399-415.
Sobotzik, J. M., J. M. Sie, C. Politi, D. Del Turco, V. Bennett, T. Deller, and C. Schultz. 2009. 'AnkyrinG is required to maintain axo-dendritic polarity in vivo', *Proc Natl Acad Sci U S A*, 106: 17564-9.
Sohal, V. S. 2012. 'Insights into cortical oscillations arising from optogenetic studies', *Biol Psychiatry*, 71: 1039-45.
Sohal, V. S., and J. L. R. Rubenstein. 2019. 'Excitation-inhibition balance as a framework for investigating mechanisms in neuropsychiatric disorders', *Mol Psychiatry*.
Sohal, V. S., F. Zhang, O. Yizhar, and K. Deisseroth. 2009. 'Parvalbumin neurons and gamma rhythms enhance cortical circuit performance', *Nature*, 459: 698-702.
Somogyi, P. 1977. 'A specific 'axo-axonal' interneuron in the visual cortex of the rat', *Brain Res*, 136: 345-50.
Somogyi, P., L. Katona, T. Klausberger, B. Lasztoczi, and T. J. Viney. 2014. 'Temporal redistribution of inhibition over neuronal subcellular domains underlies state-dependent rhythmic change of excitability in the hippocampus', *Philos Trans R Soc Lond B Biol Sci*, 369: 20120518.
Song, A. H., D. Wang, G. Chen, Y. Li, J. Luo, S. Duan, and M. M. Poo. 2009. 'A selective filter for cytoplasmic transport at the axon initial segment', *Cell*, 136: 1148-60.
Sousa, A. D., and M. A. Bhat. 2007. 'Cytoskeletal transition at the paranodes: the Achilles' heel of myelinated axons', *Neuron Glia Biology*, 3: 169-78.
Spruston, N. 2008. 'Pyramidal neurons: dendritic structure and synaptic integration', *Nature Reviews Neuroscience*, 9: 206-21.
Stahl, E. A., G. Breen, A. J. Forstner, A. McQuillin, S. Ripke, V. Trubetskoy, M. Mattheisen, Y. Wang, J. R. I. Coleman, H. A. Gaspar, C. A. de Leeuw, S. Steinberg, J. M. W. Pavlides, M. Trzaskowski, E. M. Byrne, T. H. Pers, P. A. Holmans, A. L. Richards, L. Abbott, E. Agerbo, H. Akil, D. Albani, N. Alliey-Rodriguez, T. D. Als, A. Anjorin, V. Antilla, S. Awasthi, J. A. Badner, M. Baekvad-Hansen, J. D. Barchas, N. Bass, M. Bauer, R. Belliveau, S. E. Bergen, C. B. Pedersen, E. Boen, M. P. Boks, J. Boocock, M. Budde, W. Bunney, M. Burmeister, J. Bybjerg-Grauholm, W. Byerley, M. Casas, F. Cerrato, P. Cervantes, K. Chambert, A. W. Charney, D. Chen, C. Churchhouse, T. K. Clarke, W. Coryell, D. W. Craig, C. Cruceanu, D. Curtis, P. M. Czerski, A. M. Dale, S. de Jong, F. Degenhardt, J. Del-Favero, J. R. DePaulo, S. Djurovic, A. L. Dobbyn, A. Dumont, T. Elvsashagen, V. Escott-Price, C. C. Fan, S. B. Fischer, M. Flickinger, T. M. Foroud, L. Forty, J. Frank, C. Fraser, N. B. Freimer, L. Frisen, K. Gade, D. Gage, J. Garnham, C. Giambartolomei, M. G. Pedersen, J. Goldstein, S. D. Gordon, K. Gordon-Smith, E. K. Green, M. J. Green, T. A. Greenwood, J. Grove, W. Guan, J. Guzman-Parra, M. L. Hamshere, M. Hautzinger, U. Heilbronner, S. Herms, M. Hipolito, P. Hoffmann, D. Holland, L. Huckins, S. Jamain, J. S. Johnson, A. Jureus, R. Kandaswamy, R. Karlsson, J. L. Kennedy, S. Kittel-Schneider, J. A. Knowles, M. Kogevinas, A. C. Koller, R. Kupka, C. Lavebratt, J. Lawrence, W. B. Lawson, M. Leber, P. H. Lee, S. E. Levy, J. Z.

Li, C. Liu, S. Lucae, A. Maaser, D. J. MacIntyre, P. B. Mahon, W. Maier, L. Martinsson, S. McCarroll, P. McGuffin, M. G. McInnis, J. D. McKay, H. Medeiros, S. E. Medland, F. Meng, L. Milani, G. W. Montgomery, D. W. Morris, T. W. Muhleisen, N. Mullins, H. Nguyen, C. M. Nievergelt, A. N. Adolfsson, E. A. Nwulia, C. O'Donovan, L. M. O. Loohuis, A. P. S. Ori, L. Oruc, U. Osby, R. H. Perlis, A. Perry, A. Pfennig, J. B. Potash, S. M. Purcell, E. J. Regeer, A. Reif, C. S. Reinbold, J. P. Rice, F. Rivas, M. Rivera, P. Roussos, D. M. Ruderfer, E. Ryu, C. Sanchez-Mora, A. F. Schatzberg, W. A. Scheftner, N. J. Schork, C. Shannon Weickert, T. Shehktman, P. D. Shilling, E. Sigurdsson, C. Slaney, O. B. Smeland, J. L. Sobell, C. Soholm Hansen, A. T. Spijker, D. St Clair, M. Steffens, J. S. Strauss, F. Streit, J. Strohmaier, S. Szelinger, R. C. Thompson, T. E. Thorgeirsson, J. Treutlein, H. Vedder, W. Wang, S. J. Watson, T. W. Weickert, S. H. Witt, S. Xi, W. Xu, A. H. Young, P. Zandi, P. Zhang, S. Zollner, QTLGen Consortium e, Bios Consortium, R. Adolfsson, I. Agartz, M. Alda, L. Backlund, B. T. Baune, F. Bellivier, W. H. Berrettini, J. M. Biernacka, D. H. R. Blackwood, M. Boehnke, A. D. Borglum, A. Corvin, N. Craddock, M. J. Daly, U. Dannlowski, T. Esko, B. Etain, M. Frye, J. M. Fullerton, E. S. Gershon, M. Gill, F. Goes, M. Grigoroiu-Serbanescu, J. Hauser, D. M. Hougaard, C. M. Hultman, I. Jones, L. A. Jones, R. S. Kahn, G. Kirov, M. Landen, M. Leboyer, C. M. Lewis, Q. S. Li, J. Lissowska, N. G. Martin, F. Mayoral, S. L. McElroy, A. M. McIntosh, F. J. McMahon, I. Melle, A. Metspalu, P. B. Mitchell, G. Morken, O. Mors, P. B. Mortensen, B. Muller-Myhsok, R. M. Myers, B. M. Neale, V. Nimgaonkar, M. Nordentoft, M. M. Nothen, M. C. O'Donovan, K. J. Oedegaard, M. J. Owen, S. A. Paciga, C. Pato, M. T. Pato, D. Posthuma, J. A. Ramos-Quiroga, M. Ribases, M. Rietschel, G. A. Rouleau, M. Schalling, P. R. Schofield, T. G. Schulze, A. Serretti, J. W. Smoller, H. Stefansson, K. Stefansson, E. Stordal, P. F. Sullivan, G. Turecki, A. E. Vaaler, E. Vieta, J. B. Vincent, T. Werge, J. I. Nurnberger, N. R. Wray, A. Di Florio, H. J. Edenberg, S. Cichon, R. A. Ophoff, L. J. Scott, O. A. Andreassen, J. Kelsoe, P. Sklar, and Consortium Bipolar Disorder Working Group of the Psychiatric Genomics. 2019. 'Genome-wide association study identifies 30 loci associated with bipolar disorder', *Nature Genetics*, 51: 793-803.

Steinlein, O. K. 2014. 'Mechanisms underlying epilepsies associated with sodium channel mutations', *Prog Brain Res*, 213: 97-111.

Susuki, K., K. J. Chang, D. R. Zollinger, Y. H. Liu, Y. Ogawa, Y. Eshed-Eisenbach, M. T. Dours-Zimmermann, J. A. Oses-Prieto, A. L. Burlingame, C. I. Seidenbecher, D. R. Zimmermann, T. Oohashi, E. Peles, and M. N. Rasband. 2013. 'Three Mechanisms Assemble Central Nervous System Nodes of Ranvier', *Neuron*, 78: 469-82.

Swanwick, C. C., N. R. Murthy, Z. Mtchedlishvili, W. Sieghart, and J. Kapur. 2006. 'Development of gamma-aminobutyric acidergic synapses in cultured hippocampal neurons', *J Comp Neurol*, 495: 497-510.

Talkowski, M. E., J. A. Rosenfeld, I. Blumenthal, V. Pillalamarri, C. Chiang, A. Heilbut, C. Ernst, C. Hanscom, E. Rossin, A. M. Lindgren, S. Pereira, D. Ruderfer, A. Kirby, S. Ripke, D. J. Harris, J. H. Lee, K. Ha, H. G. Kim, B. D. Solomon, A. L. Gropman, D. Lucente, K. Sims, T. K. Ohsumi, M. L. Borowsky, S. Loranger, B. Quade, K. Lage, J. Miles, B. L. Wu, Y. P. Shen, B. Neale, L. G. Shaffer, M. J. Daly, C. C. Morton, and J. F. Gusella. 2012. 'Sequencing Chromosomal Abnormalities Reveals Neurodevelopmental Loci that Confer Risk across Diagnostic Boundaries', *Cell*, 149.

Tamas, G., E. H. Buhl, A. Lorincz, and P. Somogyi. 2000. 'Proximally targeted GABAergic synapses and gap junctions synchronize cortical interneurons', *Nat Neurosci*, 3: 366-71.
Tan, H. L., B. N. Queenan, and R. L. Huganir. 2015. 'GRIP1 is required for homeostatic regulation of AMPAR trafficking', *Proc Natl Acad Sci U S A*, 112: 10026-31.
Tatti, R., M. S. Haley, O. K. Swanson, T. Tselha, and A. Maffei. 2017. 'Neurophysiology and Regulation of the Balance Between Excitation and Inhibition in Neocortical Circuits', *Biol Psychiatry*, 81: 821-31.
Tesli, M., P. Koefoed, L. Athanasiu, M. Mattingsdal, O. Gustafsson, I. Agartz, L. M. Rimol, A. Brown, K. V. Wirgenes, L. L. Smorr, A. K. Kahler, T. Werge, O. Mors, E. Mellerup, E. G. Jonsson, I. Melle, G. Morken, S. Djurovic, and O. A. Andreassen. 2011. 'Association analysis of ANK3 gene variants in nordic bipolar disorder and schizophrenia case-control samples', *Am J Med Genet B Neuropsychiatr Genet*, 156B: 969-74.
Thaxton, C., A. M. Pillai, A. L. Pribisko, J. L. Dupree, and M. A. Bhat. 2011. 'Nodes of Ranvier act as barriers to restrict invasion of flanking paranodal domains in myelinated axons', *Neuron*, 69: 244-57.
Thielmann, Y., J. Mohrluder, B. W. Koenig, T. Stangler, R. Hartmann, K. Becker, H. D. Holtje, and D. Willbold. 2008. 'An indole-binding site is a major determinant of the ligand specificity of the GABA type A receptor-associated protein GABARAP', *Chembiochem*, 9: 1767-75.
Thomas, G. M., T. Hayashi, S. L. Chiu, C. M. Chen, and R. L. Huganir. 2012. 'Palmitoylation by DHHC5/8 targets GRIP1 to dendritic endosomes to regulate AMPA-R trafficking', *Neuron*, 73: 482-96.
Toma, C., A. D. Shaw, R. J. N. Allcock, A. Heath, K. D. Pierce, P. B. Mitchell, P. R. Schofield, and J. M. Fullerton. 2018. 'An examination of multiple classes of rare variants in extended families with bipolar disorder', *Transl Psychiatry*, 8: 65.
Torrey, E. F., B. M. Barci, M. J. Webster, J. J. Bartko, J. H. Meador-Woodruff, and M. B. Knable. 2005. 'Neurochemical markers for schizophrenia, bipolar disorder, and major depression in postmortem brains', *Biol Psychiatry*, 57: 252-60.
Trunova, S., B. Baek, and E. Giniger. 2011. 'Cdk5 Regulates the Size of an Axon Initial Segment-Like Compartment in Mushroom Body Neurons of the Drosophila Central Brain', *Journal of Neuroscience*, 31: 10451-62.
Tseng, W. C., P. M. Jenkins, M. Tanaka, R. Mooney, and V. Bennett. 2015. 'Giant ankyrin-G stabilizes somatodendritic GABAergic synapses through opposing endocytosis of GABAA receptors', *Proc Natl Acad Sci U S A*, 112: 1214-9.
Turrigiano, G. 2011. 'Too many cooks? Intrinsic and synaptic homeostatic mechanisms in cortical circuit refinement', *Annu Rev Neurosci*, 34: 89-103.
Turrigiano, G. G. 2008. 'The self-tuning neuron: synaptic scaling of excitatory synapses', *Cell*, 135: 422-35.
Turrigiano, G. G., K. R. Leslie, N. S. Desai, L. C. Rutherford, and S. B. Nelson. 1998. 'Activity-dependent scaling of quantal amplitude in neocortical neurons', *Nature*, 391: 892-6.
Turrigiano, G. G., and S. B. Nelson. 2000. 'Hebb and homeostasis in neuronal plasticity', *Curr Opin Neurobiol*, 10: 358-64.
Tuvia, S., T. D. Garver, and V. Bennett. 1997. 'The phosphorylation state of the FIGQY tyrosine of neurofascin determines ankyrin-binding activity and patterns of cell segregation', *Proc Natl Acad Sci U S A*, 94: 12957-62.

Uemoto, Y., S. Suzuki, N. Terada, N. Ohno, S. Ohno, S. Yamanaka, and M. Komada. 2007. 'Specific role of the truncated betaIV-spectrin Sigma6 in sodium channel clustering at axon initial segments and nodes of ranvier', *J Biol Chem*, 282: 6548-55.

Vallee, R. B., and J. W. Tsai. 2006. 'The cellular roles of the lissencephaly gene LIS1, and what they tell us about brain development', *Genes & Development*, 20: 1384-93.

Vosseller, K., J. C. Trinidad, R. J. Chalkley, C. G. Specht, A. Thalhammer, A. J. Lynn, J. O. Snedecor, S. H. Guan, K. F. Medzihradszky, D. A. Maltby, R. Schoepfer, and A. L. Burlingame. 2006. 'O-linked N-acetylglucosamine proteomics of postsynaptic density preparations using lectin weak affinity chromatography and mass spectrometry', *Molecular & Cellular Proteomics*, 5: 923-34.

Wagnon, J. L., and M. H. Meisler. 2015. 'Recurrent and Non-Recurrent Mutations of SCN8A in Epileptic Encephalopathy', *Front Neurol*, 6: 104.

Wang, C., Z. Wei, K. Chen, F. Ye, C. Yu, V. Bennett, and M. Zhang. 2014. 'Structural basis of diverse membrane target recognitions by ankyrins', *Elife*, 3.

Wang, C., C. Yu, F. Ye, Z. Y. Wei, and M. J. Zhang. 2012. 'Structure of the ZU5-ZU5-UPA-DD tandem of ankyrin-B reveals interaction surfaces necessary for ankyrin function', *Proceedings of the National Academy of Sciences of the United States of America*, 109: 4822-27.

Wang, R., Z. Y. Wei, H. Jin, H. Wu, C. Yu, W. Y. Wen, L. N. Chan, Z. L. Wen, and M. J. Zhang. 2009. 'Autoinhibition of UNC5b Revealed by the Cytoplasmic Domain Structure of the Receptor', *Molecular Cell*, 33: 692-703.

Watanabe, K., S. Al-Bassam, Y. Miyazaki, T. J. Wandless, P. Webster, and D. B. Arnold. 2012. 'Networks of polarized actin filaments in the axon initial segment provide a mechanism for sorting axonal and dendritic proteins', *Cell Rep*, 2: 1546-53.

Weber, P., U. Bartsch, M. N. Rasband, R. Czaniera, Y. Lang, H. Bluethmann, R. U. Margolis, S. R. Levinson, P. Shrager, D. Montag, and M. Schachner. 1999. 'Mice deficient for tenascin-R display alterations of the extracellular matrix and decreased axonal conduction velocities in the CNS', *J Neurosci*, 19: 4245-62.

West, A. E., and M. E. Greenberg. 2011. 'Neuronal activity-regulated gene transcription in synapse development and cognitive function', *Cold Spring Harb Perspect Biol*, 3.

Wierenga, C. J., K. Ibata, and G. G. Turrigiano. 2005. 'Postsynaptic expression of homeostatic plasticity at neocortical synapses', *J Neurosci*, 25: 2895-905.

Williams, D. L., H. A. Pretus, R. B. McNamee, E. L. Jones, H. E. Ensley, and I. W. Browder. 1992. 'Development of a water-soluble, sulfated (1-->3)-beta-D-glucan biological response modifier derived from Saccharomyces cerevisiae', *Carbohydr Res*, 235: 247-57.

Winckler, B., P. Forscher, and I. Mellman. 1999. 'A diffusion barrier maintains distribution of membrane proteins in polarized neurons', *Nature*, 397: 698-701.

Wirgenes, K. V., M. Tesli, E. Inderhaug, L. Athanasiu, I. Agartz, I. Melle, T. Hughes, O. A. Andreassen, and S. Djurovic. 2014. 'ANK3 gene expression in bipolar disorder and schizophrenia', *Br J Psychiatry*, 205: 244-5.

Witte, H., D. Neukirchen, and F. Bradke. 2008. 'Microtubule stabilization specifies initial neuronal polarization', *Journal of Cell Biology*, 180: 619-32.

Wolswijk, G., and R. Balesar. 2003. 'Changes in the expression and localization of the paranodal protein Caspr on axons in chronic multiple sclerosis', *Brain*, 126: 1638-49.

Woodin, M., P. P. Wang, D. Aleman, D. McDonald-McGinn, E. Zackai, and E. Moss. 2001. 'Neuropsychological profile of children and adolescents with the 22q11.2 microdeletion', *Genet Med*, 3: 34-9.
Woolfe, A., M. Goodson, D. K. Goode, P. Snell, G. K. McEwen, T. Vavouri, S. F. Smith, P. North, H. Callaway, K. Kelly, K. Walter, I. Abnizova, W. Gilks, Y. J. Edwards, J. E. Cooke, and G. Elgar. 2005. 'Highly conserved non-coding sequences are associated with vertebrate development', *PLoS Biol*, 3: e7.
Xiao, Z. C., D. S. Ragsdale, J. D. Malhotra, L. N. Mattei, P. E. Braun, M. Schachner, and L. L. Isom. 1999. 'Tenascin-R is a functional modulator of sodium channel beta subunits', *J Biol Chem*, 274: 26511-7.
Xu, K., G. Zhong, and X. Zhuang. 2013. 'Actin, spectrin, and associated proteins form a periodic cytoskeletal structure in axons', *Science*, 339: 452-6.
Xu, M., and E. C. Cooper. 2015. 'An Ankyrin-G N-terminal Gate and Protein Kinase CK2 Dually Regulate Binding of Voltage-gated Sodium and KCNQ2/3 Potassium Channels', *J Biol Chem*, 290: 16619-32.
Yamada, R., and H. Kuba. 2016. 'Structural and Functional Plasticity at the Axon Initial Segment', *Front Cell Neurosci*, 10: 250.
Yang, Y., Y. Ogawa, K. L. Hedstrom, and M. N. Rasband. 2007. 'beta IV spectrin is recruited to axon initial segments and nodes of Ranvier by ankyrinG', *Journal of Cell Biology*, 176: 509-19.
Yokoi, N., Y. Fukata, A. Sekiya, T. Murakami, K. Kobayashi, and M. Fukata. 2016. 'Identification of PSD-95 Depalmitoylating Enzymes', *J Neurosci*, 36: 6431-44.
Yoshimura, T., and M. N. Rasband. 2014. 'Axon initial segments: diverse and dynamic neuronal compartments', *Curr Opin Neurobiol*, 27: 96-102.
Yu, W., and E. Krook-Magnuson. 2015. 'Cognitive Collaborations: Bidirectional Functional Connectivity Between the Cerebellum and the Hippocampus', *Front Syst Neurosci*, 9: 177.
Zhang, A., A. Desmazieres, B. Zonta, S. Melrose, G. Campbell, D. Mahad, Q. Li, D. L. Sherman, R. Reynolds, and P. J. Brophy. 2015. 'Neurofascin 140 is an embryonic neuronal neurofascin isoform that promotes the assembly of the node of Ranvier', *J Neurosci*, 35: 2246-54.
Zhang, X., and V. Bennett. 1996. 'Identification of O-linked N-acetylglucosamine modification of ankyrin(G) isoforms targeted to nodes of Ranvier', *Journal of Biological Chemistry*, 271: 31391-98.
Zhang, X., J. Q. Davis, S. Carpenter, and V. Bennett. 1998. 'Structural requirements for association of neurofascin with ankyrin', *J Biol Chem*, 273: 30785-94.
Zhong, G., J. He, R. Zhou, D. Lorenzo, H. P. Babcock, V. Bennett, and X. Zhuang. 2014. 'Developmental mechanism of the periodic membrane skeleton in axons', *Elife*, 3.
Zhou, D. X., S. Lambert, P. L. Malen, S. Carpenter, L. M. Boland, and V. Bennett. 1998. 'Ankyrin(G) is required for clustering of voltage-gated Na channels at axon initial segments and for normal action potential firing', *Journal of Cell Biology*, 143: 1295-304.
Zhu, S., Z. A. Cordner, J. Xiong, C. T. Chiu, A. Artola, Y. Zuo, A. D. Nelson, T. Y. Kim, N. Zaika, B. M. Woolums, E. J. Hess, X. Wang, D. M. Chuang, M. M. Pletnikov, P. M. Jenkins, K. L. Tamashiro, and C. A. Ross. 2017. 'Genetic disruption of ankyrin-G in adult

mouse forebrain causes cortical synapse alteration and behavior reminiscent of bipolar disorder', *Proc Natl Acad Sci U S A*, 114: 10479-84.

Zhuang, X., R. S. Oosting, S. R. Jones, R. R. Gainetdinov, G. W. Miller, M. G. Caron, and R. Hen. 2001. 'Hyperactivity and impaired response habituation in hyperdopaminergic mice', *Proc Natl Acad Sci U S A*, 98: 1982-7.

Zonta, B., S. Tait, S. Melrose, H. Anderson, S. Harroch, J. Higginson, D. L. Sherman, and P. J. Brophy. 2008. 'Glial and neuronal isoforms of Neurofascin have distinct roles in the assembly of nodes of Ranvier in the central nervous system', *Journal of Cell Biology*, 181: 1169-77.